BEDROCK STRUCTURE, LITHOLOGY AND GROUND WATER: INFLUENCES ON SLOPE FAILURE INITIATION IN DAVIS COUNTY, UTAH

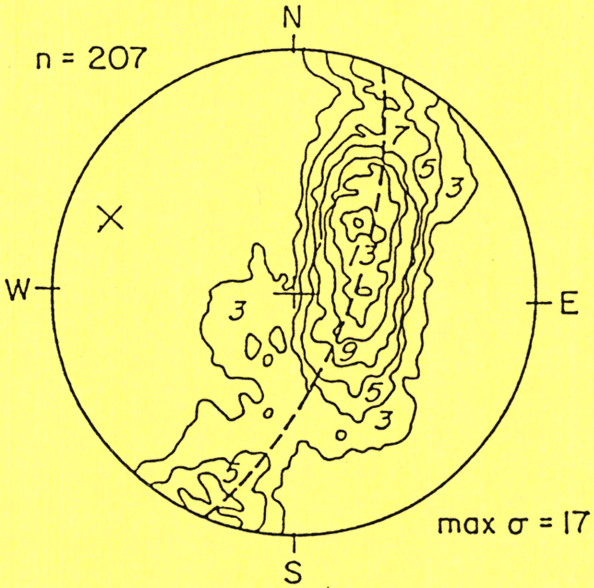

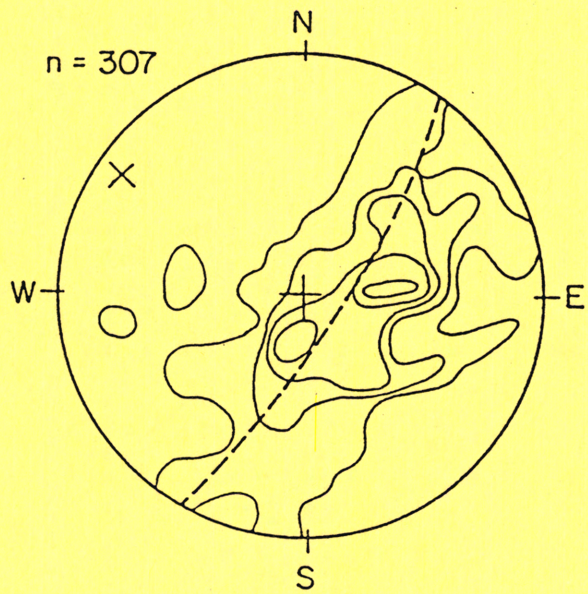

by

Souren Nariman Ala

CONTRACT REPORT 95-4 **January 1995**

UTAH GEOLOGICAL SURVEY

a division of

UTAH DEPARTMENT OF NATURAL RESOURCES

This Contract Report represents material that may not have undergone policy, technical, or editorial review required for other UGS publications. It provides information that, in part, may be interpretive or incomplete and readers are to exercise some degree of caution in the use of the data. The UGS makes no warranty as to the accuracy of the information contained in this publication.

BEDROCK STRUCTURE, LITHOLOGY AND GROUND WATER: INFLUENCES ON SLOPE FAILURE INITIATION IN DAVIS COUNTY, UTAH

A Thesis

by

SOUREN NARIMAN ALA

Submitted to the Office of Graduate Studies of
Texas A&M University
in partial fulfillment of the requirements
for the degree of

MASTER OF SCIENCE

December 1990

Major Subject: Geology

ABSTRACT

Bedrock Structure, Lithology and Ground Water:
Influences on Slope Failure Initiation
In Davis County, Utah
(December 1990)

Souren Nariman Ala
B.A., Princeton University
Chair of Advisory Committee: Dr. Christopher C. Mathewson

During May and June of 1983 and 1984, an unusually large number of land slips and debris flows occurred along the Wasatch Front, in north-central Utah. Failures on slopes underlain by rocks of the Precambrian Farmington Canyon Complex were often followed by new and sustained ground-water discharge. It has been proposed that elevated pore water pressures within the intensely fractured bedrock contribute to the initiation of slope failures.

In order to better understand the behavior of ground water in the mountain block, it was necessary to characterize the geological properties of the bedrock, and evaluate their influence on preferential ground-water flow paths. This investigation considers the roles of faults, lithological variations, fractures, fracture intersection lines and foliation planes in affecting the local and

regional hydrogeology.

The detailed geology of the Farmington Canyon Complex is extremely heterogeneous. Statistical and geological analyses of fractures, faults, foliation and lithologic variations reveal that spatial variability overrides any one factor contributing to the geometry of the structural fabric. However, inter-regional geological parameters such as lithology and proximity to faults do have an effect on the dispersion and orientation of fracture sets.

The overall fracture pattern in foliated rocks is resolved into a predictable form when variations in the orientation of foliation planes are removed. The resultant fracture geometry may indicate the direction of the greatest principal stress during the Sevier and Laramide orogenies.

The fractured bedrock constitutes an aquifer of highly variable properties. Analysis of stream discharge data suggests that a net northwestward flow of ground water is taking place along major structural lineaments. The distribution of ground-water discharge points is controlled by topography and by geological features including lithologic changes and/or low-angle fractures and foliation planes.

A comparison of slope aspects upon which slope failures have occurred indicates that slopes perpendicular to the main trend of faults (interpreted from aerial photographs) experience the greatest number of slope failures. Neither fractures, fracture intersection lines nor foliation planes correlate systematically with these slopes.

This work is dedicated to

Jeff, Julie, Jennifer and Laurie Keaton.

ACKNOWLEDGEMENTS

I am indebted to a large number of people who helped me to complete this report. I am primarily grateful to my thesis committee: Dr. Christopher C. Mathewson gave me much support, and showed me the importance of synthesizing information; Dr. J. Richard Giardino helped me greatly in my data analysis; Dr. John H. Spang gave me valuable advice, especially with respect to the regional structural geology.

I am grateful to Dr. David V. Wiltschko for access to and help with the "Structure Graphics" program; Dr. Jeffrey R. Keaton for his expert help and encouragement; Dr. C. Brann Johnson for his teaching and insights; Dr. Dale F. Morgan for help in analyzing the results of the geophysical surveys. Ted Apotria's guidance in the field, and the excellent work and general example provided by Paul Santi were gratefully accepted.

Materials and expert advice were gladly received from Dr. Loren Anderson, Adolf Yonkee, Gary Christensen, Mike Lowe, Scott Williams and Sara Monteith. In addition, the United States Forest Service, Soil Conservation Service, and Davis County Planning Commission gave us information and materials. I also thank Dr. Bill Hicks, with the Forest Service in Oregon, for his input.

The Salt Lake City office of Dames and Moore generously provided for me to print the results of my geophysical surveys. Mr. Roger Fallon of Salt Lake City did us a great service by flying us around the Wasatch Front canyons; much of the regional geological picture only became apparent after viewing photographs taken during that flight.

I thank the Keaton family for their hospitality. I am grateful to Kevin Coleman for his help and patience in the field, and for bringing out the the common ground shared by our complementary research efforts.

Lili Lyddon drafted almost all the figures in this report, with a masterful hand.

I thank the Utah Geological and Mineral Survey for their financial support (contract #89-0327). I thank the Center for Engineering Geosciences, Department of geology, Texas A&M University for funding, equipment, and moral support. I thank the Department of Geology, Texas A&M University, for funding the rental of the VLF geophysical tool.

I will be forever grateful for the love and support of my family: Ann, Fereydoun, Arjan, Tour and Natalyn.

TABLE OF CONTENTS

TABLE OF CONTENTS, CONTINUED

TABLE OF CONTENTS, CONTINUED

LIST OF TABLES

LIST OF FIGURES

LIST OF FIGURES, CONTINUED

LIST OF FIGURES, CONTINUED

LIST OF FIGURES, CONTINUED

LIST OF FIGURES, CONTINUED

LIST OF FIGURES, CONTINUED

LIST OF FIGURES, CONTINUED

INTRODUCTION

Rapid population growth in the urban area along the eastern border of the Great Salt Lake, Utah, has led to residential development in the western foothills of the Wasatch Range (Figure 1). Such sites are conveniently located as well as being aesthetically attractive. However, much of this area is susceptible to debris flow and flood hazards. A large number of debris flows occurred on the Wasatch Front during May and June of 1983 and 1984. Although no lives were lost, there was significant damage to structures, and cumulative costs for the state ran in excess of 400 million dollars (Anderson et al., 1985).

Several studies have been conducted in the area since 1983, with the goal of defining the severity and extent of flood and debris flow hazards along the Wasatch Front (Pack, 1985; Brooks, 1986; Jadkowski, 1987; Keaton, 1988b; Monteith, 1988; Santi, 1988; Weiczorek et al., 1989; Mathewson et al., 1990). Attention has been focused on 1) identifying susceptible areas, 2) gaining a better understanding of failure mechanisms, and 3) determining the amount and velocity of sediment reaching the canyon mouth. This study is an attempt to clarify parts of categories 1 and 2, by considering the source of elevated

---

The style and format of this report follow that of <u>The Bulletin of the Association of Engineering Geologists</u>.

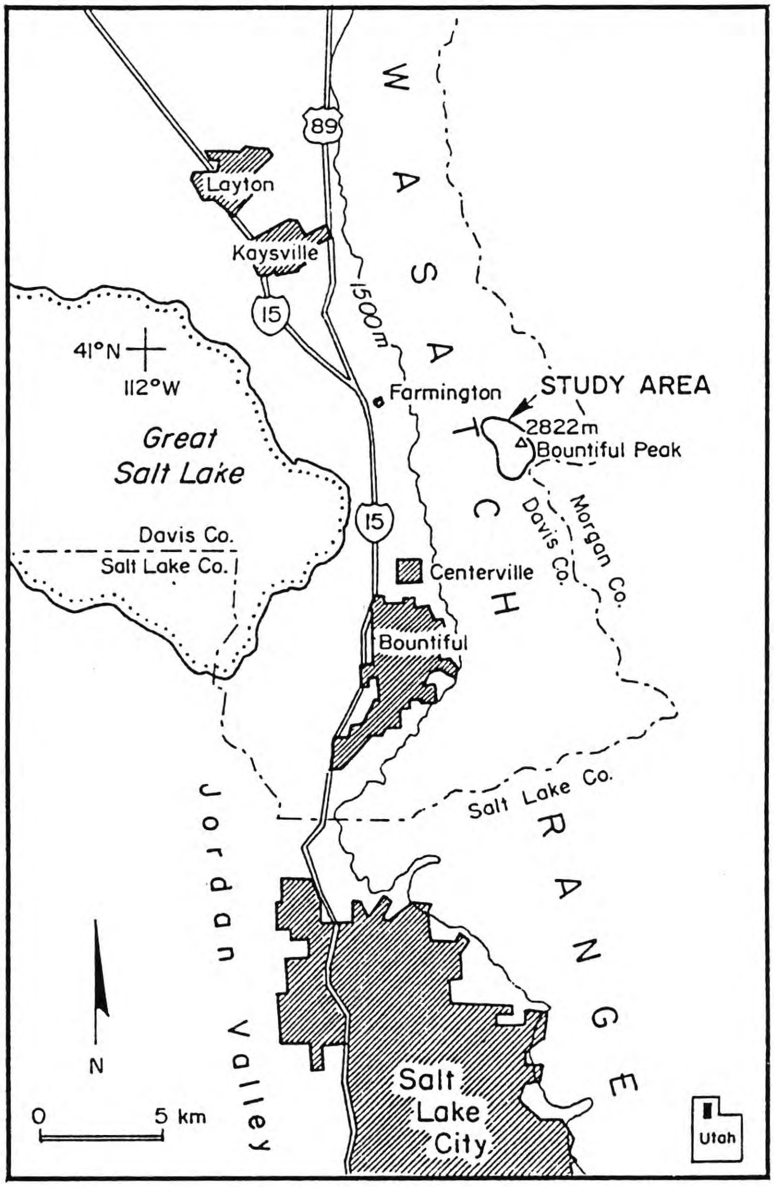

Figure 1. Location of the study area in the Wasatch Range, north central Utah. The 1500 m contour shows the elevation of the general slope gradient change at the base of the mountains. Numerous historical floods and debris flow sedimentation events have occurred at this elevation.

pore water pressures leading to slope failure. The main focus will be on characterizing the bedrock as a ground-water delivery system, by addressing the question "how and where do elevated pore water pressures develop?"

Ground Water and Hillslope Processes

Bedrock ground water is active in the evolution of hillslope landforms. Long term weathering of fractured metamorphic rocks under saturated conditions produces residual "saprolitic" soils which vary greatly in depth and composition (Figure 2). Differences in the resistance of the bedrock to weathering gradually become expressed in the topography, leading to the development of hollows on colluvial slopes. These in turn become loci for further weathering and accumulation of soil, debris and ground water (Reneau and Dietrich, 1987; Sidle, 1987). Areas of more highly fractured, weathered and thus, more permeable bedrock become sites of recurrent debris flow activity (Alger and Ellen, 1987; Tsukamoto and Minematsu, 1987).

Slope Failure Mechanisms

Failure of a slope takes place when the downslope component of applied shear stress overcomes the shear strength of the material (Chorley et al., 1984). Often, the slope is in a meta-stable condition, and failure is triggered by a sudden event. Possible examples are an increase in shear stress by added load from upslope, or a reduction in shear strength caused by removal of toe

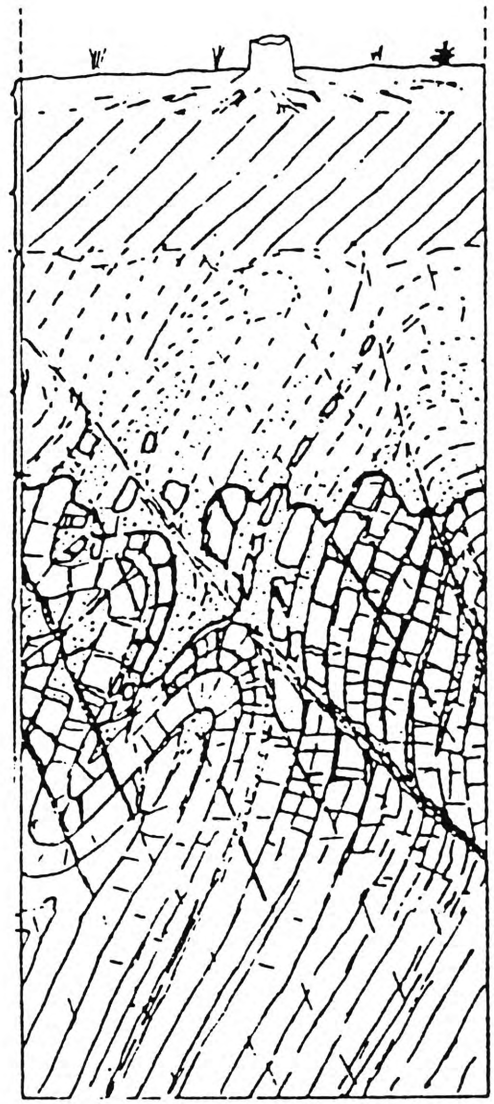

Figure 2. Schematic cross-section of a typical soil profile in weathered metamorphic terrain (adapted from Deere and Patton, 1971).

support, seismic shock or most commonly, an increase in pore water pressure at the incipient failure surface.

Debris flows can be distinguished from block glides or slumps by their more fluid behavior, brought about by a greater water content. They are almost always preceded by extremely heavy rainfall or the melting of snow or frozen ground (Schuster and Krizek, 1978).

Antecedent rainfall of at least 25 cm followed by storms with an intensity of 0.6 cm/hr or greater initiated a series of damaging debris flows in the Santa Monica mountains of southern California (Campbell, 1975). These events took place in colluvial soils underlain by sedimentary, volcanic and low-grade metamorphic rocks ranging in age from Quaternary to Triassic (State of California Department of Natural Resources, 1954). The observed failure mechanism was a critical reduction of effective stress in the colluvium, due to an increase in pore water pressure. The pore water pressure increase was brought about by continued infiltration of surface water into saturated colluvium at a rate which exceeded the hydraulic conductivity of the underlying bedrock. A schematic diagram of this process is shown in Figure 3. Failures generally began as areally extensive blocks of colluvium, that subsequently disaggregated into flows (Campbell, 1975).

Tsukamoto and Minematsu (1987) have subdivided

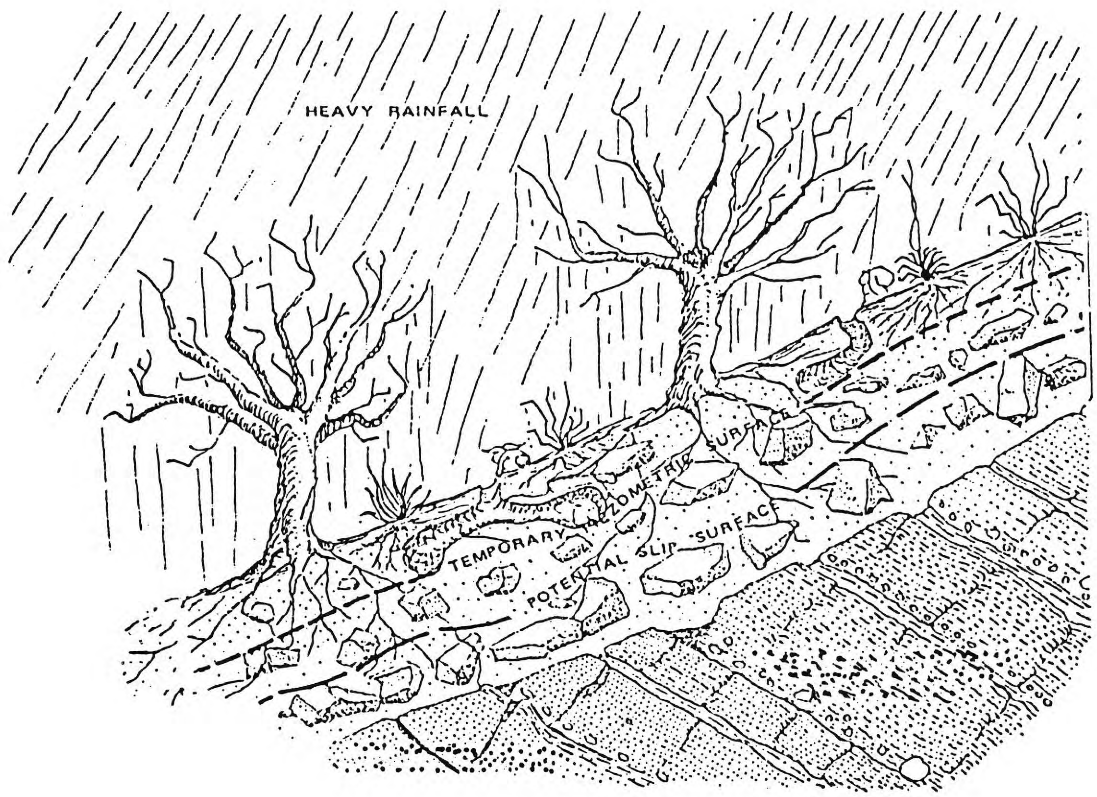

Figure 3. Schematic diagram of a slope failure mechanism in which pore water pressure is increased through rapid infiltration of rainfall into saturated colluvial soil (adapted from Campbell, 1975).

hydrologic conditions leading to hillslope erosion according to the relative permeabilities of three shallow subsurface units: soil, "underlying soil", and weathered bedrock. When rainfall intensity greatly exceeds infiltration, surface erosion occurs. When infiltration greatly exceeds the permeability of the underlying soil, shallow slides take place. When the permeability of the underlying soil greatly exceeds that of the weathered bedrock, shallow to deep slides can occur (Tsukamoto and Minematsu, 1987).

An alternative mechanism to those discussed above involves the contribution of upwelling ground water from permeable zones in bedrock, rather than downward infiltration of water through the soil. If regional ground-water flow lines are projected onto a slope, the lower section of the slope is in a zone of discharge. Where low permeability rock units or clays prevent discharge, pore water pressure rises and the potential for slope failure is increased. Campbell (1975) notes that a bedrock source of ground water is generally associated with deep seated landslides rather than debris flows. However, upwelling ground water can cause piping in cohesionless soil (Deere and Patton, 1971), and this process has been recognized as a contributor to slurry flows (Howard and McLane, 1988).

Slope failures initiated by ground water from bedrock have hitherto also been associated with heavy rainfall. Eisenlohr (1952) correlated ground-water "blowouts" with layers of shattered rock recharged by rainfall on higher ground. Hack and Goodlett (1960) found "water blowouts" along the lower contact of an impermeable diabase sill within a hillside composed mainly of permeable clastic sedimentary rocks.

Everett (1979) observed that landslide sources on forested slopes in Mingo County, West Virginia were associated with the upper surfaces of relatively less permeable sandstones, interbedded with highly fractured coal beds. These events were, therefore, associated with perched rather than artesian water table conditions.

Evidence exists that artesian ground-water conditions helped initiate debris flows on slopes underlain by Precambrian metamorphic rocks of the Farmington Canyon Complex, Wasatch Front, Utah (Mathewson et al., 1990). In May and June of 1983 and 1984, the Wasatch Front was the site of numerous debris flows and floods. Many of these originated as small water blowouts which gathered material during their progress down the channel (Santi, 1988). Failures were not correlated with heavy rainfall, but with rapid spring snowmelt. Several debris flow scars experienced new discharge, which was sustained for up to six months after failure (Mathewson and Santi, 1987;

Mathewson et al., 1990).

Mathewson and Santi (1987) proposed that hydrostatic head in the fractured bedrock, combined with variations in topography, led to elevated pore water pressures in the axes of upper mountain swales. This hypothesis has been confirmed in at least one case: a study by Monteith (1988) showed that a landslide and debris flow in Steed Canyon (immediately south of Farmington Canyon) was initiated by artesian ground-water conditions.

Schematic diagrams of the mechanisms proposed by Mathewson and others (1990), Hack and Goodlett (1960), and Everett (1979) are shown in Figures 4 and 5. A third mechanism, observed by Hicks (1988) in the Cascade Mountains, Oregon, is shown in Figure 6.

A large number of landslides and debris flows have occurred in colluvial soils in hilly terrain overlying the highly fractured metamorphic Franciscan melange in Marin County, California. In a small test area in this region, Wilson and Dietrich (1987) were able to construct a contoured hydraulic conductivity profile along the axis of a hollow, using constant head permeability tests in more than 30 piezometer nests (Figure 7).

During a 25-year scale storm that occurred from February 12-20, 1986, water levels along the basin axis were monitored. Results implied that subsurface flow through bedrock was forced up to the surface at point B,

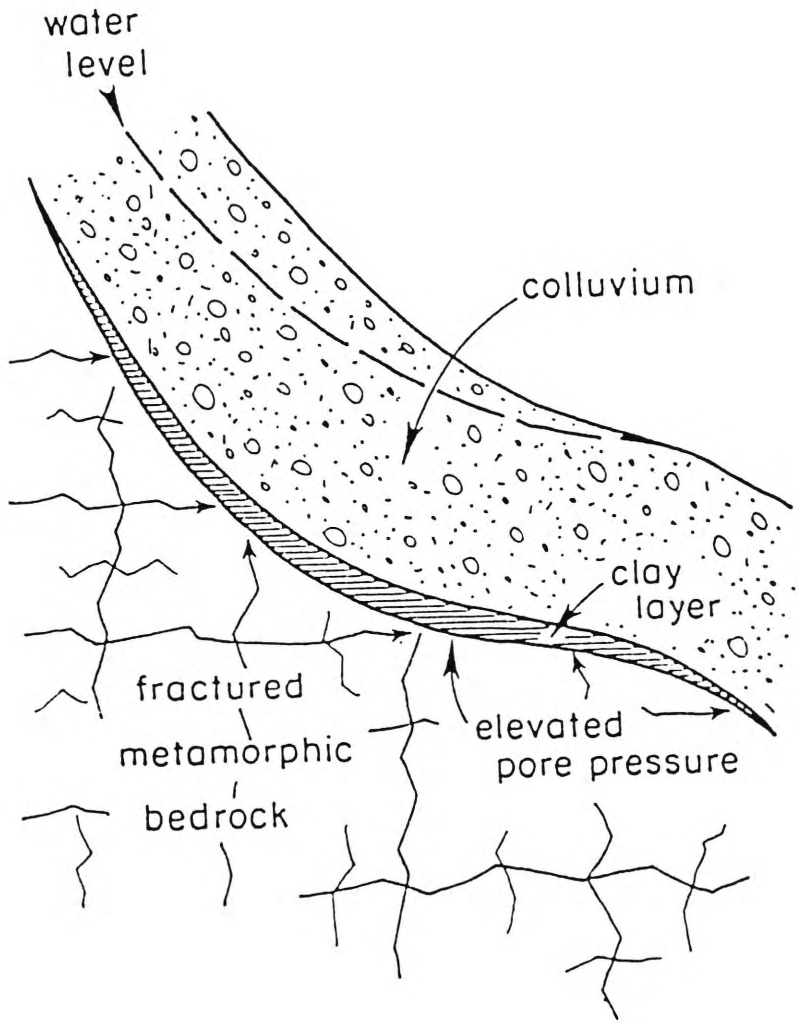

Figure 4. Schematic diagram of a slope failure mechanism in which ground water under significant hydrostatic pressure increases pore water pressures at the base of the soil profile. Communication to the surface is provided by low-angle fractures (adapted from Mathewson and Santi, 1987).

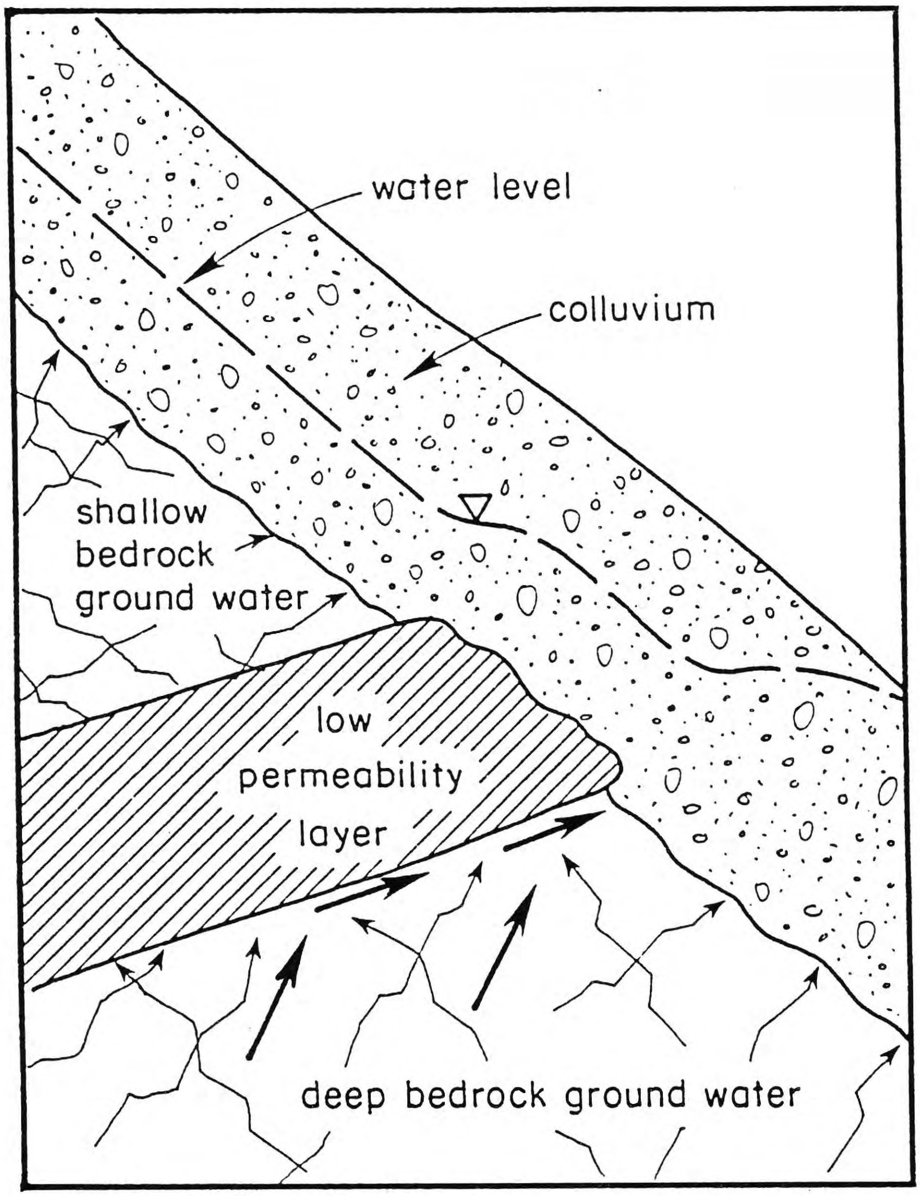

Figure 5. Schematic diagram of a slope failure mechanism in which pore water pressures in the soil are raised by perched and/or artesian ground-water conditions created by a relatively less permeable rock unit (based on concepts from Hack and Goodlett, 1960; and Everett, 1979).

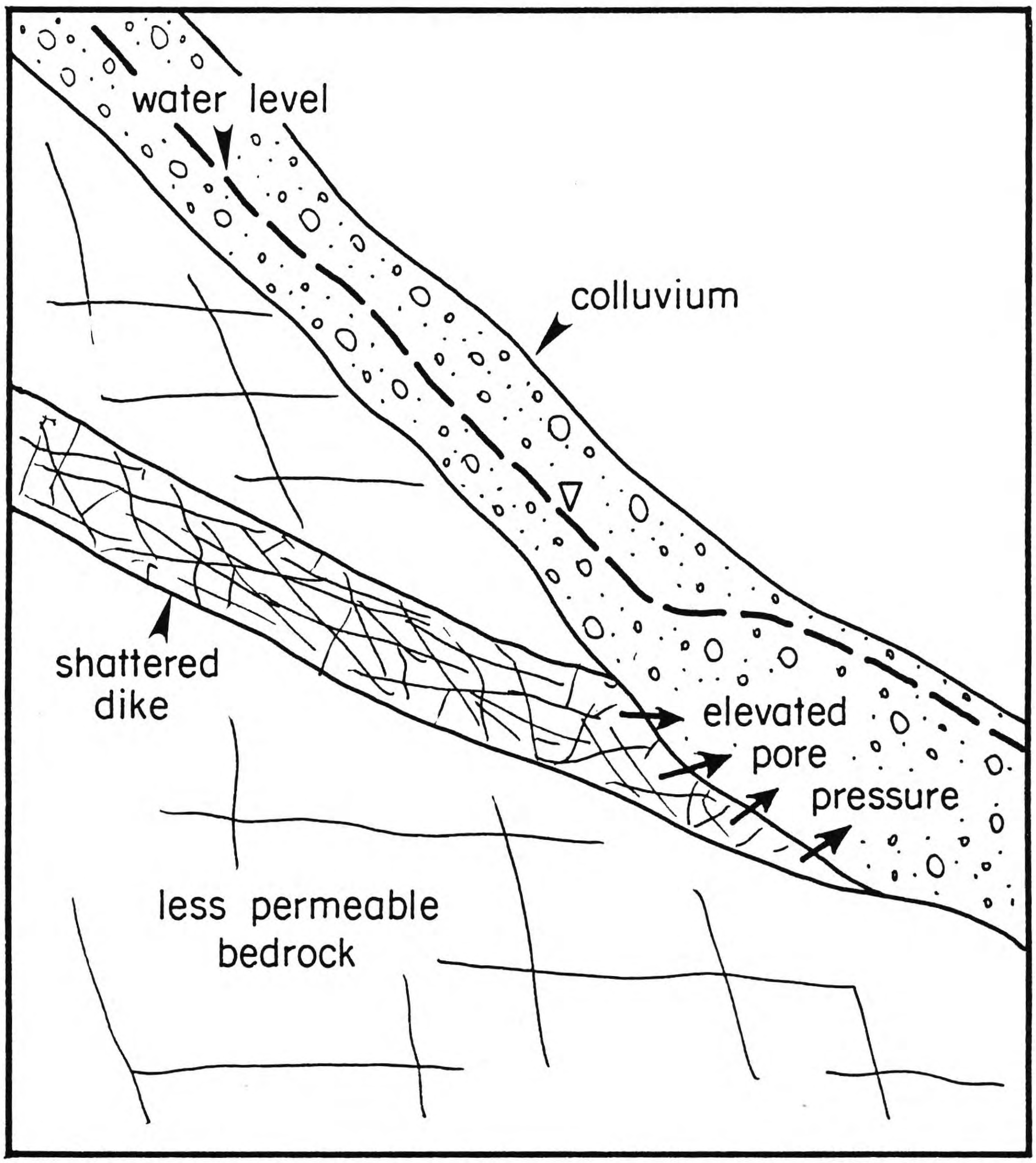

Figure 6. Schematic diagram of a slope failure mechanism in which pore water pressures in the soil are raised by ground-water discharge via a relatively more permeable rock unit (after Hicks, 1988).

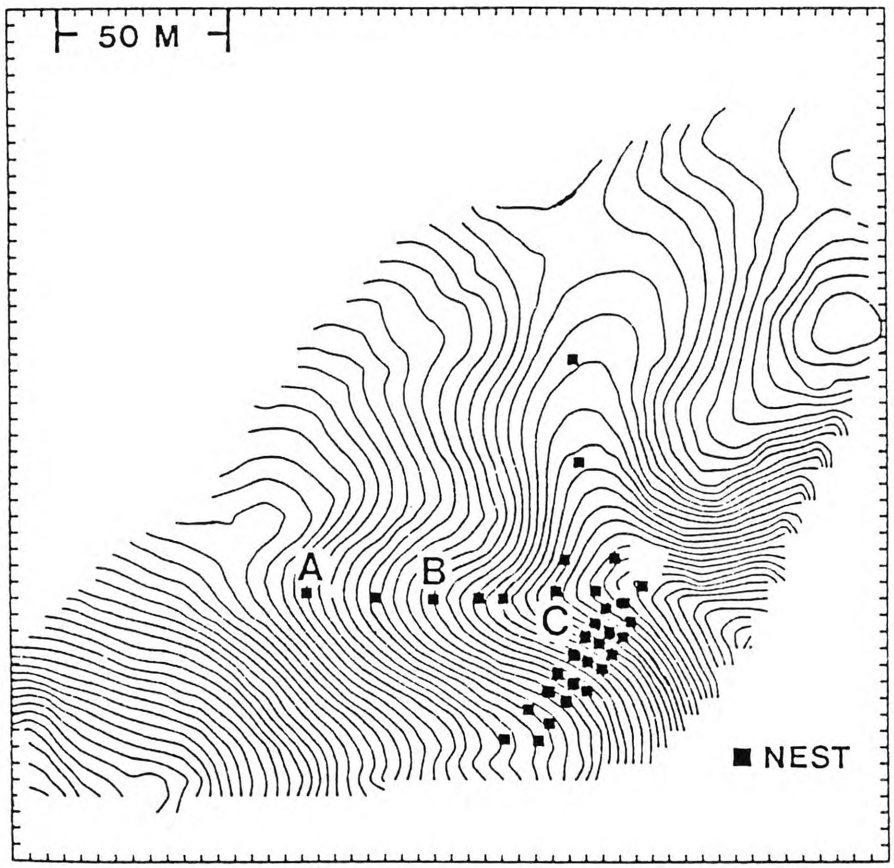

Figure 7. Location of piezometers in a study site in Marin County, CA (after Wilson and Dietrich, 1987).

at $K=10^{-7}$ cm/sec, and was then able to drain back down at point C, at $K=10^{-4}$ cm/sec (Figure 8). The authors concluded that permeability changes in bedrock may provide an important mechanism for debris flow initiation during periods of intense precipitation. The Franciscan formation, like the Farmington Canyon Complex, is highly fractured and lithologically heterogeneous.

The geology of the Farmington Canyon Complex undoubtedly affected the distribution of slope failures in this section of the Wasatch Front. Pack (1985) presents a multi-component model to predict landslide susceptibility in this area; he mentions that local geology is an important factor in determining landslide locations. However, he does not consider local geology in his model, declaring that bedrock variations are too site-specific for regional study. Olson (1985) states that, although an active ground-water system exists in this section of the Wasatch Front, the hydrogeology is poorly understood.

The slope failures of 1983 and 1984 in this section of the Wasatch Front have been correlated with an ancient uplifted erosional surface identified by Eardley (1944; cited in Vandre, 1985). Vandre (1985) shows that there is a relative increase in debris flow occurences, as well as drainage heads, at the approximate elevation of the ancient surface. It is possible that this surface acts as a shelf, causing ponding and discharge of ground water

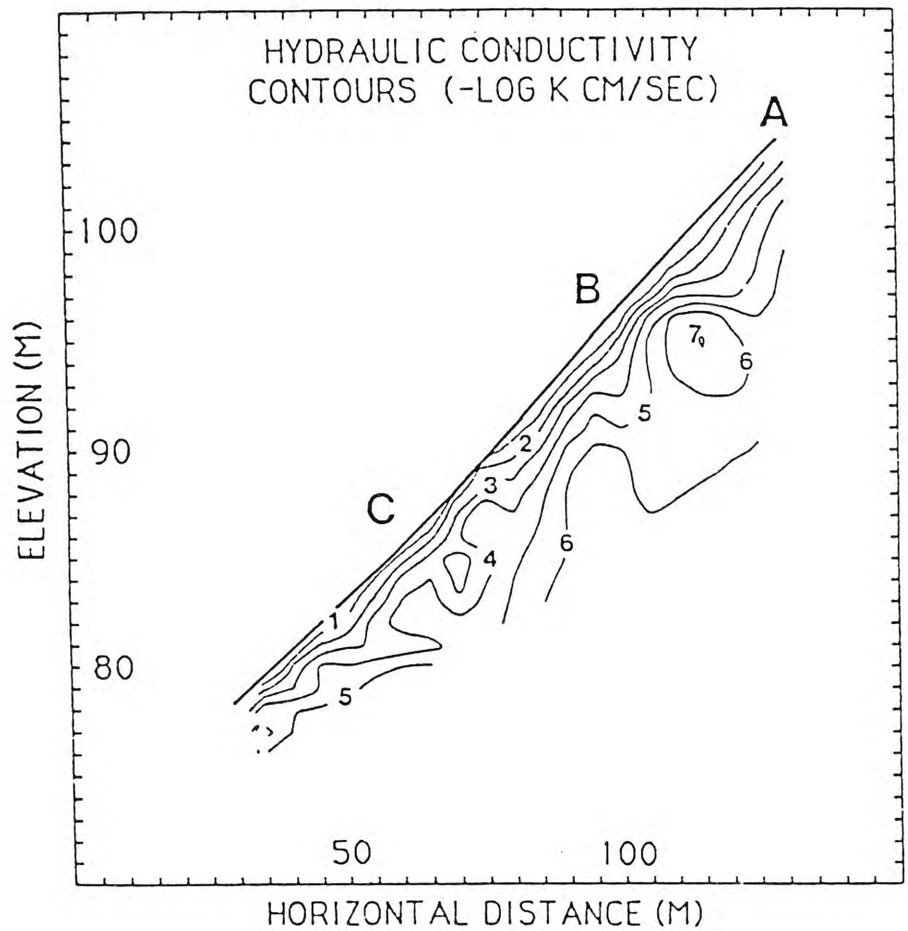

Figure 8. Contours of hydraulic conductivity in cross-sectional view along the axis of the Marin County study site. Contoured values are hydraulic conductivity, from 10^{-1} to 10^{-7} cm/sec (after Wilson and Dietrich, 1987).

to the surface. In addition, a relatively thicker soil profile (evident above the upper Rudd Creek failure scar) may have developed on top of the ancient surface. The role of this feature in the distribution of slope failure events was not analyzed in this study.

Purpose of Study

The purpose of this study was to test the hypothesis of Mathewson and Santi (1987) that elevated pore water pressure in colluvium is derived from ground water in the Farmington Canyon Complex. The objective then was to characterize the structure and lithology of the bedrock in terms of its ground-water storage and permeability characteristics.

STUDY AREA

Physiography

The study area is in Davis County, Utah, which includes a portion of the Wasatch Front, which comprises the western flank of the Wasatch Range, in north-central Utah. The western edge of the Front forms an approximate boundary between the uplifted Colorado plateau to the east and the extensional Basin and Range province to the west (Figure 9). The relief on the Wasatch Front is due to approximately 4 km of displacement on the Wasatch fault during the last 12 Ma (Naeser et al., 1983). A series of steep westward-draining canyons have eroded down into the mountain block.

The total relief on this part of the Wasatch Front is approximately 1200 m. Average annual precipitation increases 10 cm for every 200 m increase in elevation; above 2500 m, 90 percent of this is in the form of snow (Pankey and DeByle, 1984). The area is also subject to intense orographic rainstorms during the summer months.

The study area is located on rocks of the Farmington Canyon Complex, which is exposed east of the Wasatch Fault, and extends eastward to the highest ridge on the Front, beyond which it is buried by sediments of Paleozoic through Quaternary age (Figure 10). Although outcrops are common, the great majority of the land area is covered by

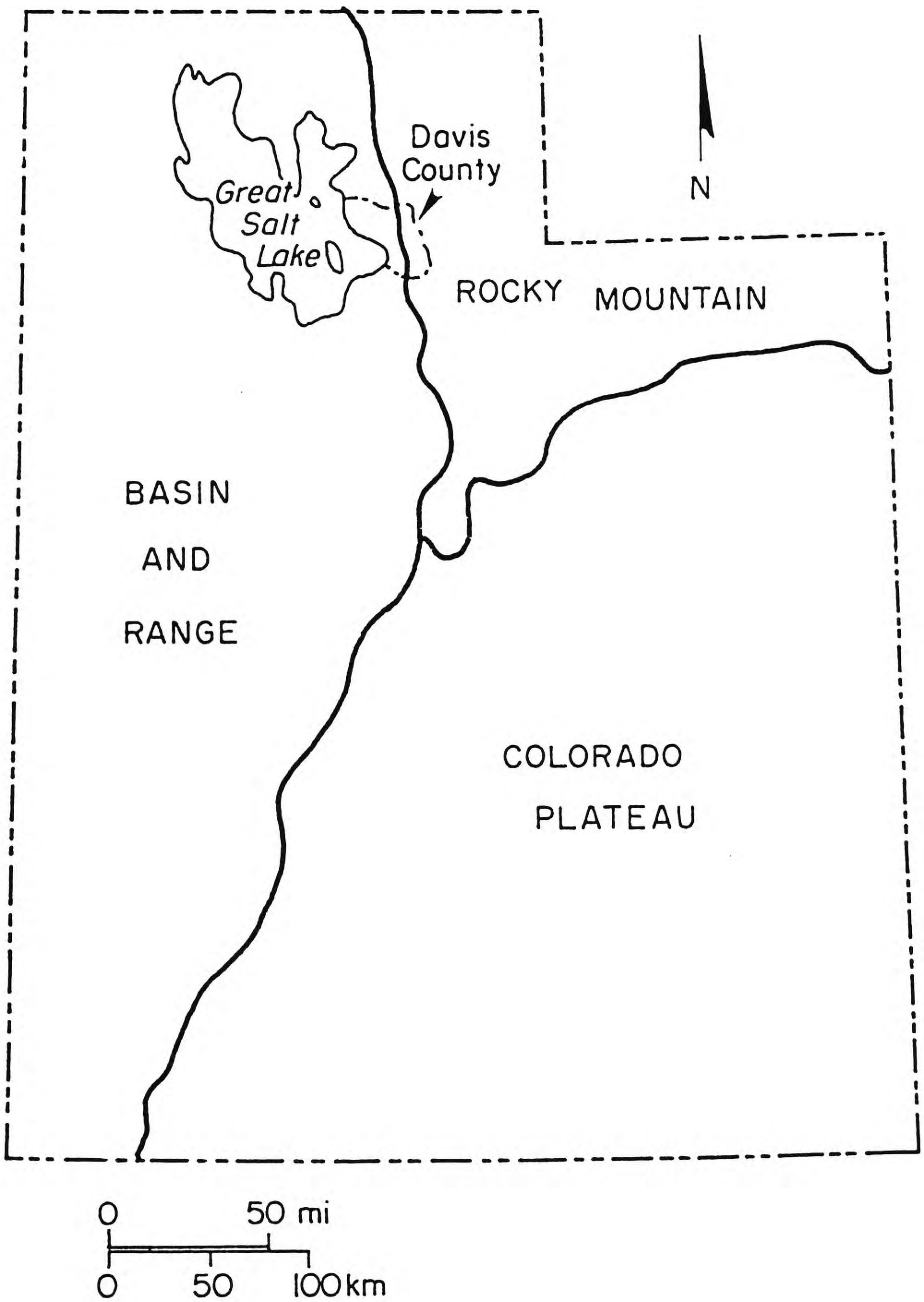

Figure 9. Davis County, Utah, is located in the zone dividing the Basin and Range province from the middle Rocky Mountains. The Farmington Canyon Complex outcrops in eastern Davis County.

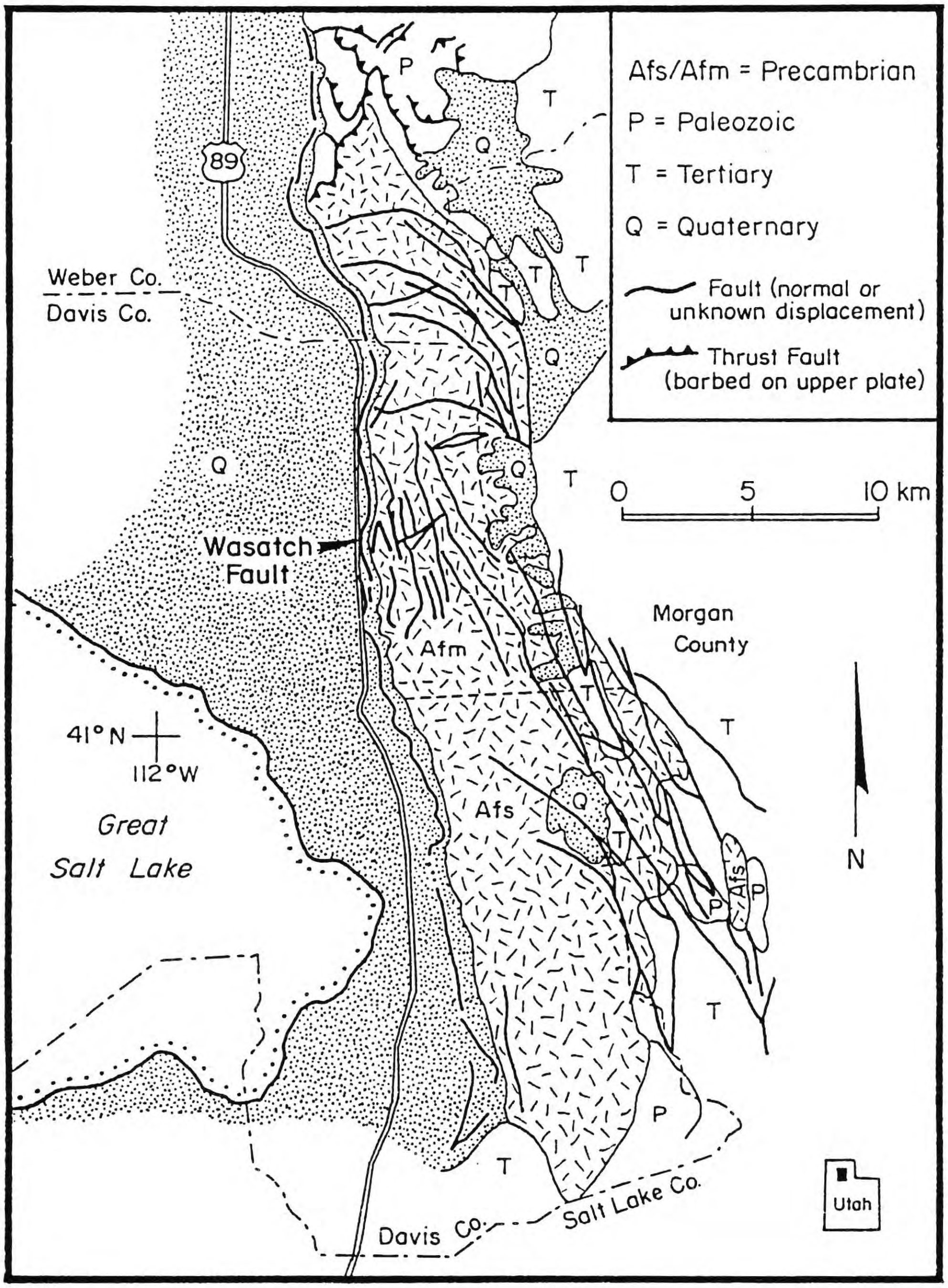

Figure 10. Geologic map of the Precambrian Farmington Canyon Complex (simplified from Bryant, 1988).

vegetation, in the form of trees, scrub and grasses. The ridge crests, where much of the field data were gathered, have little or no vegetation or soil cover.

Regional Geology

Petrology

The Farmington Canyon Complex consists of Precambrian metasediments which have experienced a long history of deformation and igneous intrusion. The dominant lithologies along the Wasatch Front between Bountiful and Ogden, Utah, consist of two generalized units. The first unit, "Afs", covering the southern portion of the Precambrian exposure, is made up of quartzofeldspathic gneiss, sillimanite-grade pelitic schist/gneiss, some quartzite, amphibolite lenses and numerous pegmatite dikes and sills. North of the town of Farmington, this unit grades into "Afm", a migmatite with interlayered and intergradational quartz monzonite gneiss, grey pelitic and quartzofeldspathic schist, greenish-black amphibolite, and pegmatite dikes (Bryant, 1988). Figure 10 shows the location of the gradational boundary between Afm and Afs. Within these two lithologic units are mapped several lenses of quartz monzonite gneiss (containing amphibolite lenses), quartzite, and amphibolite bodies. Localized zones of intensely sheared and mylonitized rocks are found at the base of the outcrop near the Wasatch Fault. Oval to highly elongate pegmatite dikes (quartz and microcline) are abundant (Bryant, 1988). Figure 11 is a geologic map of the study area.

The oldest rocks in the Farmington Canyon Complex are the schists and gneisses. Detailed radiometric dating by Hashad and others (1970) and Hedge and others (1984) suggests the following events during the Precambrian era: Archean sandstones and shales were deposited between 3.0 and 3.6 Ga; a major igneous/metamorphic event occurred at 2.6 Ga, intruding and extruding gabbros and basalts. Another high temperature metamorphic episode took place at 1.8 Ga, which sheared and partly migmatized these rocks; at the same time they were intruded by quartz monzonite (Hedge et al., 1984). A late Precambrian or early Paleozoic metamorphism of lesser intensity was accompanied by local uplift at approximately 0.5 Ga.

Structural History of the Region

Precambrian and Paleozoic: The geologic evolution of this part of Utah includes periods of marine deposition, compression, intense volcanism and extension. Hintze (1982) divides the Phanerozoic in Utah into six phases, as seen in Figure 12. At the time of diagram 12I, the Farmington Canyon Complex was already in place, had experienced two episodes of intense metamorphism, and was either involved in, or was just emerging from, a lesser stage of metamorphism that generated the structural uplifts of the Northern Utah

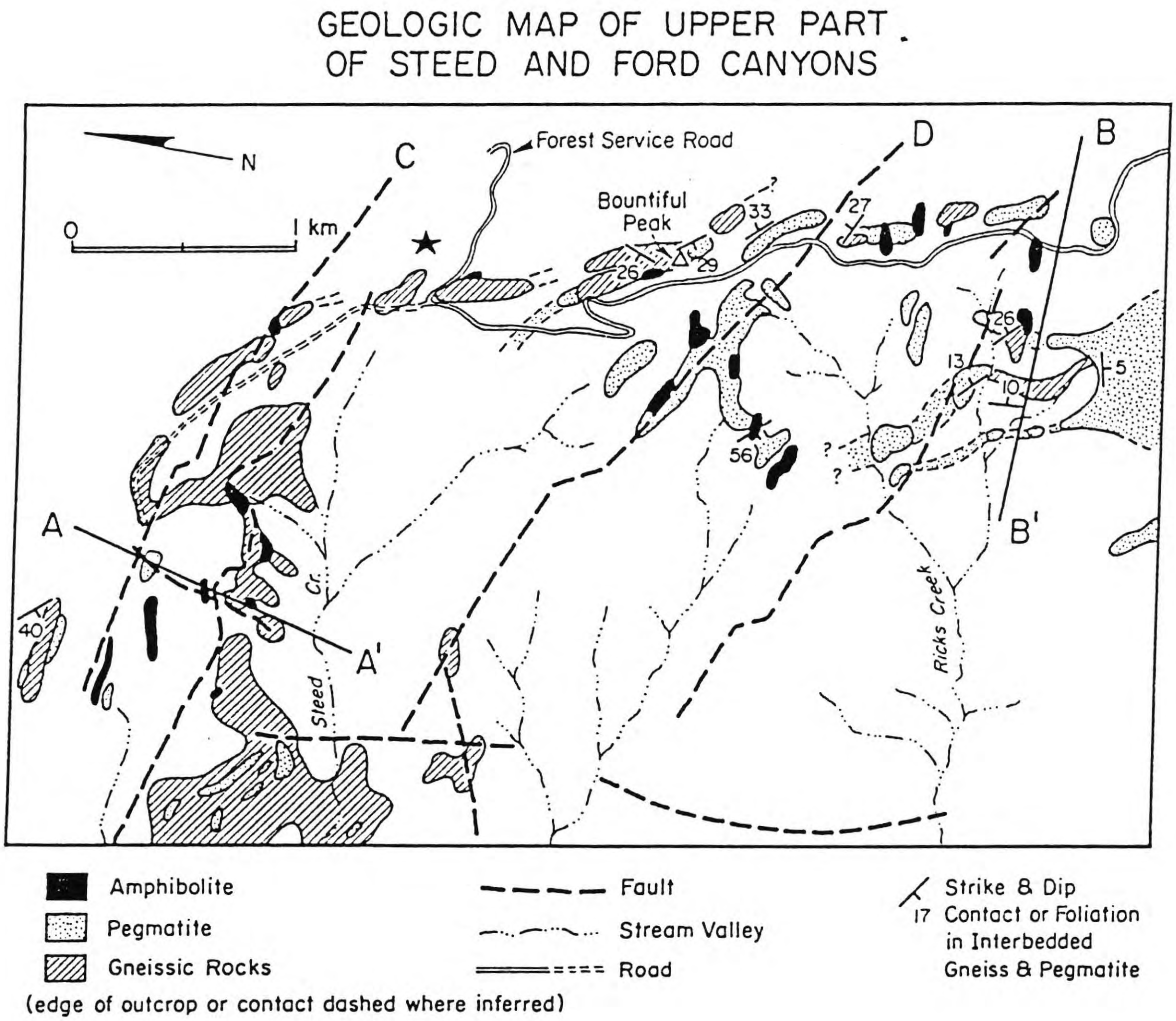

Figure 11. Geologic map of the study area; developed from photogeology and field investigation. Star indicates position of a spring feeding Farmington Lake (see Figure 55).

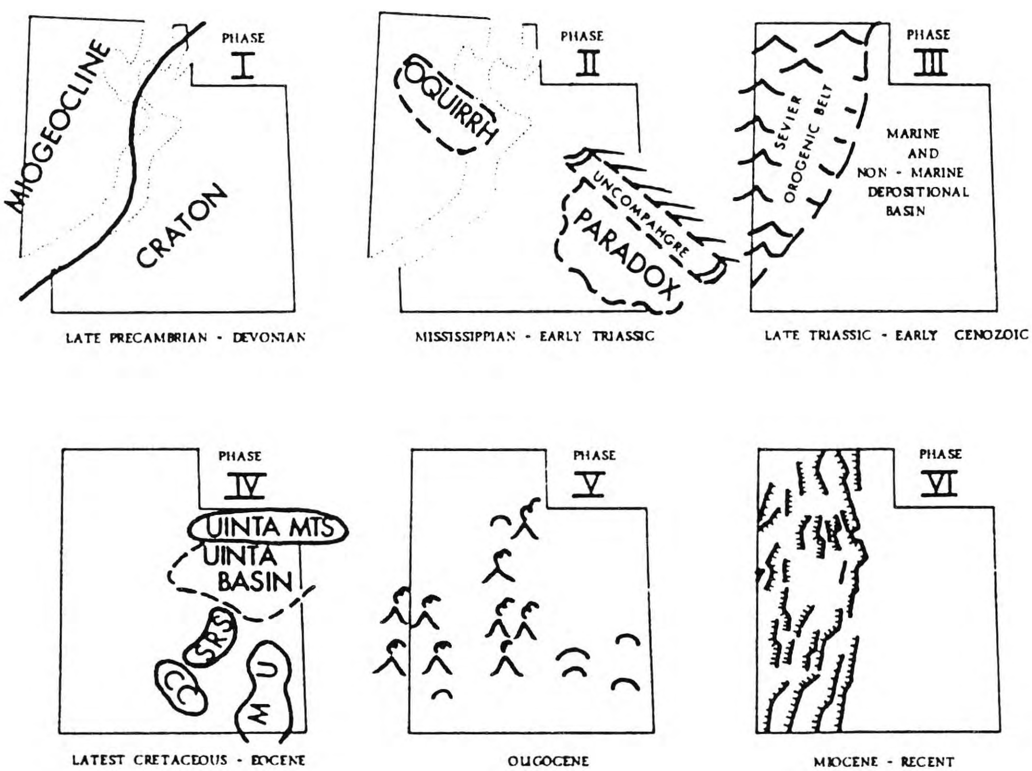

Figure 12. Six phases of the geologic evolution of Utah. Note the importance of the northeast-trending "Paleozoic hinge line" in the development of the state (after Hintze, 1982).

Highland, (not shown in Figure 12) and the Uinta mountains.

The Paleozoic and early Mesozoic eras in this region were tectonically quiet, and consisted of shallow to intermediate marine deposition of clastics and carbonates. Sediment transport was westward from the craton until the Mississippian Antler Orogeny uplifted rocks to the west and reversed the direction of transport.

As shown by Young (1984), a number of large scale trends or "megalineaments" divide this region (Figure 13). Of particular interest is the junction of the Wasatch East and Uinta megalineaments, which can be traced to the location of the Cottonwood igneous stock. The Wasatch fault itself lies along the "Paleozoic hinge line", which is generally acknowledged to be the division between the late Precambrian through early Paleozoic uplifted craton and the miogeosyncline to the west, also known as the Wasatch line. This corresponds to the transition zone separating the Colorado Plateau and Rocky Mountain regions from the Basin and Range Province. The development of this trend as a major crustal boundary is evident in Figure 12.

The Northern Utah Highland, shown in Figure 14, includes the area around the outcropping Farmington Canyon Complex and its equivalent on Antelope Island. Eardley (1939) claims that early Paleozoic sediments up to 5,500 m

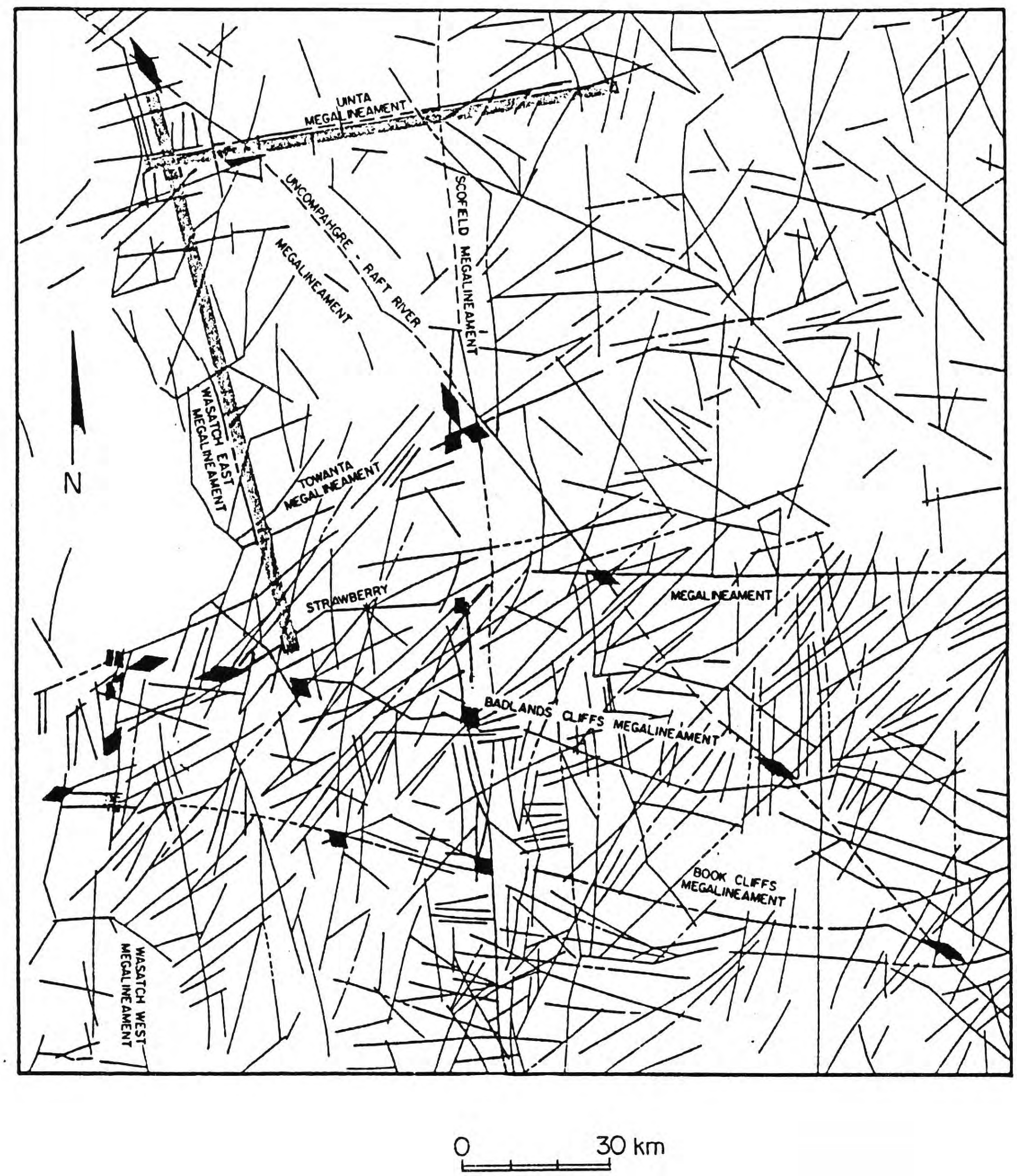

Figure 13. ERTS imagery showing major lineaments in the earth's crust in northest Utah. Note the Wasatch East and Uintah megalineaments (shaded), mentioned in the text. The Wasatch Fault, which forms the western border of the Farmington Canyon Complex outcrop, lies along the Wasatch East Megalineament (adapted from Young, 1984).

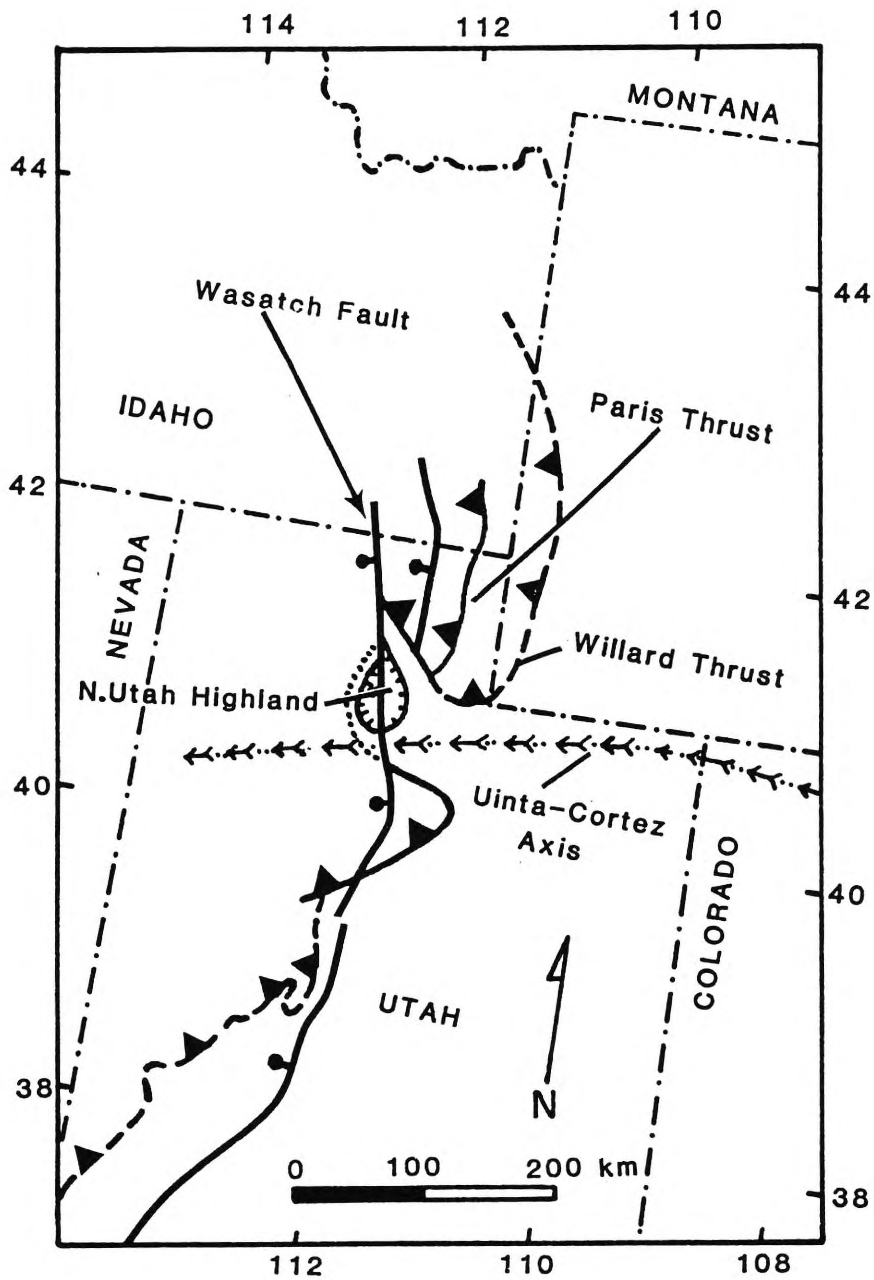

Figure 14. The Northern Utah Highland distorted the geometry of thrust faults of the Sevier/Laramide orogenies (adapted from Tooker, 1983).

thick in adjacent basins pinched out completely on the flanks of this structure before Cretaceous (Laramide) age thrust-faulting began. According to Crittenden (1972), however, there was a considerable thickness of late Precambrian and early Cambrian sediments overlying the Northern Utah Highland, which were "tectonically stripped" by the Willard thrust sheet as it partially over-rode the structure. The thrust plate was being rapidly eroded synorogenically, and continued uplift of the Northern Utah Highland accelerated this process. In either interpretation, the Northern Utah Highland stood as a basement high at the start of Sevier/Laramide deformation.

Mesozoic through early Cenozoic: The Sevier/Laramide orogenies in the vicinity of the Wasatch Front consisted of eastward thrust-faulting of sediments, both broad and narrow-curvature folding, high angle reverse-faulting, normal faulting on the flanks of uplifts, and "transcurrent" strike-slip faulting through thrust sheets (Tooker, 1983). Eardley (1944) states that several stages of Sevier motion took place, resulting in a complex geometry of folds and thrust faults.

The main causes of asymmetry in the Sevier folds and thrusts west of the Wasatch front are the Precambrian autochthons. According to Eardley (1939), the Northern Utah Highland acted as a buttress in the way of the advancing thrust sheets, forcing them to wrap around it.

The westward face of the Northern Utah Highland was, therefore, an area of major stress concentration and realignment. Figure 15 shows the great influence of the these uplifts, particularly the Northern Utah Highland, on the regional structure.

The concentration of stress on the rocks of the Farmington Canyon Complex from Sevier/Laramide deformation could be responsible for the dense network of faults in the northern half of Davis County, shown in Figure 10. It is possible that these faults are Precambrian features reactivated by the new stress regime. However, many of the early Precambrian faults and fractures are filled by pegmatite dikes with a different orientation to this fault network. The late Precambrian uplift may not have been strong enough to produce such faulting. It is likely, then, that a new fracture/fault network has been overprinted on the Precambrian structure, at least locally. A combination of compression during the Sevier orogeny, followed by a relaxation of compressive stress, may be the cause of the orthogonal fracture pattern in the rocks (Friedman, 1963).

Miocene through Recent: Faulting in the Basin and Range began about 12 Ma. Physiographically, the eastern margin of Basin and Range extension is represented by the Wasatch fault scarp. This fault trends approximately 12 degrees

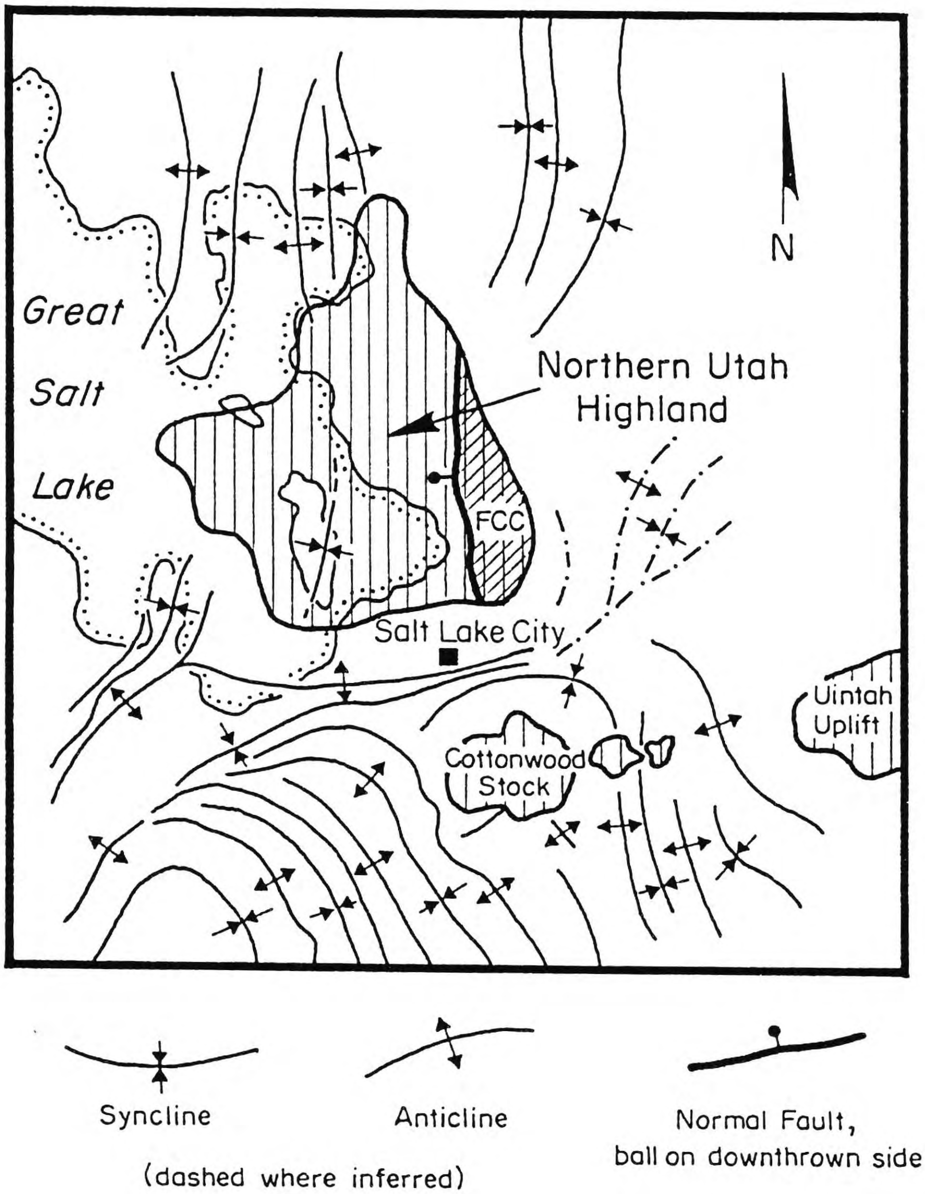

Figure 15. Fold axes associated with Sevier/Laramide compression are distorted by the existing uplifts. FCC=Farmington Canyon Complex (adapted from Eardley, 1944).

west of north. It is locally discontinuous, and has an en echelon surface expression in the southern Wasatch Range (Eardley, 1939).

Investigators have generally had a difficult time interpreting seismic data from the Jordan and Sevier valleys (Zoback, 1983; Arabasz and Julander, 1986). They mention problems associated with complex subsurface structure and heterogeneous mechanical properties of rock units, multiple microseismic events within Range blocks rather than discrete events at block boundaries, and the disagreement of calculated earthquake slip vectors at depth with surface fault attitudes (Zoback, 1983; Arabasz and Julander, 1986). These phenomena are the result of structural constraints imposed by the complicated geologic development of the area, particularly the skewed fault and fold geometry created by Sevier thrusting around Precambrian autochthons.

Both Zoback (1983) and Arabasz and Julander (1986) characterize their study areas as complex transition zones between the Colorado Plateau and the Basin and Range provinces (Figure 16). Both document isolated occurrences of events generated by compressive stress and cases of strike-slip faulting.

Zoback (1983) mentions the low seismicity of the Farmington Canyon Complex relative to the adjacent basin and speculates that it is because of the greater competence of these rock units. It may also be due to the

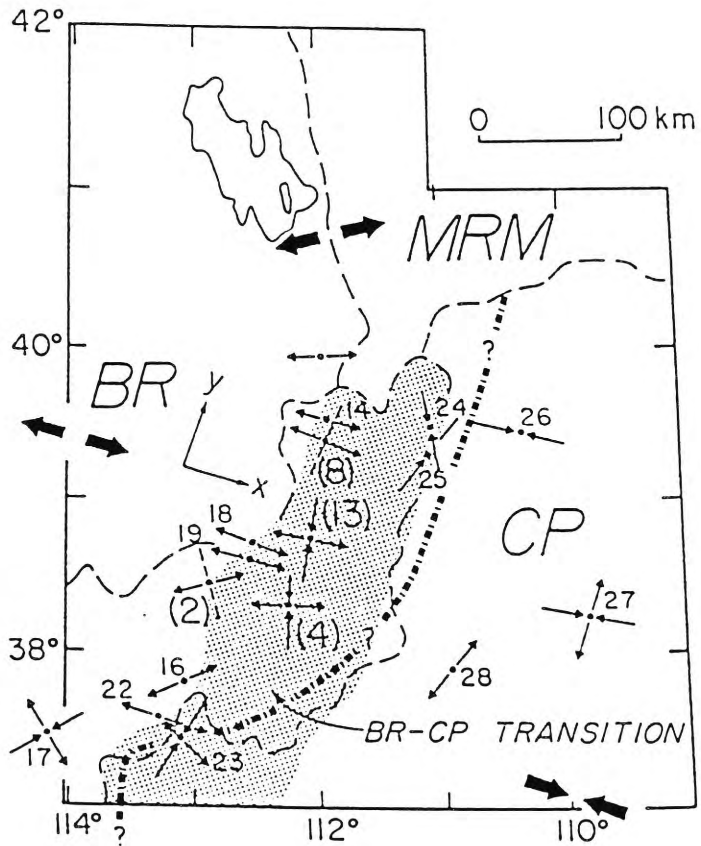

Figure 16. Seismic slip vectors indicate a complex variety of stress orientations in the transition zone between the CP (Colorado Plateau) and the BR (Basin and Range) (after Arabasz and Julander, 1986).

deep fracture network in the bedrock, which allows it to adjust and compensate for applied stress.

The orientation of the least principal stress (the direction of crustal extension) in the Jordan Valley is along azimuth 255° (Zoback, 1983). In the Sevier valley, it is along azimuth 282° (Arabasz and Julander, 1986). The latter is in line with the Basin and Range as a whole. Zoback (1983) accounts for her data by offering two possibilities: that the relative rotation is due to compensation for ongoing spreading in the Rio Grande rift, or that it is a result of anisotropy imparted by the "late Precambrian rift margin", a reference to the Paleozoic hinge line discussed earlier.

STATISTICAL ANALYSIS OF BEDROCK STRUCTURE IN THE STUDY AREA

The Farmington Canyon Complex has undergone multiple episodes of deformation, particularly by late Mesozoic through early Cenozoic age compression associated with the Sevier and Laramide orogenies. It is likely that Sevier and Laramide deformation has overprinted previous structures. The origin of this geologic structure has been discussed in the previous section. The function of this section is to characterize the present structural and lithologic configuration of the Farmington Canyon Complex.

A term commonly used to describe fractured rock masses is "complex". This term reveals nothing about the actual properties of the rock mass. It is hypothesized here that a comprehensive study of the "complex" structural fabric of bedrock can yield valuable information about its hydraulic properties and weathering characteristics. Thus, the main task of the following section is to further examine and refine the general phrase "complex structural fabric". "Structural fabric" here refers to photogeologically identified lineaments, macroscopic lithologic trends and the geometry of fractures and foliation viewed in the field. The study of the properties of these rock masses, individually and as groups, should produce a clearer and more detailed picture of bedrock trends.

This section is a statistical characterization of the structural fabric of the Farmington Canyon Complex; its aim is to define similar structural domains within the study area. The next section correlates the regional view of lineaments obtained from photogeologic analysis with the detailed view of fracture geometries in the field, and attempts to interpret them geologically.

It is important to distinguish the statistical analysis in this section from the geological analysis in the next section. This section describes the dispersion of fracture orientations regardless of their actual orientation. In the next section, both the dispersion and the orientation of fracture sets are considered in their geological context.

Conclusions from these two sections are used in inferring potential ground-water flow paths in the bedrock, discussed in the section on hydrogeologic implications of the structural fabric.

Data Acquisition

Because the ultimate goal of this study is to better understand the hydrogeology of the bedrock in the study area, the properties chosen for study were those considered important in determining the hydraulic behavior of fractured rocks. In this study, no attempt has been made to arrive at quantitative values for bedrock porosity, storativity, or hydraulic conductivity. Instead, a regional picture of hydrogeologic trends is developed.

There is a debate as to which geometric parameters among fracture orientation, length, spacing, aperture, surface roughness, density of interconnections, and/or other properties are the most important in determining hydraulic conductivity. According to Pollard and Aydin (1988), they are fracture spacing, orientation and aperture, and their connectivity, which is a function of the first two as well as fracture length. From a numerical simulation, Long and Witherspoon (1985) found that the degree of interconnectivity of fracture sets (a function of length and density) controls permeability, and that fracture length is more important than density in determining interconnectivity.

Of the categories of data mentioned above, orientation, length and spacing were readily obtainable in the field. The following physical features and their spatial distribution were studied: fracture orientation, length, spacing and aperture, and the orientation of major structural lineaments.

Once joint data have been gathered, how should they be analyzed? The appropriate probability distributions are not well known as yet (Baecher et al., 1977; Jones et al., 1985). At best, mathematical models of fractured rock permeability can be summed up in the "Principle of Indeterminacy" (Leopold and Langbein, 1963; cited in Legrand, 1979, p. 344):

> ...the applicable physical laws may be satisfied by a large number of combinations of values of interdependent variables. As a result, a number of individual cases will differ among themselves, although their average is reproducible in different samples. Any individual case, then, cannot be forecast or specified except in a statistical sense. The result of an individual case is indeterminate.

Fracture and foliation orientations were gathered from 64 stations within the study area (Figure 17). A limited amount of fracture length and spacing data were also gathered. Stations where length and spacing information was obtained are also marked in Figure 17. Fracture apertures at the surface were approximated for a single outcrop in the study area, also shown in Figure 17.

Avoiding Bias

Bias in sampling fracture populations is almost inevitable, because outcrops are commonly two-dimensional, and fracture populations are not. There are many other sources of bias in the field sampling of fracture distributions and characteristics (Baecher et al., 1977; LaPointe and Hudson, 1985). In addition, the angle at which fractures intersect a free surface affects how the population will be represented; for instance, in aerial photography, steeply dipping fractures are more visible than flat-lying ones. The same is true at most physically

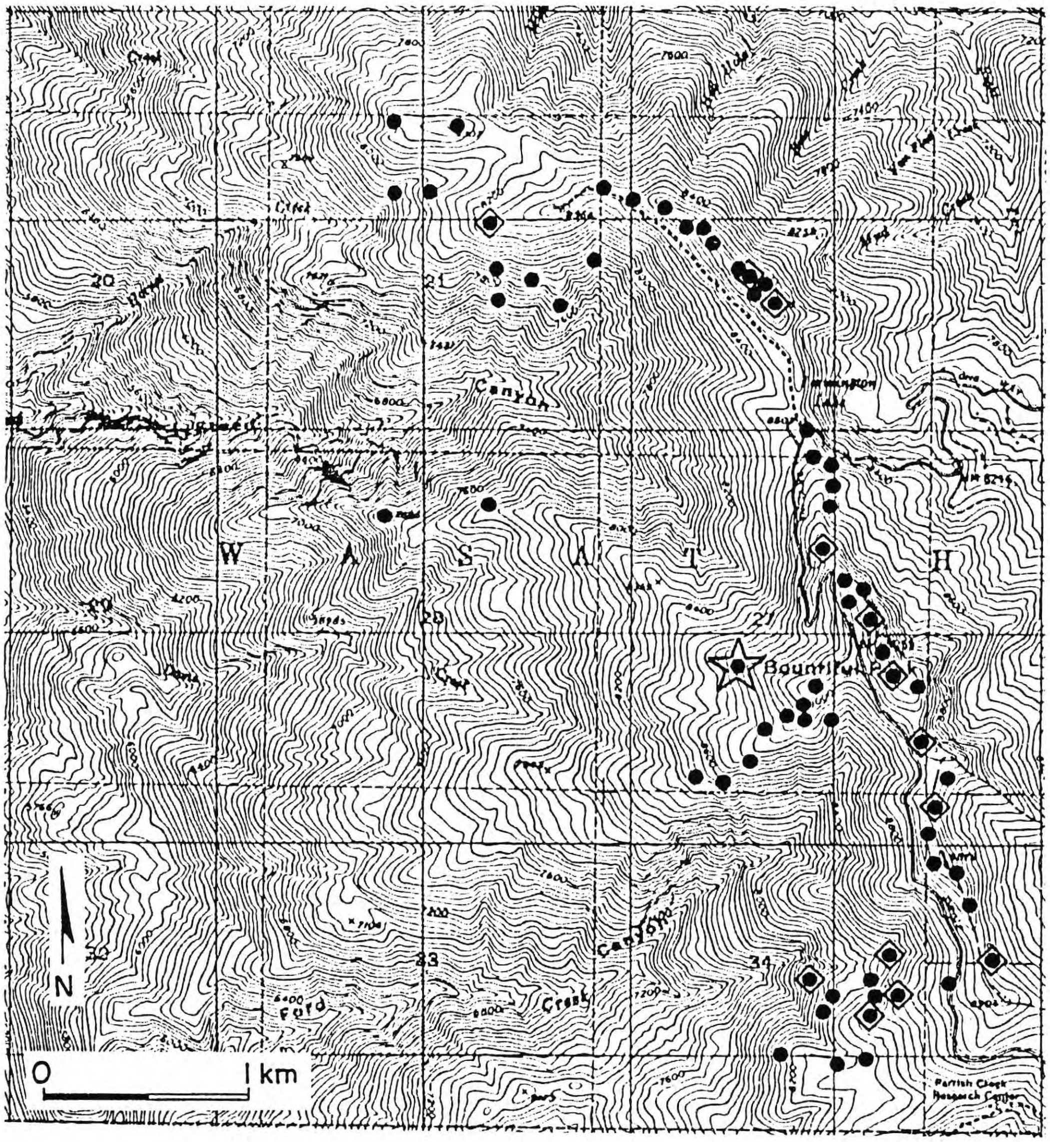

Figure 17. Stations where fracture orientation data were gathered are shown with dots. Diamonds show where fracture half-length and spacing data were taken. The star shows outcrop A98, where orientation, half-length, spacing and aperture data were taken along a scan line.

accessible outcrops. However, in the study area, many of the outcrops were found to have two or more exposed faces. In addition, fractures tended to be well exposed at the surface, allowing measurement of dip as well as strike. Figure 18 shows the distribution of outcrops in which more than one face is exposed.

Some of the sources of bias in the study area were:

1) the great majority of sampled outcrops were on ridges. Fractures perpendicular to the ridge trend are more likely to be encountered than those that parallel the ridge. Thus a regional bias is introduced.

2) Fractures are less likely to be filled with weathered material on the ridges than in the valleys.

3) In ground-level outcrops (see Figure 18) high angle fractures are more likely to be encountered than low-angle fractures.

Measures taken to obtain a truly representative sample were:

1) a large number of observations were made (over 1400 observations). At each outcrop, an effort was made to take a number of fractures from each visible set.

2) In the case of three-dimensional outcrops, which are common throughout the study area, orientation data were obtained from more than one exposed face of the outcrop. The majority of fracture dips appear to be steep. However, dip orientations for foliation planes are much less steep, within the same study area. This fact

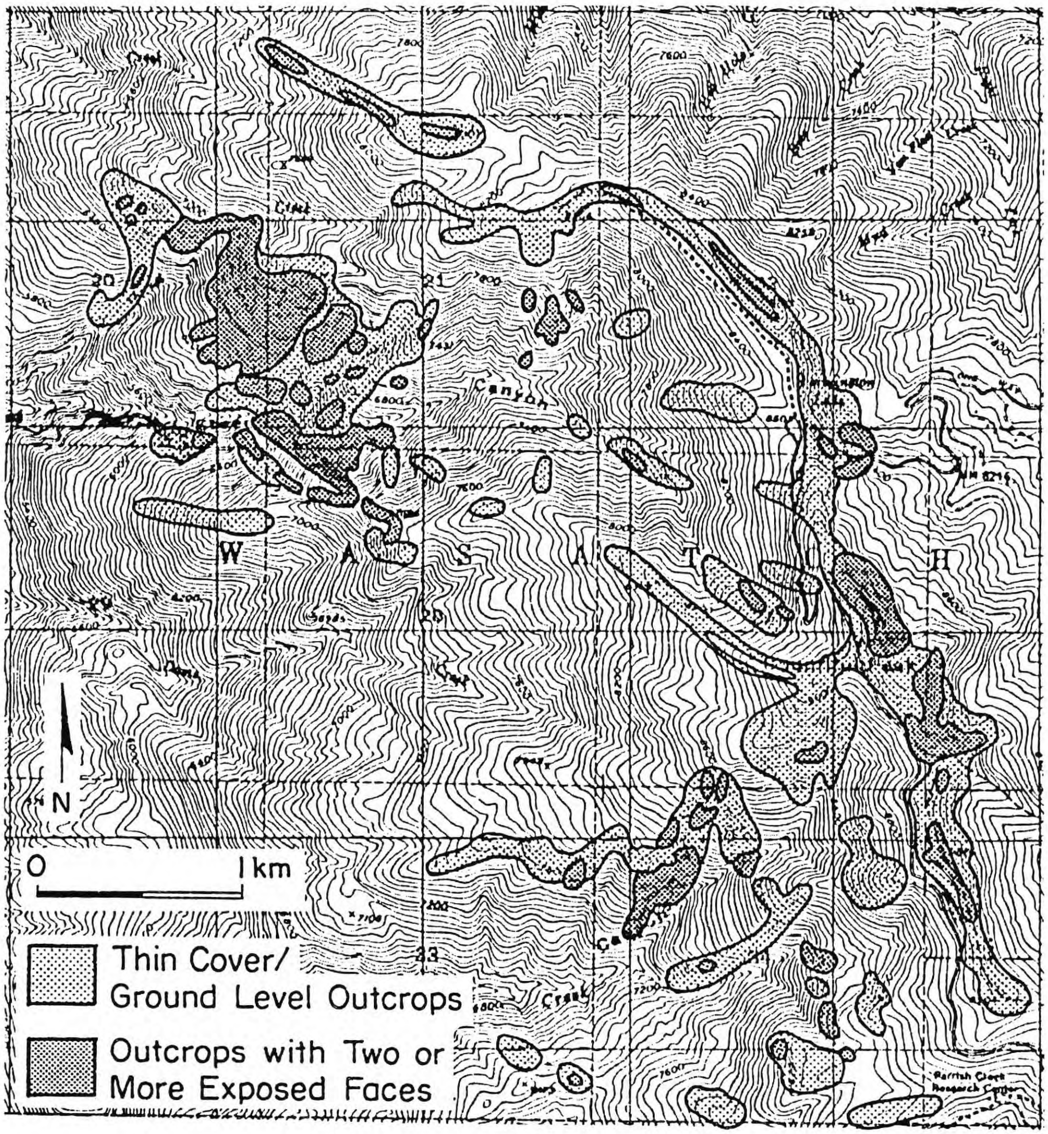

Figure 18. Distribution of bedrock outcrops in the study area.

supports the contention that orientation data are relatively unbiased.

3) The lithology of the bedrock was noted for each fracture orientation.

4) Length and spacing data as well as orientation data were obtained using a scanline method in which only the trace lengths on one side of the tape are sampled. This method simplifies the mathematical estimation of the true (uncensored) trace length distribution from the raw (censored) data (Warburton, 1980). Although this conversion was not done for outcrops sampled in this study, the field technique itself was quicker and more suited to the irregular shape of outcrops in the study area. Thus, trace length data are presented as "half-lengths".

Plotting the Data

Fracture analysis involving Fisher statistics and Kamb contouring, and presentation of stereonets and rose diagrams were carried out using the "Structure Graphics" program written by Wiltschko (1990).

Scatter Diagrams

Initially, fracture orientations for each station and lithology were plotted on lower hemisphere Schmidt nets, in the form of scatter diagrams. Discrete joint sets are apparent in many of these diagrams, as in Figure 19 A. When orientation data for the same lithology for a number of local outcrops are combined, joint sets are less clearly defined, as in Figure 19 B. If all the data for one locality are combined, orientations appear to be more or less randomly oriented, as in Figure 19 C.

This apparent randomness is actually the effect of mixing outcrops with different fracture sets into a single group. To avoid mixing different populations, principal fracture sets were determined, by eye, from the original data: one for each lithology within a single outcrop. These principal orientations were then ranked qualitatively as very good, good, fair, poor and very poor, depending on the visually determined tightness of each grouping; poor and very poor were not used. The remainder were compiled into a data set of "principal fracture orientations" for subsequent analysis.

Random or Not?

Both the "principal fracture orientations" data set and different groups of raw data were analyzed statistically to determine whether or not they were random, and also to further characterize their distributions. If the fracture orientation data recorded in the field were truly randomly distributed, then anisotropies in hydraulic properties of the bedrock must be attributed to other factors. Therefore the first step in characterizing fracture orientations was to establish whether any or all of the data sets were randomly

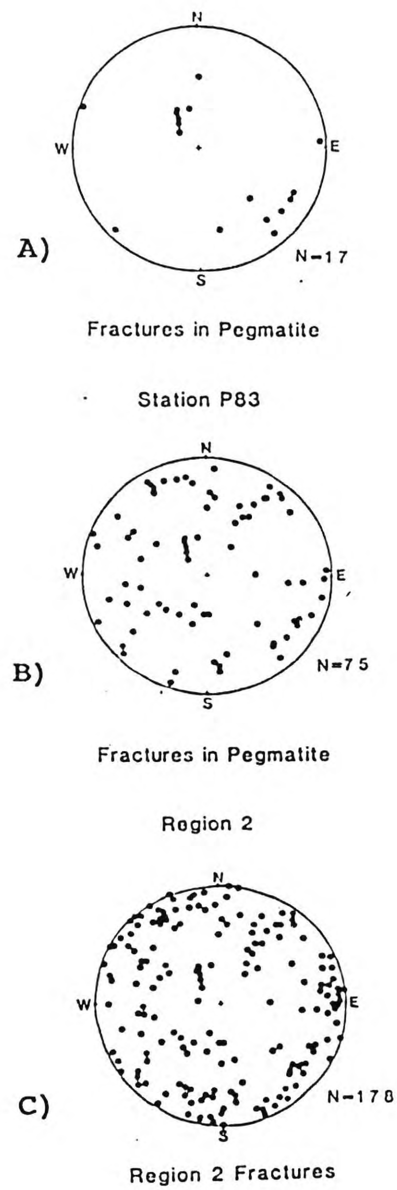

Figure 19. Scatter diagrams of fracture poles in Schmidt nets. **A.** Poles to fractures at one outcrop form discrete sets. **B** and **C.** No individual sets can be distinguished when the area of observation is increased.

oriented. Two methods were used to do this.

The Fisher Method

The first method was to view the poles to fracture planes as unit vectors in a sphere, and to compare the magnitude of the resultant vector, **R**, for each data set with that of **Ro**, a resultant vector calculated for random spherical distributions at 95 percent confidence (Tabulated by Irving, 1964, and included in Appendix 2). The magnitude of the resultant vector is calculated as follows:

$$R=S^2(l)+S^2(m)+S^2(n),$$

where S^2 is the sum of squares of l, m and n, which are the components of each of the three-dimensional vectors in a data set (Fisher, 1953, p. 296).

Fisher described the distribution of unit vectors in three-dimensional space with the probability density function P, where

$$P=[K/4(pi)\sinh K]e^{K\cos\beta};$$

β is the angular distance between a given point and the true population mean, and K is the precision parameter, discussed below (Tarling, 1983, p. 118). This equation has traditionally been most useful in paleomagnetic studies, where a spherical mean direction of remanent magnetism is sought among a distribution of orientations in an area. The mean is the resultant vector with the greatest magnitude of direction cosines.

This method is applicable to the analysis of fracture pole distributions. However, it must be used with caution when data sets are broadly distributed throughout the sphere, or when more than one fracture set is present. The majority of data sets from the study area fall into one or both of the above categories. Figure 20 shows how an inappropriate mean can be generated for a population of fractures.

Rotating Data

In order to overcome problems with broad distributions and/or multiple fracture sets, a technique similar to the one suggested by Andrews (1971) was used. The procedure involves finding the best-fit plane to all the poles in a data set; this divides the data set into roughly symmetrical halves. Then all the data points on one side of that plane are rotated by 180° about the vertical axis in the center of the hemisphere, and superimposed on the other half. This technique works best for distributions with two symmetrical fracture sets, which are common in outcrop data from the Farmington Canyon Complex; but it is applicable to all diffuse and disparate orientation distributions. An example from Andrews (1971) is shown in Figure 21.

Rotated data sets were analyzed by the Fisher method. Obviously, the rotated data are not truly representative either of the orientation or the grouping of the original

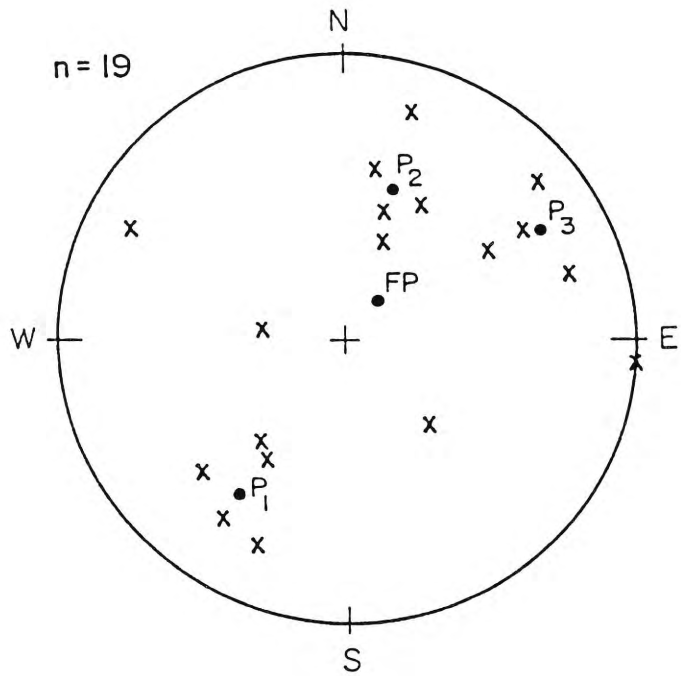

Figure 20. The Fisher mean pole of the data set of poles to fractures is labeled FP. A more accurate representation of the distribution of the data is P_1, P_2 and P_3, representing three <u>separate</u> poles.

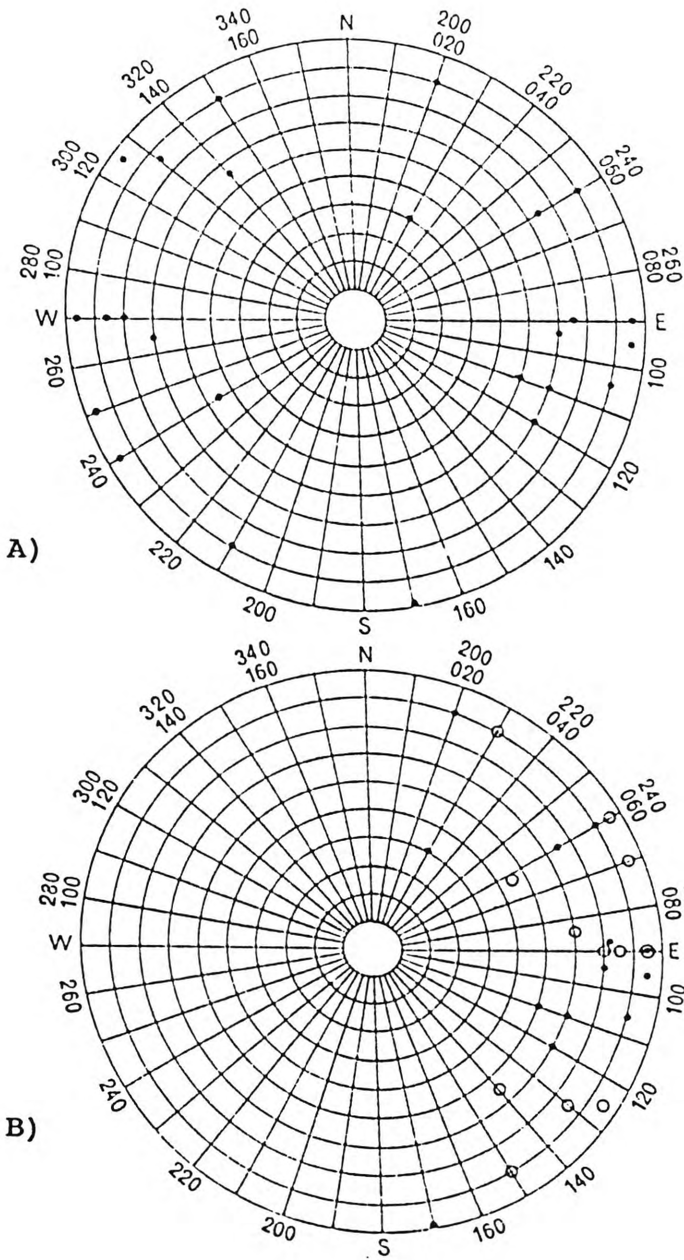

Figure 21. A. An equatorial plot of bi-modal orientation data. B. The points on the left of the N-S line have been rotated by 180° and overlain on the right side. Open circles are the rotated points (after Andrews, 1971).

data sets. However, because the problem with disparate data is eliminated, the result is a better <u>relative</u> representation of the data sets, for purposes of comparison. Since the objective is simply to compare dispersion parameters for different data sets, the mathematical conversion between axial and vectorial data was deemed unnecessary. In addition, the rotated data sets are closer to spherical normal, which is required by the Fisher method. The statistical comparisons in this section use the rotated data sets.

The Fisher distribution is not entirely satisfactory for describing the orientation of poles to fractures, for two reasons: 1) it is a parametric method, which assumes that the data are grouped in a "spherical normal" array (Fisher, 1953), and 2) the Fisher distribution considers the dispersion of vectors on the entire surface of a sphere, where each vector is unidirectional. Fracture orientations are plotted as points on a lower hemisphere projection for convenience, and so may be characterized by Fisher statistics. However, they are really <u>axes</u>, which would be represented by two diametrically opposed points on the surface of an entire sphere (Mardia, 1972). Thus the dispersion of raw axial data cannot properly be analyzed using vectorial criteria (Mark, 1974; Yonkee, 1990).

In conclusion, it may not be advisable to use the Fisher method for 1) determining the randomness of groups of axial data, or 2) finding the trend and plunge of the spherical mean of widely dispersed or multi-modal pole orientations. However, it is believed that the Fisher method is useful for comparative purposes between data sets, particularly if the data are rotated.

The Eigenvalue Method

An alternative analytical method makes use of the eigenvalues of the orientation tensor calculated from the direction cosines of each data set (Woodcock and Naylor, 1983). These values are the magnitudes of the three axes of an ellipsoid that describes the shape of the distribution of orientations in the data set. The eigenvalues are normalized to the population of each data set, and the ratios between the greatest (S_1), middle (S_2) and least (S_3) are compared. End members of ellipsoid shapes are elongate clusters, where S_1 is much greater than S_2 and S_3, and girdles, where S_1 and S_2 are similar, and S_3 is much smaller (Woodcock and Naylor, 1983).

The other application of the eigenvalue technique is to test the randomness of groups of orientations. An ellipsoid that is not significantly different from a sphere cannot be described either as a cluster or a girdle. Woodcock and Naylor (1983) developed a statistic to test the "strength" of a group of orientations for different confidence intervals, based on the ratio S_1/S_3.

Just as with the Fisher distribution, it is dangerous to use the eigenvalue method indiscriminately, particularly for data sets that have two or more preferred orientations. As shown in Figure 20, many of the data sets from the Farmington Canyon Complex are of this type.

Comparisons of "Goodness of Fit"

The precision of a spherical distribution as described by Fisher (1953) is determined by two methods:

1) The k parameter

This is an approximation of the true precision parameter K. K is 0 for completely uniform spherical distributions, and infinite for a single unit vector. K is a property of an entire population, so it cannot be known in a realistic field survey; but it can be approximated by the sample parameter k, which is given as

$$k=(n-1)/(n-R)$$

(Fisher, 1953, p. 303), where n is the sample population, and R is the magnitude of the resultant vector; thus the larger the value of k, the tighter the grouping. This relationship works for k greater than 3 and n greater than 7 (Tarling, 1983). If k is greater than 10, the calculated mean of a Fisher distribution of vectors is a good approximation of the true mean (Tarling, 1983). The maximum k for data sets from the Farmington Canyon Complex is 4.57, and most are well below this value. However, the concern here is simply to characterize the dispersion of fracture orientations; the Fisher distribution is not used for analysis of the actual orientations of fracture sets in this study. Orientations have been determined by contouring the data, as discussed later in this section.

2) The radius of alpha95

This is a graphical way to compare spherical data. The radius of a circle on the surface of the unit sphere which contains 95 percent of the observations, centered on the resultant vector, is calculated (McElhinney, 1973). The smaller the radius, known as alpha95, the tighter the grouping. Alpha95 gives a good visual idea of groupings of fracture orientations about a mean value.

The two methods are similar in that they describe the closeness of the clustering of values around the mean vector. One difference between them is that k takes the entire sample into account, while alpha95 disregards the "worst 5 percent" of the observations. This means that k is more susceptible to outliers than alpha95. It is not known which of the two parameters is most suitable for the description of fracture sets in a hydrogeological context.

Results of Randomness and Goodness of Fit Analyses

Randomness

1) Fisher method

Table 1 shows that 71 percent of the unrotated fracture orientation data sets used in this analysis have a ratio of R/Ro of greater than 1, indicating a non-random distribution at 95 percent confidence. For the remainder, R/Ro is less than 1, so they would seem to lack preferred orientation. These conclusions are not necessarily correct; certain distributions of points on a sphere are inappropriate for analysis using the Fisher method, as discussed above.

Table 1. Comparing values of R for each data set with Ro for an equivalent randomly oriented data set. Left column is for raw data; right column shows effect of rotation procedure (discussed above). Data sets marked by an asterisk (*) are from principal fracture sets determined by eye from scatter diagrams of individual outcrops. XNFC and XNFD refer to fractures in outcrops adjacent to faults labeled C and D in Figure 11. 71 percent of the unrotated data sets are non-random at 95 percent confidence.

Data Set Name	Sample size (n)	R/Ro Unrotated	Rotated
*All Fracs	68	2.49	3.88
*Gneiss	49	1.80	3.39
*Amphibolite	33	2.11	2.62
*Pegmatite	21	1.24	2.03
XNFD	99	2.78	4.57
XNFC	82	2.17	4.19
*Region 1	10	0.83	1.45
*Region 2	9	1.14	1.46
*Region 3	20	1.41	2.04
*Region 4	15	1.19	1.93
*Region 5	10	0.99	1.74
*Region 6	10	0.99	1.62
*Region 7	10	0.93	1.38
*Region 8	13	1.16	1.62

Table 1 also compares unrotated and rotated R/Ro values for the data sets. All the rotated sets are nonrandomn at 95 percent confidence; but this result is also misleading, because values may be inflated above their "true" level. Nevertheless, although the value of R/Ro cannot prove that the remaining 29 percent of the original data sets are non-random, it provides a better description of the data. Eigenvalues were not calculated for the rotated data.

Fracture intersection lines were computed from the data in regions 1 through 8. R/Ro analysis for these (unrotated) data sets shows that they are all non-random at 95 percent confidence (see Table 2 below). A more complete explanation of the importance of fracture intersection lines is given further ahead.

Table 2. R/Ro values for fracture intersection lines in regions 1 through 8. The value for region 3 was not computed since the Ro value for n=190 was not available. Ro for Reg4int was estimated from the tabulated value for n=100. All samples were computed from the "principal fracture orientations" data set. All are comfortably non-random at 95 percent confidence.

Data Set Name	Sample Pop.(n)	R/Ro
Reg1int	45	2.88
Reg2int	36	2.76
Reg3int	190	
Reg4int	105	3.51
Reg5int	45	2.32
Reg6int	45	2.15
Reg7int	45	2.35
Reg8int	78	2.63

2) Eigenvalue method

Figure 22 shows that poles to fracture sets for

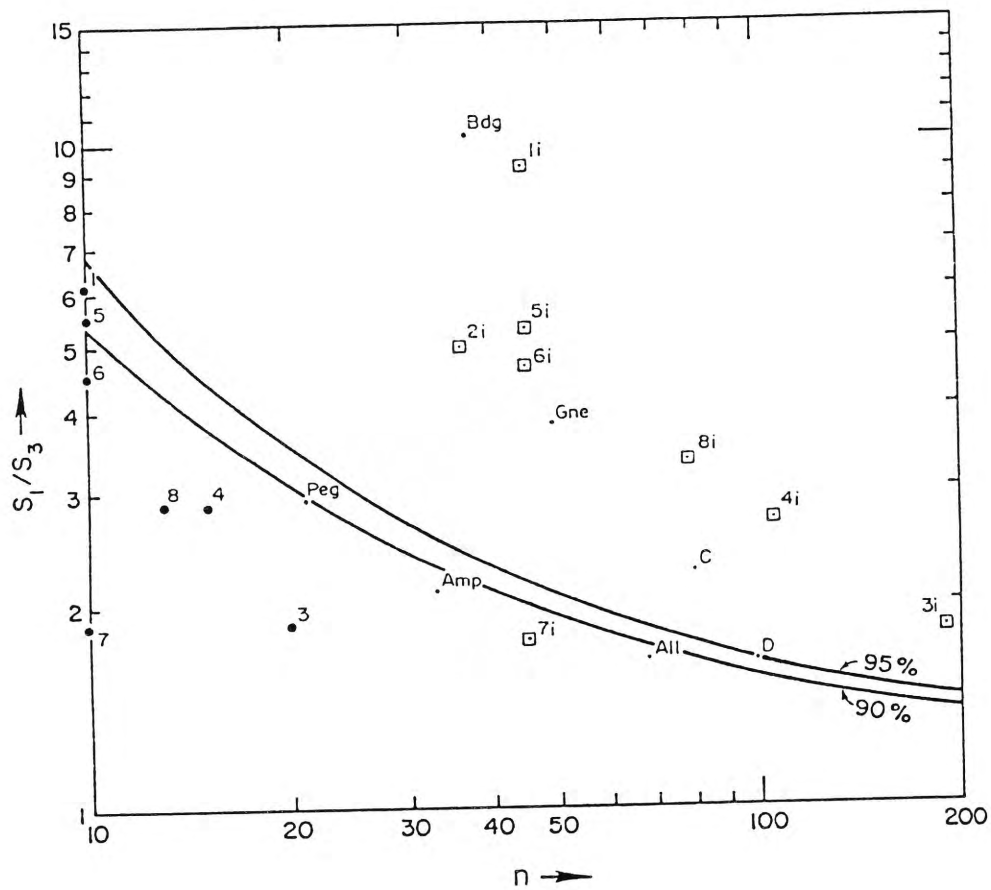

Figure 22. A plot of the randomness of fracture pole orientation distributions at 90 and 95 percent confidence. Numbers 1 to 8 are for poles to fractures, by region. Numbers followed by "i" are for intersection lines, by region. C and D=data sets XNFC and XNFD. Gne=gneiss; Amp=amphibolite; Peg=pegmatite; All=entire study area; Bdg=foliations in study area. Region 2 has only 9 data points and would plot in the random field (adapted from Woodcock and Naylor, 1983).

regions 1 through 8 are random at 95 percent confidence. Therefore, at this confidence level, no preferred fracture orientations exist. However, at 90 percent confidence, regions 1 and 5 are non-random, indicating that these two data sets contain preferred orientations of fractures. The distribution of fractures adjacent to fault C is non-random at 95 percent confidence; fractures adjacent to fault D are non-random at 90 percent confidence (refer to the geologic map in Figure 11 for the location of faults C and D).

Poles to fractures in pegmatite and amphibolite are random, but in gneiss they are non-random; this is in agreement with the R/Ro analysis. Finally, the principal trends of fracture intersections for seven of the eight sub-regions plot well into the non-random field. This too is in agreement with the R/Ro analysis.

Statistical Comparisons

1) Fisher method

An attempt was made to quantify differences in goodness of fit, or the "tightness" of groupings, for fracture sets within the study area, according to different geological criteria. These criteria were A) lithology, B) proximity to major lineaments, C) geomorphic (and perhaps structural) regions, D) different lithologies within geomorphic regions. Values of k and alpha95 were computed for these criteria. The rotated data sets were used for comparison. In cases A) and B) the raw data are plotted next to the rotated data for reference.

A) Lithology

Variations in lithology have been simplified into gneiss, amphibolite and pegmatite, as shown in the geologic map in Figure 11. It was hypothesized that the foliated metamorphic rocks classified as gneiss should have more consistent fracture orientations than pegmatites. The results show that k is greatest for gneiss and least for pegmatite; alpha95 is smallest for gneiss and greatest for pegmatite (Figures 23 and 24). The two parameters show that gneiss has the narrowest spread of fracture orientations, and pegmatite has the widest.

B) Proximity to major lineaments

At least three lineaments, interpreted to be faults, were mapped in the study area (Figure 11). It was hypothesized that the strain associated with faulting would have imposed a local disturbance on the regional fracture pattern. Figures 23 and 24 also show the statistical parameters for fracture orientations taken from outcrops adjacent to lineaments in the study area. The values of k and alpha95 for these two data sets reflect values of k and alpha95 for the entire study area. This implies that the distribution of orientations for sites adjacent to faults in the study area is not

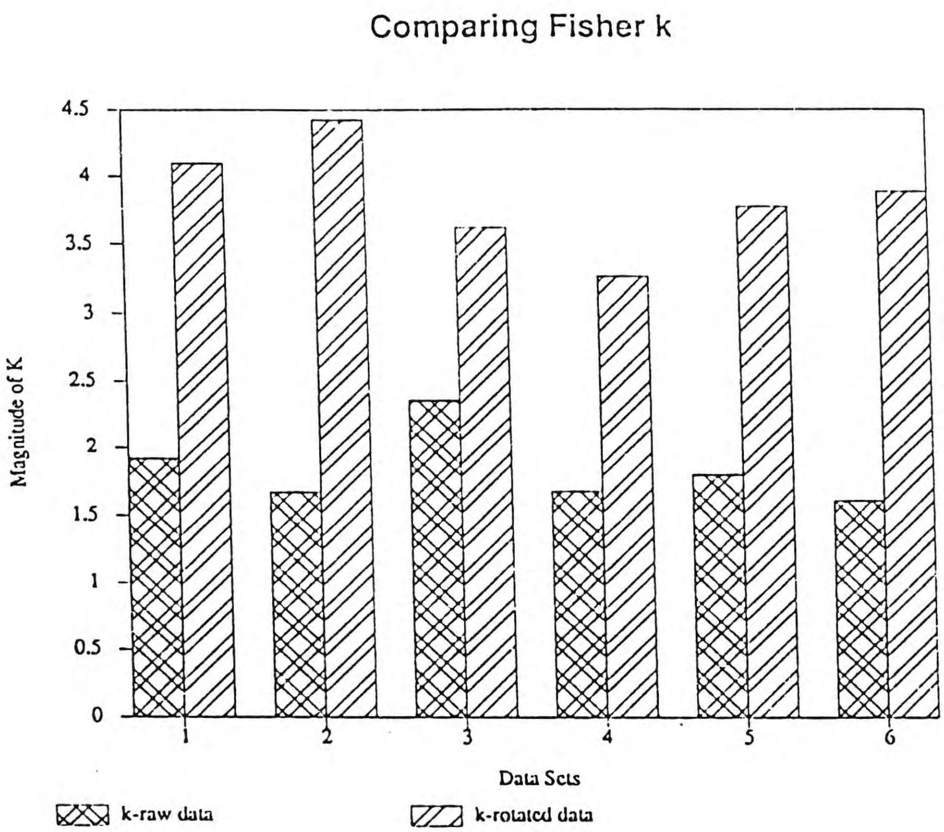

Figure 23. Fisher k parameters compared for different data sets in the study area. 1=all fracture sets; 2=fracture sets in gneiss; 3=fracture sets in amphibolite; 4=fracture sets in pegmatite; 5=fracture sets adjacent to fault C; 6=fracture sets adjacent to fault D. The rotated k value is greatest for gneiss and least for pegmatite.

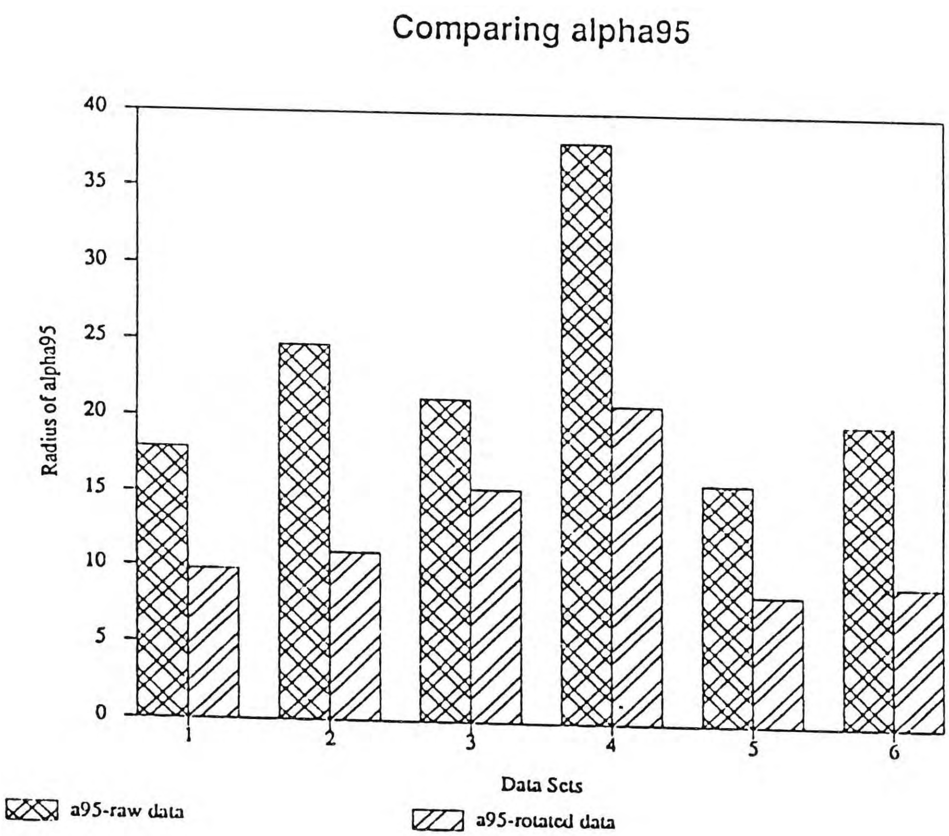

Figure 24. The rotated alpha95 value is smallest for gneiss (#2) and largest for pegmatite (#4).

significantly different from that of the "background", or entire study area.

C) Geomorphic regions

The field study area was divided into eight regions, corresponding to different geomorphic environments (Figure 25). Regions 1, 4, 5 and 6 are along sharp ridges forming the crest of the Wasatch Front; outcrops here are well exposed, and vegetation is sparse. Regions 2, 3 and 8 are located on less steep, wider, west-trending ridges between canyons; aspen and other trees and scrub are present here, and outcrops are less well exposed. Region 7 is on a steep south-facing slope. It was thought that fracturing on sharp ridges would be more consistently oriented than in the other regions.

The following paragraph is a review of results shown in Figures 26 and 27. The highest k values belong to regions 4, 5 and 6. The smallest values of alpha95 are found in regions 3, 4, 5 and 6. Altogether, it appears that regions 4, 5 and 6 have the tightest grouping of fracture orientations. These correspond to three out of the four sharp ridges. Region 7 appears to be the most widely scattered, followed by region 2. The other regions have intermediate statistical properties.

D) Different lithologies within regions 1 through 8

The field data on fracture orientations included an identifier of location as well as lithology; this allowed

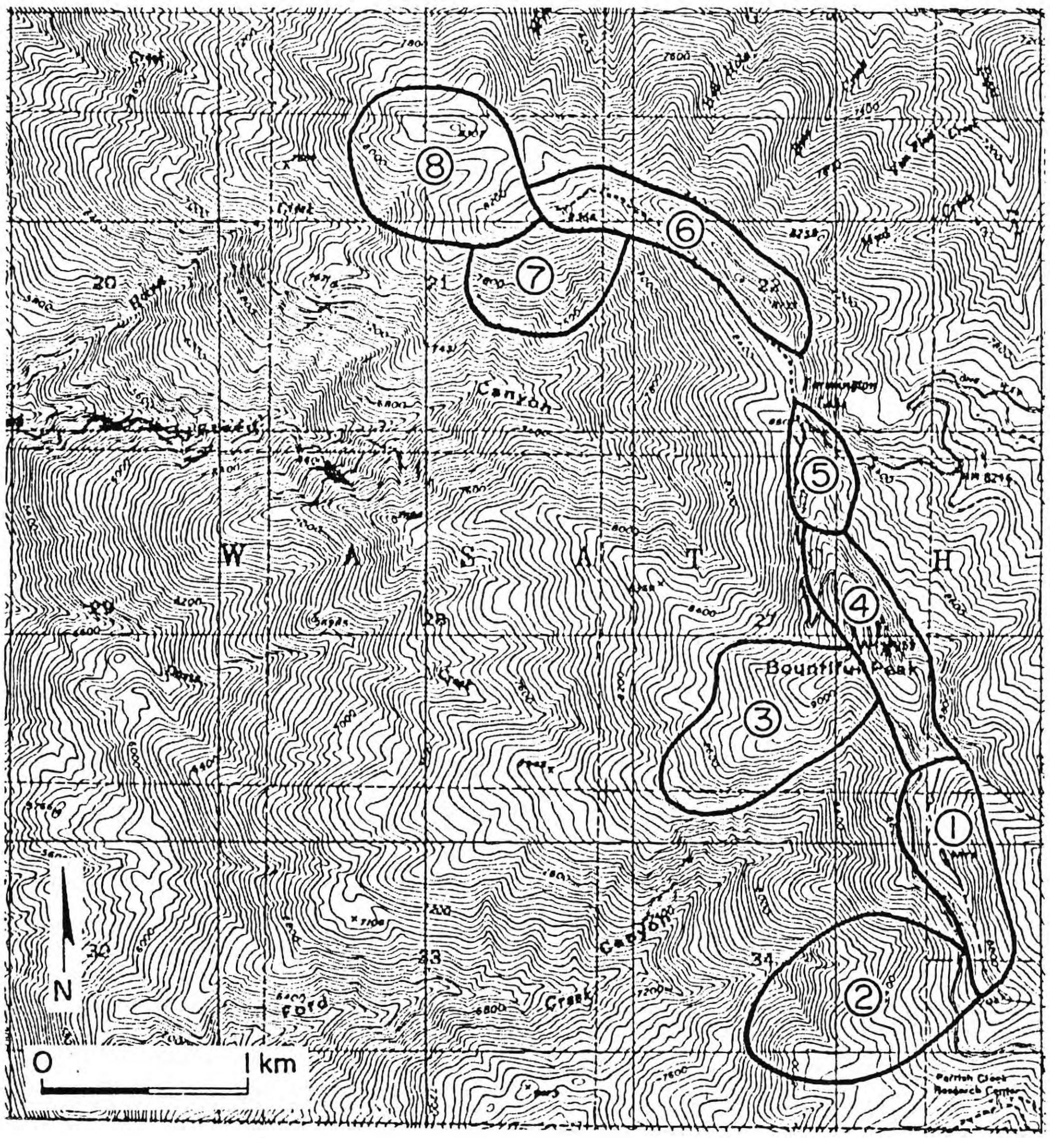

Figure 25. Regions 1 through 8, separated on the basis of geomorphic appearance. Fracture orientation data were classified by region.

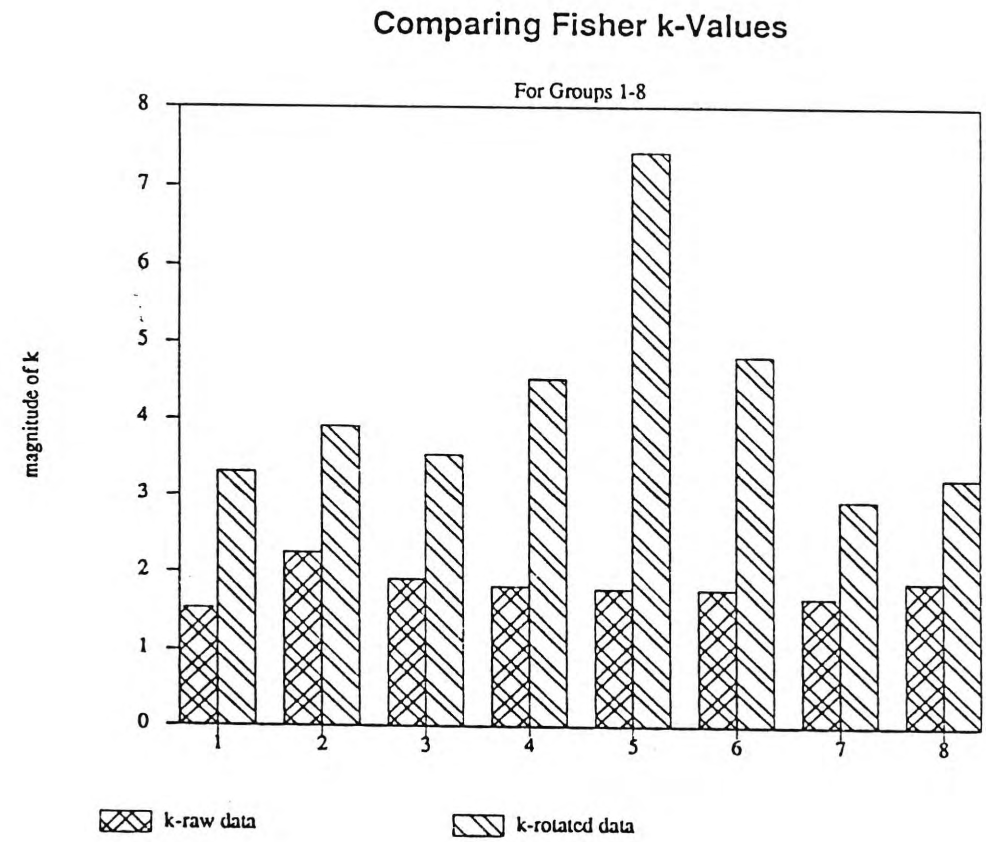

Figure 26. The rotated k values are largest for regions 4, 5 and 6.

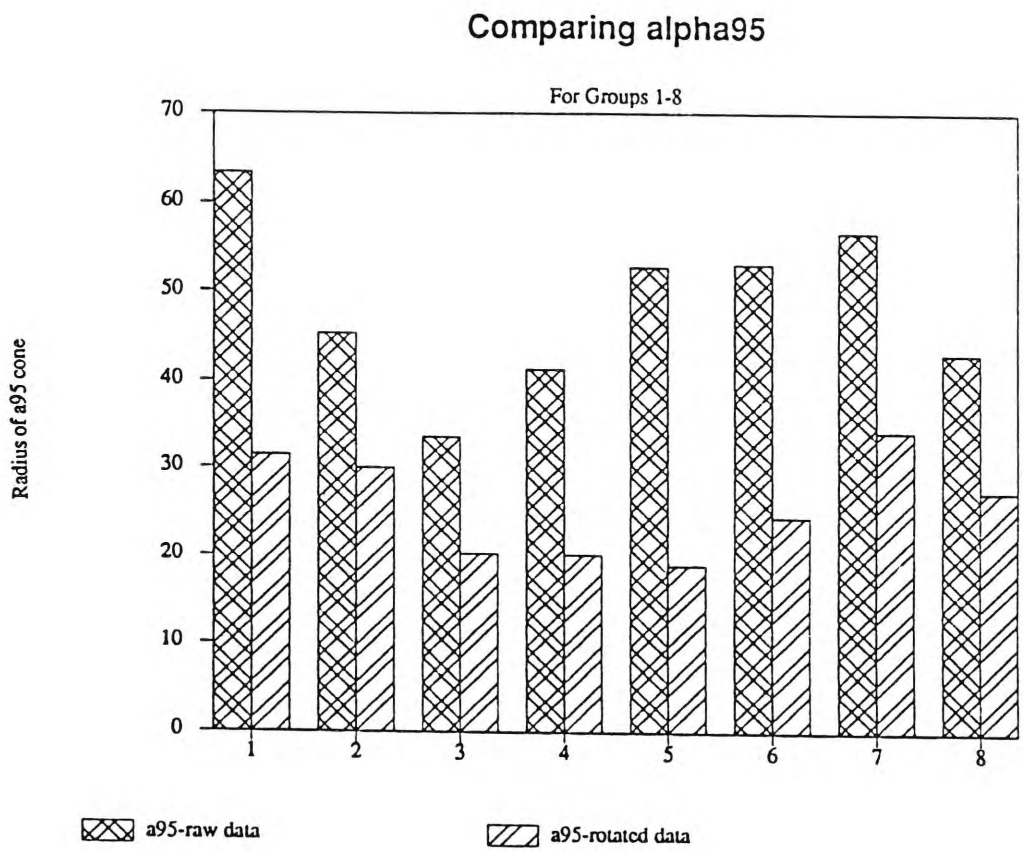

Figure 27. The rotated alpha95 values are smallest for regions 3, 4, 5 and 6.

the same data to be grouped in two different ways. The purpose of doing this was to see which criterion of lithology or spatial location had a greater influence on fracture orientation distribution. It was reasoned that if, for instance, sample parameters k and alpha95 were not statistically different for different lithologies, then lithology in itself was not a significant influence on the distribution of fracture orientations.

The statistical test employed to compare the two groupings of sample parameters was the Kruskal-Wallis test. This is a nonparametric or "distribution-free" statistical test. It does not require that the sample be from a normal population (Davis, 1986). Nonparametric tests cannot be used for analyzing interval or ratio data, as can the sophisticated tests based on normal distributions (Conover, 1980). However, for this simple application, the Kruskal-Wallis test is adequate.

The original data were classified according to the two criteria; k and alpha95 were calculated for each, forming two 3 by 8 matrices of 21 sample parameters (3 slots were empty due to a lack of data) as shown in Table 3. For each criterion, the null hypothesis stated that the given parameters were from the same population (i.e., not significantly different at 95 percent confidence).

Table 3. Descriptive parameters of fracture orientation distributions, grouped by lithology (rows) and by geomorphic region (columns).

	Lithology					
	Gneiss		Amphibolite		Pegmatite	
	k	95	k	95	k	95
Region						
1	6.32	11.4	5.06	10.4	4.81	8.8
2	3.44	22.0	2.99	13.8	3.22	10.3
3	-	-	3.68	10.1	3.15	9.6
4	4.12	8.2	4.45	24.5	4.05	8.7
5	3.62	11.6	4.83	15.8	-	-
6	4.26	8.5	4.84	15.1	4.07	17.6
7	3.46	11.8	3.14	18.9	-	-
8	4.92	8.1	4.06	11.6	6.19	40.2

The Kruskal-Wallis test shows that k and alpha95 for gneiss, amphibolite and pegmatite are not significantly different at 95 percent confidence. None of the alpha95 values for regions 1 through 8 are significantly different either. However, one or more of the k values for regions 1 through 8 <u>are</u> different. This can be seen qualitatively in histograms of the parameters for different lithologies, and different regions (Figures 28 through 31).

It was mentioned above that the parameter k is more sensitive to data outliers than alpha95. This is probably the reason why the Kruskal-Wallis test showed significant differences in k for regions 1 through 8, but not for alpha95.

It is concluded that geomorphic environment is a more important influence on the distribution of fracture orientations than lithology. The test results, and the

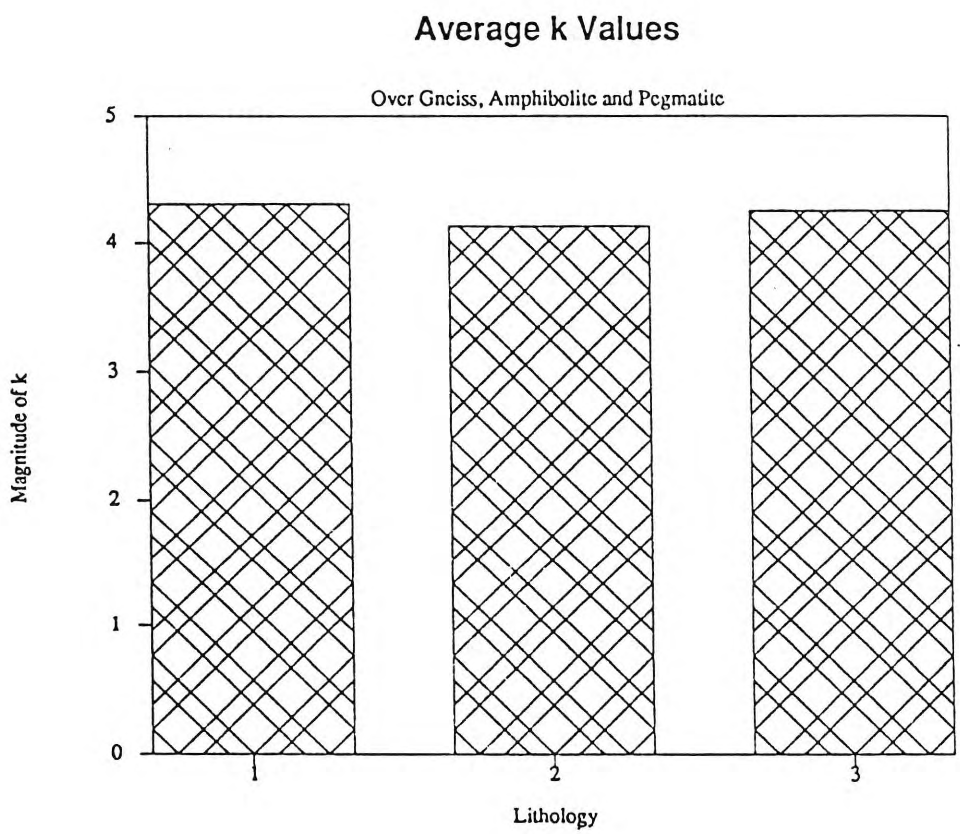

Figure 28. Variability in k for gneiss (#1), amphibolite (#2), and pegmatite (#3). Average values range from near 4.0 to near 4.3.

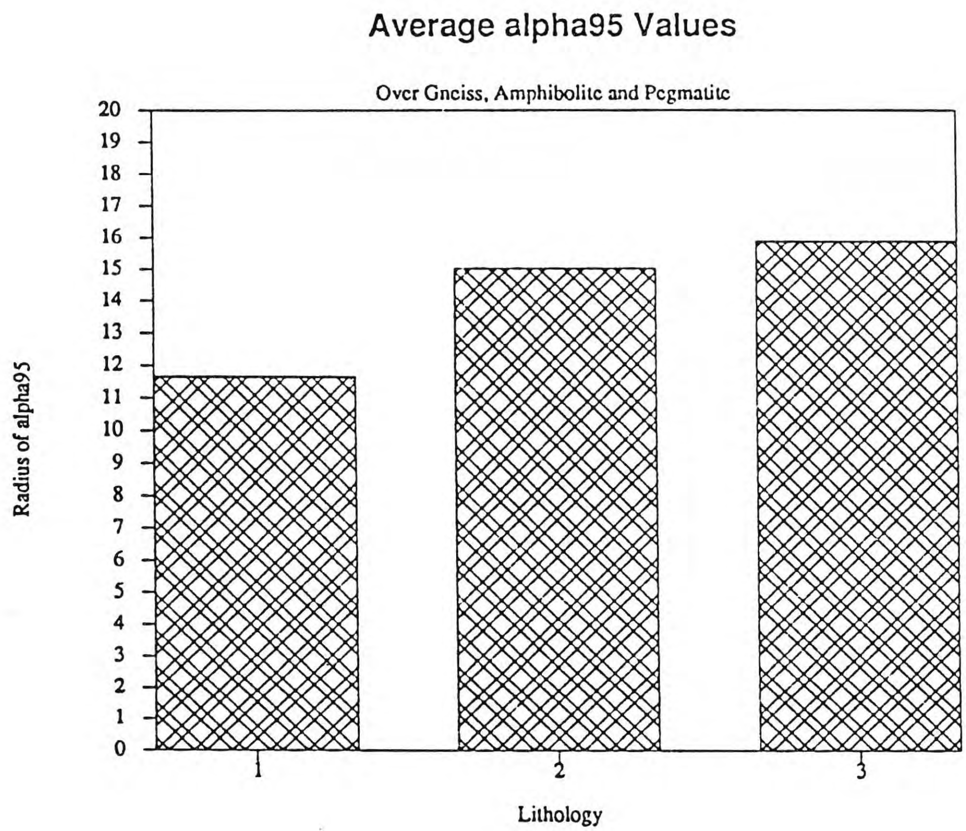

Figure 29. Variability in alpha95 for the three lithologies. Average values range from near 11.5 to near 16.0.

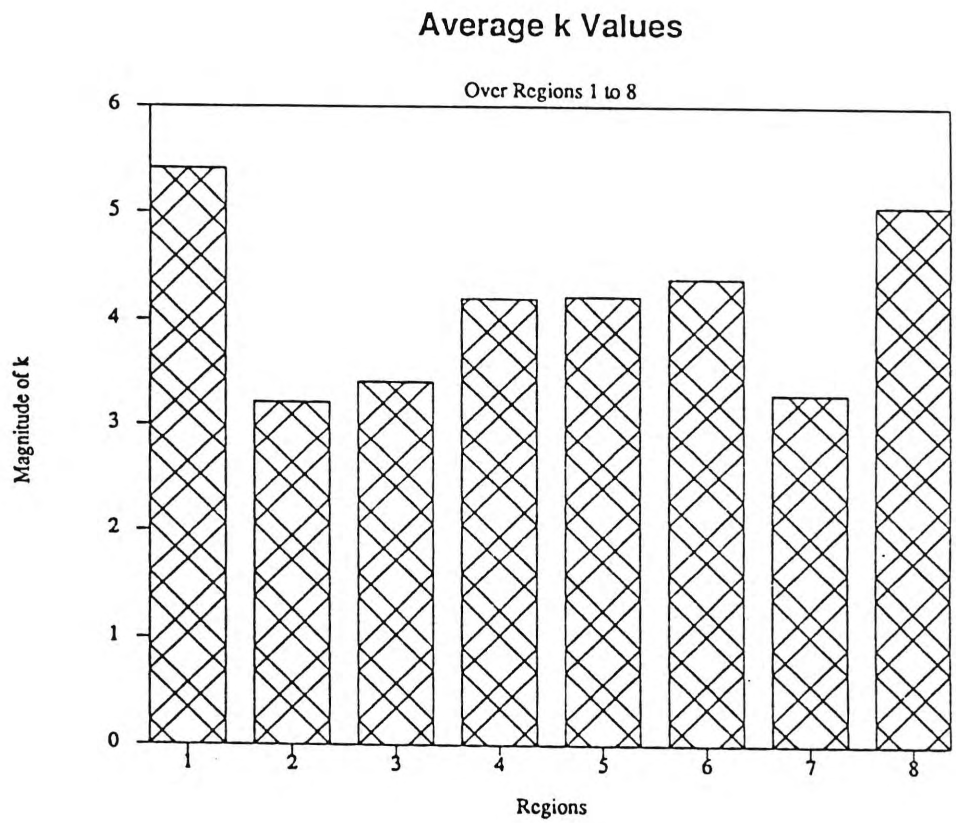

Figure 30. Variability in k for regions 1 through 8. Average values range from near 3.0 to near 5.5.

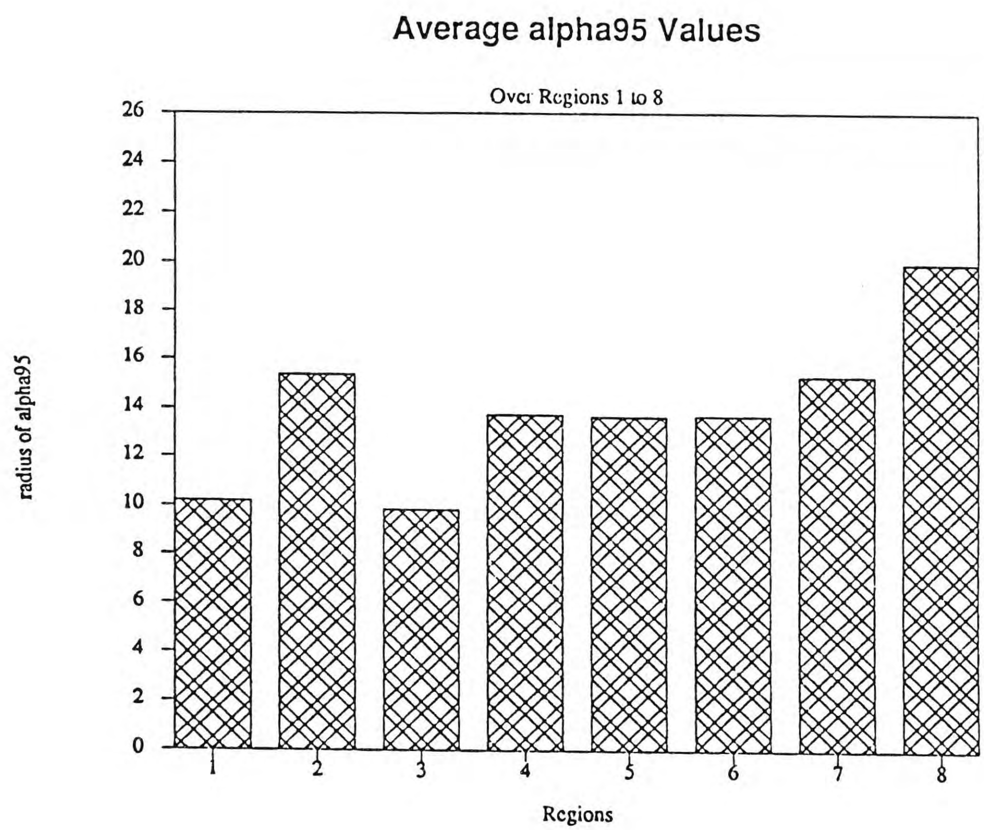

Figure 31. Variability in alpha95 for regions 1 through 8. Average values range from near 10 to near 20.

steps involved in calculating the Kruskal-Wallis statistics are shown in Appendix 3.

An important assumption in this test is that the two criteria (lithology and geomorphic region) are independent (Milton and Arnold, 1986). It is likely that there is a geological link between the distribution of lithologies and the geomorphic character of regions; for example, the sharp ridges are in many cases the site of elongate pegmatite outcrops. However, for the Kruskal-Wallis tests, the assumption of independence was justified, because statistical comparisons were made <u>within</u> each classification of variables. In other words, lithology was analyzed separately from regions.

2) Eigenvalue method

The normalized eigenvalue ratios of each data set were compared to show the general shape of the distributions (i.e. towards clusters or girdles). Figure 32 shows how the shapes of the fracture pole orientations can be described by the relative magnitudes of S_1, S_2 and S_3. The data sets for the Farmington Canyon Complex are shown in Figure 33. In the perspective offered by Figure 32, most of these data have "weak" fabric strength. Few of the groupings represent either clusters or girdles. The only obvious girdles are for Bdg (the set of foliations) and the fractures in region 2. Relatively strong clusters are seen for fracture intersection lines

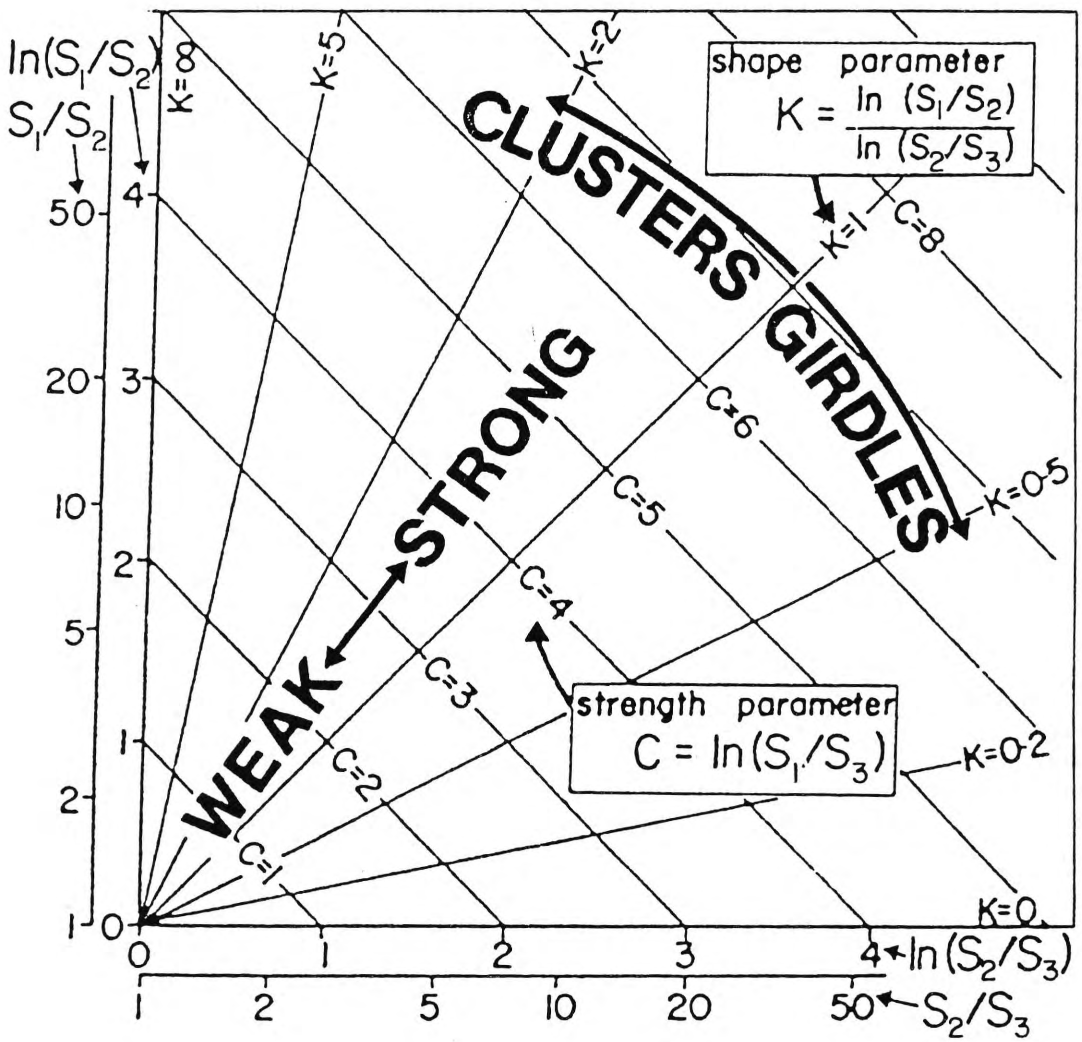

Figure 32. A Plot of ellipsoid shapes described by the relative lengths of their axes, as indicated by the relative magnitudes of the normalized eigenvalues S_1, S_2 and S_3. C is a measure of departure from sphericity of the ellipsoid; data at the origin are spheres (after Woodcock and Naylor, 1983).

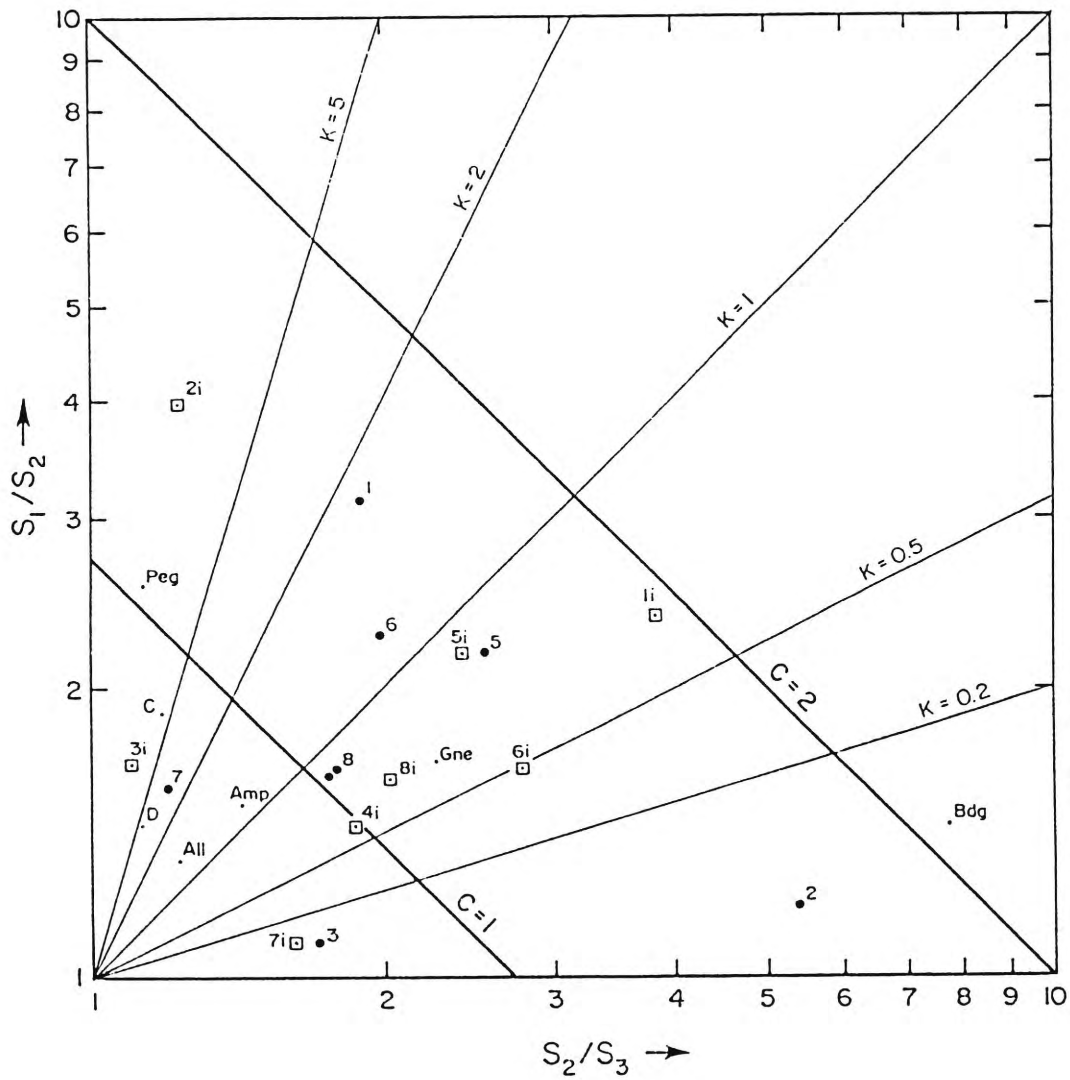

Figure 33. Eigenvalue ratio plot showing the shape of fracture orientation sets from the Farmington Canyon Complex. Dots are poles to fractures; squares are intersection lines; abbreviations are the same as for Figure 22 (adapted from Woodcock and Naylor, 1983.)

in region 2, and for fractures in pegmatite.

An interesting observation from Figure 33 is that poles to fractures plot opposite to fracture intersection lines generated from the same data set. Thus, a well-defined girdle configuration of fracture orientations will have a tight cluster of intersection lines.

Summary and Discussion of Results

The R/Ro analysis of unrotated data suggests that at least 71 percent of the fracture orientation distribution samples selected from the field data in the study area are non-random at a 95 percent confidence level. These findings are incompatible with the results of the eigenvalue tests for the same data sets (Figure 22), which finds them all to be random at 95 percent, except gneiss and data set XNFC. In addition, at 90 percent confidence, regions 1 and 5 and data set XNFD are non-random.

In view of the limitations of the Fisher method (discussed above), the results from the eigenvalue analysis are accepted: 1) there are no preferred orientations in principal fracture sets for the entire study area, for pegmatites or amphibolites, or for any of the eight sub-regions of the study area at 95 percent confidence, and 2) contrary to the Fisher analysis results, it appears that there <u>is</u> a significant difference (at 90 percent confidence) between the dispersion of fractures adjacent to faults and those of the "background", or entire study area.

Among rotated data sets analyzed by the Fisher method, the most tightly focused fracture orientation groups were found in gneiss, and in regions 4, 5 and 6. This agrees to some extent with the eigenvalue analysis of unrotated data sets, which found fractures in gneiss, and in regions 1 and 5, to be non-random at 90 percent confidence. Both the R/Ro and eigenvalue tests on (unrotated) fracture intersection lines for regions 1 through 8 indicate non-randomness at 95 percent confidence, except for region 7, which is random according to the eigenvalue analysis.

The fact that the majority of data sets of fracture intersections are non-random suggests that a preferred orientation of the structural fabric <u>does</u> exist, which is not apparent in the analyses of the fractures themselves. This implies that fracture sets are not truly randomly oriented, and that neither the Fisher nor the eigenvalue analyses are completely satisfactory for such complex and poorly focused orientation data. The Kamb contouring method (discussed ahead) also supports the idea that there are preferred orientations of fractures in these data sets.

The Kruskal-Wallis test on the dispersion parameter k shows that variations in fracturing style between lithologies are overshadowed by the variation between geomorphic environments. However, it is important to recognize that the differences between these regions are the result of geological processes of various types. More resistant lithologies exist along ridges (regions 1, 4, 5 and 6). Regions 2, 3 and 8 are cut by faults; Bryant (1988, p. 43) notes the sites of high-angle faults are wide zones of thicker soil development, "marked by gullies, notches, and vegetation", as shown in Figure 34. The areas depicted in this figure have a similar geomorphic appearance to regions 2, 3 and 8.

These results bring out the truly heterogeneous geological nature of this part of the Farmington Canyon Complex, consistent with its complex geologic history. It is also seen that care must be taken in applying statistical analyses to real geological data, in order to obtain meaningful results. A further implication for this area is that detailed analyses over the entire study area, or within small blocks of the study area, may be less useful than analyses that determine the size and extent of more or less homogeneous regions, such as photogeologic investigation.

Contouring Preferred Orientations

Having statistically characterized the data in terms of randomness and precision, a method was sought which would display the orientation as well as the dispersion of fracture sets. This was accomplished by contouring

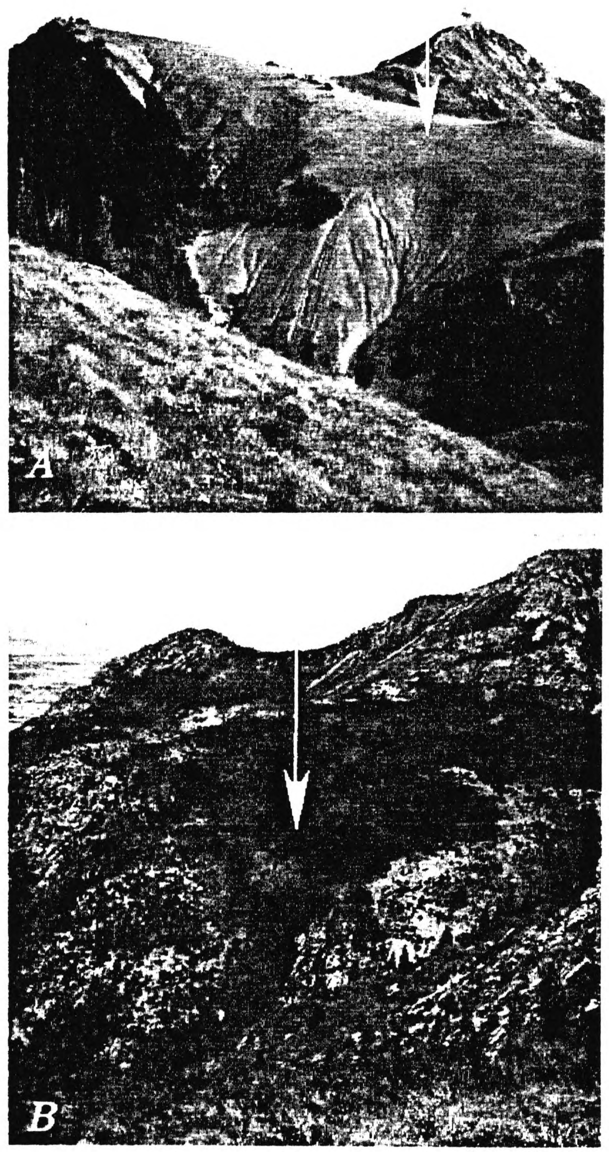

Figure 34. Geomorphic expression of two high-angle faults in the Farmington Canyon Complex. **A.** Francis Peak Fault **B.** A fault near Bountiful Peak (after Bryant, 1988).

observations by their density on the lower surface of a hemisphere stereonet.

Contouring the orientations of poles to fracture planes clearly identifies fracture sets. Commonly, poles to fractures are contoured by the number of observations within a specified percentage of the area of the hemisphere. This method can be inconclusive for large data sets, because, as the number of poles to be contoured increases, their density increases throughout the hemisphere, and much "noise" may be generated.

The contouring procedure used in this analysis was developed by W.B. Kamb (1959). The Kamb method works independently of the number of observations in the data set. A counting area "A" is assigned such that the number of observations "E" falling within A is equal to 3 times the standard deviation of n, the number of points that will fall within A if the sampling is random (i.e., no preferred orientations). The reason that 3σ is chosen as the lower threshold of significant non-randomness is that randomly oriented groupings of fractures may coincidentally contain points in close proximity to each other, thus imitating a non-random grouping. Raising the requirement for non-randomness allows for this problem. For a population of vectors on a sphere, with no preferred orientation, the following equation can be written (Kamb, 1959, Appendix):

$$\sigma/E=([1-A]/nA)^{1/2}, \text{ where } E=nA.$$

Contours were drawn to separate densities up to 3σ, above 3σ to 5σ, above 5σ to 7σ, and so on. Kamb contours of the data sets described in the previous section are shown in the next section.

Orientations of Fracture Intersections

The degree of interconnection of fractures has a great effect on fluid flow through fractured rocks (Long and Witherspoon, 1985). Fracture connectivity is not simple but depends on fracture orientation, length and density.

It has already been shown that samples of fracture intersection lines computed from fractures in regions 1 through 8 of the study area are clearly non-randomly distributed, except for region 7. The Structure Graphics program (Wiltschko, 1990) calculates and plots the orientations of all possible lines of intersection between planes in a data set, assuming fractures are infinite planes. This is an important assumption, and may be unreasonable as a basis for computing hydraulic permeability if the fracture length and density of a sample are non-uniform; if this is the case, longer, more closely spaced fractures will be better connected than shorter, more widely spaced ones, which might greatly affect the main permeability trends (Long and Witherspoon, 1985).

A scan-line survey of one outcrop in the region (Station 98) revealed the following information about the orientations of fractures of different lengths and apertures:

1) Longer fractures were oriented similarly to the complete data set (Figures 35 A and B).

2) Open fractures were oriented similarly to the complete data set (Figure 35 C).

If outcrop A98 is representative of the region, the three-dimensional structure of shallow bedrock fractures is relatively uniform for fractures of different lengths and apertures. Other outcrops were qualitatively observed to have similar properties. This analysis helps justify the method used for calculating fracture intersection lines, because if fractures of different types are similarly oriented, their intersection line (and relative permeability) trends should also be similar.

Fracture Spacing and Length

Fracture spacing and length data were collected for a few of the stations, as shown in Figure 17. The data collection technique has already been described. In each case, the scan line was oriented as near as possible to perpendicular to the principal fracture set. Fracture half-lengths, and the spacing between them, were recorded. In some cases, fractures extended to the edges of outcrops. The lengths of these fractures are not known,

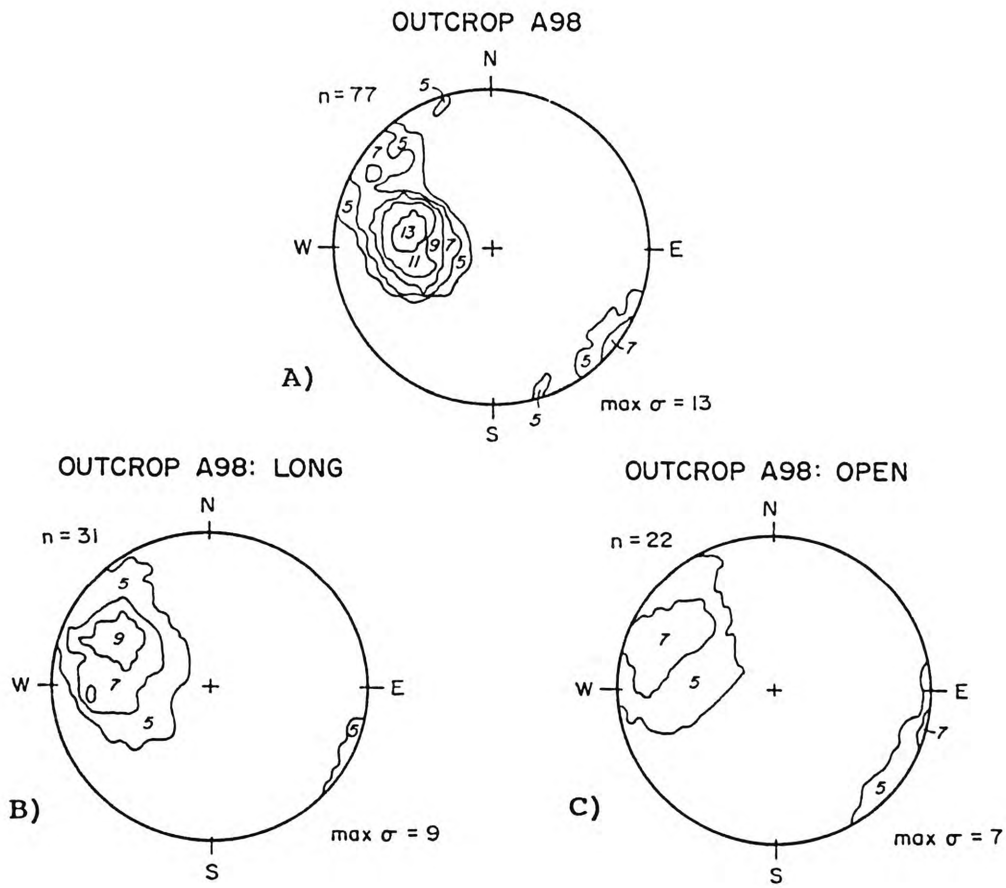

Figure 35. Contoured Schmidt nets of poles to fractures at outcrop A98. **A.** All fractures **B.** Fractures with half-lengths greater than 80 mm **C.** Fractures with apertures greater than approximately 0.5 mm.

but the observed lengths were used in subsequent analyses. The irregular surface and elongate shape of most of the outcrops limited the utility of fracture length information.

Results are similar for most stations. Examples are presented, for three different lithologies, in Figures 36, 37 and 38. Both length and spacing data are exponentially or lognormally distributed: most of the fractures are short and closely spaced. There is a lack of longer, more widely spaced fractures. The same distribution was found at almost all outcrops, regardless of lithology. It is not clear what these distributions imply for the hydrogeologic behavior of the rock mass.

FRACTURE SPACING

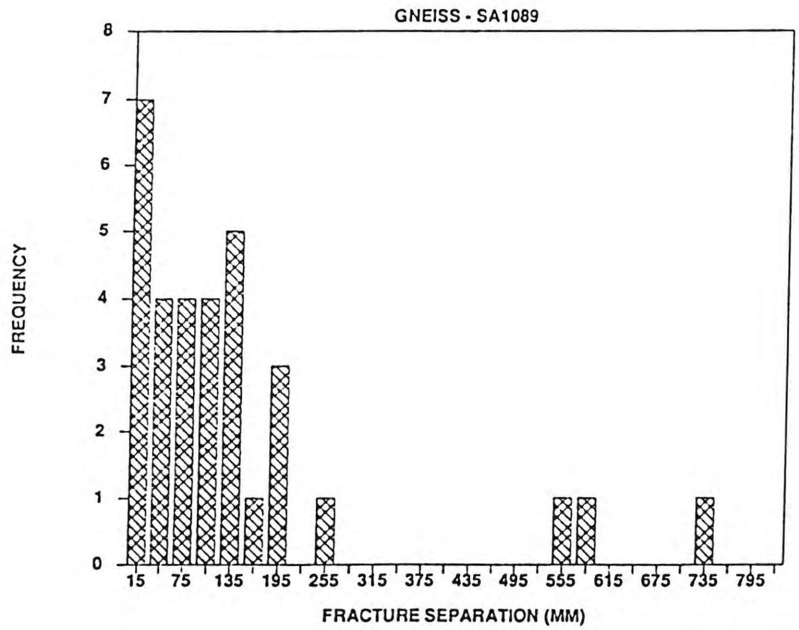

FRACTURE LENGTH

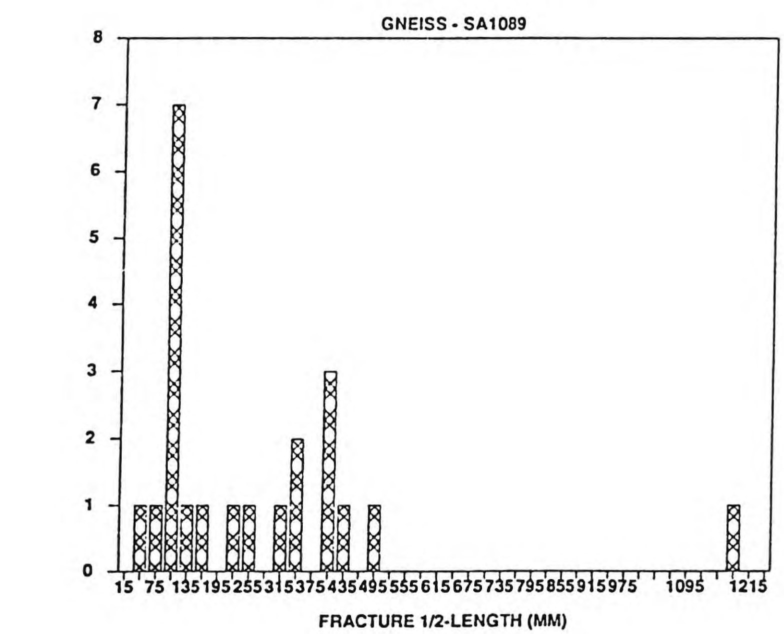

Figure 36. Fracture spacing and half-length for a gneiss outcrop (scan line technique).

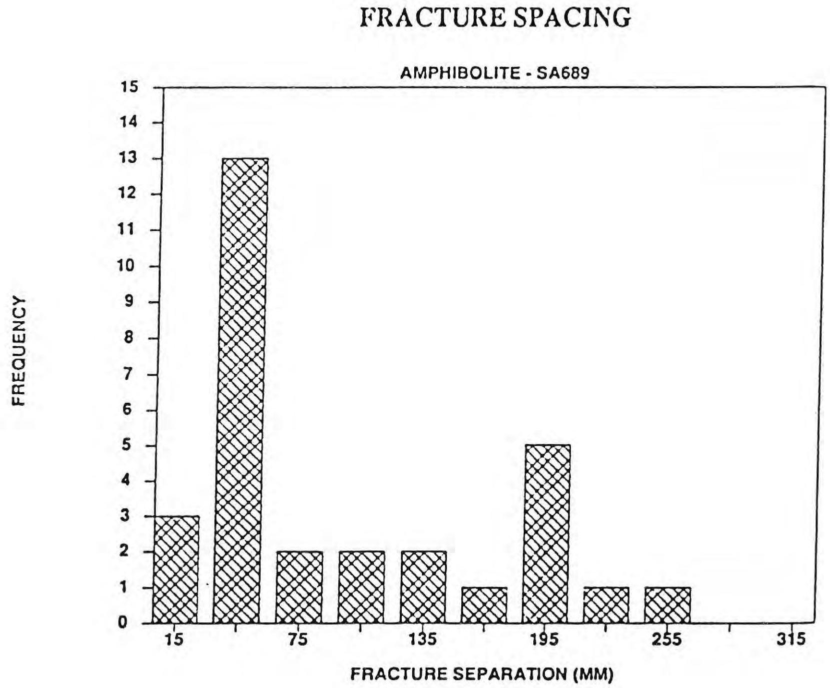

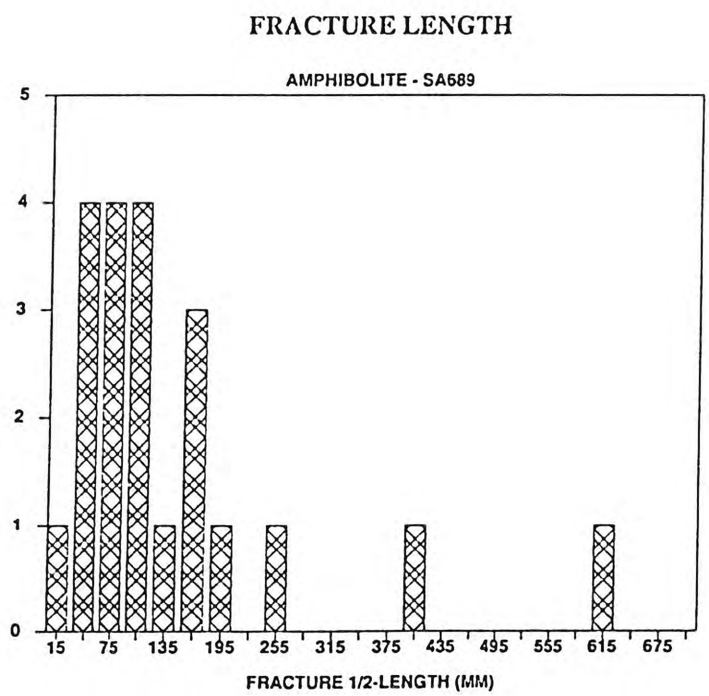

Figure 37. Fracture spacing and half-length for an amphibolite outcrop (scan line technique).

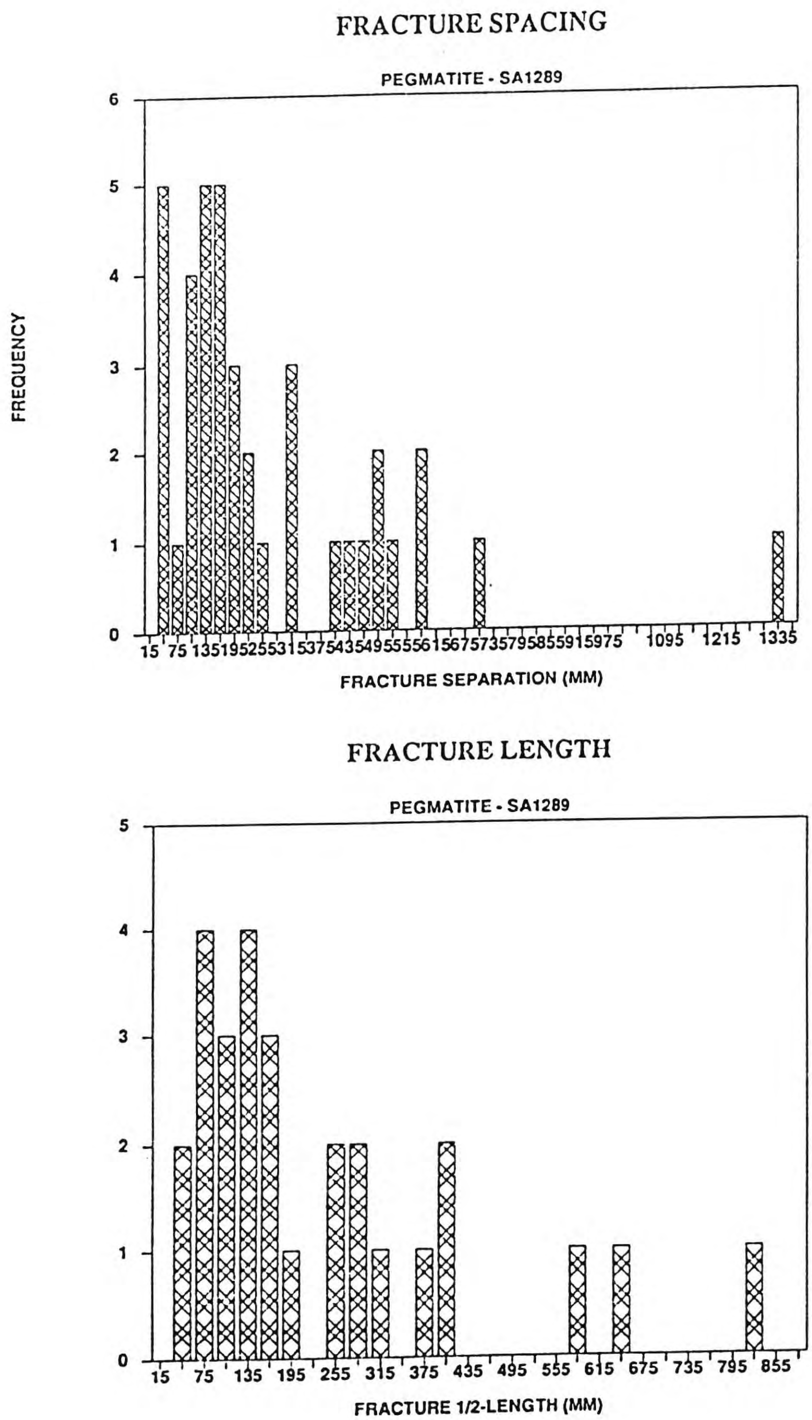

Figure 38. Fracture spacing and half-length for a pegmatite outcrop (scan line technique).

GEOLOGIC INTERPRETATION OF THE STRUCTURAL FABRIC

Orientations of Fractures and Foliation

Entire Study Area

The principal pole(s) for each outcrop were contoured in one diagram for the entire study area (Figure 39). The density of poles is a maximum of 7σ. There are two clusters of poles, as shown in Table 4. The strike of the most pervasive set of fracture planes is approximately 57° from the trend of major faults in this area (shown as dashed lines in Figure 11), and 65° from the orientation of the Wasatch Fault. (Structural trends are given in azimuth angle from true north, generally between 180° and 359°). The average dip for this set is 79° SE.

Table 4. Mean orientations of the principal fracture and foliation sets estimated from Figures 39 and 40 A.

Data Set	Poles Trend/Plunge	Planes Strike/dip
All Fractures	323°/11°	233°/79°SE
	196°/40°	286°/50°N
All Foliations	221°/57°	311°/33°SW

Figure 40 A shows Kamb contours of poles to observable foliation planes within the study area. The orientation of the greatest density of poles to foliations is listed in Table 4. The poles form a girdle configuration about a pole located at 291°, 20°. This distribution agrees well with similar data obtained by

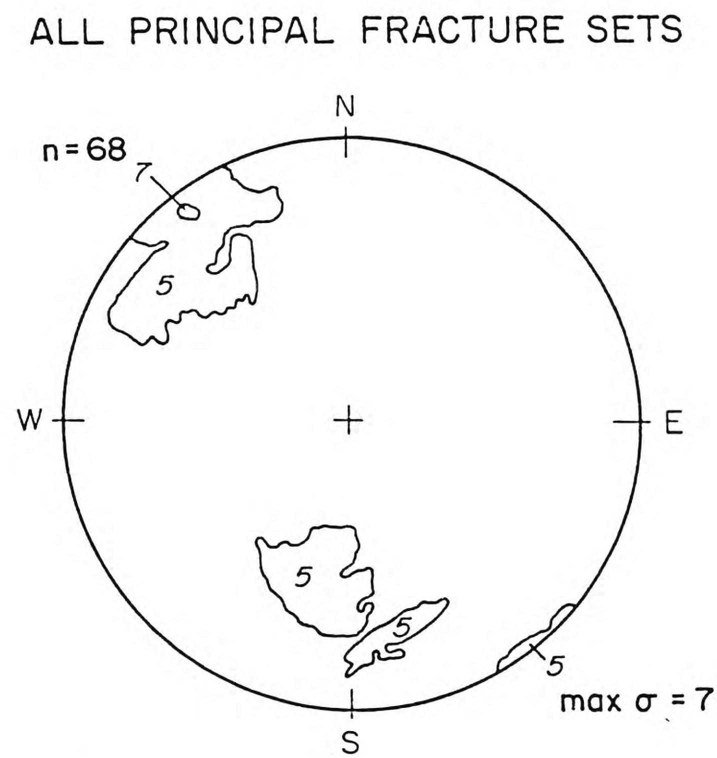

Figure 39. Contoured Schmidt net of poles to fracture sets for the entire study area.

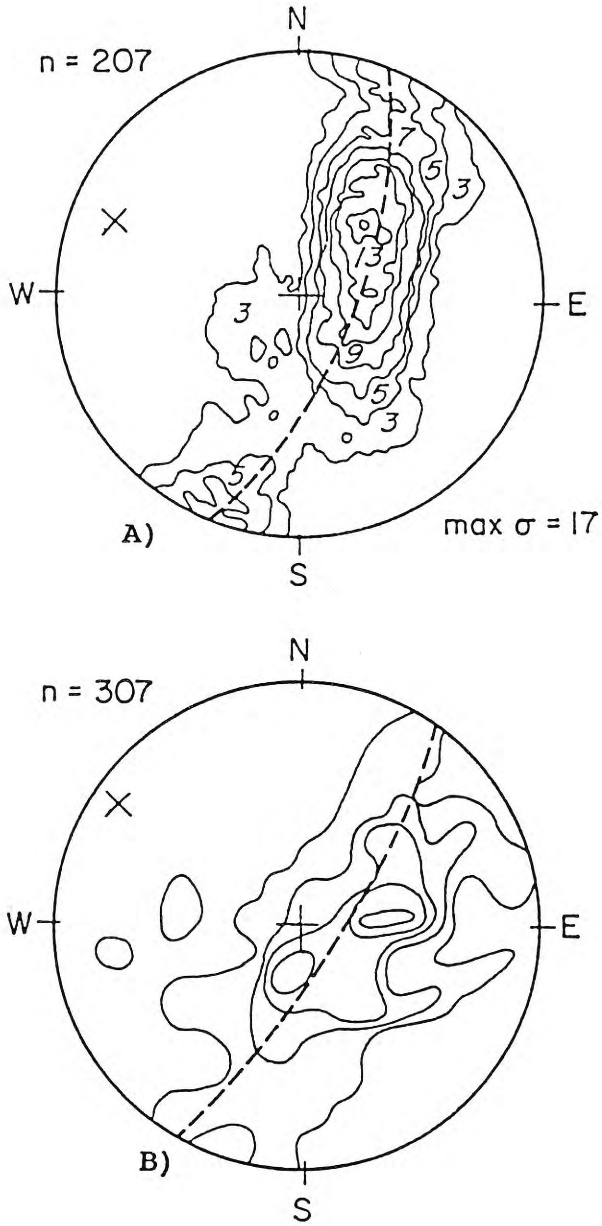

Figure 40 A. Contoured Schmidt net (Kamb method) of poles to all foliations in the study area, showing a girdle around a pole at azimuth 291°, dip 20°. **B.** Contoured poles to foliation for non-cataclastic rocks in Bountiful Peak quadrangle form a girdle around a pole at azimuth 303°, dip 10° (after Bryant, 1988). Contours in this diagram are for pole density percent (0.65, 2, 3.3, 4.5 and 6 percent) within a fixed area of the sphere (1 percent).

Bryant (1988), shown in Figure 40 B. Comparing Figure 40 A with Figure 39, it is apparent that the principal set of poles to fractures and the greatest density of poles to foliation planes are very nearly orthogonal in three dimensions.

<u>Lithologic control:</u> Rocks of different lithologies have different moduli and will fracture in different ways. Lithologic control of fracture orientations accounts for some of the variability in orientations in Figure 39. Figures 41 A, B and C show these differences graphically. Table 5 lists the orientations of the principal fracture sets for each lithology. Note that the contoured poles for pegmatite outcrops are distinctly different from the other two.

Table 5. Mean orientations of the principal fracture sets estimated from Figure 41 A, B and C. Data sets are from principal fracture sets estimated by eye from scatter diagrams for individual outcrops.

Data Set	**Poles Trend/Plunge**	**Planes Strike/Dip**
Gneiss	178°/21°	268°/69°N
	307°/29°	217°/61°SE
	330°/5°	240°/85°SE
Amphibolite	309°/20°	219°/70°SE
Pegmatite	3°/8°	273°/82°S
	197°/9°	287°/81°N

The similarity of amphibolite and gneiss fracture orientations implies a similar geologic and structural history for these lithologies, in contrast to the pattern

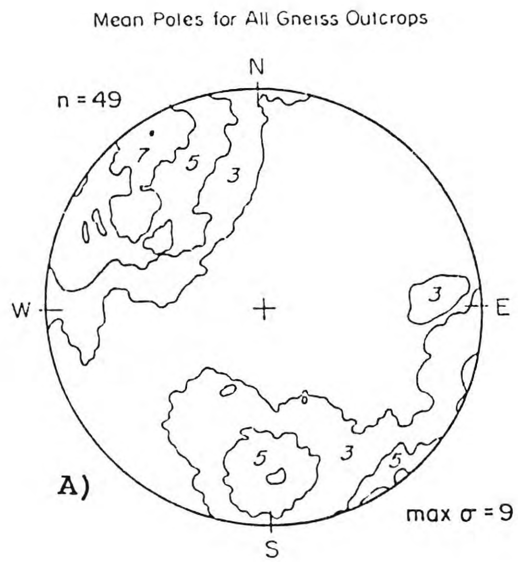

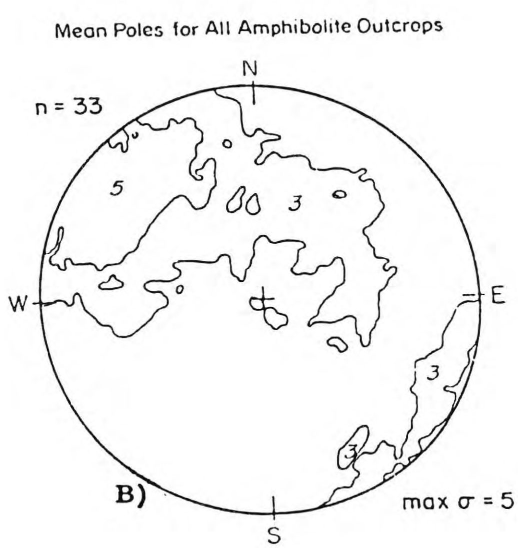

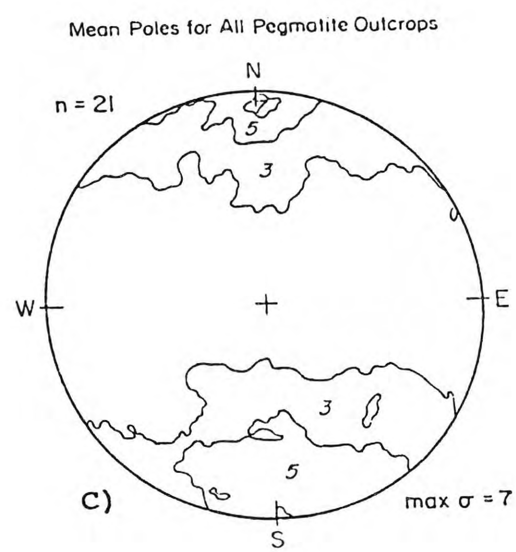

Figure 41. Contoured poles to principal fracture sets over the entire study area for different lithologies: A=gneiss; B=amphibolite; C=pegmatite.

observed in pegmatite outcrops. This is what would be expected, given the lithologic and genetic similarity of the amphibolite and felsic gneisses, and their dissimilarity with pegmatite (Bryant, 1988). The different engineering properties of pegmatite are also significant, in that they must have produced local changes in stress distribution during structural deformation.

Rotating fracture orientations: The above analyses are useful in determining an overall picture of fracture set orientations in the study area. However, from the evidence presented in the previous section, it could be argued that any "global" method of characterizing fracture orientations in this part of the Farmington Canyon Complex misrepresents the data because it does not take spatial variability into account.

Geological controls on the regional variability of fracture orientations were discussed to some extent in the previous section. The geological evolution of structures in the Farmington Canyon Complex has also been discussed, in a regional context. Unfortunately, the very complicated geology of the Farmington Canyon Complex makes it difficult to identify regionally consistent structures within the study area. Differences in rock strengths and pre-existing structures have complicated subsequent patterns of deformation.

In the study area, no coherent pattern of folding is apparent; however, the majority of the metamorphic rocks are foliated. Foliation is a regionally consistent characteristic of rocks, in that it may indicate the direction of the greatest principal stress during metamorphism. Bryant (1988) suggests that foliation follows the general pattern of folding within the Farmington Canyon Complex, though both are locally contorted. With this in mind, it was considered that "unfolding" the folded foliation would reveal a regionally pervasive structural fabric.

To allow for regional variability, it was assumed that all foliation planes were originally parallel and horizontal. Differences in foliation orientations were removed so that all fractures were oriented relative to horizontal foliation planes. The unfolding procedure used the fact that most outcrops contained both fractures and well-defined foliation planes. The principal pole(s) to foliation for a given outcrop were determined. If more than one set of foliation planes existed, that outcrop was not used. The pole was rotated to vertical (to bring the principal foliation plane to horizontal). Fractures from that outcrop were then rotated by the same amount.

Rotated and unrotated fractures are compared for the entire study area (Figures 42 A and B) and for different lithologies within the entire study area (Figures 43 and

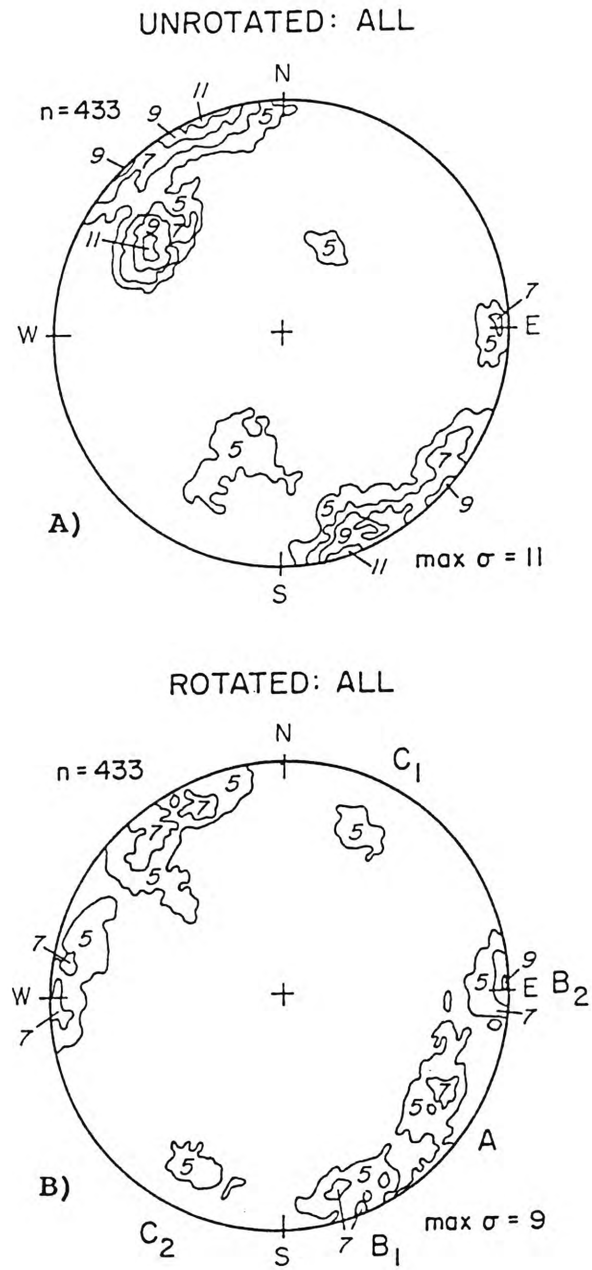

Figure 42. Contoured poles to fractures for all outcrops that included foliation as well as fracture data. **A.** Before rotation to a common horizontal foliation plane **B.** After rotation. A, B_1, B_2, C_1 and C_2 are zones of high pole density referred to in the text, and in Figure 45.

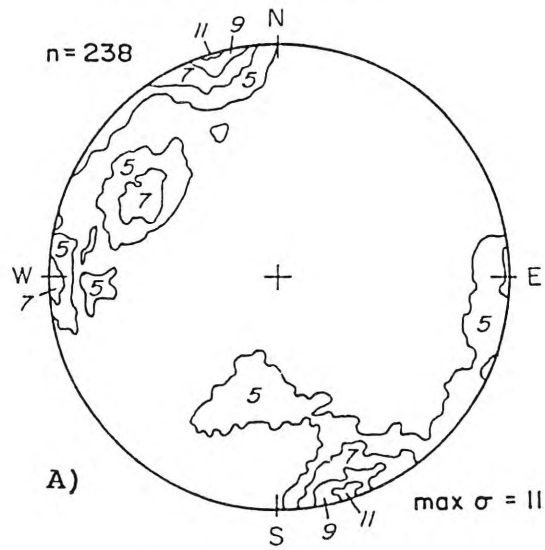

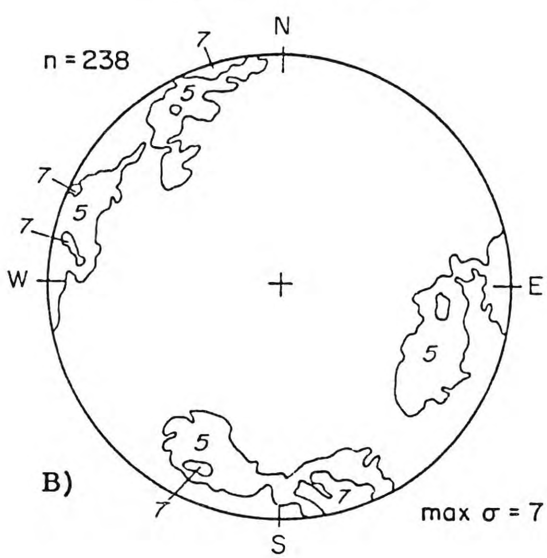

Figure 43. Contoured poles to fractures for gneiss outcrops. **A.** Before rotation to a common horizontal foliation plane **B.** After rotation.

44, A and B). Although the general spread of fracture orientations showed very little change, some differences can be seen between unrotated and rotated data sets. It appears that fracture dips are steeper overall, and perpendicular to foliation. This is to be expected if fractures post-date foliation; fractures form early in the lithification history of sedimentary rocks, and are commonly perpendicular to bedding (Nickelsen, 1974; Hodgson, 1961). Mechanically, the relationship of fractures to foliation bands in rocks of the Farmington Canyon Complex appears to be similar to that of fractures in layered sedimentary rocks.

The data set containing all the rotated fractures (Figure 42 B) shows an interesting grouping around the perimeter of the stereonet. There are two areas of high fracture pole density, 76° apart (B_1 and B_2), approximately bisected by a third group of poles. This central group of poles (A) corresponds to a group of fracture planes striking along azimuth 211° and dipping 75° northwest.

According to Friedman (1963), the maximum principal compressive stress for rock deformation is oriented parallel to a plane bisecting shear planes which are generally 60° apart (Figure 45). In addition, a fourth fracture develops orthogonal to the greatest principal stress if any relaxation of compression occurs (Friedman,

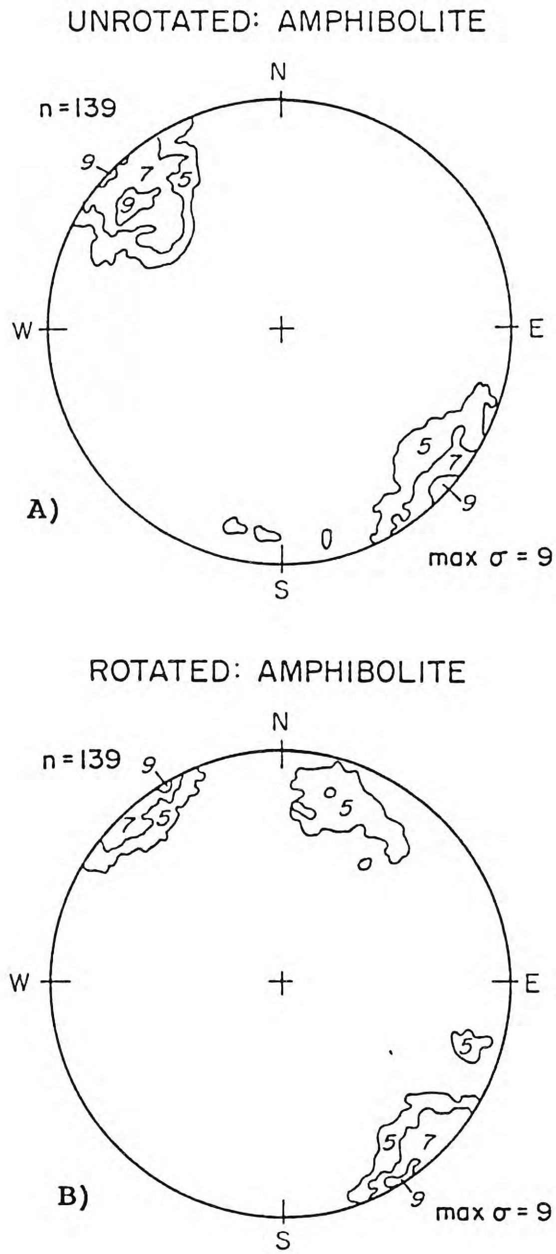

Figure 44. Contoured poles to fractures for amphibolite outcrops. **A.** Before rotation to a common horizontal foliation plane **B.** After rotation.

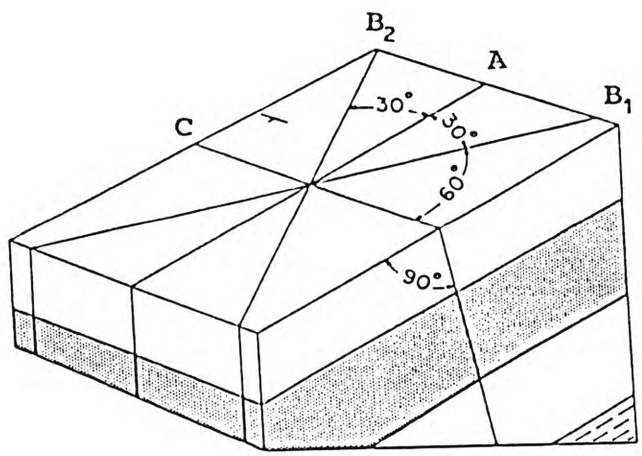

Figure 45. Fractures forming under applied stress. A is parallel to the greatest principal compressive stress. B_1 and B_2 are shear planes 60° apart, bisected by A. C is orthogonal to A, and is a relaxation feature (after Friedman, 1963).

1963).

This model appears to have been reproduced in Figure 42 B. Two less well defined sets of poles to fracture planes are shown in this figure (poles are labelled as C_1 and C_2: fracture set orientations are 294°, 63° SW and 298°, 71° NE) whose orientations fit this model. If foliation planes were approximately horizontal at the onset of regional compression, then the rotated fracture pattern in the metasedimentary rocks of the study area may be associated with regional stresses leading up to the Sevier and Laramide orogenies. Similar patterns have been observed in structural forelands by Engelder (1982), Engelder and Geiser (1980) and Babcock (1973). In the Farmington Canyon Complex, such a pattern may subsequently have been broken up by folding and faulting associated with intense deformation during the Laramide orogeny.

If the idea of shear planes is ignored, figure 42 B can be interpreted differently: the planes corresponding to C_1 and C_2 could represent the orientation of the greatest principal stress during Sevier/Laramide compression, and the set of planes corresponding to A could be relaxation fractures which developed after the end of compression. This is more consistent with the estimated <u>southeasterly</u> trajectory of compression during the Sevier orogeny (Hollet et al., 1978).

Influence of Faults

Fracture and foliation orientations at outcrops were also grouped according to their position with respect to mapped faults. The analyses in the previous section showed that fractures in outcrops adjacent to faults are non-randomly oriented at 95 percent confidence. For the two faults considered, the contoured hemisphere plots (Figures 46 A and B) are very similar to the overall orientation of fractures shown in Figure 39.

Mapping Fracture Data

Another way to account for spatial variability is to map the data. The spatial distribution of rock types and faults within the study area is shown in Figure 11. This geologic map shows observed and inferred outcrop patterns, lithologies, and best estimates of strike and dip, taken from foliated gneisses and interbedded gneiss and pegmatite. The variety of lithologies has been generalized into amphibolite, pegmatite, and gneissic rocks (generally felsic gneiss).

The strikes of principal fracture sets for the entire study area, presented (as poles) in stereonet form in Figure 39, are shown in Figure 47. Only the strikes are shown here for simplicity; this is justified because the majority of fracture dips are relatively uniform and steep. This figure illustrates the fact that the majority of sampled fractures are roughly perpendicular to the

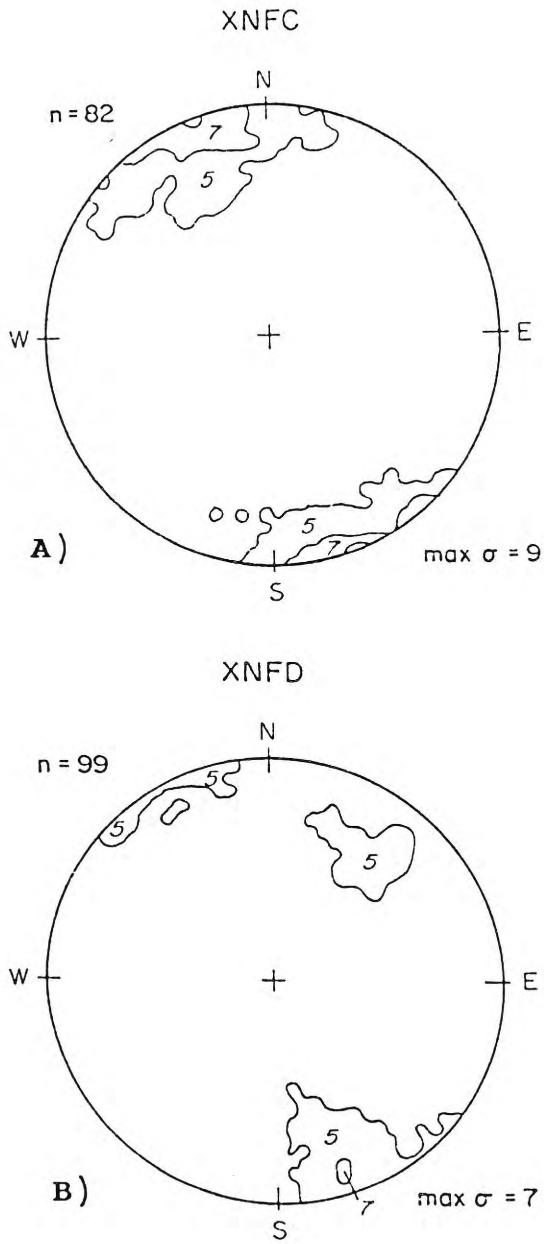

Figure 46. Contoured poles to fractures adjacent to faults in the study area. **A.** Data set XNFC, corresponding to the fault labeled C in Figure 11. **B.** Data set XNFD, corresponding to the fault labeled D in Figure 11.

summit ridge. It is not known how much of this pattern is the result of sampling bias.

Figure 48 shows the orientations of fracture intersection lines calculated from the "principal orientations" data set, for geomorphic regions 1 through 8. The spread of orientations is generally smaller for intersection lines than for the fracture planes themselves, with the exception of region 7. The overall trend is northeasterly, as shown in Figure 49; but there are local exceptions, such as in regions 3 and 4, where two of the three principal trends are sub-parallel to a fault running through the area. In region 7, several diffuse trends exist; they coincide with more intense faulting in that locality. Because of this inconsistency, it is not clear exactly what geometric relationship exists between the orientation of fracture intersections and the trend of faults.

Aerial Photograph Analysis

Stereoscopic aerial photographs at 1:12000 scale, taken in 1980 and 1981, were used to develop a rose diagram of all visible surface lineaments in the study area (Figure 50). These lineaments trend most strongly toward azimuths 185°, 295° and 355°. The generally north-trending group is sub-parallel to the Wasatch Fault; the other is oriented northwest, approximately 60° from the first.

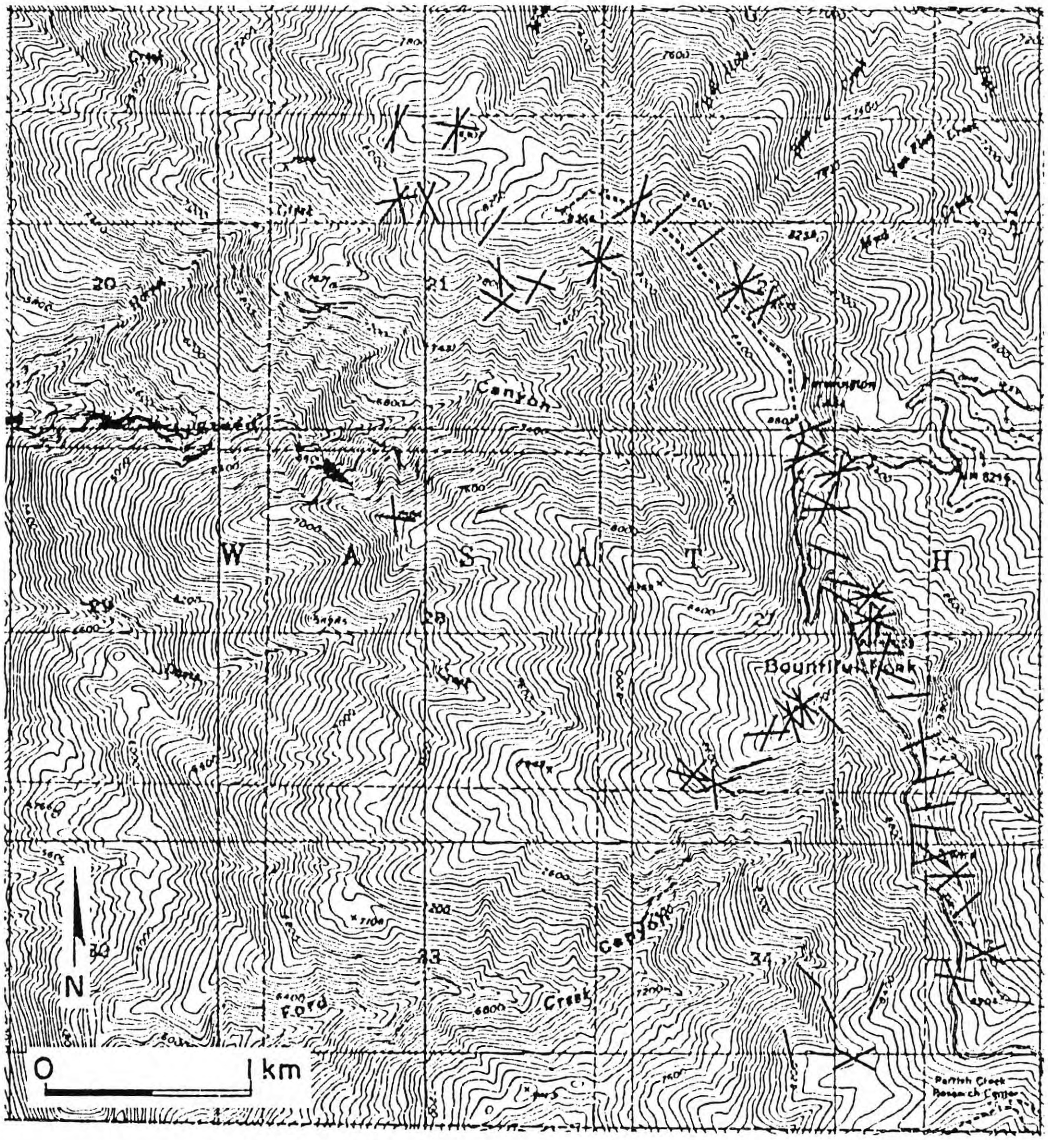

Figure 47. Strikes of the principal fracture sets in the study area.

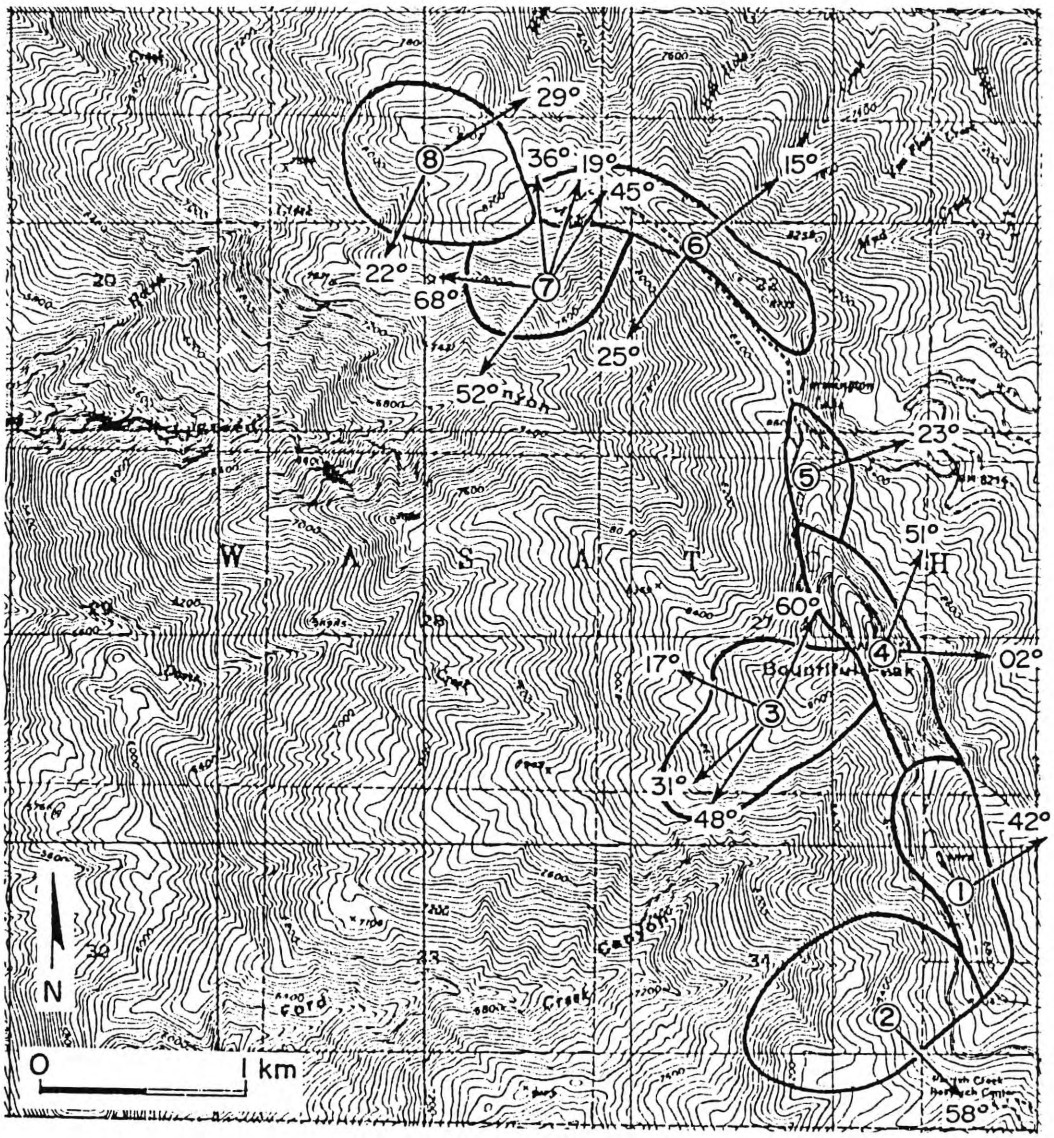

Figure 48. Trend and plunge of the principal sets of fracture intersection lines for regions 1 through 8.

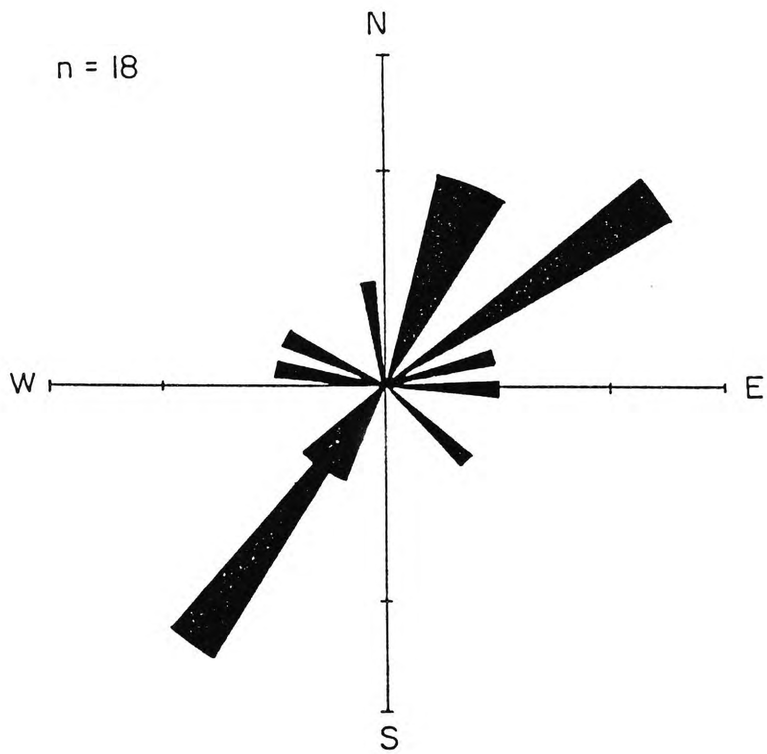

Figure 49. Rose diagram of the trends of intersection lines mapped in Figure 48.

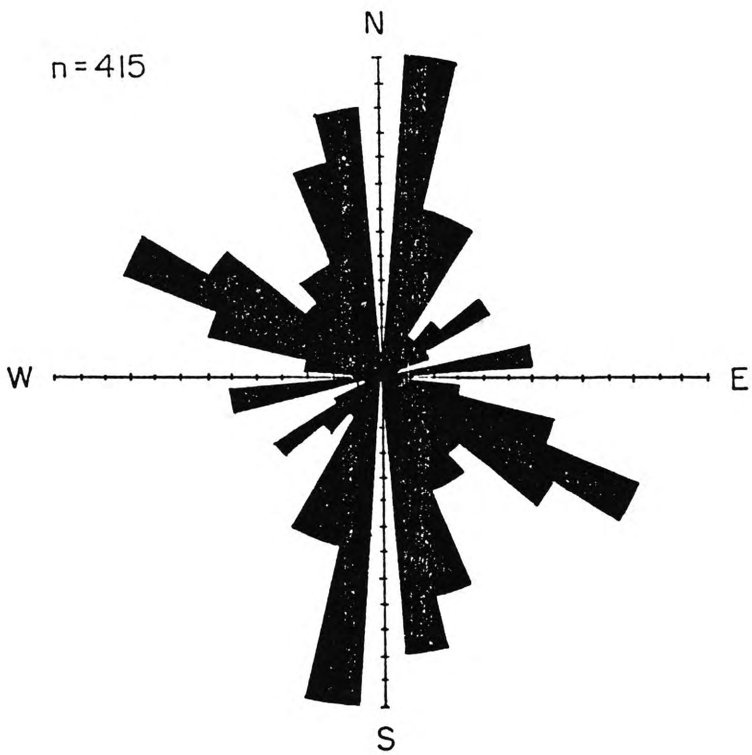

Figure 50. Rose diagram of all structural lineaments in the study area visible in stereoscopic color aerial photographs at 1:12000 scale.

The structural lineament groupings correspond well with the principal trends (approximately 180° and 290°) of large-scale faults in the study area. These were taken from Bryant (1988), and also independently interpreted from 1946 1:20000-scale black and white aerial photographs; some sections were checked in the field. They are shown as dashed lines in Figure 11. The trends of these two groups of lineaments are perpendicular and oblique to the overall (westward) topographic slope. They also appear to be rotated westward from the generally north-trending regional orientation of faults in this section of the Wasatch Front, seen in Figure 10.

Many of the creeks in the vicinity of the study area have a linear appearance. The easiest places for streams to erode should be where the bedrock is already weakened by tectonic deformation. Thus it is believed that the paths of streams reflect the trends of faults or fracture zones in the bedrock. The general trend of stream channels is approximately 270°.

Large pegmatite bodies in the study area crop out across the slope, and trend along a range of azimuths from 302° to 333°. Locally, they dip gently eastward, as shown in the geological map of the study area (Figure 11).

Discussion

Statistical and geological analyses of fractures show that the dominant characteristic of fracture patterns is their great spatial variability. However, lithology is a spatially consistent control on the style and orientation of fracture populations. The distribution of fractures in gneissic rocks is significantly non-random. The principal orientation of fractures in pegmatites is different from those in gneiss and amphibolite.

It is concluded that an overall fracture pattern does exist, which was mainly imprinted by stresses associated with the Sevier and Laramide orogenies. The geological complexity of the Farmington Canyon Complex is responsible for widely disparate <u>fracturing styles</u> at different localities.

Rotation of the fracture sets suggests that:

1) major lineaments in the study area that trend along azimuth 290° are subparallel to the direction of the greatest principal stress during the Sevier orogeny, and that

2) the majority of rotated fractures are orthogonal to this direction (i.e., parallel to the least principal stress during Sevier compression), and therefore may be "relaxation" fractures, which have been further opened by Basin and Range extension. This subsequent extension may also explain why the northeast-trending fractures are better represented at the outcrop than other orientations of fractures in the study area.

Regions classified according to their geomorphology appear to have significantly different fracturing styles. It is most likely, however, that their geomorphology is a function of their geology. It is concluded that regional tectonic stress, followed by folding, and compounded by lithological variation, along with an unknown degree of topographically induced sampling bias, has resulted in the observed distribution of fracture and foliation orientations in the study area.

HYDROGEOLOGIC IMPLICATIONS OF BEDROCK STRUCTURE

This section integrates information from multiple sources in an attempt to comprehensively describe the hydrogeology of the Farmington Canyon Complex in the study area. Before addressing the the hydrological implications of the bedrock structure, some general properties of this and other consolidated bedrock aquifers are discussed.

Regional Hydrogeology in the Basin and Range

Circulation of ground water through deep flow systems contributes significantly to the hydrologic balance in the southwestern Basin and Range province. Miflin (1968) emphasizes the importance of interbasin flow for the Nevada water budget. He states that avenues for water transport through carbonates exist at great depths along shear zones created by intense and repeated structural deformation associated with the development of the Basin and Range. Continuous interbasin flow has maintained or enlarged these flow routes. The author mentions that deep flow systems may also be present in lithologies other than carbonates (Miflin, 1968).

In the Death Valley salt pan of California, major differences in water chemistry were found between springs on the eastern and western edges of the salt pan (Hunt and Robinson, 1960). The authors attribute this to interbasin flow along faults connecting the eastern springs to

Mesquite Flat, 16 km northwest in an adjacent basin. Springs on the western edge are linked to Ash Meadows Springs, 80 km to the east (Figure 51). The differences in water chemistry shown in Figure 52 support the authors' hypothesis.

Recharge from mountain blocks bordering alluvial valleys in the Basin and Range province accounts for a substantial portion of the available ground water. Extensively fractured bedrock, underlying saprolites and colluvium, can constitute a large ground-water reservoir (Mundorff et al., 1963). Discharge is via springs, or directly into the valley alluvium at depth (Figure 53).

Hydrogeology of the Farmington Canyon Complex

Little has been written about the hydrogeology of this part of the Wasatch Front. A study by Feth (1964) shows evidence of recharge to the Jordan Valley (Lake Bonneville sediments) from the Farmington Canyon Complex. He cites water chemistry similarities, analogous seasonal level fluctuations in mountain and valley water tables, and the position of equipotential lines in concluding that the mountain block is an aquifer which provides significant recharge to the basin reservoir. Feth (1964) also mentions that during the construction of Gateway Tunnel, a water supply tunnel dug parallel to the Weber River, a ground-water source was encountered approximately 305 m into rocks of the Farmington Canyon Complex, which yielded a steady discharge of 19 to 38 l/s.

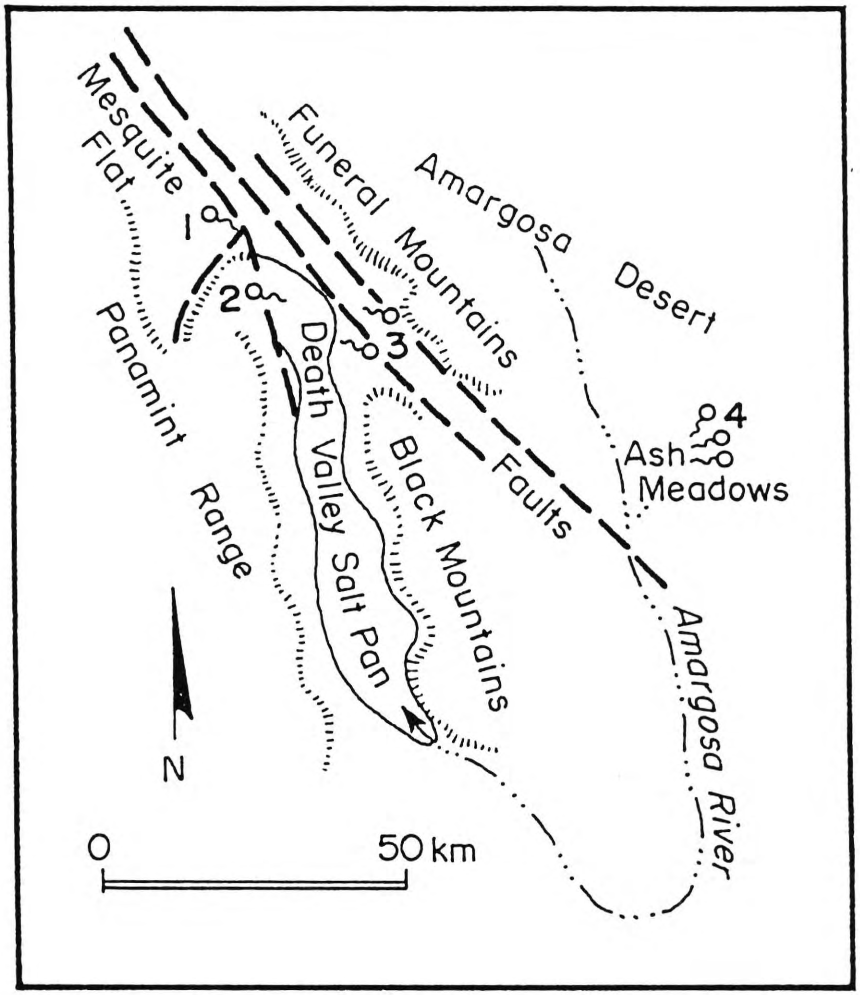

Figure 51. Location map of the four springs discussed in the text (after Hunt and Robinson, 1960).

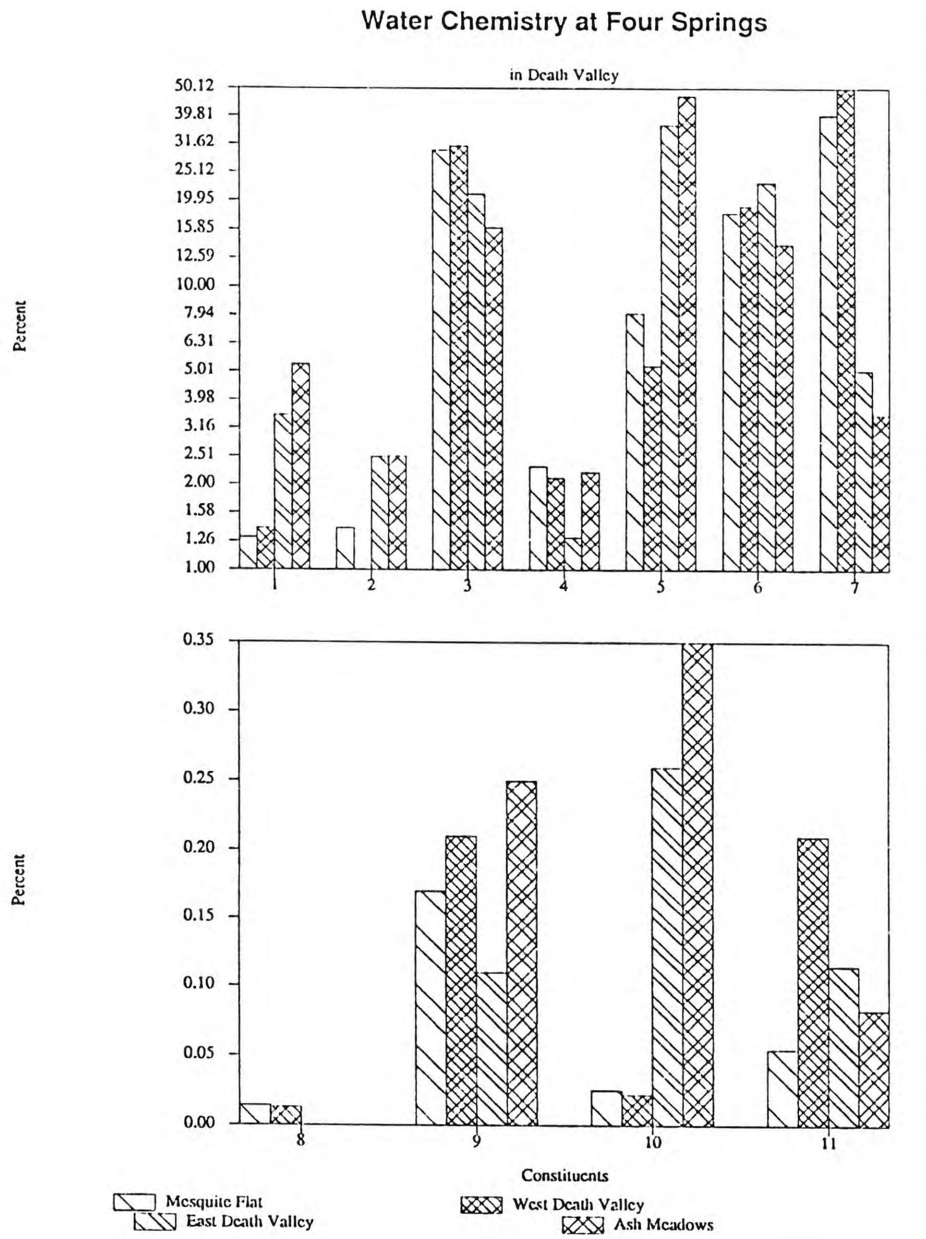

Figure 52. Histograms comparing the water chemistry of springs at Mesquite Flat (1), western Death Valley (2), eastern Death Valley (3) and Ash Meadows (4). 1=Ca; 2=Mg; 3=Na; 4=K; 5=HCO_3; 6=SO_4; 7=Cl; 8=As(x100); 9=Sr; 10=F; 11=B (adapted from Hunt and Robinson, 1960).

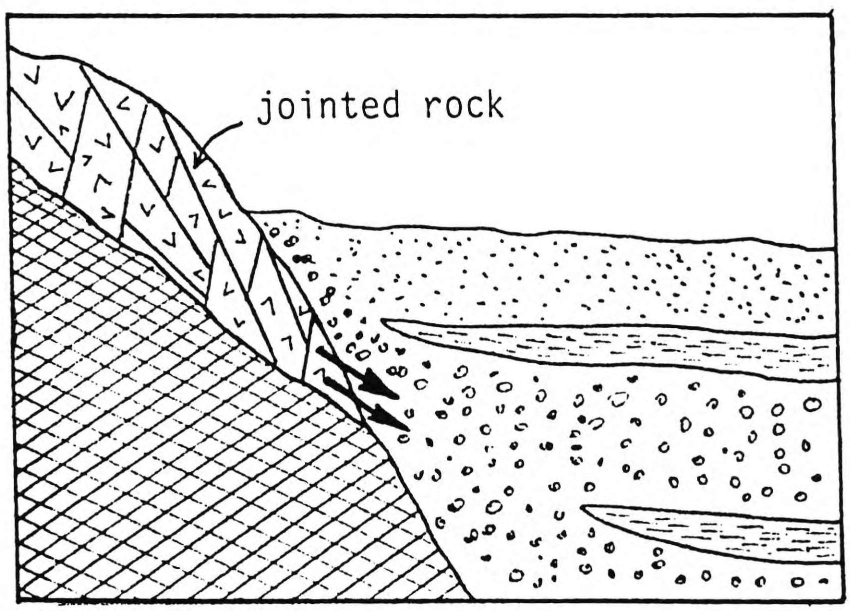

Figure 53. Schematic diagram suggesting paths by which recharge through jointed crystalline rocks reaches aquifers in alluvial basins (after Feth, 1964).

Feth's study is primarily concerned with the state of the alluvial aquifer at the base of the Wasatch Front. He does not discuss ground-water discharge within the mountain block, which is the concern of this study. The cross-sections in Figure 54 were developed from investigations in the study area. They show inferred downslope ground-water flow paths, and different bedrock controls on ground-water discharge. The locations of these cross-sections are shown in Figure 11.

Many springs and seeps are known to exist along the Front (Skelton, 1990; Olson, 1985). A number of springs in Rudd Canyon were developed to supply water for the town of Farmington. These springs were abandoned when they could no longer meet demand and a water supply aqueduct became available (Keaton, 1987).

A number of springs were observed in the study area during the summer of 1988. Outflow from one of these (shown with a star in Figure 11) was measured on a daily basis after a significant local rain on August 8, 1988. A best-fit recession curve was plotted for these data (Figure 55). Recession curves can be used to estimate aquifer properties, including specific yield (Weeks, 1964; Domenico, 1972). Fractured aquifers in crystalline rock generally have low porosity, and therefore low specific yield (Freeze and Cherry, 1979).

The base discharge for the spring is unknown; but the

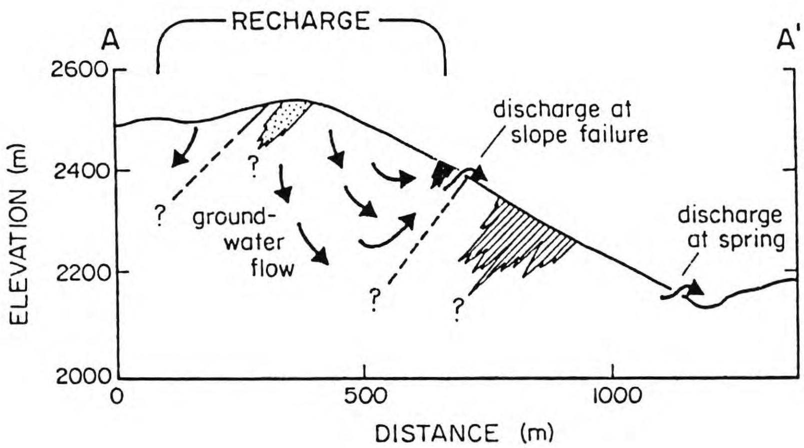

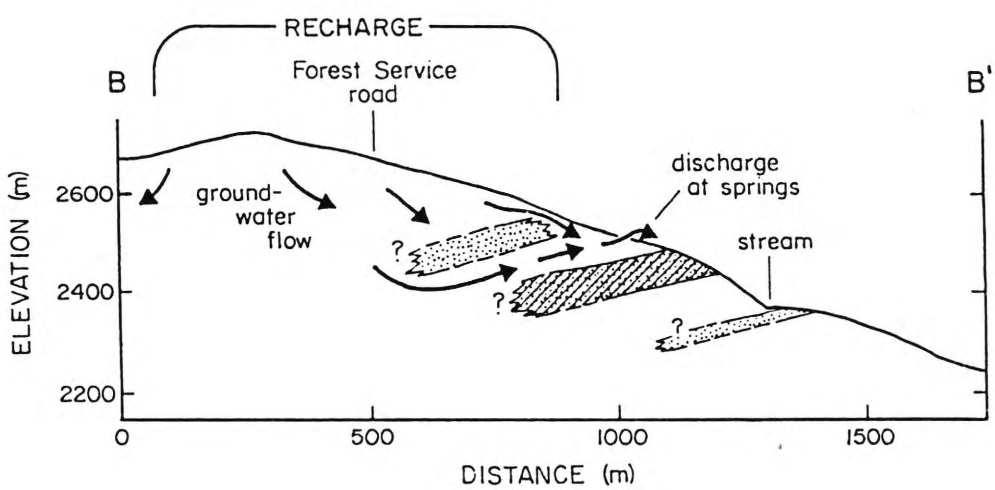

Figure 54. Geologic cross-sections AA' and BB' from Figure 11. Arrows show inferred paths of ground-water flow. Discharge is due locally to the influence of faults or lithologic contacts.

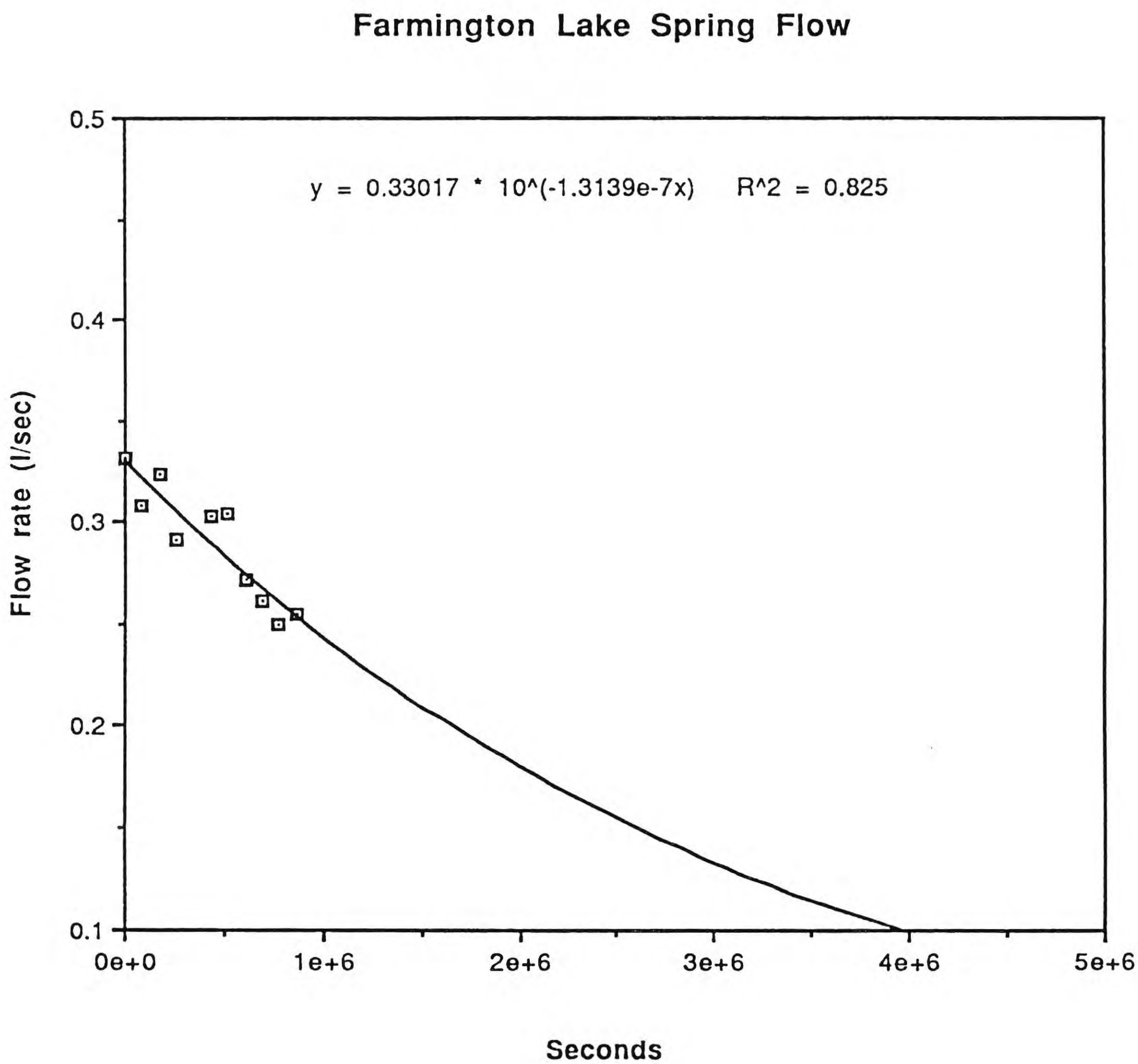

Figure 55. Decline in spring flow after a rainstorm on August 8, 1988. Time (x-axis) is measured in seconds, starting from 0 at the time of the first measurement.

presence of a large pond fed by this and other local springs implies that it does not dry up completely during the year. Projected forward, the spring discharge curve decreases to 0.1 l/s in just over 46 days. The total volume of water discharged by the spring over this time is approximately 765,695 l, or 766 m^3.

This result indicates that the specific yield of the aquifer tapped by this spring is low. This means that for a given recharge volume, the aquifer fills up more rapidly than a porous medium aquifer with a greater specific yield. Thus a critical pore water pressure can be achieved earlier in these fractured rocks than in porous media, assuming the head difference is the same for the two cases.

It could be argued in this case that the rapid decline in spring flow is simply due to the aquifer having a very limited areal extent. A small, highly permeable porous media aquifer would behave in the same way. Indeed, it is likely that structural and lithological heterogeneities compartmentalize the bedrock aquifer to a considerable extent. However, some new springs emerging from debris flow scars in this area have flowed continuously for up to five months after the event. Springs feeding a stream in Lightning Canyon, north of the study area, had a total estimated discharge of 388,000 m^3 for the calendar year 1984 (Mathewson et al., 1990). In view of the inferred low specific yield of the rocks that make up the aquifer, this implies that the areal extent of aquifer compartments can be very great, and that large sections of the subsurface are in hydraulic communication.

Sustained post-storm flow can be seen in the hydrograph of Halfway Creek, a tributary of Farmington Creek, just north of the study area, shown in Figure 56 (Davis County Planning Commission, 1989). A storm on August 10, 1989 caused an immediate rise in the stream level, due to surface runoff. The stream level then decreased to 10 cm above pre-storm levels, and stayed constant for at least 26 hours.

Halfway Creek is in a steep tributary canyon of Farmington Creek. Aerial photographs show that bedrock exposures are common, especially on the southeast-facing flanks. It appears that colluvial cover is minimal on these slopes, particularly on the southeast-facing flanks. In addition, some large contour trenches have been cut into the head of the drainage; these probably enhance recharge to the fractured bedrock. In view of the character of the Halfway Creek watershed, it is concluded that the hydrograph in Figure 56 shows post-runoff drainage out of a fractured bedrock aquifer.

Directional Permeability of Fractured Rocks

The Farmington Canyon Complex consists primarily of crystalline rocks, which generally have very little

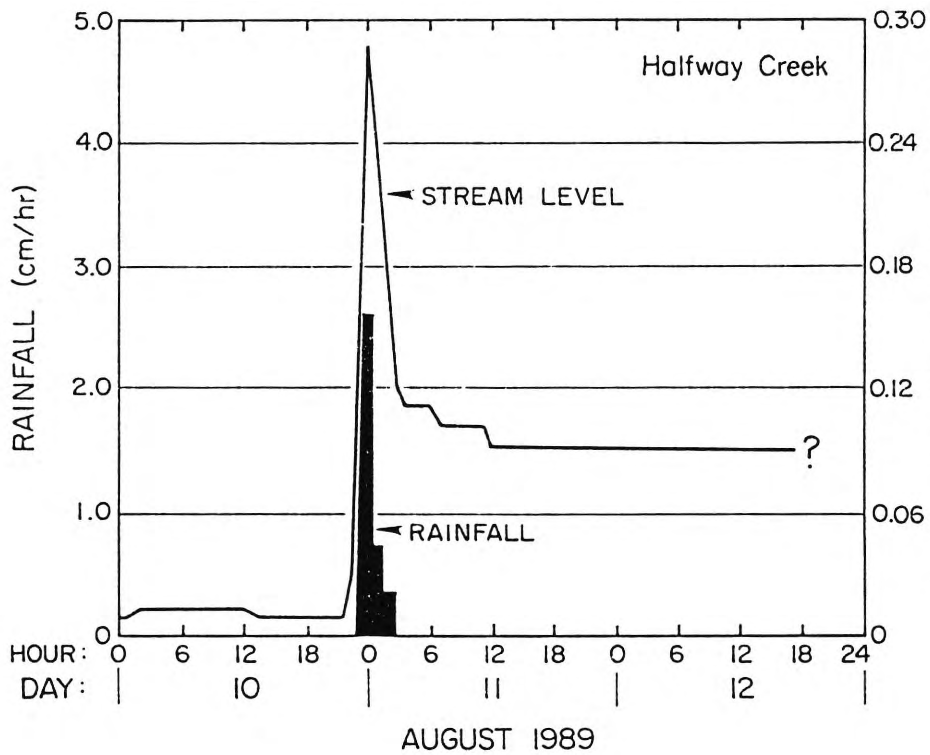

Figure 56. Hydrograph of Halfway Creek, showing the response of stream level to a rainstorm on August 10, 1989.

intergranular porosity. However, the rocks are ubiquitously fractured. In this study, it is assumed that fractures control the porosity and permeability of the bedrock. As a result, the permeability may be highly anisotropic, making it very difficult to predict flow paths (Neretnieks, 1985).

Much work has been done on evaluating reliable permeability parameters in fractured rock. The recent interest in tracing the flow directions of solutes in ground water has added momentum to this research. Studies generally approach the subject from opposite extremes: the microscale (non-continuum) or the megascale (continuum). The megascale approach is to evaluate basin-scale regions in terms of average values of hydraulic conductivity and effective porosity. Results can be very useful but may mask important local anomalies.

Examples of microscale work are papers by Witherspoon and others (1980) and Brown (1987), who discuss the applicability of the parallel plate model for flow through a single fracture, first put forward by D. T. Snow in 1965. The basic equation is derived from Darcy's Law: flow rate is proportional to the difference in hydraulic head and the fracture aperture cubed (Gale et al., 1985, p. 1). The model appears to be reliable in laboratory experiments, for a range of fracture apertures (down to 4 microns), even when surfaces are quite rough (Witherspoon et al., 1980; Brown, 1987).

It is difficult to adapt such detailed theoretical studies to realistic in situ conditions, especially when dealing with an extensive and geologically heterogeneous study area. Complex numerical methods have been developed for this (e.g., Long and Witherspoon, 1985). Another method of characterizing the hydraulic conductivity of an area is to interpolate between known values (such as boreholes) using geostatistical methods (Jones et al., 1985). If fracture density is great enough, the aquifer can be modeled as an equivalent anisotropic porous medium (Greenkorn et al., 1960; Long et al., 1985).

Fracture Connectivity

Long and Witherspoon (1985) found that the degree of interconnection of a network of fractures greatly affects its hydraulic conductivity. LaPointe and Hudson (1985) used a printed electrical circuit board analog to model two-dimensional hydraulic conductivity. They found that the direction of greatest hydraulic conductivity was approximately parallel to the direction of maximum fracture interconnectivity.

Taylor and Fleming (1988) used azimuthal resistivity surveys (Wenner array) to characterize the hydraulic conductivity of fractured rocks. In all cases, they found that the major axis of the resistivity ellipse corresponded to the direction of greatest hydraulic conductivity. This direction also coincided with the direction of greatest joint connectivity (Taylor and Fleming, 1988). Based on this work, it is believed that the principal direction of fracture intersection lines (shown for regions 1 through 8 in Figure 49) is a good indicator of the direction of maximum bedrock permeability, at least in areas unaffected by large-scale features such as faults or major lithological boundaries.

Effect of Large-Scale Features

Regional Ground-Water Flow

The principal trend of faults interpreted from aerial photographs in the study area is 290°. The trend of pegmatite outcrops across the study area is between 302° and 333°. In contrast, the principal strike of fracture sets is 223°, and, based on Figure 49, the principal trends of fracture intersection lines are 22°, 54° and 215°, with very flat plunges. It has not been possible to directly assess the relative contribution of each type of structural discontinuity to regional permeability trends in this part of the Farmington Canyon Complex. Some indirect comparisons have been made using available data, to infer the dominant trend of ground-water transport, and hence to identify the most influential bedrock feature(s).

Figure 57 shows the location of several creeks flowing through rocks of the Farmington Canyon Complex along the Wasatch Front. Discharge data from these creeks

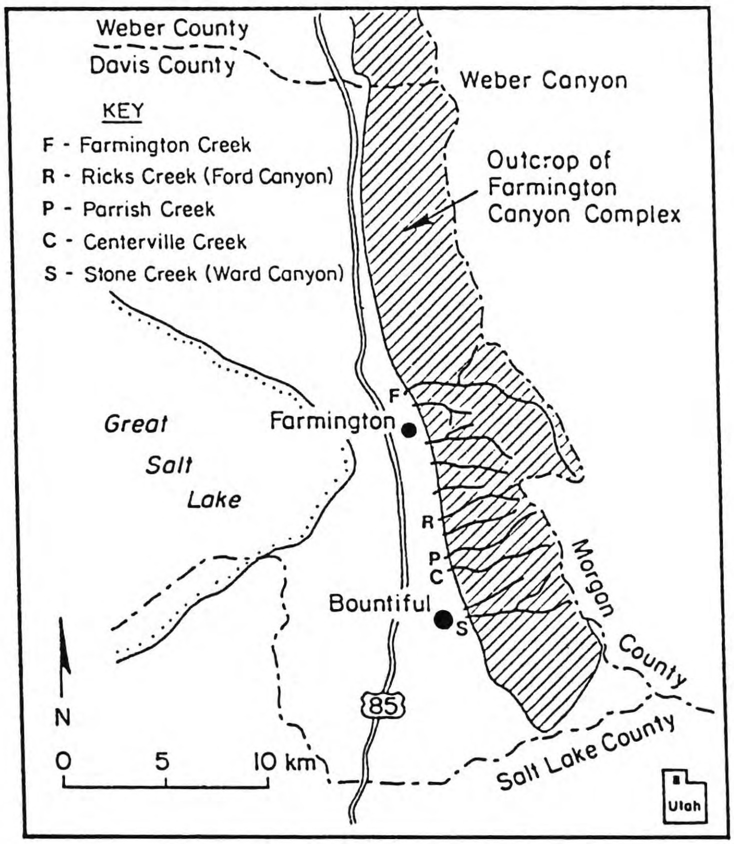

Figure 57. Location of creeks along the Wasatch Front that were used in the comparison of normalized discharge.

for the available years are shown in Figure 58. Discharge data were obtained from United States Geological Survey records, for the years 1952 through 1963. Average annual discharge has been divided by the drainage basin area to normalize the values. Overall, the pattern is of increasing discharge northward. An explanation for this trend is that northwestward "inter-canyon" transfer of ground water takes place at depth along faults and fracture zones.

The exception to this trend is Centerville Creek, which has a higher discharge per drainage area than Parrish Creek even though it is located southward of it. Possible reasons for this are: 1) Centerville Canyon has a different land use history than the other creeks. It is the only one whose pristine condition has been preserved (Croft and McDonald, 1944). Thus, clayey residual soils may be better developed, inhibiting recharge to deep bedrock conduits, and directing interflow back into Centerville Creek. 2) A broad area to the southeast of Centerville Canyon is free of other canyons. Thus Centerville Creek may be recharged by ground water moving along northwest-trending fault zones. The southeast flank of Parrish Canyon is much narrower, so recharge to deep structures is likely to be much less.

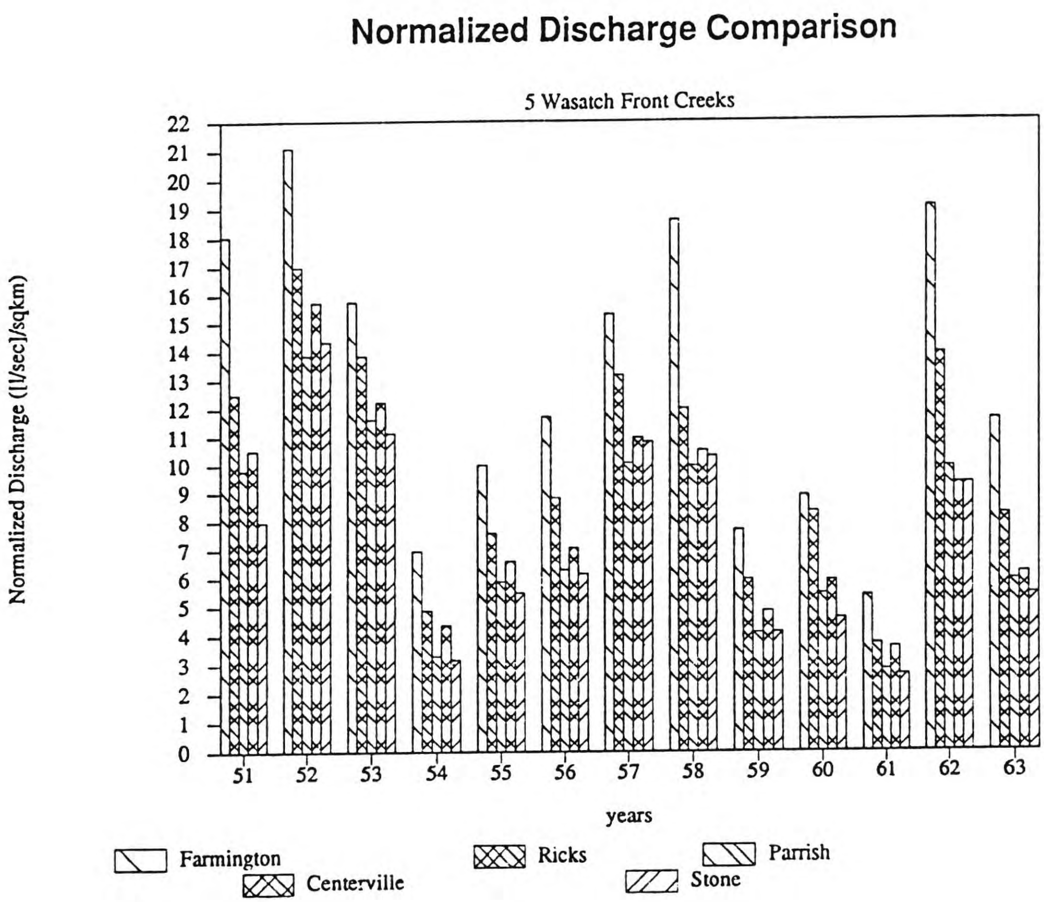

Figure 58. Discharge data for the years 1951 through 1963 show that, except for Centerville Creek, discharge per unit area of drainage increases northward.

Debris Flow Initiation and Prolonged Discharge

The largest debris flow along the Wasatch Front during 1983 was in Rudd Creek. Approximately 63,000 m^3 of material was deposited at the mouth of the creek (Keaton, 1988b). After the debris flow at Rudd, water continued to flow out of the slide scar well into the summer (a small but steady stream was observed there by this writer in August 1988).

Figure 59 shows the topography of the area around the Rudd Creek debris flow scar. Failure occurred at an elevation of approximately 2109 m. Thus the maximum head that could have developed, from the highest point in the recharge area to the failure scar, is approximately 420 m, equivalent to 42 kg/cm^2 in an open conduit. Even through a network of fractured rock, substantial pressures would be generated. However, it seems unlikely that the small recharge area directly above Rudd Creek (shown with a dotted line in Figure 59) could have sufficient storage to provide water for year-round flow.

Taking into account the possibility of cross-slope discharge along a fault, the recharge area for Rudd Creek can be greatly expanded (Keaton, 1988a). The inferred boundary for the <u>structurally-controlled</u> recharge area is shown with a dashed line in Figure 59. In addition, approximately 116 m can be added to the pressure head column above the point of debris flow initiation.

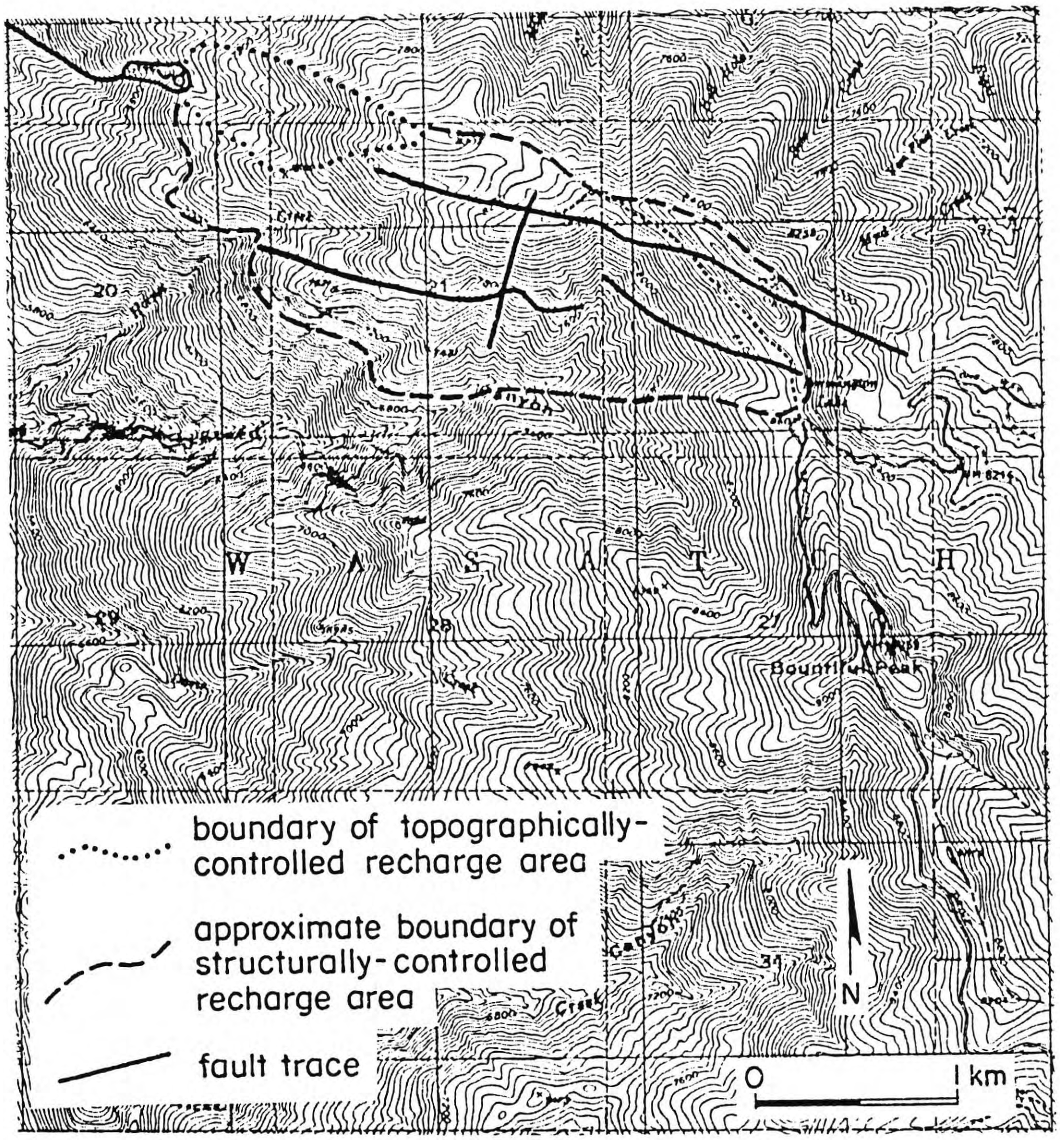

Figure 59. Boundary of the topographically-controlled recharge area for the head of Rudd Creek is shown with a dotted line. Inferred boundary of the recharge area controlled by bedrock structure is shown with a dashed line. Faults are heavy solid lines. Note debris flow failure scar and spring in northwest corner.

Structural Fabric and the Distribution of Slope Failures

Slope Aspect

In order to assess the relative contribution of fractures and faults to the initiation of slope failures, the aspects of slopes (i.e. the direction faced by the slope) on which slope failures occurred were measured for 74 mapped shallow landslides and debris flows (compiled by Lowe, 1989). Slope aspect at the failure scar was determined at the highest point of the failure. A sampling circle with a diameter equal to twice the width of the widest mapped debris flow scar was used to standardize the areas measured. The circle was positioned such that the topographic contour nearest to the failure scar touched the circle on diametrically opposite sides. The direction of the (downslope) normal to this diameter was taken to be the aspect of the slope failure.

It was thought that slopes perpendicular to structural features conducting significant amounts of ground water would have the greatest chance of experiencing high pore water pressures leading to slope failure. Conversely, slopes parallel to discontinuities would have little chance of intersecting major ground-water pathways, and should therefore have fewer slope failures. This analysis assumes that all other conditions are the same for the slopes.

Figure 60 shows that the majority of slope failures occurred on slopes facing azimuth 290°. This corresponds to the orientation of large scale structural lineaments in the study area. There are very few slope failures on slopes facing azimuth 110°, diametrically opposite 290°. This is because of the general westward aspect of this section of the Wasatch Front.

There is no increase over background in slope failure occurrences for any other azimuth. Therefore, it does not appear that the main trends of fractures, fracture intersection lines, or pegmatites in the study area play a significant role in the regional control of ground-water flow paths. However, these may be more important in contributing to local failure mechanisms, as discussed below.

Daylighting Fracture and Foliation Planes

There is some evidence that gently-dipping bedrock discontinuities exert a more localized control on the initiation of debris flows. One of the possible failure mechanisms discussed earlier involved gently-dipping fracture and foliation plane sets intersecting the slope at the base of the soil mantle, and thus allowing communication between the bedrock aquifer and the surface (Figure 4). For these gently-dipping planes, dip direction rather than strike was considered to be more important in controlling ground-water flow paths.

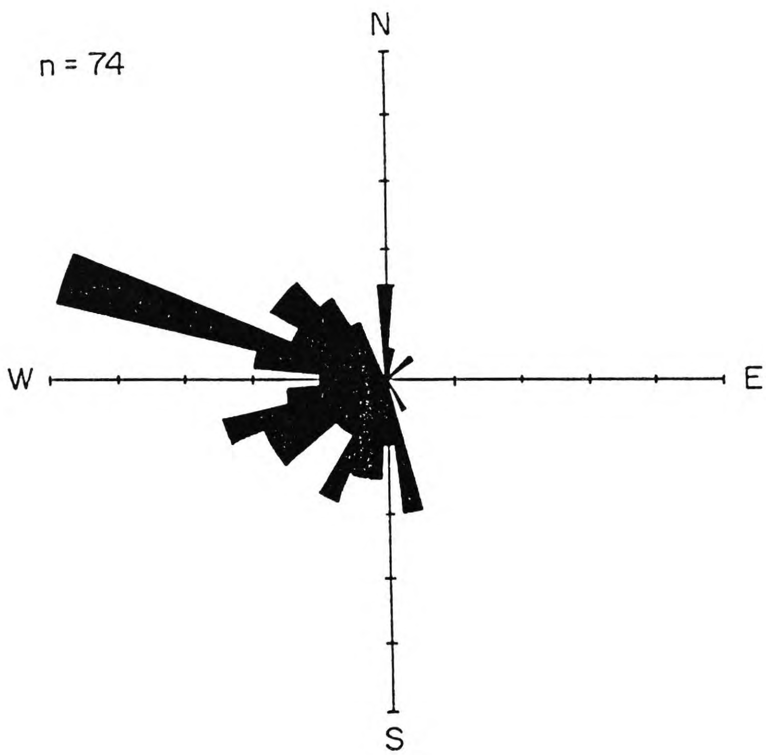

Figure 60. Slope aspect, shown as the normal to the trend of the slope, for 74 mapped slope failures.

Figure 61 shows the location, dip angle, and dip direction of principal foliation planes and fractures that dip less steeply and up to 10° steeper than the topographic slope. (The latter were included because slope angles might locally be steeper than the mean angle calculated from the topographic map). Figure 62 is a rose diagram of the dip directions mapped in Figure 61. Three major trends are apparent; toward azimuths 45°, 235° and 296°.

The location of data points depended on the distribution of accessible outcrops, so the direct utility of this analysis is limited with respect to areas susceptible to soil slips or debris flows. Most of the gently-dipping discontinuities were found on ridges, where there is little or no soil cover, and no hydrostatic column within the aquifer. The swales, where such data would have been most useful, were often covered by vegetation, or were too remote. However, the fracture and foliation sets shown in Figure 61 may persist within the local area, so it may be possible to extrapolate the effect of daylighting planes to swales adjacent to the outcrops shown. Information from Figure 61 forms part of the composite map of structural features and mapped slope failures compiled by Lowe (1989), shown in Figure 63 (in pocket).

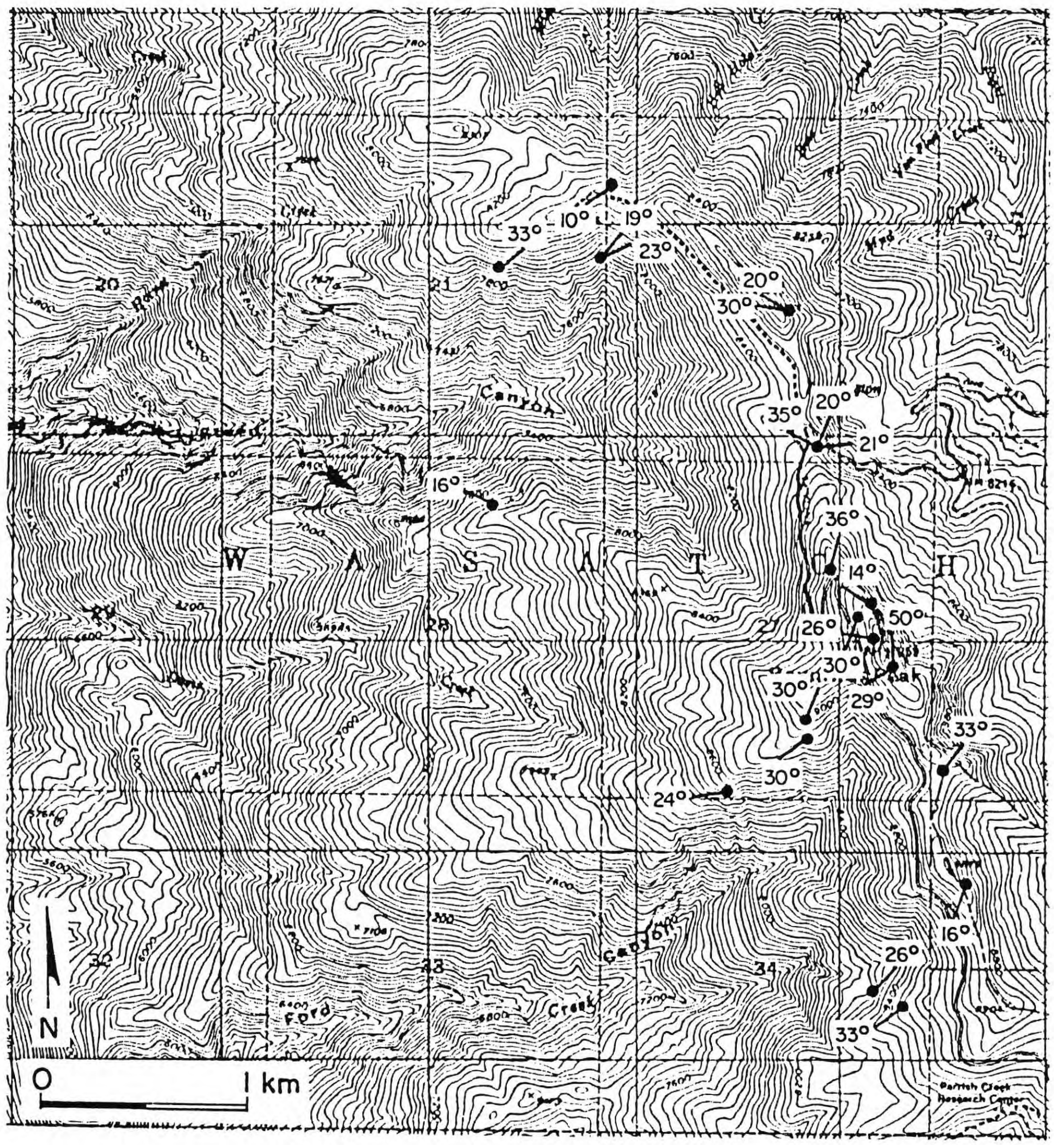

Figure 61. Location, dip directions and dip angles of principal fracture sets that dip less steeply, and up to 10° more steeply, than the topography.

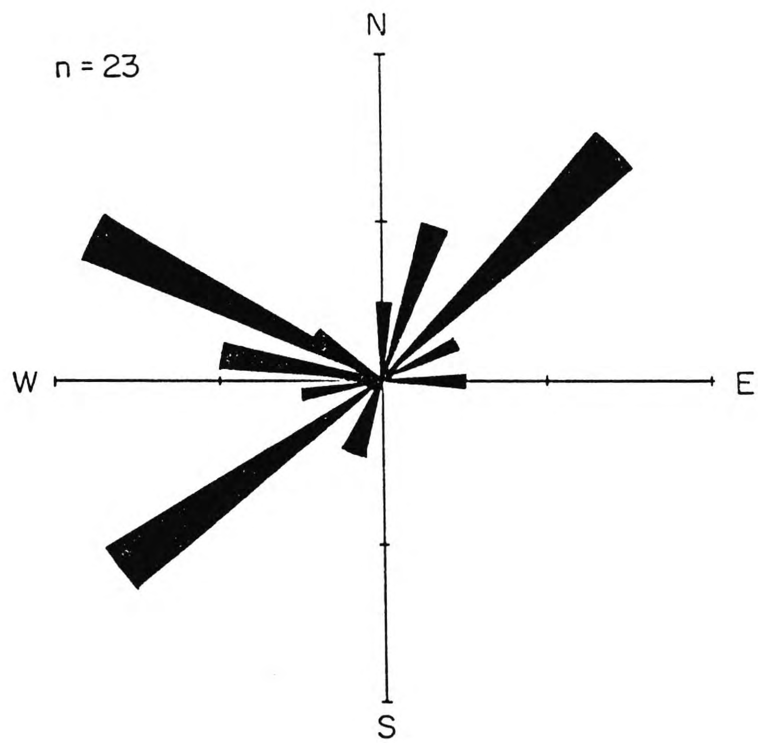

Figure 62. Rose diagram of the dip directions of low-angle discontinuities mapped in Figure 61.

Another thing to note about Figure 62 is that many of the locations are included because of having extremely steep slopes rather than extremely flat discontinuities. Such steep slopes are unlikely to be the sites of landslides or slope failures, because of a lack of soil development. However, the locations do correlate with several rock failures observed in the study area, particularly on the east side of the ridge crest.

Gently-dipping contacts between gneiss and pegmatite were also proposed as potential sites for ground-water discharge and/or slope failure (Figure 5). In Ford Canyon, a shelf-like pegmatite outcrop trends across the slope, and is associated with several springs and at least one recent shallow soil slip (Figure 64). Pegmatite outcrops have also been included in Figure 63 (in pocket).

Discussion

What appears to exist in the region are two separate structural and ground-water environments, conceptually divided into "shallow" and "deep". Each exerts different controls on ground-water flow. Where they are in communication, the potential for prolonged discharge or a rise in pore water pressure is increased. Thus, the controlling influence on ground-water discharge of a given spring or seep is how well it is connected to a high volume compartment within the aquifer.

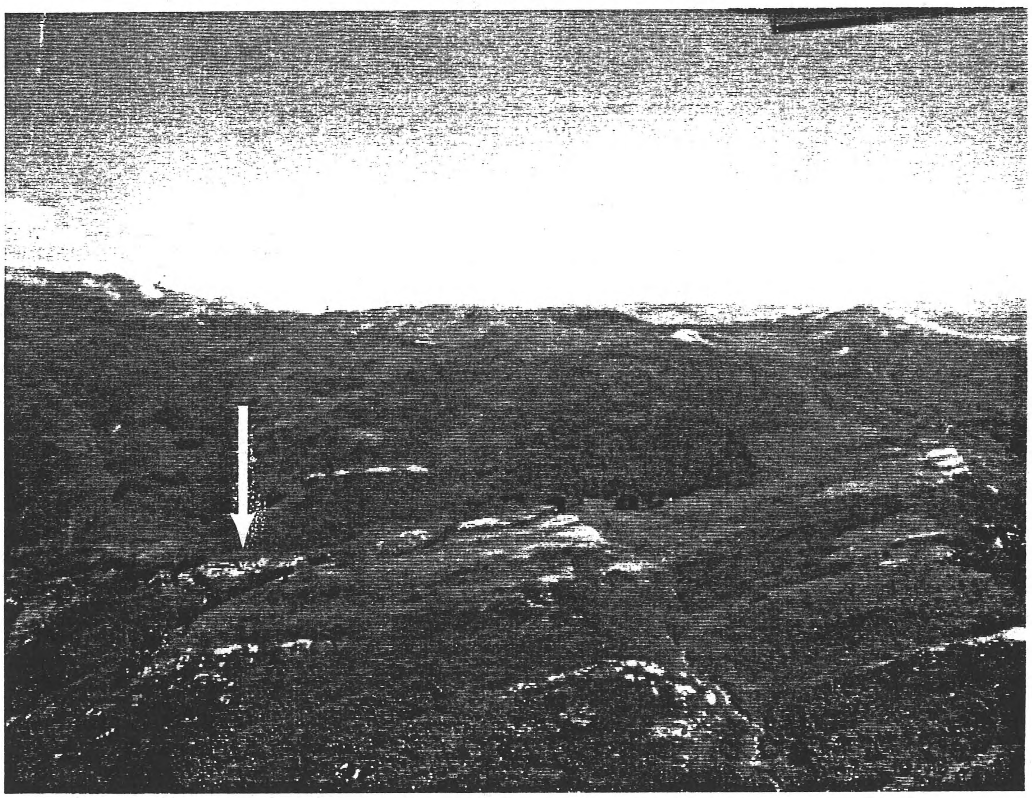

Figure 64. Oblique aerial photograph (looking east) of pegmatite outcrops cutting across slopes in the study area. Arrow shows Ford Canyon swale (site of a WADI survey) underlain by a pegmatite unit. Directly west of the flat swale is a wide, shallow soil slip.

At a regional scale, major structural lineaments may be responsible for significant cross-slope transport of ground water. More locally, heterogeneities in lithology and bedrock discontinuities control the distribution of discharge points. The cross-slope trend of low-permeability rock units, together with the dip directions of low-angle discontinuities (Figure 62) identify the particular slopes on which ground-water discharge is more likely to take place.

GEOPHYSICAL SURVEYS

Introduction

Three geophysical surveys were conducted in the study area to get an idea of bedrock structural fabric at depth. The VLF (very low frequency) electromagnetic method was used, with a hand-held receiver marketed under the name of "WADI" by Saga Geophysics of Austin, Texas. The instrument makes use of an existing 15-30 KHz EM field emitted by various stations around the world, normally used for worldwide navigation purposes.

Theory

The horizontal component of the magnetic field reaches the study area. When a steeply dipping planar subsurface conductor (for example, a fracture containing ion-rich water) is encountered by the primary field, eddy currents are induced on the edges of the conductor; an associated vertical magnetic field is induced. The WADI measures the addition of the primary (source) and secondary (induced) fields, thus yielding a ratio of $([e_p+e_s]/e_p)$ denoted as "ECD" (equivalent current density), where e_p is the in-phase component of the primary magnetic field and e_s is the in-phase component of the secondary magnetic field. In this way, conductive planar features in the subsurface are recorded as positive anomalies over a background established for the survey.

The magnitude of the quadrature, (i.e. the vertical, out-of-phase component) of the secondary magnetic field gives a measure of the capacitance, or ability to hold current, of the subsurface conductor. The larger the quadrature, the greater the capacitance of the feature; thus fractures filled with saturated clays or metallic mineralization, being excellent conductors, should have high values for both ECD and quadrature. Fresh-water-bearing fractures are much less conductive, though still more conductive than most rock, especially dense metamorphic rock; thus they do not hold current well, and should have lower quadrature values (Morgan, 1990; Saga Geophysics, 1989).

Intact cystalline rocks typically have very high resistivities, as shown in Table 6. Therefore, saturated fractures or fracture zones are likely to be represented by lower resistivity (higher conductivity) values over a background established in rocks of the Farmington Canyon Complex. These would be recorded as positive conductivity anomalies by the WADI.

For this study, anomalously high ECD values occuring in conjunction with low quadrature values were taken to be water-bearing fractures. The following hypothesis was advanced: linear conductivity anomalies are water-bearing fractures that represent preferential pathways for ground-water flow through bedrock. Conversely, if the bedrock is so pervasively fractured that it is isotropically and homogeneously permeable to ground water, conductivity values will be relatively uniform.

Table 6. Resistivities of some consolidated and unconsolidated rocks. Note that unconsolidated sediments have much lower resistivities than consolidated rocks (adapted from a table compiled by Heiland, 1968).

Material	Locality	Res.(Ohm-m)
Lab specimens:		
Garnet gneiss	Bavaria	$2x10^9$
Hornblende gneiss	Mineville	$1-6x10^{10}$
Gray biotite gneiss	Mineville	$4x10^{10}$
In situ:		
Graphitic schist	Normandy	$1-10x10^5$
Schists	Missouri	$2-60x10^5$
Hard calc. schist	Belgian Congo	$2-11x10^6$
Mica schist (hard packed)	Washington D.C.	$1.3x10^7$
Quartz porphyry (slightly altered)	Newfoundland	$3.4x10^6$
Slightly altered syenite	Ontario	$2.4-3.7x10^7$
Serpentine	Ontario	$2.1-5.3x10^6$
Clays with Mg salts	Australia	1-2
Wet clay	New Jersey	51
Dry clay	New Jersey	80
Alluvium (moist)	Montana	23
Silt (dry)	Montana	20

Survey Techniques and Results

A VLF transmission station in Seattle, Washington was used for all the surveys. This station transmits a 125 kW, 24.8 kHz signal; thus its wavelength is approximately 20 km (Halliday and Resnick, 1978). As discussed below, it is preferable to use at least two transmitters for any VLF survey, but this was not done in the study area.

Steed Canyon Survey

A VLF survey was carried out in Steed Canyon, in two adjoining swales along the northern flank of the canyon (Figure 65). The eastern swale is the site of a 1983 landslide and debris flow that has been studied by researchers at Utah State University (Brooks, 1986; Monteith, 1988). The bedrock in this area consists of layered to migmatized gneiss, some of which grades into amphibolite. No pegmatites were found in the surveyed area. The two swales contain a relatively thicker soil column than the surrounding slopes.

Four parallel conductivity profiles were recorded at this site. Each reading was spaced 10 m apart, and profiles were 30 m apart. The results were contoured in separate maps for ECD and quadrature, shown in Figures 66 and 67.

Figure 68 shows the general topography of the survey area. In the east swale, ECD values are generally low. There is an elongate zone of higher ECD on the eastern flank of the ridge separating the two swales; this also corresponds to a quadrature high. This feature is interpreted to be a north-trending fault or fracture zone containing moist clayey material. In the west swale, there is a relatively higher ECD zone trending northwest across the swale axis. There is no increase in the quadrature over the area, so this feature could be a

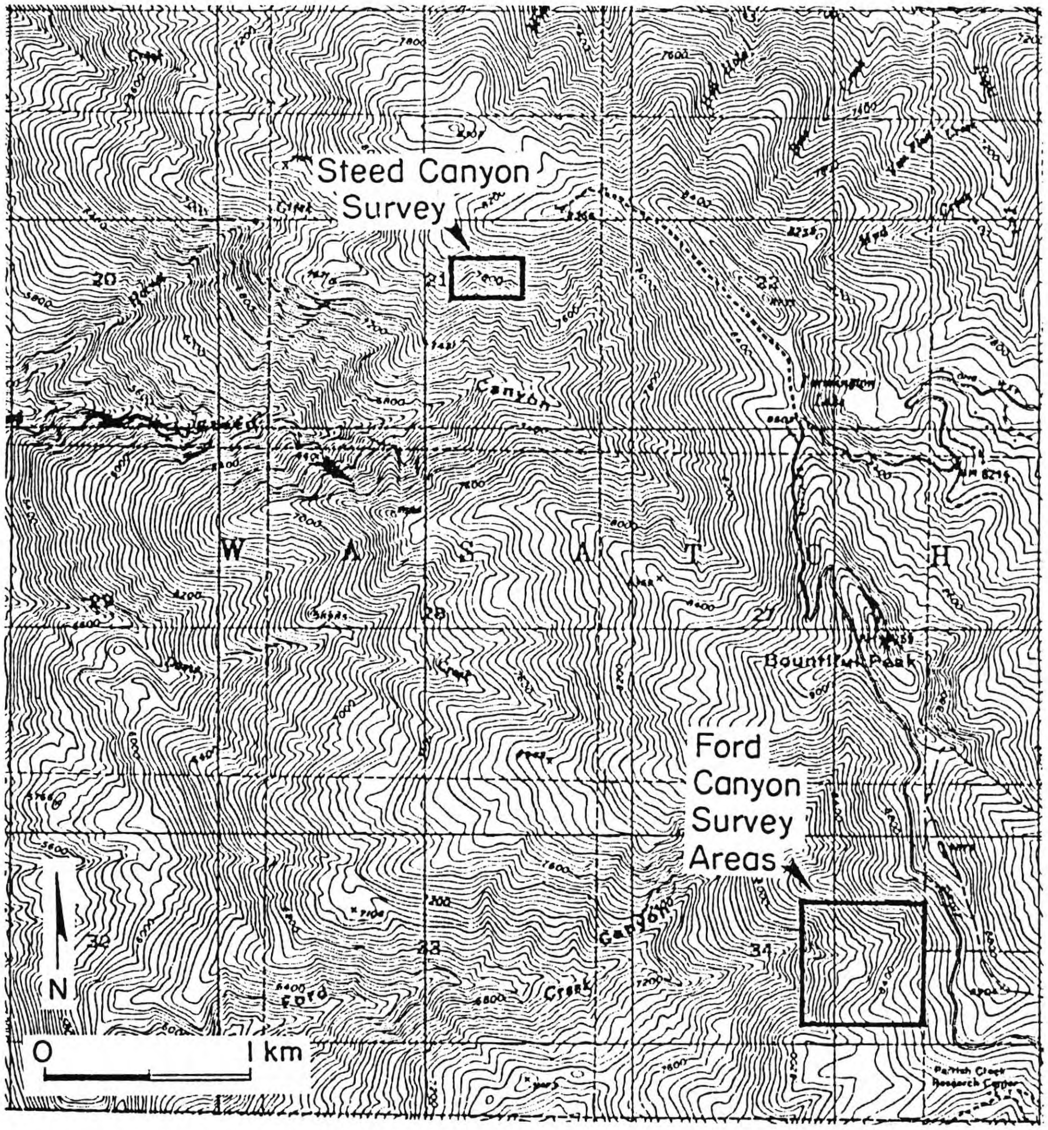

Figure 65. Location of the WADI surveys in Steed and Ford canyons.

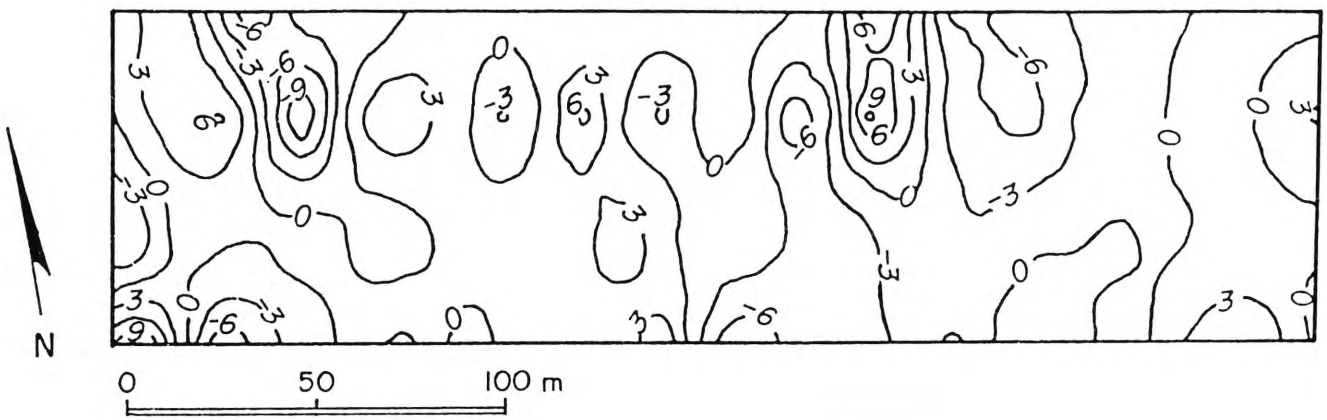

Figure 66. Contoured ECD values from the Steed Canyon WADI survey. Conductivity anomalies trend north in the east swale, and northwest in the west swale.

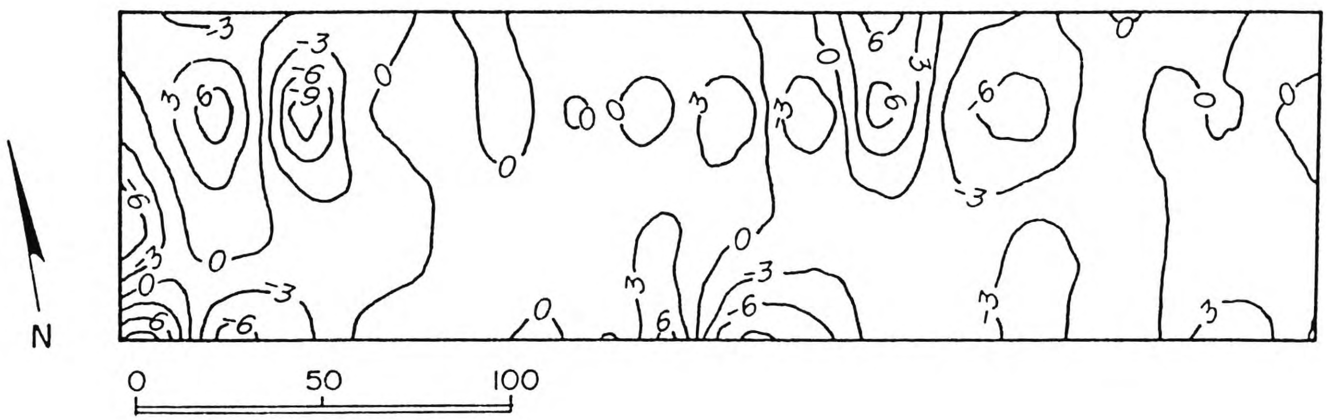

Figure 67. Contoured quadrature values from the Steed Canyon WADI survey.

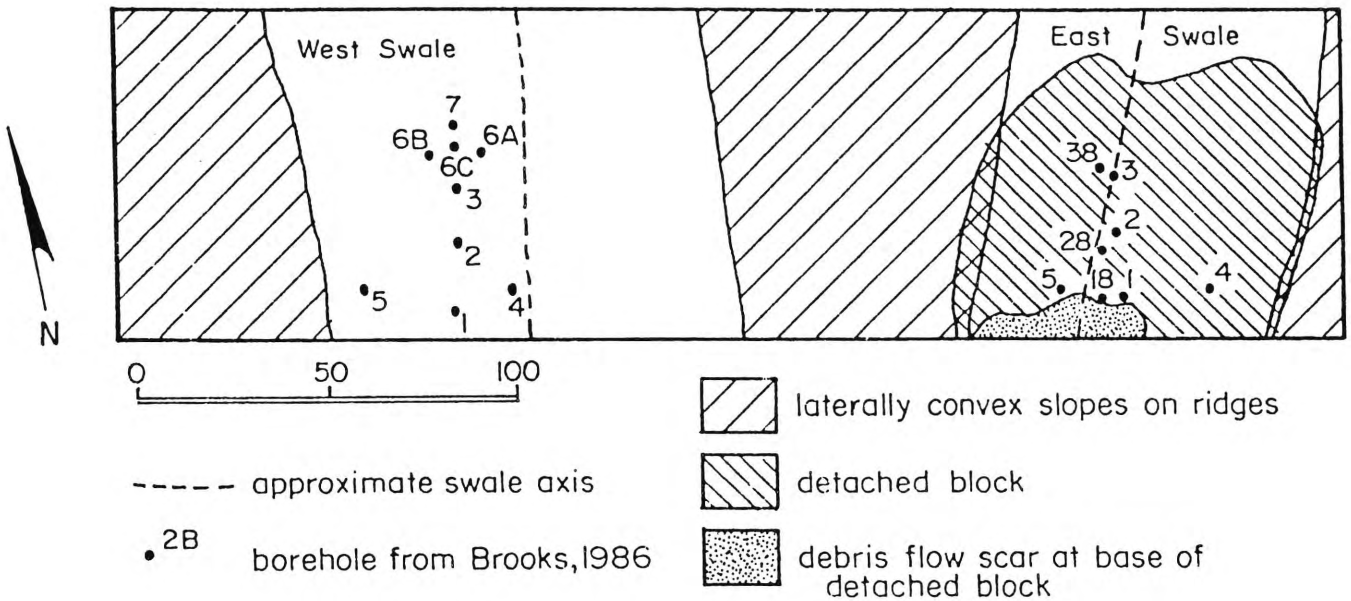

Figure 68. Generalized topography of the Steed Canyon WADI survey area and location of the Steed Canyon landslide and debris flow. Also shown are the locations of boreholes from a study by Brooks (1986). In the text, boreholes in the east and west swales are distinguished by E or W before the borehole number.

broad, unevenly saturated fracture zone with little or no clay.

West of and sub-parallel to this zone is a narrow trend of negative ECD and quadrature values. This feature, located on the western edge of the west swale, could be interpreted either as a hard bedrock ridge or as an unsaturated fracture zone. Finally, an ECD high on the far west side of the survey corresponds to a quadrature high, and appears to be another clay-filled structure.

In a previous study, Brooks (1986) logged several boreholes in each of the Steed Canyon swales. Figure 68 shows the locations of the boreholes. In the east swale, almost all the borings encountered a layer of rock or rock fragments at approximately 3 m. Soils beneath this layer were found to be non-plastic. In borings E1 and E1B, a plastic, silty to clayey sand layer was found overlying the ledge. If it is assumed that higher plasticity corresponds to lower hydraulic conductivity (Brooks, 1986), then it is possible that ground water in and under the fractured ledge was prevented from discharging, and pore water pressures built up to a critical level in the vicinity of E1 and E1B.

Borings in the west swale indicated the presence of a rocky ledge which divides the swale into an upper and a lower part. Brooks (1986) found evidence of large voids in the bedrock in borehole W5. A water hose with 122 m of head on it failed to fill borehole W6B, "regardless of the quantity of water poured down the hole" (Brooks, 1986, p. 46). Boreholes 5 and 6B in the west swale correspond to the edges of the northwest-trending low-conductivity anomaly found by the WADI. This supports the interpretation of the anomaly as an unsaturated fracture zone. It appears, therefore, that a deep, highly permeable fracture zone cuts across the west side of this swale, which is capable of draining great volumes of water during flood conditions, but is dry for most of the year. This feature probably prevented the development of elevated pore water pressures in the west swale during May and June of 1983 and 1984, which may explain why slope failure did not occur in this swale.

In the Steed Canyon survey, the overall low ECD values in the hollows compared with the ridges are thought to be due to masking of the signal by electrically conductive clays in the subsurface. Topographic ridges have higher ECD values, consistent with the greatly decreased (to non-existent) soil cover in these areas. In addition, the depths of conductors found by the WADI are greater on the ridges: between the two swales, these values range from 2 to 10 m, averaging 6.3 m; on the ridge west of the western swale, values range from 4 to 16 m, averaging 9 m. In the hollows, the depths of conductors average 3.2 m (east swale) and 5.4 m (west swale). Brooks

(1986) found the depth to "true" bedrock (not the rocky ledge) to be between 5 and 10 m for the east swale, and between 3.7 and 12 m for the west swale. This range is similar to the depths of the conductors recorded on ridges by the WADI, which appears to be more realistic than the depths recorded in the hollows.

Monteith (1988) mentions that the clay layer in the east swale is thick at the downslope end of the swale, and thins upslope. This correlates with higher ECD values at the north edge of the WADI survey, and supports the claim that readings were suppressed by electrically conductive clayey soils toward the south.

The WADI also indicates the apparent dip of a planar conductive feature, by determining the lateral changes in conductivity at different depths for a given conductivity peak (Karous and Hjelt, 1983). Table 7 shows the distribution of dips for the Steed Canyon survey area. Since the survey was carried out along azimuth 270°, all values are apparent dips along this strike. The majority of features have a westward apparent dip, at an average angle of 42°. Table 7 shows that this is not in agreement with the fracture and foliation orientations measured at the surface.

The validity of dip values given by the WADI is questionable for this survey. Furthermore, it is unlikely that individual fractures are being recorded by the WADI.

Table 7. **A.** Apparent dip angles and directions for planar conductivity anomalies in the Steed Canyon survey area. **B.** Dip angles and directions for principal orientations of (i) fractures in the area adjacent to the northern mapped fault (data set XNFC), and (ii) foliations over the entire study area; both projected along the same strike (az. 270°) as the WADI survey line.

Dip direction	Avg.Dip angle	Std.Dev.	Number
A) **WADI:** west	42°	11°	14
east	28°	5.5°	5
vertical	90°		1
B) **OUTCROP:**			
(i) Fractures from data set XNFC:			
east	84°		
(ii) Foliations over entire study area:			
west	23°		
(iii) Geomorphic region 7: no resolvable principal sets.			

It is more likely that a larger feature such as a fault or fracture zone is being recorded. In Figure 69 a line of anomalies appears to trend northwestward (approximate azimuth 315°) across the survey area. This follows the trend of the broad, high ECD/low quadrature zone shown in Figures 66 and 67, and may be more representative of the scale of bedrock features best suited for investigation by the WADI.

Ford Canyon Surveys

Two surveys were run in the upper part of Ford Canyon. The survey areas are located on the flank and at the base of a large swale which appears to have been the site of Holocene land slips (Lowe, 1989). The location and topography of the survey areas are shown in Figure 70.

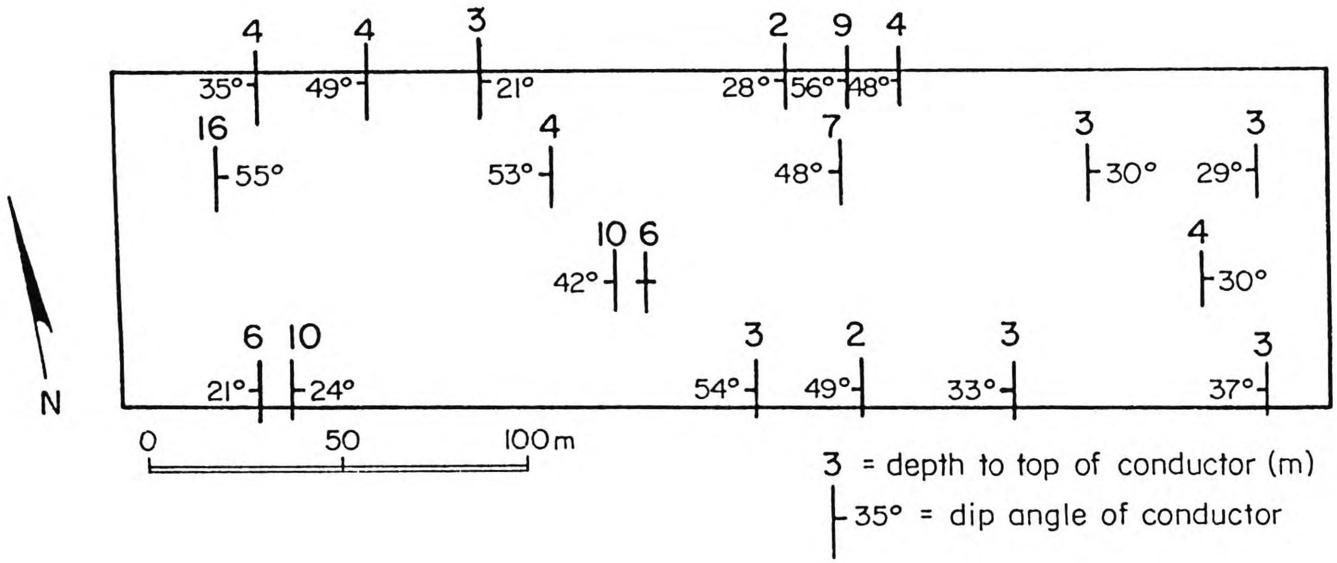

Figure 69. Location, apparent dip angle and dip direction of planar conductors interpreted by the WADI. Note the northwest trend of conductors across the west swale.

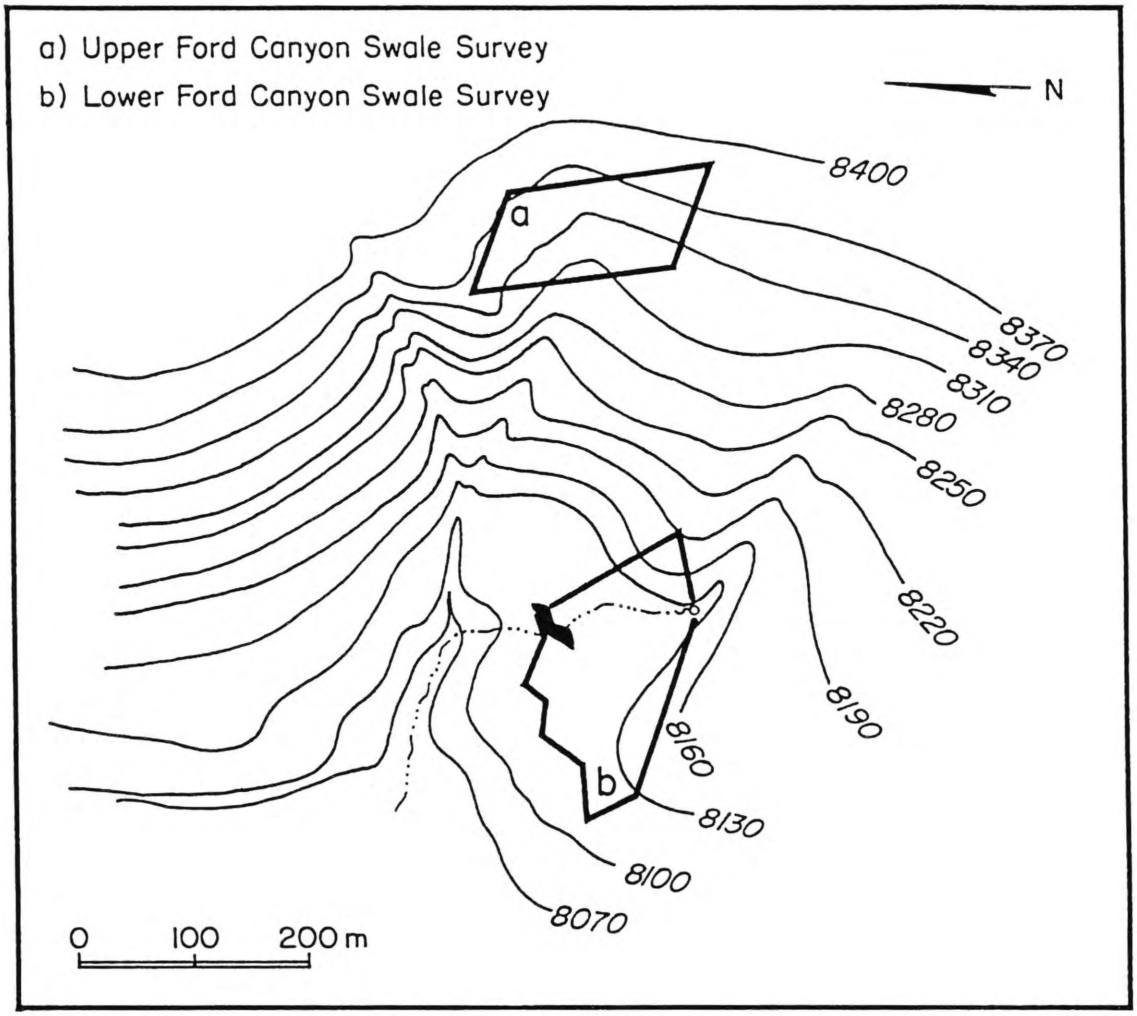

Figure 70. Location and topography of the upper and lower Ford Canyon swale WADI surveys. Note the pond created by a beaver dam.

This swale is underlain by a gently eastward-dipping series of interbedded pegmatite and gneiss units of varying thickness. At least one shallow soil slip from 1984 is located at the head of the steeper slope just beyond the western edge of the swale. No direct subsurface information was available for these sites, although the descriptions in Harp and others (1990) indicate that the soil stratigraphy is similar to that of the Steed Canyon area.

Contour maps were generated for ECD and quadrature for the upper and lower Ford Canyon surveys, as shown in Figures 71 through 74. Linear conductivity anomalies for both surveys trend approximately due north and due west. The quadrature for the entire lower swale is near zero, except in the northeastern and southern corners (Figure 74). In the upper swale, ECD highs roughly correspond to quadrature lows. Therefore it is reasonable to conclude that these linear anomalies are water-bearing fracture zones. The west-trending subsurface features parallel the general orientation of fractures measured at the outcrop for pegmatites, shown in the lower hemisphere plot in Figure 41 C.

The low ECD values along the southern edge and in the northeastern corner of the lower Ford Canyon swale survey (Figure 73) indicate the presence of extremely poor conductors. These are discussed below.

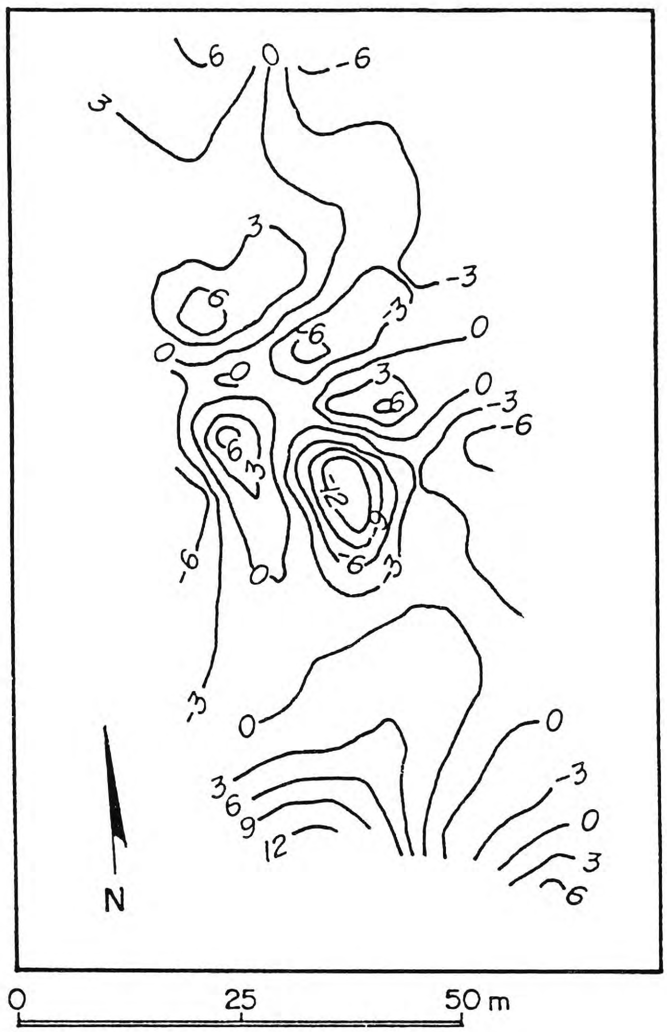

Figure 71. Contoured ECD values for the upper Ford Canyon swale WADI survey. Linear anomalies in the center of the plot trend approximately north and west.

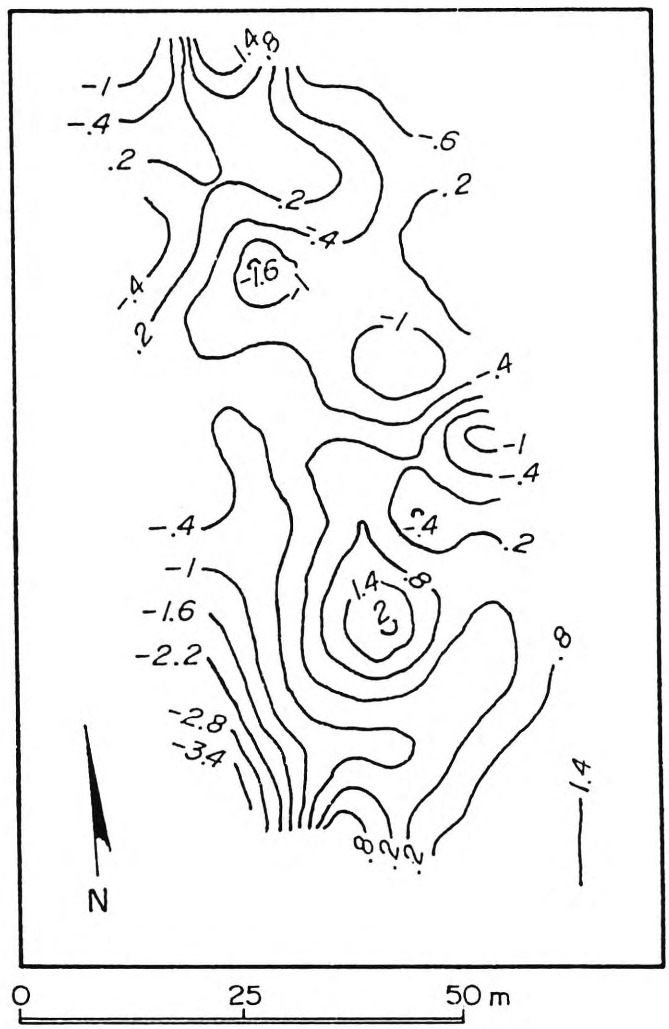

Figure 72. Contoured quadrature values for the upper Ford Canyon swale WADI survey.

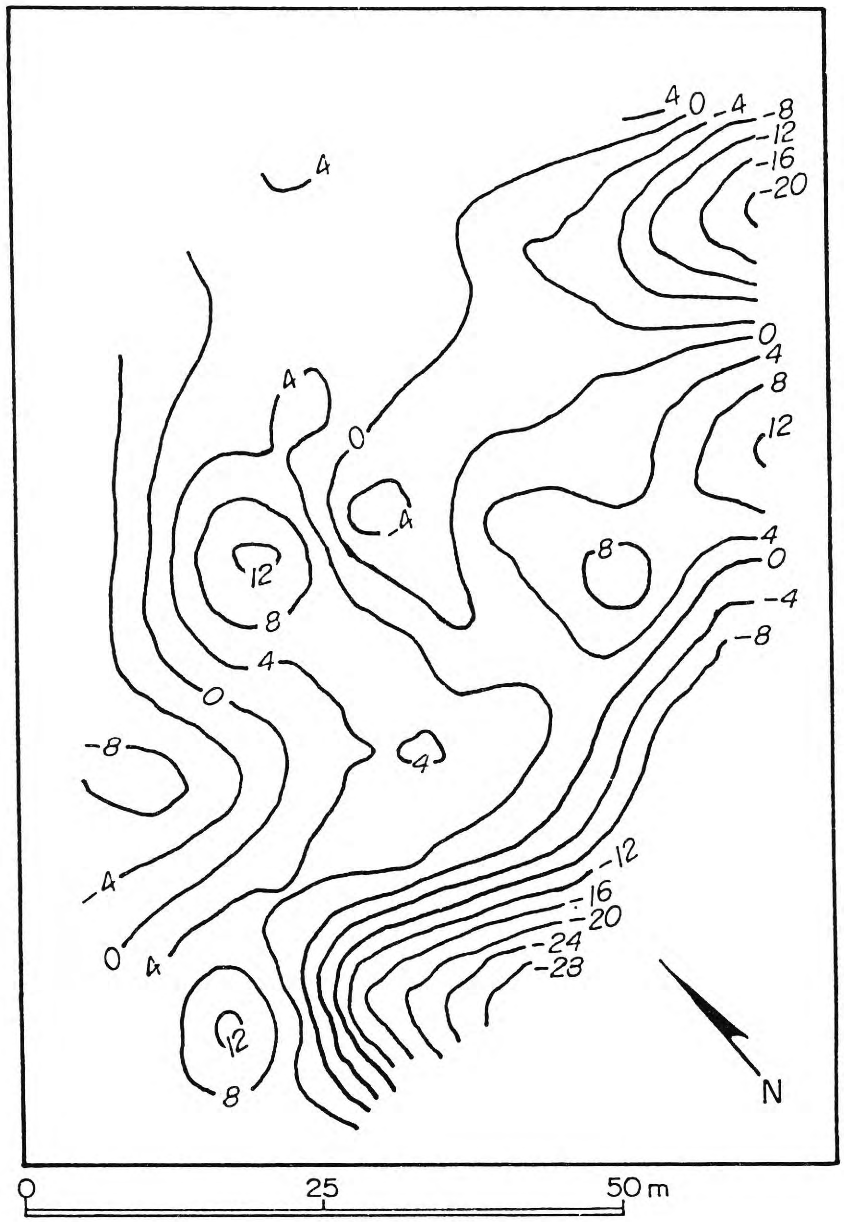

Figure 73. Contoured ECD values for the lower Ford Canyon swale WADI survey. Anomalies trend north and west.

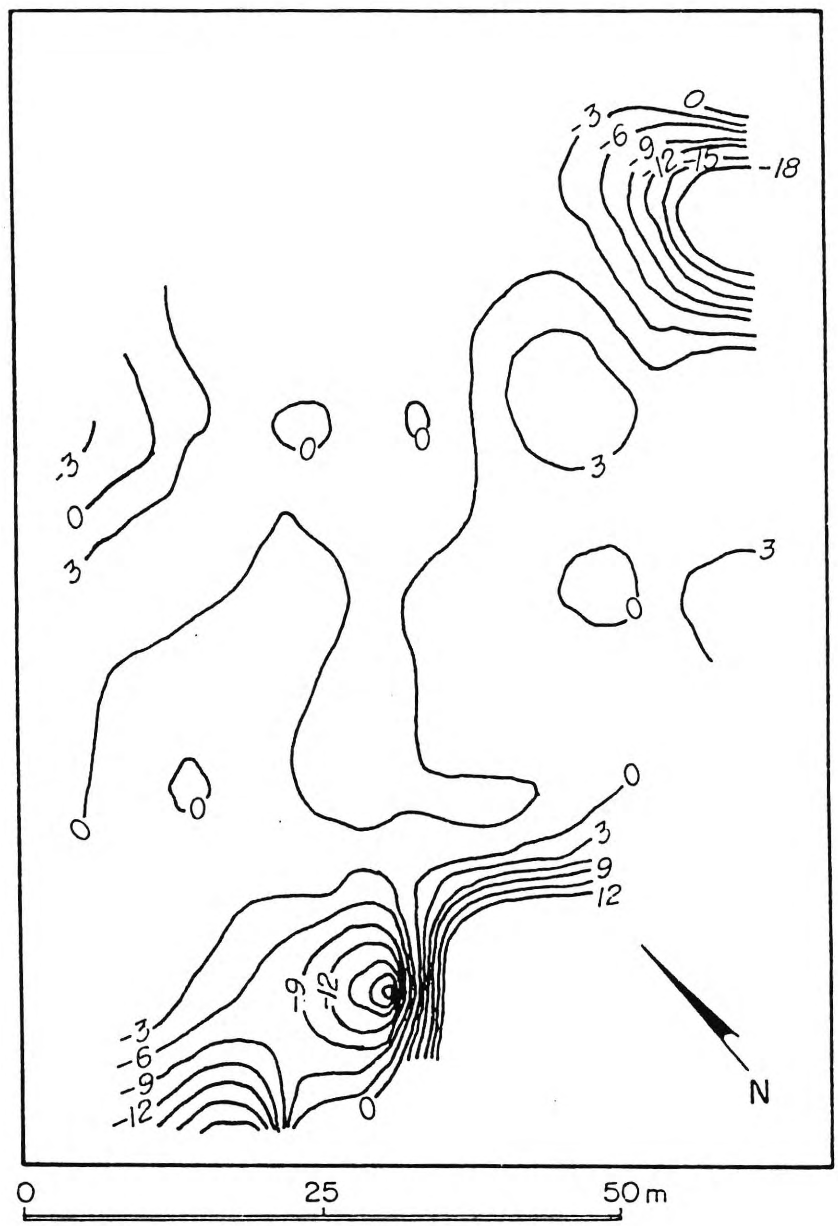

Figure 74. Contoured quadrature values for the lower Ford Canyon swale WADI survey.

Dips recorded by the WADI in the upper and lower Ford Canyon Swale surveys are compared with outcrop-derived orientation data in Table 8 below. Apparent dips do not appear to match between surface information and interpretations made by the WADI.

Table 8. **A.** Apparent dips of conductors in upper and lower Ford canyon swales, from WADI. **B.** Dip directions and apparent dip angles for (i) fractures adjacent to the central fault (data set XNFD), and (ii) fractures in pegmatite over the entire study area.

Dip Direction	Avg.Dip Angle	Std. Dev.	Number
A) WADI:			
(i) Conductors in upper Ford Canyon Swale			
west	36°	9.5	8
east	43°		1
(ii) Conductors in lower Ford Canyon Swale			
west	41°	7.3	11
east	42°		1
vertical	90°	0	2
B) OUTCROP:			
(i) Fractures from data set XNFD:			
1 - Projected to trend of upper swale survey line			
west	24°		
east	31°		
2 - Projected to trend of lower swale survey line			
west	66°		
east	30°		
(ii) Fractures from Pegmatite over entire study area:			
1 - Projected to trend of upper swale survey line			
east	61°		
2 - Projected to trend of lower swale survey line			
east	76°		
(iii) Geomorphic region 2: no resolvable fracture sets.			

The depths to conductors in the Ford Canyon surveys are shown in Figures 75 and 76. There was no independent subsurface information with which to compare these readings. The north-trending, higher ECD zone in Figure

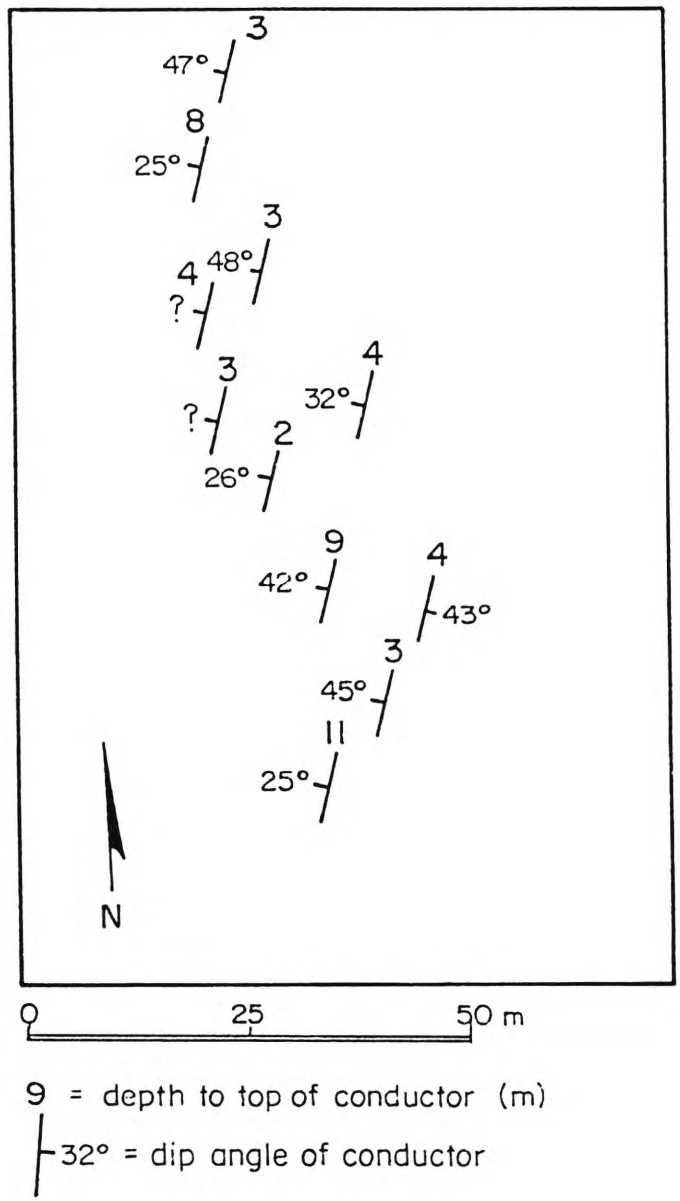

Figure 75. Apparent dip angle and dip direction of planar conductors interpreted by the WADI, for the upper Ford Canyon swale.

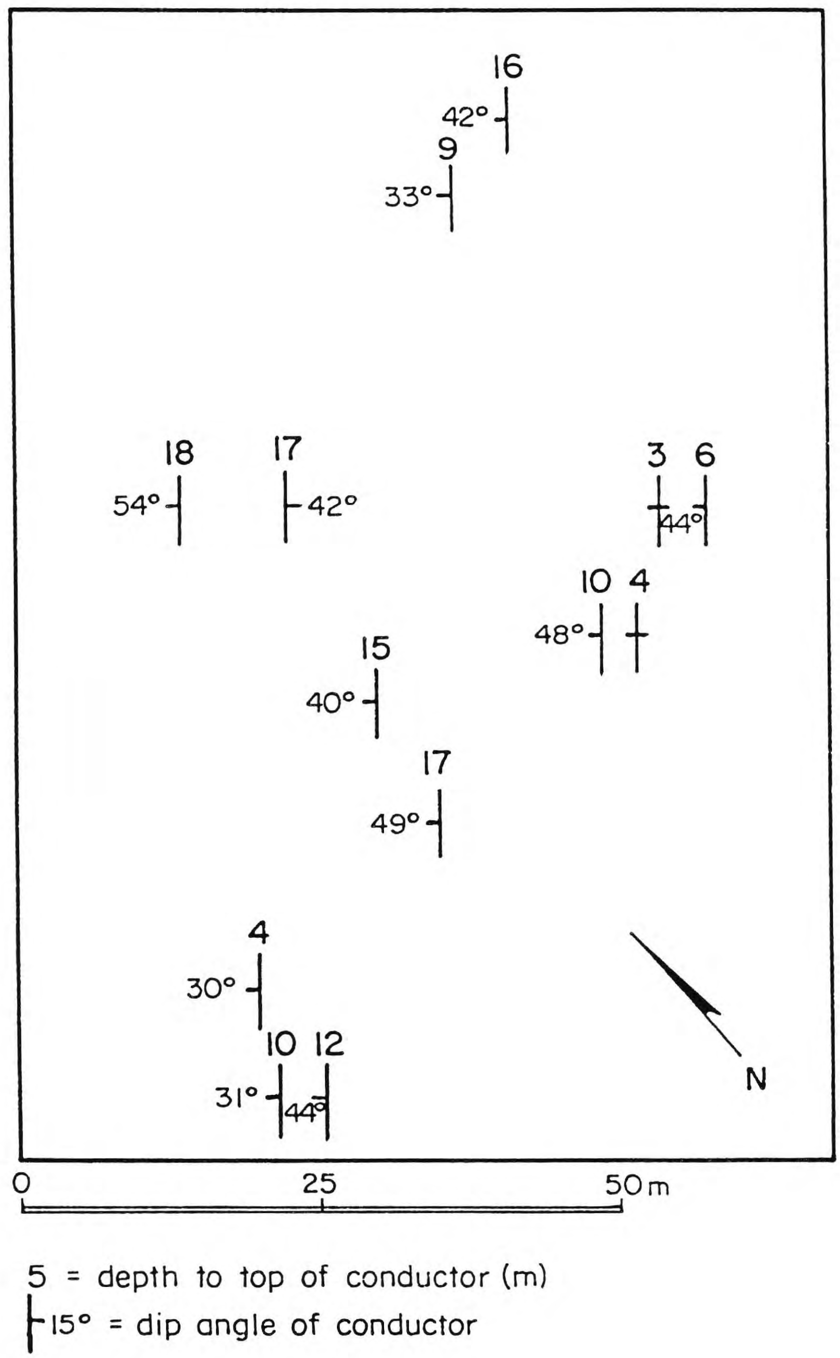

Figure 76. Apparent dip angle and dip direction of planar conductors interpreted by the WADI, for the lower Ford Canyon swale.

73 (lower swale) corresponds to depth readings in Figure 76 which average 13.4 m. This may indicate the depth to water in the fractured bedrock. In contrast, the west-trending higher ECD zone at the slope break averages 7.9 m in depth. Both of these readings appear too deep, considering the numerous springs and seeps in theimmediate area. No individual trends are distinguishable in the upper survey.

The depths to conductors recorded by the WADI in these surveys are highly variable. This is consistent with the picture of the subsurface obtained from boreholes in the Steed Canyon survey area. In general, little can be concluded from the data on the dip of, or the depth to, conductors in the two Ford Canyon surveys, beyond the fact that the soil/bedrock interface is highly irregular.

A curious feature in the lower Ford Canyon swale survey is the pattern of strong negative values at the southern edge and northeasten corner of the survey. Assuming these are not due to instrument malfunction, they may be due to distortion of the primary magnetic field by topographic effects, because the anomalous values correspond approximately to the edge of steeper slopes on the southeastern edge of the swale. Another possible cause for the low conductivity readings is that the water table is deeper in these zones of higher topography, although evidence from the Steed Canyon survey showed a general increase in conductivity over topographic highs. A third possibility is that the negative anomalies are electrical edge effects on either end of a conductive zone of saturated fractured bedrock (seen as a long west-trending higher ECD zone in the southern part of the survey in Figure 73).

A hypothesis for the development of the apparent bedrock ground-water condition in the lower Ford Canyon swale is that the bedrock ledge north of the slope break has been downdropped, forming a shelf which has become a ground-water discharge area, as well as a repository for residual soil and colluvium. Ground water has been impounded due to the (post-faulting) geometry of the less permeable bedrock. A conceptual diagram of this feature is presented in Figure 77.

The presence of springs and seeps as well as water in fractures (inferred from the Wadi survey) during August 1988, one of the driest summers on record for this region, indicates perched water table conditions. Discharge through this system is probably greatly increased during times of peak runoff and snowmelt. This area of ground-water discharge was created by the anomalous presence of a relatively less permeable rock body, as shown schematically in Figure 5. The area is presented as one example of bedrock control over ground-water discharge and/or slope failure in the study area.

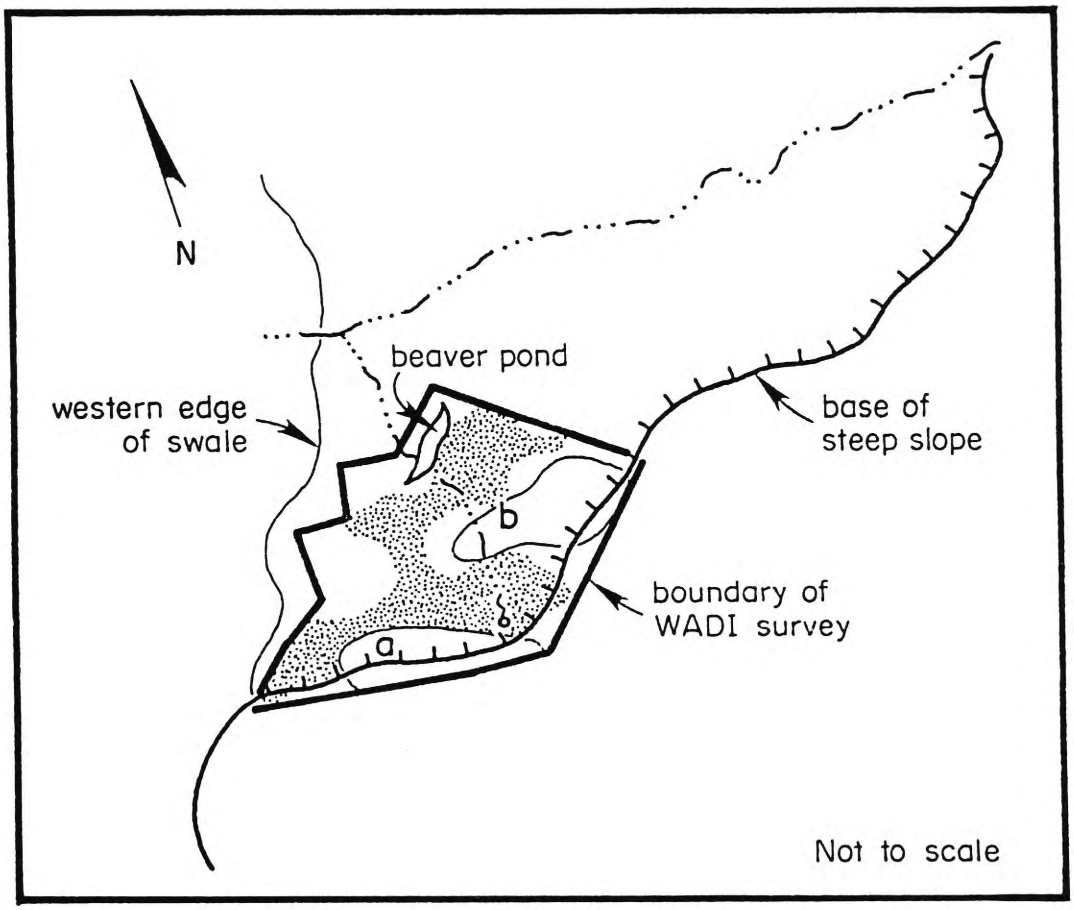

Figure 77. Schematic diagram of the site of the lower Ford Canyon WADI survey. The pegmatite unit underlying this area has been down-dropped across a fault or fracture zone trending approximately due west. This has created a ground-water discharge zone throughout the Ford Canyon Swale. The fault hanging wall is marked with hachures; **a** and **b** denote the low ECD areas next to the fault scarp; the patterned area shows high ECD, corresponding to saturated fractured bedrock.

Discussion

Method

The WADI, and the VLF method, are excellent reconnaissance tools for a number of reasons. The WADI is light and compact; it was found to have great utility in the rough terrain of the study area. Surveys for quite large areas can be conducted rapidly. Each data point recorded in a survey contains information on in-phase and out-of-phase components of the induced field. Anomalies can be interpreted in situ. The lateral and vertical position of the anomaly, and a value for the dip of the feature are presented graphically. Up to approximately 4000 measurements can be held in the memory (Saga Geophysics, 1988).

The low frequency of the waves allows them to penetrate some distance into the ground, depending on the conductivity of the material. The remoteness of the primary field source means that the field is essentially uniform for surveys of the size used in this study (Telford et al., 1985).

Interpretation of Results

The principal drawbacks of this method, as with any geophysical method, lie in the ambiguity of the results. Some of the causes of ambiguity are listed below.

1) Resolution is poor; conductive features must be on the order of 10 m or more in length to be detected.

2) The dip of the subsurface conductor affects the magnitude of the secondary field. Since the primary field is dominantly horizontal, more steeply dipping planes present a larger conductive area; so the greater the dip, the greater the induced field. Thus an apparently poor conductor may simply be oriented near to horizontal, while a less conductive, more steeply dipping feature may appear to be a stronger conductor than it really is.

3) In order for the secondary field to be maximized, the subsurface conductor must be aligned perpendicular to the primary field. Deviation from this orientation results in distortion of the secondary field read by the VLF instrument. If the primary field is near parallel to the trend of the conductor, the secondary field may be severely inhibited (Telford et al., 1985). Thus it is recommended that the same area be traversed at least twice, using different stations for each survey. This was done by White and Gainer (1985), in their reconnaissance for fractures around a uranium mill tailings pond.

4) The WADI measures all conductivity values with respect to the first data point of the survey. Thus, if the first point is taken on a highly conductive (or highly resistive) material, subsequent points might all show excessively low (or high) conductivities because of the contrast with the first point. However, relative values should not be affected. In this study, a procedure

suggested by Morgan (1990) was followed, in order to normalize conductivity values between surveys. The average conductivity over the entire survey was calculated, and was set equal to zero. The data for that survey are then shifted by the same amount. All the ECD and quadrature grids shown in Figures 66, 67, and 71 through 74 were normalized to their average value.

5) Results can be affected by topography, and by the in situ properties of surface and subsurface materials. Topography can affect induced conductivity readings by "channelizing" the primary field and creating higher readings in valleys than on ridges (Morgan, 1990). It is not known how local topography has affected these results, though Lagmanson (1990) states that the filtering method incorporated into the WADI accounts for topographic changes. At any rate, the Steed and lower Ford Canyon swale surveys have <u>opposite</u> correlations with topography (Figures 66 and 73), so other factors must be more important than topography in producing the observed conductivity distributions.

6) Changes in the conductivity of the overburden may mask the response from bedrock; highly conductive surficial materials such as clays may completely preclude this method (Saga Geophysics, 1988). However, surface water bodies do not induce a noticeable secondary field, probably because of their horizontal upper surface; this

was observed in the lower Ford Canyon swale, where a beaver dam has impounded spring discharge (Figure 70).

In contrast to surface water, subsurface clayey zones may have a near-vertical tabular geometry, as in the case where a highly fractured or weathered zone has been filled by clay minerals. Clay-filled fractures should be distinguishable from water-bearing fractures by the magnitude of their quadrature.

Finally, as with any geophysical method, it is important to have independent geological verification of the results. This type of supporting data was lacking in the Ford Canyon study area.

Summary

The clayey subsoils which are present in the Steed Canyon survey area (Brooks, 1986) and probably also in the Lower Ford Canyon swale, may have dampened the secondary field response from deeper conductive features in the bedrock. In spite of this, several linear anomalies were recorded.

A trend of anomalies was recorded by the WADI in the Steed Canyon survey, along azimuth 315°. This does not correspond to the trend of the fault mapped through this region using aerial photographs and surface information (azimuth 290°). However, north-trending anomalies in the east Steed Canyon swale, and north and west-trending anomalies in the Ford Canyon swales do correspond to the trends of faults and fracture sets observed at the surface.

The WADI survey in Steed Canyon correlates with a change in soil properties found in borings (Brooks, 1986), and may have identified a fault or fracture zone in the west swale. In Ford Canyon, little direct confirmation of the WADI data was available. Conductivity anomalies were generally aligned due north and west, and a possible fault-controlled ground-water discharge mechanism was hypothesized for the lower swale. The geophysical data correlated well with surface observations, and were supported by geomorphic and hydrologic evidence.

SUMMARY AND CONCLUSIONS

This study has attempted to characterize the large and small scale structural fabric of the Farmington Canyon Complex, to infer ground-water flow directions in the bedrock, and to determine the distribution of ground-water discharge points at the surface. Several slope failures in the study area were initiated by ground-water discharge; thus the main application of this research was to establish a link between the structural fabric of the bedrock and the distribution of slope failures.

The following sections summarize the findings of this research. The bedrock features and distribution of slope failures discussed in this section refer to several different figures in the text. Most of these are combined in Figure 63 (in pocket).

Structural Fabric

1) Randomness

A. Analysis of the randomness of different families of fractures indicates that preferred orientations exist in only a small percentage of the data sets. These are fractures in gneiss, fractures adjacent to faults in the study area, and foliations. Therefore, the character of fracturing has been significantly influenced by regional geologic conditions such as faulting, metamorphism and the juxtaposition of different rock types.

B. The study area was divided into eight regions on the basis of geomorphology. None of the fracture sets in any of the eight regions have preferred orientations at 95 percent confidence. Regions 1 and 5, representing two of the four sharp north to northwest-trending ridges, have preferred orientations at 90 percent confidence. This may be due to topographic sampling bias and/or the uniformity of bedrock characteristics along ridges.

C. The orientation of principal trends of intersection lines between fracture planes in regions 1 through 8 were tested for randomness. All regions except region 7 are non-random at 95 percent confidence.

In summary, although most of the data sets of fractures proved to be randomly distributed at 95 percent confidence, fracture intersections have statistically significant preferred orientations.

2) General trends

Contouring sets of poles to fractures shows that the orientations of principal fracture sets in pegmatite are different from fractures in gneiss and amphibolite. The principal strike of fracture sets adjacent to faults is approximately 40° from the trend of the faults.

3) Regional structural influence

It appears that the distribution of fracture orientations, as observed in outcrops, is mainly derived from late Jurassic through Eocene (Sevier/Laramide) compression. Rotation of fracture sets to a common horizontal foliation plane suggests that the majority of fractures formed during the earliest stages of Sevier/Laramide compression, and were subsequently contorted by complex folding. Subsequent Miocene through Recent (Basin and Range) extension resulted in further development of the northeast-trending fractures.

4) Controls on fracture characteristics

A comparison of twenty-one data sets grouped by region and by lithology shows that regional location has a significant influence on fracture orientation dispersion parameter k, while lithology does not. Thus geomorphic environment accounts for a greater variability in fracture orientations than lithology. Geomorphic character is not directly a geological criterion; however, it describes the cumulative expression of an indeterminate combination of physical parameters. From this test it is concluded that the observed fracture geometry of the Farmington Canyon Complex is due to a combination of factors (including lithologic variability and sampling bias) which cannot be resolved separately.

5) Fracture half-length, spacing and intersections

Fracture half-length and spacing distributions appear to be exponential or lognormal, irrespective of lithology or regional position. At one station it was found that longer and more open fractures are similarly oriented to all the fractures for that station. Based on this example, it was assumed that the theoretical distribution of fracture intersection lines as calculated by the Structure Graphics program is representative of the true distribution of fracture intersection lines in the Farmington Canyon Complex.

6) Geophysical surveys

WADI surveys in Steed and Ford canyons suggested the presence of elongate to linear saturated and unsaturated fracture zones in the bedrock. In the west swale of the Steed Canyon survey, a fracture zone functions as a drain; in the lower Ford Canyon swale, fracture zones appear to be sites of ground water accumulation.

Hydrogeology and Application to Slope Failures

1) The role of fracture intersections

Previous studies have pointed out the importance of fracture interconnectivity in influencing ground-water flow in fractured rock masses (Long and Witherspoon, 1985; Pollard and Aydin, 1988). The distribution of intersection lines for the eight sub-regions in the study area is non-random at 95 percent confidence. However, this study did not find evidence confirming that preferential ground-water flow takes place parallel to the principal trends of fracture intersections. In the absence of such evidence, it is believed that the trends of fracture intersection lines for regions 1, 2, 3, 4, 5, 6 and 8 are the directions of maximum bedrock permeability in these regions.

2) Aquifer characteristics

Hydrogeologic evidence suggests that the shallow bedrock forms an aquifer of low specific yield. However, long-term discharge has been observed from some springs and debris flow scars underlain by the Farmington Canyon Complex (Mathewson and Santi, 1987). Therefore, the aquifer is divided into compartments of different sizes. It is believed that faults, fracture zones and/or lithological contacts control the partitioning of the aquifer, by acting either as conduits for deep ground-water flow or as barriers against topographically driven interflow, and thus re-direct ground water obliquely across the slope. The area around the head of Rudd Creek appears to be recharged in this manner (Keaton, 1988a). Further support for this hypothesis is provided by the WADI surveys, which indicated the the presence of water-bearing fractures in the vicinity of a fault in Steed Canyon, and near pegmatite outcrops in Ford Canyon.

3) Permeability trends

Two forms of indirect evidence support the hypothesis that ground water travels preferentially along faults. First, a generally northwestward increase in stream discharge (normalized to drainage area) is apparent for five westward-draining canyons in this region. Second, the greatest number of slope failures within the study area occurred on slopes perpendicular to the principal trend of faults in the study area. No such correlations were found between slope failures and the strikes of fractures or the trends of fracture intersection lines.

The role of steeply-dipping fractures and fracture intersection lines appears to be one of recharge to the deep permeable zones in the bedrock. The extent of communication between shallow structures (fractures and foliation) and deep structures (faults) is important: the greater the permeability of the shallow bedrock, the greater the recharge to the deeper aquifer. Where the fractured shallow bedrock is not near a deep conduit, downslope movement of ground water occurs as interflow, until a permeable zone is encountered, or surface discharge occurs.

4) Surface discharge mechanisms

Bedrock features causing surface discharge of interflow may be relatively less permeable rock bodies such as pegmatite, and/or fracture and foliation sets that intersect the slope, as hypothesized by Mathewson and Santi (1987). A number of gently dipping fractures and foliation planes dip toward the northwest, corresponding to the slopes on which the greatest number of debris flows occurred.

Extrapolating the surficial bedrock structure observed in the study area to all of eastern Davis County, it is concluded that the density of structural discontinities near the surface is uniformly high. Thus, while the principal trends of discontinuities may vary considerably, overall permeability characteristics of the near-surface bedrock are interpreted to be uniform and nearly isotropic.

Figure 78 A (in pocket) shows the proposed ground-water flow system in the Farmington Canyon Complex between Farmington Canyon and Ward Canyon. Permeability trends in the bedrock <u>between</u> major linears are nearly perpendicular to the linears, allowing for rapid recharge to the deeper flow system. Linears are interpreted to be ground-water conduits. Some, however, may have <u>lower</u> permeability than the material around them, and thus may be barriers to ground-water flow. The barriers that trend across the general westward slope of the Wasatch Front cause ground water to be conducted down and across the slope, parallel to and uphill of the linear feature.

Application to the Debris Flow Hazard

It is concluded from this study that the distribution of slope failures, particularly debris flows, underlain by the Farmington Canyon Complex is at least partially dependent on bedrock geology. Two general ground-water conditions can lead to a debris flow, consistent with two different meteorologic conditions. First, intense and localized summer rainstorms may lead to rapid interflow and discharge at contacts with pegmatite, and through low-angle fractures and partings in well-foliated gneisses. Second, spring snowmelt may saturate deep ground-water conduits, causing prolonged discharge and/or slope failure through the localized elevation of pore water pressure in the manner described by Mathewson and Santi (1987).

The results of this study suggest that the future occurrence of slope failures associated with spring snowmelt in this region will take place on slopes perpendicular to regional faults, and at discharge points along fault traces, created by local variations in the permeability of fault zones and the presence of favourably oriented fractures or foliations. Debris flows and shallow landslides associated with intense summer rainfall may correlate more strongly with the occurrence of "daylighting" fractures and foliation, and along contacts between pegmatite and other lithologies.

The proposed distribution of ground-water discharge points and shallow ground water for both of the conditions discussed in the previous paragraph is shown in Figure 78 B (in pocket). Many are located adjacent to creeks, most of which appear to mark the trace of bedrock faults or fracture zones. Thus in the wet season, the entire length of a stream valley becomes a ground-water discharge zone.

In this way, sufficient pore water pressure is maintained along a canyon to allow the continuous mobilization of colluvium in a debris flow, as proposed by Santi (1988).

RECOMMENDATIONS FOR FURTHER WORK

The traces of regional faults and the trends of lithologic contacts are best identified using aerial photographs. A large percentage of slope failures in this study area correlate with these features. Aerial photograph analysis, with a limited amount of field checking, would provide useful input to slope failure hazard maps of larger regions. Digital image processing would help in identifying these regionally important bedrock features.

The conclusions drawn from the detailed analysis of fracture and foliation orientations may not be directly applicable outside the study area. Because of the heterogeneous geology of the Farmington Canyon Complex, orientations are likely to be quite different elsewhere. In new areas, data collection at the outcrop level may be necessary for comparison with the data sets in this study.

Further work is necessary to test the hypothesized relationship between structural fabric and ground-water flow directions. Useful field techniques might include measuring spring discharge and water chemistry, and conducting tracer tests to investigate the areal extent of aquifer compartments, and travel times.

The relative permeability of gneissic, amphibolitic and pegmatitic rocks should be better established. In this study, geomorphic and hydrologic evidence was used to infer that pegmatites (at least in the subsurface) are the least permeable rock type.

Slope failure scars in part or all of the study area could be field checked to distinguish those which involved significant deep ground-water discharge from those which may have been initiated by pore water pressures in colluvium or shallow bedrock. This would refine the correlations found in this study between ground-water trends and slope failures.

Finally, the statistical techniques used here for characterizing the dispersion and orientation of families of structural discontinuities can be used in other applications, such as in predicting the fate of solutes in the ground water within fractured rock masses. This is particularly true of regions with less complex fracture geometries. Some preliminary conclusions about the permeability characteristics of a fractured rock mass could be drawn from an analysis of eigenvalues, k, alpha95, and Kamb contours of fracture poles and intersection lines. The data for these analyses can be gathered relatively quickly. In comparison, in situ hydrogeologic investigations of fractured rock masses can involve very large amounts of money and time; and mathematical treatments are generally extremely complex.

REFERENCES

Alger, C.S., and Ellen, S.D., 1987, Zero-order Basins Shaped by Debris Flows, Sunol, California, U.S.A. In Beschta, R.L.; Blinn, T.; Grant, G.E.; Ice, G.G.; and Swanson, F.J., (editors) Erosion and Sedimentation in the Pacific Rim: Publication No. 165, International Association of Hydrological Sciences, Washington, D.C., p. 111.

Anderson, L.R.; Keaton, J.R.; Saarinen, T.F.; and Wells, W.G. III, 1985, The Utah Landslides, Debris Flows, and Floods of May and June 1983, in Bowles, D.S., (editor), Delineaton of Landslide, Flash Flood, and Debris Flow Hazards in Utah, Utah Water Research Laboratory, Utah State University, Logan, UT, 592 p.

Andrews, J.T., 1971, Techniques of Till Fabric Analysis; in Brunsden D. and Thornes, J.B., (editors), British Geomorphological Research Group, Technical Bulletin No. 6, British Geomorphological Research Group, (Private Collection, J.R. Giardino), 43 p.

Arabasz, W.J., and Julander, D.R., 1986, Geometry of Seismically Active Faults and Crustal Deformation Within the Basin and Range-Colorado Plateau Transition in Utah, in Mayer, L., (editor), Extensional Tectonics of the Southwestern United States: a Perspective on Processes and Kinematics, Geological Society of America Special Paper No. 208, p. 43-74.

Babcock, E.A., 1973, Regional Jointing in Southern Alberta, Canadian Journal of Earth Science, Vol. 10, p. 1769.

Baecher, G.B.; Lanney, N.A.; and Einstein, H.H., 1977, Statistical Description of Rock Properties and Sampling, in Wang, F.D., and Clark, G.B., (editors), Energy Resources and Excavation Technology: Proceedings of the 18th United States Symposium on Rock Mechanics, Keystone, CO, Colorado School of Mines Press, Golden, CO, p. 5C11-8.

Brooks, R.K., 1986, Instrumentation of the Steed Canyon Landslide, Unpublished Master of Science Thesis, Department of Civil and Environmental Engineering, Utah State University, Logan, UT, 183 p.

Brown, S.R., 1987, Fluid Flow Through Rock Joints: the Effect of Surface Roughness, Journal of Geophysical Research, Vol. 92, No. B2, p. 1337-1347.

Bryant, Bruce, 1988, Geology of the Farmington Canyon Complex, Wasatch Mountains, Utah, United States Geological Survey Professional Paper 1476, United States Government Printing Office, Washington, D.C., 54 p.

Campbell, R.H., 1975, Soil Slips, Debris Flows, and Rainstorms in the Santa Monica Mountains and Vicinity, Southern California, United States Geological Survey Special Paper 851, Denver, CO, 51 p.

Chorley, R.J.; Schumm, S.A.; and Sugden, D.E., 1984, Geomorphology: Methuen and Company, New York, NY, 605 p.

Conover, W.J., 1980, Practical Non-Parametric Statistics, Second Edition, John Wiley and Sons, New York, NY, 493 p.

Crittenden, M.D. Jr., 1972, Willard Thrust and the Cache Allochthon, Utah, Geological Society of America Bulletin, Vol. 83, p. 2871-2880.

Croft, A.R., and McDonald, L.W., 1944, Centerville, Utah, A Pattern for Progress, The Centerville Newsette, Centerville, UT, November 1944.

Davis County Planning Commission, 1989, Unpublished Stream flow and Precipitation Data for Halfway Creek, Davis County Courthouse, Farmington, UT.

Davis, J.C., 1986, Statistics and Data Analysis in Geology, Second Edition, John Wiley and Sons, New York, NY, 646 p.

Deere, D.H. and Patton, F.D., 1971, Slope Stability in Residual Soils. In Proceedings of the Fourth Panamerican Conference on Soil Mechanics and Foundation Engineering, Vol. 1, American Society of Civil Engineers, New York, NY, p. 87-170.

Domenico, P.A., 1972, Concepts and Models in Groundwater Hydrology, McGraw Hill, New York, NY, p. 48-52.

Eardley, A.J., 1939, Structure of the Wasatch-Great Basin region, Geological Society of America Bulletin, Vol. 50, p. 1277-1310.

______________, 1944, Geology of the north-central Wasatch mountains, Utah, Geological Society of America Bulletin, Vol. 55, p. 819-894.

Eisenlohr, W.S. Jr., 1952, Floods of July 18, 1942, Pennsylvania, in Notable Floods of 1942-3, United States Geological Survey Water Supply paper 1134-B, United States Government Printing Office, Washington, D.C., p. 75-79.

Engelder, T., 1982, Is There a Genetic Relationship Between Selected Regional Joints and Contemporary Stress Within the Lithosphere of North America ? Tectonics, Vol. 1, No. 2, p. 161-177.

____________, and Geiser, P., 1980, On the Use of Regional Joint Sets as Trajectories of Paleostress Fields During the Development of the Appalachian Plateau, New York, Journal of Geophysical Research, Vol. 85, No. B11, p. 6319-6341.

Everett, A.G., 1979, Secondary Permeability as a Possible Factor in the Origin of Debris Avalanches Associated with Heavy Rainfall, Journal of Hydrology, Vol. 43, p. 347-354.

Feth, J.H., 1964, Hidden Recharge, United States Geological Survey Water Resources Division, United States Government Printing Office, Washington, D.C., p. 14-17.

Fisher, Sir Ronald, 1953, Dispersion on a sphere, Proceedings of the Royal Society, Series A, Vol. 217, No. 1130, Cambridge University Press, London, England, p. 295-305.

Freeze, R.A., and Cherry, J.A., 1979, Groundwater, Prentice-Hall, Englewood Cliffs, NJ, p. 472.

Friedman, M., 1963, Petrofabric techniques for the determination of principal stress directions in rocks, in Rudd, W.R., (editor), International Conference on the State of Stress in the Earth's Crust, Proceedings, Elsevier Publishing Company, New York, NY, p. 474.

Gale, J.E.; Rouleau, A.; and Atkinson, L.C., 1985, Hydraulic Properties of Fractures, in Hydrogeology of Rocks of Low Permeability, International Association of Hydrogeologists Memoires, Tucson, AZ, Vol. XVII, Part 1 (Proceedings), p. 1-16.

Greenkorn, R.A.; Johnson, C.R.; and Shallenberger, L.K., 1964, Directional Permeability of Heterogeneous Anisotropic Porous Media, Society of Petroleum Engineers Journal, June 1964, p. 124.

Hack, J.T. and Goodlett, J.C., 1960, Geomorphology and Forest Ecology of a Mountain Region in the Central Appalachians, United States Geological Survey Professional Paper #347, United States Government Printing Office, Washington, D.C., p. 41-56.

Halliday, D. and Resnick, R., 1978, Physics: Part Two, Third Edition, John Wiley and Sons, New York, NY, 894 p.

Harp, E.L.; Wells, W.G. II; and Sarmiento, J.G., 1990, Pore Pressure Response During Failure in Soils, The Geological Society of America Bulletin, Vol. 102, No. 4, p. 428-438.

Hashad, A.H.; Damon, P.; and Whelan, J.A., 1970, Precambrian Geology of the Central Wasatch mountains, in Whelan J.A., (editor), Radioactive and isotopic determinations of Utah rocks, Utah Geological and Mineral Survey, affiliated with The College of Mines and Mineral Industries Bulletin 81, Salt Lake City, UT, p. 15-17.

Hedge, C.E.; Stacey, J.S.; and Bryant, Bruce, 1984, Geochronology of the Farmington Canyon Complex, Wasatch Mountains, Utah, in Miller, D.M., Todd, V.R., and Howard, K.A., (editors), Tectonic and stratigraphic studies in the Eastern Great Basin, Geological Society of America Memoir 157, Denver, CO, p. 37-45.

Heiland, C.A., 1968, Geophysical Exploration, Hafner Publishing Co., New York, NY, 1013 p.

Hicks, B.G., 1988, Personal Communication, Geologist, Rogue River National Forest, Medford, OR.

Hintze, L.F., 1982, Geologic History of Utah, Department of Geology, Brigham Young University, Provo, UT, 181 p.

Hodgson, R.A., 1961, Regional Study of Jointing in Comb Ridge-Navajo Mountain Aera, Arizona and Utah, American Association of Petroleum Geologists Bulletin, Vol. 45, No. 1, p. 38.

Hollet, D.W.; Bruhn, R.L.; and Parry, W.T., 1978, Physicochemical Aspects of Thrust Faulting in Precambrian Gneiss, Sevier Orogenic Belt, Utah, Geological Society of America Abstracts With Programs, Vol. 15, No. 5, p. 402.

Howard, A.D., and McLane, C.F. III, 1988, Erosion of Cohesionless Sediment by Groundwater Seepage, Water Resources Research, Vol. 24, No. 10, p. 1659-74.

Hunt, C.B., and Robinson, T.W., 1960, Possible Interbasin Circulation of Ground Water in the Southern Part of the Great Basin, in Geological Survey Research, United States Geological Survey Professional Paper 400-B, United States Government Printing Office, Washington, D.C., p. 273.

Irving, E., 1964, Palaeomagnetism and its Application to Geological and Geophysical Problems, John Wiley and Sons, Inc., New York, NY, 399 p.

Jadkowski, M.A., 1987, Multispectral Remote Sensing of Landslide Susceptible Areas: Unpublished Ph.D. Dissertation, Department of Civil and Environmental Engineering, Utah State University, Logan, UT, 264 p.

Jones, J.W.; Simpson, E.S.; Neuman, S.P.; and Keys, W.S., 1985, Field and Theoretical Examinations of Fractured Crystalline Rock Near Oracle, Arizona, Division of Radiation Programs and Earth Sciences, Office of Nuclear Regulatory Research, United States Nuclear Regulatory Commission, Washington, D.C., 104 p.

Kamb, W.B., 1959, Ice Petrofabric Observations from Blue Glacier, Washington, in Relation to Theory and Experiment, Journal of Geophysical Research, Vol. 64, No. 11, p. 1891-1909.

Karous, M., and Hjelt, S.E., 1983, Linear Filtering of VLF Dip-Angle Measurements, Geophysical Prospecting, Vol. 31, p. 782-794.

Keaton, J.R., 1987, Personal Communication, Senior Engineering Geologist, Sergent, Beckwith and Hauskins, Salt Lake City, UT.

____________, 1988a, A Probabilistic Model For Hazards Related to Sedimentation Processes on Alluvial Fans in Davis County, Utah: Unpublished Ph.D. Dissertation, Department of Geology, Texas A&M University, College Station, TX, 441 p.

____________, 1988b, Personal Communication, Senior Engineering Geologist, Sergent, Beckwith and Hauskins, Salt Lake City, UT.

Lagmanson, M., 1990, Personal Communication, Saga Geophysics, Austin, TX.

LaPointe, P.R., and Hudson, J.A., 1985, Characterization and Interpretation of Rock Mass Joint Patterns, Geological Society of America Special Paper 199, Boulder, CO, 37 p.

Legrand, H., 1979, Evaluation Techniques in Fractured-Rock Hydrology, Journal of Hydrology, Vol. 43, p. 333-346.

Long, J.C.S.; Endo, H.K.; Karasaki, K; Pyrak, L; MacLean, P.; and Witherspoon, P.A., 1985, Hydrogeologic Behavior of Fracture Networks, in Hydrogeology of Rocks of Low Permeability, International Association of Hydrogeologists Memoires, Tucson, AZ, Vol. XVII, Part 1 (Proceedings), p. 449.

Long, J.C.S., and Witherspoon, P.A., 1985, The Relationship of the Degree of Interconnection to Permeability in Fracture Networks, Journal of Geophysical Research, Vol. 90, No. B4, p. 3087-3098.

Lowe, M., 1989, Slope Failure Inventory Map; Bountiful Peak Quadrangle, Unpublished Davis County Planning Commission Map, Farmington, UT, 1:24000 scale.

Mardia, K.V., 1972, Statistics of Directional Data, Academic Press, New York, NY, 357 p.

Mark, D.M., 1974, On the Interpretation of Till Fabrics, Geology, Vol. 2, p. 101-104.

Mathewson, C.C. and Santi, P.M., 1987, Bedrock Ground Water: Source of Sustained Post-Debris Flow Stream Discharge. In Proceedings of the 23rd Symposium on Engineering Geology and Soils Engineering, Utah State University, Logan, UT, p. 253.

______________; Keaton, J.R.; and Santi, P.M., 1990, Role of Bedrock Ground Water in Debris Flows and Sustained Post-Flow Stream Discharge, The Bulletin of the Association of Engineering Geologists, Vol. XXVII, No. 1, p. 73-83.

McElhinny, M.W., 1973, Palaeomagnetism and Plate Tectonics, Cambridge University Press, New York, NY, 358p.

Miflin, M.D., 1968, Delineation of Ground-Water Flow Systems in Nevada, Technical Report Series H-W, Hydrology and Water Resources Publication No. 4, Center for Water Resources Research, Desert Research Institute, University of Nevada System, NV, p. 35-45.

Milton, J.S., and Arnold, J.C., 1986, Probability and Statistics in the Engineering and Computing Sciences, McGraw-Hill Book Company, New York, NY, 643 p.

Monteith, S., 1988, Stability Analysis of the Steed Canyon Landslide, Unpublished Master of Science Thesis, Department of Civil and Environmental Engineering, Utah State University, Logan, UT, 107 p.

Morgan, D.F., 1990, Personal Communication, Associate Professor, Department of Geophysics, Texas A&M University, College Station, TX.

Mundorff, M.J.; Broom, H.C.; and Kilburn, C., 1963, Reconnaissance of the Hydrology of the Little Lost River Basin, Idaho, United States Geological Survey Water Supply Paper 1539Q, United States Government Printing Office, Washington, D.C., p. Q22.

Naeser, C.W.; Bryant, Bruce; Crittenden, M.D. Jr.; and Sorensen, M.L., 1983, Fission-track Ages of Apatite in the Wasatch Mountains, Utah: an Uplift Study, in Miller, D.M.; Todd, V.R.;and Howard, K.A., (editors), Tectonic and Stratigraphic Studies in the Eastern Great Basin, Geological Society of America, Boulder, CO, Memoir 157, p. 29-36.

Neretnieks, I., 1985, Transport in Fractured Rocks. In Hydrogeology of Rocks of Low Permeability, International Association of Hydrogeologists Memoires, Tucson, AZ, Vol. XVII, Part 1 (Proceedings), p. 301.

Nickelsen, R.P., 1974, Early Jointing and Cumulative Fracture Patterns, in Hodgson, R.A., and Gay, S.P. Jr., (editors), Proceedings of the First International Conference on the New Basement Tectonics No. 23, Utah Geological Association Publication No. 5, Salt Lake City, UT, p. 193-199.

Olson, E.P., 1985, East Layton Debris Flow, Environmental Geology, Level 2 Case Study, Report G R-4, 85-2, United States Department of Agriculture, Forest Service, R-4 Intermountain Region, Ogden, UT, 25 p.

Pack, R.T., 1985, Multivariate Analysis of Landslide-Related Variables in Davis County, Utah, in Bowles, D.S. (editor), Delineation of Landslide, Flash Flood, and Debris Flow Hazards in Utah, Utah Water Research Laboratory, Utah State University, Logan, UT, p. 50-66.

Pankey, J. M., and DeByle, N.V., 1984, Streamflow Summaries from Twelve Tributaries of Farmington Creek, Davis County Experimental Watershed, Northern Utah, General Technical Report INT-162, United States Department of Agriculture, Forest Service, Ogden, UT, 133 p.

Pollard, D.D., and Aydin, A., 1988, Progress in Understanding Jointing Over the Past Century, Geological Society of America Bulletin, Vol. 100, p. 1181-1204.

Reneau, S.L., and Dietrich, W.E., 1987, The Importance of Hollows in Debris Flow Studies: Examples from Marin County, California, Geological Society of America Reviews in Engineering Geology, Boulder, CO, Vol. VII, p. 165-179.

Saga Geophysics, 1988, Unpublished WADI User's Manual, Saga Geophysics, Austin, TX, 64 p.

Santi, P.M., 1988, The Kinematics of Debris Flow Transport Down a Canyon, Unpublished Master of Science Thesis, Department of Geology, Texas A&M University, College Station, TX, 85 p.

Schuster, R.L., and Krizek, R.J., (editors), 1978, Landslides, Analysis and Control, Transportation Research Board Special Report 176, National Academy of Sciences, Washington, D.C., p. 18.

Sidle, R.C., 1987, A dynamic model of slope stability in zero-order Basins. In Beschta, R.L.; Blinn, T.; Grant, G.E.; Ice, G.G.; and Swanson, F.J., (editors), Erosion and Sedimentation in the Pacific Rim: Publication No. 165, International Association of Hydrological Sciences, Washington, D.C., p. 101.

Skelton, R.K., 1989, Personal Communication, Department of Geology, Texas A&M University, College Station, TX.

Snow, D.T., 1965, A Parallel Plate Model of Fractured Permeable Media, Ph.D. Thesis, University of California, Berkeley, CA, 331 p.

State of California Department of Natural Resources, 1954, Geology of Southern California, Bulletin 170, Division of Mines, San Francisco, CA, 527 p.

Tarling, D.H., 1983, Palaeomagnetism: Principles and Applications in Geology, Geophysics and Archaeology, Chapman and Hall, New York, NY, 379 p.

Taylor, R.W., and Fleming, A.H., 1988, Characterizing Jointed Systems by Azimuthal Resistivity Surveys, Ground Water, Vol. 26, No. 4, p. 464-474.

Telford, W.M.; Geldhart, L.P.; Sheriff, R.E.; and Keys, D.A., 1985, Applied Geophysics, Cambridge University Press, New York, NY, 860 p.

Tooker, E.W., 1983, Variations in the Structural Style and Correlation of Thrust Plates in the Sevier Foreland Thrust Belt, Great Salt Lake Area, Utah, in Miller, D.M.; Todd, V.R.; and Howard, K.A., (editors), Tectonic and Stratigraphic Studies in the Eastern Great Basin, Geological Society of America Memoir 157, Boulder, CO, p. 37-45.

Tsukamoto, Y., and Minematsu, H., 1987, Hydrogeomorphological Characteristics of a Zero-Order Basin, in Beschta, R.L.; Blinn, T.; Grant, G.E.; Ice, G.G.; and Swanson, F.J., (editors), Erosion and Sedimentation in the Pacific Rim: Publication No. 165, International Association of Hydrological Sciences, Washington, D.C., p. 61.

United States Department of the Interior, Geological Survey, 1952, Surface Water Supply of the United States, 1950, Part 10, The Great Basin, United States Geological Survey Water Supply Paper No. 1180, United States Government Printing Office, Washington, D.C., 234 p.

_________________, 1953, Surface Water Supply of the United States, 1951, Part 10, The Great Basin, United States Geological Survey Water Supply Paper No. 1214, United States Government Printing Office, Washington, D.C., 247 p.

_________________, 1954, Surface Water Supply of the United States, 1952, Part 10, The Great Basin, United States Geological Survey Water Supply Paper No. 1244, United States Government Printing Office, Washington, D.C., 247 p.

_________________, 1955, Surface Water Supply of the United States, 1953, Part 10, The Great Basin, United States Geological Survey Water Supply Paper No. 1284, United States Government Printing Office, Washington, D.C., 227 p.

__________________, 1956, <u>Surface Water Supply of the United States, 1954, Part 10, The Great Basin</u>, United States Geological Survey Water Supply Paper No. 1344, United States Government Printing Office, Washington, D.C., 252 p.

__________________, 1957, <u>Surface Water Supply of the United States, 1955, Part 10, The Great Basin</u>, United States Geological Survey Water Supply Paper No. 1394, United States Government Printing Office, Washington, D.C., 232 p.

__________________, 1958, <u>Surface Water Supply of the United States, 1956, Part 10, The Great Basin</u>, United States Geological Survey Water Supply Paper No. 1444, United States Government Printing Office, Washington, D.C., 231 p.

__________________, 1959, <u>Surface Water Supply of the United States, 1957, Part 10, The Great Basin</u>, United States Geological Survey Water Supply Paper No. 1514, United States Government Printing Office, Washington, D.C., 233 p.

__________________, 1960a, <u>Surface Water Supply of the United States, 1958, Part 10, The Great Basin</u>, United States Geological Survey Water Supply Paper No. 1564, United States Government Printing Office, Washington, D.C., 279 p.

__________________, 1960b, <u>Surface Water Supply of the United States, 1959, Part 10, The Great Basin</u>, United States Geological Survey Water Supply Paper No. 1634, United States Government Printing Office, Washington, D.C., 247 p.

__________________, 1961a, <u>Surface Water Supply of the United States, 1960, Part 10, The Great Basin</u>, United States Geological Survey Water Supply Paper No. 1714, United States Government Printing Office, Washington, D.C., 270 p.

__________________, 1961b, <u>Surface Water Records of Utah</u>, United States Geological Survey, Water Resources Division, United States Government Printing Office, Washington, D.C., 272 p.

__________________, 1962, <u>Surface Water Records of Utah</u>, United States Geological Survey, Water Resources Division, United States Government Printing Office, Washington, D.C., 270 p.

__________________, 1963, Surface Water Records of Utah, United States Geological Survey, Water Resources Division, United States Government Printing Office, Washington, D.C., 272 p.

Vandre, B.C., 1985, Rudd Creek Debris Flow, in Bowles, D.S., (editor), Delineation of Landslide, Flash Flood, and Debris Flow Hazards in Utah, Utah Water Research Laboratory, Utah State University, Logan, UT, p. 117-132.

Warburton, P.M., 1980, A Stereological Interpretation of Joint Trace Data, International Journal of Rock Mechanics, Mining Science and Geomechanics Abstracts, Vol. 17, p. 181-190.

Weeks, E.P., 1964, Use of Water-Level Recession Curves to Determine the Hydraulic Properties of Glacial Outwash in Portage County, Wisconsin, United States Geological Survey Professional Paper 501-B, United States Government Printing Office, Washington, D.C., p. B181-B184.

White, R.B., and Gainer, R.B., 1985, Control of Ground Water Contamination at an Active Uranium Mill, Groundwater Monitoring Review, Vol. 5, No. 2, p. 75-82.

Wieczorek, G.F.; Lips, E.W.; and Ellen, S.D., 1989, Debris Flows and Hyperconcentrated Floods Along the Wasatch Front, Utah, 1983 and 1984: The Bulletin of the Association of Engineering Geologists, Vol. XXVI, No. 2, p. 191.

Wilson, C., and Dietrich, W.E., 1987, The Contribution of Bedrock Groundwater Flow to Storm Runoff and High Pore Pressure Development in Hollows, in Beschta, R.L.; Blinn, T.; Grant, G.E.; Ice, G.G.; and Swanson, F.J., (editors), Erosion and Sedimentation in the Pacific Rim: Publication No. 165, International Association of Hydrological Sciences, Washington, D.C., p. 41.

Wiltschko, D.V., 1990, Structure Graphics, Unpublished Computer Program, Department of Geology and Center for Tectonophysics, Texas A&M University, College Station, TX.

Witherspoon, P.A.; Wang, J.S.Y.; Iwai, K.; and Gale, J.E., 1980, Validity of Cubic Law for Fluid Flow in a Deformable Rock Fracture, Water Resources Research, Vol. 16, No. 6, p. 1016-1024.

Woodcock, N.H., and Naylor, M.A., 1983, Randomness Testing in Three-Dimensional Orientation Data, Journal of Structural Geology, Vol. 5, No. 5, p. 539-548.

Yonkee, A., 1990, Personal Communication, Utah Geological and Mineral Survey, Salt Lake City, UT.

Young, R.B., 1984, A Geologic Analysis of a Part of Northeastern Utah Using ERTS Multispectral Imagery, in Brigham Young University Geology Studies, Vol. 31, Part 1, Provo, UT, p. 187.

Zoback, M.L., 1983, Structure and Cenozoic Tectonism Along the Wasatch Fault Zone, Utah, in Miller, D.M.; Todd, V.R.; and Howard, K.A., (editors), Tectonic and Stratigraphic Studies in the Eastern Great Basin, Geological Society of America Memoir 157, Denver, CO, p. 3-28.

APPENDIX 1

TABLE OF NOMENCLATURE

Ma: Mega-annum (million years)

Ga: Giga-annum (billion years)

R: Resultant vector

Ro: Resultant vector for a random distribution of vector orientations at 95 percent confidence

R: Magnitude of resultant vector

S^2: Sum of squares

l: east direction cosine

m: north direction cosine

n: vertical (down) direction cosine

P: Probability density function describing the Fisher distribution of vectors

K: Fisher precision parameter; in eigenvalue analysis, an indicator of the shape of the ellipsoid ($[S_1/S_2]/[S_2/S_3]$)

k: Estimate of Fisher precision parameter

β: Angular distance between a given data point on a sphere and the spherical mean

S_1, S_2, S_3: Normalized eigenvalues calculated from sums of products matrix of direction cosines

C: Strength of the structural fabric, shown by departure from sphericity of the ellipsoid (S_1/S_3)

n: Sample population

alpha95: angular radius of a circle on a sphere which contains 95 percent of the Fisher distributed data

A: Counting area on lower hemisphere for Kamb contouring

E: Expected number of observations falling in A

σ: Standard deviation of the number of points that will fall within A for a randomly distributed sample

e_p: Primary magnetic field emitted by station

e_s: Secondary field induced by current in subsurface conductor

n_j: The number of ranked observations in each sample of the Kruskal-Wallis test

R_j: The numerical value of the summed ranks within each sample of the Kruskal-Wallis test

q: The summed values of (R_j^2/n_j) for calculating H

H: The test statistic for comparison with H_0 and H_1, calculated as follows: $H = (12/n[n+1])(q)-3(n+1)$; from Conover, 1980, p. 230.

H_0: The null hypothesis

H_1: The alternative ("research") hypothesis

APPENDIX 2

TABLE OF RESULTANTS (Ro) OF RANDOMLY ORIENTED VECTORS AT 95 PERCENT CONFIDENCE

n	0	1	2	3	4	5	6	7	8	9
0	-	-	-	2.62	3.10	3.50	3.85	4.18	4.48	4.76
10	5.03	5.28	5.52	5.75	5.98	6.19	6.40	6.60	6.79	6.98
20	7.17	7.35	7.52	7.69	7.86	8.02	8.18	8.34	8.50	8.65
30	8.80	8.94	9.09	9.23	9.37	9.51	9.65	9.78	9.91	10.0
40	10.2	10.3	10.4	10.6	10.7	10.8	10.9	11.0	11.2	11.2
50	11.4	11.5	11.6	11.7	11.8	11.9	12.0	12.2	12.3	12.4
60	12.5	12.6	12.7	12.8	12.9	13.0	13.1	13.2	13.3	13.4
70	13.5	13.6	13.7	13.8	13.8	13.9	14.0	14.1	14.2	14.3
80	14.4	14.5	14.6	14.7	14.8	14.8	14.9	15.0	15.1	15.2
90	15.3	15.4	15.4	15.5	15.6	15.7	15.8	15.9	15.9	16.0

100 - 16.1

Adapted from Irving, 1964. Numbers above 10.0 have been rounded off to one decimal place.

APPENDIX 3

KRUSKAL-WALLIS ONE-WAY ANALYSES OF VARIANCE

1) To compare the Fisher k values for different lithologies.

H_0 = there is no significant difference in the Fisher k for different lithologies.

H_1 = Fisher k values for different lithologies are significantly different.

Confidence level = 95 percent

n = 21; df = 2

	RANKS	
Gneiss	Amphibolite	Pegmatite
5	1	3
6	2	4
7	8	9
12	10	11
13	14	15
18	16	20
21	17	
	19	
n_j=7	n_j=8	n_j=6
R_j=82	R_j=87	R_j=62

Sum from j=1 to j=3 for (R_j^2/n_j) = 2547.37 = "q".

H = (12/n[n+1])(q)-3(n+1) = 0.165.

For small sample sizes, the approximate value of the statistic at 95 percent confidence with df=2 is obtained from the Chi-square distribution. The value of the statistic is 5.991 (Conover, 1980, p. 432); thus H_0 cannot be rejected. It is concluded that the Fisher k values for different lithologies are the same.

2) To compare the Fisher k values for different regions.

H_0 = there is no significant difference in the Fisher k for different regions.

H_1 = Fisher k values for different regions are significantly different.

Confidence level = 95 percent

n = 21; df = 7

RANKS OF REGIONS 1-8

1	2	3	4	5	6	7	8
15	1	3	9	7	11	2	10
19	4	8	12	16	13	6	18
21	5	-	14	-	17	-	20
n_j=3	n_j=3	n_j=2	n_j=3	n_j=2	n_j=3	n_j=2	n_j=3
R_j=55	R_j=10	R_j=11	R_j=35	R_j=23	R_j=41	R_j=8	R_j=48

Sum from j=1 to j=8 for (R_j^2/n_j) = 3135.20 = "q".

H = (12/n[n+1])(q)-3(n+1) = 15.43.

The value of the statistic at 95 percent confidence with df=7 is obtained from the Chi-square distribution. The value of the statistic is 14.07 (Conover, 1980, p. 432); thus H_0 is rejected in favour of H_1. It is concluded that the Fisher k values for different regions are different.

3) To compare alpha95 values for different lithologies.

H_0 = there is no significant difference in alpha95 for different lithologies.

H_1 = alpha95 values for different lithologies are significantly different.

Confidence level = 95 percent

n = 21; df = 2

RANKS

Gneiss	Amphibolite	Pegmatite
1	7	4
2	9	5
3	11	6
10	14	8
11	15	17
13	16	21
19	18	
	20	
n_j=7	n_j=8	n_j=6
R_j=59	R_j=110	R_j=61

Sum from j=1 to j=3 for (R_j^2/n_j) = 2629.95 = "q".

H = (12/n[n+1])(q)-3(n+1) = 3.03.

For small sample sizes, the approximate value of the statistic at 95 percent confidence with df=2 is obtained from the Chi-square distribution. The value of the statistic is 5.991 (Conover, 1980, p. 432); thus H_0 cannot be rejected. It is concluded that alpha95 values for different lithologies are the same.

4) To compare alpha95 values for different regions.

H_0 = there is no significant difference in alpha95 for different regions.

H_1 = alpha95 values for different regions are significantly different.

Confidence level = 95 percent

n = 21; df = 7

RANKS OF REGIONS 1-8

1	2	3	4	5	6	7	8
5	8	6	2	11	3	13	1
9	14	7	4	16	15	18	11
10	19	-	20	-	17	-	21
n_j=3	n_j=3	n_j=2	n_j=3	n_j=2	n_j=3	n_j=2	n_j=3
R_j=55	R_j=10	R_j=11	R_j=35	R_j=23	R_j=41	R_j=8	R_j=48

Sum from j=1 to j=8 for (R_j^2/n_j) = 2678.40 = "q".

H = (12/n[n+1])(q)-3(n+1) = 4.15.

The value of the statistic at 95 percent confidence with df=7 is obtained from the Chi-square distribution. The value of the statistic is 14.07 (Conover, 1980, p. 432); thus H_0 cannot be rejected. It is concluded that alpha95 values for different regions are the same.

APPENDIX 4

ORIGINAL FRACTURE ORIENTATION DATA

1) Raw Data: "Field Observations" and "Wasatch3"

2) Reduced Data: "Wholeoutcrop" and "Mean Poles to Bedding"

FIELD OBSERVATIONS

No.	ID	Plng	Trnd	Strike	Dip	Azmth	Dip	Dip	DDir	Plt	Site
1	X	47	179	N89E	43 NW	269	43	43	359		GQ55
2	X	62	181	N89W	28 NE	271	28	28	1		GQ55
3	X	26	92	N2E	64 NW	182	64	64	272		GQ55
4	X	42	100	N10E	48 NW	190	48	48	280		GQ55
5	X	3	261	N9W	87 NE	351	87	87	81		GQ55
6	X	72	205	N65W	18 NE	295	18	18	25		GQ55
7	X	46	175	N85E	44 NW	265	44	44	355		GQ55
8	X	55	176	N86E	35 NW	266	35	35	356		GQ55
9	X	49	67	N23W	41 SW	157	41	41	247		GQ55
10	X	41	102	N12E	49 NW	192	49	49	282		P55
11	X	26	43	N47W	64 SW	133	64	64	223		P55
12	X	3	59	N31W	87 SW	149	87	87	239		P55
13	X	36	110	N20E	54 NW	200	54	54	290		P55
14	X	46	301	N31E	44 SE	31	44	44	121		A55
15	X	10	113	N23E	80 NW	203	80	80	293		A55
16	X	32	66	N24W	58 SW	156	58	58	246		A55
17	X	33	67	N23W	57 SW	157	57	57	247		A55
18	X	43	313	N43E	47 SE	43	47	47	133		A55
19	X	50	308	N38E	40 SE	38	40	40	128		A55
20	X	26	41	N49W	64 SW	131	64	64	221		A55
21	X	37	303	N33E	53 SE	33	53	53	123		A55
22	X	25	346	N76E	65 SE	76	65	65	166		A55
23	X	75	128	N38E	15 NW	218	15	15	308		A55
24	BDG	15	190	N80W	75 NE	280	75	75	10		S55
25	X	23	90	N0W	67 W	180	67	67	270		S55
26	X	41	85	N5W	49 SW	175	49	49	265		S55
27	X	30	95	N5E	60 NW	185	60	60	275		S55
28	X	14	314	N44E	76 SE	44	76	76	134		S55
29	X	6	318	N48E	84 SE	48	84	84	138		S55
30	X	1	91	N1E	89 NW	181	89	89	271		A56
31	X	25	294	N24E	65 SE	24	65	65	114		A56
32	X	10	300	N30E	80 SE	30	80	80	120		A56
33	X	30	33	N57W	60 SW	123	60	60	213		A56
34	X	35	275	N5E	55 SE	5	55	55	95		A56
35	X	59	65	N25W	31 SW	155	31	31	245		A56
36	X	68	71	N19W	22 SW	161	22	22	251		A56
37	X	65	60	N30W	25 SW	150	25	25	240		A56
38	X	32	288	N18E	58 SE	18	58	58	108		A56
39	X	5	316	N46E	85 SE	46	85	85	136		A56
40	X	47	286	N16E	43 SE	16	43	43	106		A56
41	X	22	326	N56E	68 SE	56	68	68	146		A56
42	X	39	215	N55W	51 NE	305	51	51	35		A56
43	X	53	67	N23W	37 SW	157	37	37	247		A56
44	X	52	186	N84W	38 NE	276	38	38	6		A56
45	X	41	186	N84W	49 NE	276	49	49	6		A56
46	X	4	95	N5E	86 NW	185	86	86	275		G22
47	X	90	75	N15W	0 SW	165	0	0	255		G22
48	X	3	169	N79E	87 NW	259	87	87	349		G22
49	X	4	67	N23W	86 SW	157	86	86	247		G22
50	X	4	183	N87W	86 NE	273	86	86	3		G22
51	X	7	6	N84W	83 SW	96	83	83	186		G22
52	X	55	332	N62E	35 SE	62	35	35	152		G22
53	X	25	85	N5W	65 SW	175	65	65	265		G22
54	X	10	102	N12E	80 NW	192	80	80	282		G22
55	X	4	151	N61E	86 NW	241	86	86	331		G22

FIELD OBSERVATIONS: Continued

No.	ID	Plng	Trnd	Strike	Dip	Azmth	Dip	Dip	DDir	Plt	Site
56	X	27	184	N86W	63 NE	274	63	63	4		G22
57	X	5	81	N9W	85 SW	171	85	85	261		G22
58	X	28	183	N87W	62 NE	273	62	62	3		G22
59	X	45	345	N75E	45 SE	75	45	45	165		G22
60	X	15	263	N7W	75 NE	353	75	75	83		G22
61	X	29	181	N89W	61 NE	271	61	61	1		G22
62	X	12	349	N79E	78 SE	79	78	78	169		G22
63	X	29	251	N19W	61 NE	341	61	61	71		G22
64	X	47	320	N50E	43 SE	50	43	43	140		G22
65	BDG	72	125	N35E	18 NW	215	18	18	305		G59
66	BDG	72	105	N15E	18 NW	195	18	18	285		G59
67	BDG	76	126	N36E	14 NW	216	14	14	306		G59
68	X	4	98	N8E	86 NW	188	86	86	278		G59
69	X	8	94	N4E	82 NW	184	82	82	274		G59
70	X	90	105	N15E	0 NW	195	0	0	285		G59
71	X	8	353	N83E	82 SE	83	82	82	173		G59
72	X	29	353	N83E	61 SE	83	61	61	173		G59
73	X	5	356	N86E	85 SE	86	85	85	176		G59
74	X	9	198	N72W	81 NE	288	81	81	18		G59
75	X	4	23	N67W	86 SW	113	86	86	203		G59
76	X	2	340	N70E	88 SE	70	88	88	160	2	G59
77	X	4	164	N74E	86 NW	254	86	86	344		G59
78	X	4	337	N67E	86 SE	67	86	86	157		G59
79	X	2	159	N69E	88 NW	249	88	88	339		G59
80	X	9	171	N81E	81 NW	261	81	81	351		G59
81	X	12	166	N76E	78 NW	256	78	78	346		G59
82	X	1	341	N71E	89 SE	71	89	89	161		G59
83	X	9	154	N64E	81 NW	244	81	81	334		G59
84	X	6	72	N18W	84 SW	162	84	84	252		G64
85	X	8	78	N12W	82 SW	168	82	82	258		G64
86	X	6	83	N7W	84 SW	173	84	84	263		G64
87	X	1	9	N81W	89 SW	99	89	89	189		G64
88	X	0	180	N90E	90 N	270	90	90	0		G64
89	X	10	163	N73E	80 NW	253	80	80	343		G64
90	X	12	270	N0E	78 E	0	78	78	90		G64
91	X	14	157	N67E	76 NW	247	76	76	337		Q65
92	X	2	327	N57E	88 SE	57	88	88	147		Q65
93	X	11	150	N60E	79 NW	240	79	79	330		Q65
94	X	16	327	N57E	74 SE	57	74	74	147		Q65
95	X	14	145	N55E	76 NW	235	76	76	325		Q65
96	X	10	65	N25W	80 SW	155	80	80	245		Q65
97	X	14	71	N19W	76 SW	161	76	76	251		Q65
98	X	19	81	N9W	71 SW	171	71	71	261		Q65
99	X	16	323	N53E	74 SE	53	74	74	143		Q65
100	X	17	330	N60E	73 SE	60	73	73	150		Q65
101	X	24	190	N80W	66 NE	280	66	66	10		Q65
102	X	23	186	N84W	67 NE	276	67	67	6		Q65
103	X	2	315	N45E	88 SE	45	88	88	135		Q65
104	X	2	318	N48E	88 SE	48	88	88	138		Q65
105	X	5	320	N50E	85 SE	50	85	85	140		Q65
106	X	20	192	N78W	70 NE	282	70	70	12		Q65
107	X	9	93	N3E	81 NW	183	81	81	273		Q65
108	X	15	96	N6E	75 NW	186	75	75	276		Q65
109	X	6	353	N83E	84 SE	83	84	84	173		Q65
110	X	23	186	N84W	67 NE	276	67	67	6		Q65

FIELD OBSERVATIONS: Continued

No.	ID	Plng	Trnd	Strike	Dip	Azmth	Dip	Dip	DDir	Plt	Site
111	X	15	86	N4W	75 SW	176	75	75	266		Q65
112	X	13	81	N9W	77 SW	171	77	77	261		Q65
113	X	0	84	N6W	90 SW	174	90	90	264		Q65
114	X	15	304	N34E	75 SE	34	75	75	124		P66
115	X	32	301	N31E	58 SE	31	58	58	121		P66
116	X	19	329	N59E	71 SE	59	71	71	149		P66
117	X	15	337	N67E	75 SE	67	75	75	157		P66
118	X	36	24	N66W	54 SW	114	54	54	204		P66
119	X	27	175	N85E	63 NW	265	63	63	355		P66
120	X	31	296	N26E	59 SE	26	59	59	116		P66
121	X	7	101	N11E	83 NW	191	83	83	281		P66
122	X	16	330	N60E	74 SE	60	74	74	150		P66
123	X	40	34	N56W	50 SW	124	50	50	214		P66
124	X	27	33	N57W	63 SW	123	63	63	213		Q66
125	X	36	215	N55W	54 NE	305	54	54	35		Q66
126	X	10	338	N68E	80 SE	68	80	80	158		Q66
127	X	2	336	N66E	88 SE	66	88	88	156		Q66
128	X	29	331	N61E	61 SE	61	61	61	151		KP66
129	X	28	335	N65E	62 SE	65	62	62	155		KP66
130	X	12	283	N13E	78 SE	13	78	78	103		KP66
131	X	0	108	N18E	90 NW	198	90	90	288		KP66
132	X	50	169	N79E	40 NW	259	40	40	349		KP66
133	X	48	181	N89W	42 NE	271	42	42	1		KP66
134	X	20	325	N55E	70 SE	55	70	70	145		KP66
135	X	21	25	N65W	69 SW	115	69	69	205		KP66
136	X	38	268	N2W	52 NE	358	52	52	88		KP66
137	X	20	201	N69W	70 NE	291	70	70	21		KP66
138	X	54	228	N42W	36 NE	318	36	36	48		P67
139	X	35	95	N5E	55 NW	185	55	55	275		P67
140	X	51	302	N32E	39 SE	32	39	39	122		P67
141	X	34	5	N85W	56 SW	95	56	56	185		P67
142	X	43	30	N60W	47 SW	120	47	47	210		P67
143	X	22	118	N28E	68 NW	208	68	68	298		P67
144	X	57	214	N56W	33 NE	304	33	33	34		P67
145	X	17	344	N74E	73 SE	74	73	73	164		P67
146	X	10	228	N42W	80 NE	318	80	80	48		P67
147	X	30	2	N88W	60 SW	92	60	60	182		P67
148	BDG	58	51	N39W	32 SW	141	32	32	231		G68
149	BDG	42	35	N55W	48 SW	125	48	48	215		G68
150	BDG	39	33	N57W	51 SW	123	51	51	213		G68
151	X	30	148	N58E	60 NW	238	60	60	328		G68
152	X	25	198	N72W	65 NE	288	65	65	18		G68
153	X	19	148	N58E	71 NW	238	71	71	328		G68
154	X	44	349	N79E	46 SE	79	46	46	169		G68
155	X	23	332	N62E	67 SE	62	67	67	152		G68
156	X	23	246	N24W	67 NE	336	67	67	66		G68
157	X	26	252	N18W	64 NE	342	64	64	72		G68
158	X	15	333	N63E	75 SE	63	75	75	153		G68
159	X	11	167	N77E	79 NW	257	79	79	347		G68
160	X	10	165	N75E	80 NW	255	80	80	345		G68
161	X	26	349	N79E	64 SE	79	64	64	169		G68
162	BDG	64	294	N24E	26 SE	24	26	26	114		A68
163	BDG	72	280	N10E	18 SE	10	18	18	100		A68
164	BDG	72	147	N57E	18 NW	237	18	18	327		A68
165	BDG	64	108	N18E	26 NW	198	26	26	288		A68

FIELD OBSERVATIONS: Continued

No.	ID	Plng	Trnd	Strike	Dip	Azmth	Dip	Dip	DDir	Plt	Site
166	X	16	2	N88W	74 SW	92	74	74	182		A68
167	X	46	270	N0E	44 E	0	44	44	90		A68
168	X	19	180	N90E	71 N	270	71	71	0		A68
169	X	30	345	N75E	60 SE	75	60	60	165		A68
170	X	16	5	N85W	74 SW	95	74	74	185		A68
171	X	15	13	N77W	75 SW	103	75	75	193		A68
172	X	28	235	N35W	62 NE	325	62	62	55		A68
173	X	16	353	N83E	74 SE	83	74	74	173		A68
174	X	34	226	N44W	56 NE	316	56	56	46		A68
175	X	22	237	N33W	68 NE	327	68	68	57		A68
176	X	17	321	N51E	73 SE	51	73	73	141		A68
177	BDG	55	117	N27E	35 NW	207	35	35	297		G68
178	BDG	55	105	N15E	35 NW	195	35	35	285		G68
179	BDG	52	133	N43E	38 NW	223	38	38	313		G68
180	BDG	58	105	N15E	32 NW	195	32	32	285		G68
181	BDG	58	58	N32W	32 SW	148	32	32	238		G68
182	X	11	204	N66W	79 NE	294	79	79	24		G68
183	X	26	213	N57W	64 NE	303	64	64	33		G68
184	X	26	318	N48E	64 SE	48	64	64	138		G68
185	X	34	320	N50E	56 SE	50	56	56	140		G68
186	X	32	315	N45E	58 SE	45	58	58	135		G68
187	X	21	186	N84W	69 NE	276	69	69	6		G68
188	X	40	280	N10E	50 SE	10	50	50	100		G68
189	X	20	196	N74W	70 NE	286	70	70	16		G68
190	X	42	275	N5E	48 SE	5	48	48	95		G68
191	X	30	323	N53E	60 SE	53	60	60	143		G68
192	X	27	22	N68W	63 SW	112	63	63	202		G68
193	X	35	285	N15E	55 SE	15	55	55	105		G68
194	X	4	243	N27W	86 NE	333	86	86	63		G69
195	X	42	318	N48E	48 SE	48	48	48	138		G69
196	X	33	332	N62E	57 SE	62	57	57	152		G69
197	X	21	250	N20W	69 NE	340	69	69	70		G69
198	X	43	311	N41E	47 SE	41	47	47	131		G69
199	X	83	246	N24W	7 NE	336	7	7	66		G69
200	X	40	214	N56W	50 NE	304	50	50	34		G69
201	X	30	198	N72W	60 NE	288	60	60	18		G69
202	X	28	344	N74E	62 SE	74	62	62	164		G69
203	BDG	46	160	N70E	44 NW	250	44	44	340		G69
204	BDG	5	193	N77W	85 NE	283	85	85	13		G69
205	BDG	28	29	N61W	62 SW	119	62	62	209		G69
206	BDG	13	16	N74W	77 SW	106	77	77	196		G69
207	X	47	181	N89W	43 NE	271	43	43	1		A70
208	X	20	51	N39W	70 SW	141	70	70	231		A70
209	X	11	153	N63E	79 NW	243	79	79	333		A70
210	X	10	140	N50E	80 NW	230	80	80	320		A70
211	X	15	151	N61E	75 NW	241	75	75	331		A70
212	X	14	149	N59E	76 NW	239	76	76	329		A70
213	X	20	14	N76W	70 SW	104	70	70	194		A70
214	X	11	138	N48E	79 NW	228	79	79	318		A70
215	X	35	150	N60E	55 NW	240	55	55	330		A70
216	X	20	272	N2E	70 SE	2	70	70	92		A70
217	X	3	210	N60W	87 NE	300	87	87	30		A70
218	X	30	354	N84E	60 SE	84	60	60	174		G70
219	X	49	183	N87W	41 NE	273	41	41	3		G70
220	X	40	302	N32E	50 SE	32	50	50	122		G70

FIELD OBSERVATIONS: Continued

No.	ID	Plng	Trnd	Strike	Dip		Azmth	Dip	Dip	DDir	Plt	Site
221	X	25	253	N17W	65	NE	343	65	65	73		G70
222	X	61	266	N4W	29	NE	356	29	29	86		G70
223	X	41	300	N30E	49	SE	30	49	49	120		G70
224	X	40	172	N82E	50	NW	262	50	50	352		G70
225	X	16	270	N0E	74	E	0	74	74	90		G70
226	X	41	162	N72E	49	NW	252	49	49	342		G70
227	BDG	50	102	N12E	40	NW	192	40	40	282		AG70
228	BDG	46	44	N46W	44	SW	134	44	44	224		AG70
229	BDG	54	93	N3E	36	NW	183	36	36	273		AG70
230	BDG	32	36	N54W	58	SW	126	58	58	216		G70
231	BDG	50	33	N57W	40	SW	123	40	40	213		G70
232	BDG	59	87	N3W	31	SW	177	31	31	267		A70
233	BDG	57	71	N19W	33	SW	161	33	33	251		A70
234	X	10	291	N21E	80	SE	21	80	80	111		Q71
235	X	27	72	N18W	63	SW	162	63	63	252		Q71
236	X	5	98	N8E	85	NW	188	85	85	278		Q71
237	X	5	287	N17E	85	SE	17	85	85	107		Q71
238	X	52	16	N74W	38	SW	106	38	38	196		Q71
239	X	20	11	N79W	70	SW	101	70	70	191		Q71
240	X	30	74	N16W	60	SW	164	60	60	254		Q71
241	X	60	154	N64E	30	NW	244	30	30	334		Q71
242	X	69	159	N69E	21	NW	249	21	21	339		Q71
243	X	76	155	N65E	14	NW	245	14	14	335		Q71
244	X	27	27	N63W	63	SW	117	63	63	207		Q71
245	BDG	32	25	N65W	58	SW	115	58	58	205		G71
246	BDG	32	19	N71W	58	SW	109	58	58	199		G71
247	BDG	2	195	N75W	88	NE	285	88	88	15		G71
248	X	35	165	N75E	55	NW	255	55	55	345		G71
249	X	7	158	N68E	83	NW	248	83	83	338		G71
250	X	5	159	N69E	85	NW	249	85	85	339		G71
251	X	5	156	N66E	85	NW	246	85	85	336		G71
252	X	10	58	N32W	80	SW	148	80	80	238		G71
253	X	5	247	N23W	85	NE	337	85	85	67		G71
254	X	24	295	N25E	66	SE	25	66	66	115		G71
255	X	5	70	N20W	85	SW	160	85	85	250		G71
256	X	25	280	N10E	65	SE	10	65	65	100		G71
257	X	2	345	N75E	88	SE	75	88	88	165		G71
258	X	43	10	N80W	47	SW	100	47	47	190		Q72
259	X	45	3	N87W	45	SW	93	45	45	183		Q72
260	X	38	5	N85W	52	SW	95	52	52	185		Q72
261	X	35	355	N85E	55	SE	85	55	55	175		Q72
262	X	47	356	N86E	43	SE	86	43	43	176		Q72
263	X	67	227	N43W	23	NE	317	23	23	47		Q72
264	X	60	205	N65W	30	NE	295	30	30	25		Q72
265	X	64	220	N50W	26	NE	310	26	26	40		Q72
266	X	65	214	N56W	25	NE	304	25	25	34		Q72
267	X	16	231	N39W	74	NE	321	74	74	51		Q72
268	X	51	181	N89W	39	NE	271	39	39	1		Q72
269	X	12	203	N67W	78	NE	293	78	78	23		Q72
270	X	18	195	N75W	72	NE	285	72	72	15		Q72
271	X	15	190	N80W	75	NE	280	75	75	10		Q72
272	X	14	243	N27W	76	NE	333	76	76	63		Q72
273	X	29	234	N36W	61	NE	324	61	61	54		Q72
274	X	13	1	N89W	77	SW	91	77	77	181		Q72
275	X	17	154	N64E	73	NW	244	73	73	334		Q72

FIELD OBSERVATIONS: Continued

No.	ID	Plng	Trnd	Strike	Dip		Azmth	Dip	Dip	DDir	Plt	Site
276	X	2	6	N84W	88	SW	96	88	88	186		Q72
277	X	43	350	N80E	47	SE	80	47	47	170		G72
278	X	40	346	N76E	50	SE	76	50	50	166		G72
279	X	20	343	N73E	70	SE	73	70	70	163		G72
280	X	3	81	N9W	87	SW	171	87	87	261		G72
281	X	5	264	N6W	85	NE	354	85	85	84		G72
282	X	15	262	N8W	75	NE	352	75	75	82		G72
283	BDG	60	189	N81W	30	NE	279	30	30	9		G72
284	BDG	61	140	N50E	29	NW	230	29	29	320		G72
285	BDG	58	171	N81E	32	NW	261	32	32	351		G72
286	BDG	63	132	N42E	27	NW	222	27	27	312		G72
287	BDG	55	145	N55E	35	NW	235	35	35	325		G72
288	X	60	198	N72W	30	NE	288	30	30	18		P73
289	X	66	189	N81W	24	NE	279	24	24	9		P73
290	X	0	52	N38W	90	SW	142	90	90	232		P73
291	X	3	249	N21W	87	NE	339	87	87	69		P73
292	X	0	67	N23W	90	SW	157	90	90	247		P73
293	X	7	133	N43E	83	NW	223	83	83	313		P73
294	X	6	149	N59E	84	NW	239	84	84	329		P73
295	X	6	6	N84W	84	SW	96	84	84	186		P73
296	X	45	198	N72W	45	NE	288	45	45	18		P73
297	X	57	309	N39E	33	SE	39	33	33	129		P73
298	X	38	310	N40E	52	SE	40	52	52	130		P73
299	X	28	303	N33E	62	SE	33	62	62	123		P73
300	X	59	189	N81W	31	NE	279	31	31	9		P73
301	X	15	55	N35W	75	SW	145	75	75	235		P73
302	X	30	7	N83W	60	SW	97	60	60	187		P73
303	X	34	113	N23E	56	NW	203	56	56	293		P73
304	X	13	101	N11E	77	NW	191	77	77	281		P73
305	X	9	197	N73W	81	NE	287	81	81	17		P73
306	X	25	314	N44E	65	SE	44	65	65	134		P73
307	X	13	240	N30W	77	NE	330	77	77	60		P73
308	X	17	149	N59E	73	NW	239	73	73	329		P73
309	X	21	145	N55E	69	NW	235	69	69	325		P73
310	X	58	202	N68W	32	NE	292	32	32	22		P73
311	X	4	44	N46W	86	SW	134	86	86	224		P73
312	X	26	206	N64W	64	NE	296	64	64	26		P73
313	X	30	0	N90E	60	S	90	60	60	180		P73
314	X	5	346	N76E	85	SE	76	85	85	166		P73
315	X	62	216	N54W	28	NE	306	28	28	36		P73
316	X	47	329	N59E	43	SE	59	43	43	149		P73
317	X	15	346	N76E	75	SE	76	75	75	166		P73
318	X	42	335	N65E	48	SE	65	48	48	155		P73
319	X	33	106	N16E	57	NW	196	57	57	286		P73
320	X	44	192	N78W	46	NE	282	46	46	12		P73
321	X	37	193	N77W	53	NE	283	53	53	13		P73
322	X	46	235	N35W	44	NE	325	44	44	55		P74
323	X	7	174	N84E	83	NW	264	83	83	354		P74
324	X	38	47	N43W	52	SW	137	52	52	227		P74
325	X	38	39	N51W	52	SW	129	52	52	219		P74
326	X	18	176	N86E	72	NW	266	72	72	356		P74
327	X	25	322	N52E	65	SE	52	65	65	142		P74
328	X	37	315	N45E	53	SE	45	53	53	135		P74
329	X	36	330	N60E	54	SE	60	54	54	150		P74
330	X	37	47	N43W	53	SW	137	53	53	227		P74

FIELD OBSERVATIONS: Continued

No.	ID	Plng	Trnd	Strike	Dip	Azmth	Dip	Dip	DDir	Plt	Site
331	X	14	200	N70W	76 NE	290	76	76	20		P74
332	X	25	122	N32E	65 NW	212	65	65	302		P74
333	X	20	210	N60W	70 NE	300	70	70	30		P74
334	X	49	198	N72W	41 NE	288	41	41	18		P74
335	X	32	5	N85W	58 SW	95	58	58	185		P74
336	X	18	208	N62W	72 NE	298	72	72	28		P74
337	X	20	351	N81E	70 SE	81	70	70	171		P74
338	X	30	243	N27W	60 NE	333	60	60	63		P74
339	X	24	268	N2W	66 NE	358	66	66	88		P74
340	BDG	39	154	N64E	51 NW	244	51	51	334		A75
341	BDG	36	149	N59E	54 NW	239	54	54	329		A75
342	BDG	31	149	N59E	59 NW	239	59	59	329		A75
343	BDG	42	153	N63E	48 NW	243	48	48	333		A75
344	X	50	300	N30E	40 SE	30	40	40	120		A75
345	X	20	42	N48W	70 SW	132	70	70	222		A75
346	X	30	86	N4W	60 SW	176	60	60	266		A75
347	X	17	58	N32W	73 SW	148	73	73	238		A75
348	X	12	68	N22W	78 SW	158	78	78	248		A75
349	X	62	25	N65W	28 SW	115	28	28	205		A75
350	X	62	26	N64W	28 SW	116	28	28	206		A75
351	X	26	304	N34E	64 SE	34	64	64	124		A75
352	X	20	0	N90E	70 S	90	70	70	180		A75
353	X	55	22	N68W	35 SW	112	35	35	202		A75
354	X	25	302	N32E	65 SE	32	65	65	122		A75
355	BDG	76	80	N10W	14 SW	170	14	14	260		G75a
356	BDG	72	91	N1E	18 NW	181	18	18	271		G75a
357	BDG	75	95	N5E	15 NW	185	15	15	275		G75a
358	BDG	70	176	N86E	20 NW	266	20	20	356		G75a
359	BDG	71	121	N31E	19 NW	211	19	19	301		G75a
360	BDG	69	122	N32E	21 NW	212	21	21	302		G75a
361	BDG	64	175	N85E	26 NW	265	26	26	355		G75a
362	BDG	68	147	N57E	22 NW	237	22	22	327		G75a
363	BDG	71	184	N86W	19 NE	274	19	19	4		G75a
364	BDG	67	59	N31W	23 SW	149	23	23	239		G75a
365	BDG	68	58	N32W	22 SW	148	22	22	238		G75a
366	X	35	313	N43E	55 SE	43	55	55	133		G75a
367	X	5	129	N39E	85 NW	219	85	85	309		G75a
368	X	9	131	N41E	81 NW	221	81	81	311		G75a
369	X	2	138	N48E	88 NW	228	88	88	318		G75a
370	X	12	116	N26E	78 NW	206	78	78	296		G75a
371	X	18	112	N22E	72 NW	202	72	72	292		G75a
372	X	3	354	N84E	87 SE	84	87	87	174		G75a
373	X	8	348	N78E	82 SE	78	82	82	168		G75a
374	X	39	210	N60W	51 NE	300	51	51	30		G75a
375	X	44	190	N80W	46 NE	280	46	46	10		G75a
376	X	4	310	N40E	86 SE	40	86	86	130		G75a
377	X	2	175	N85E	88 NW	265	88	88	355		G75a
378	X	13	358	N88E	77 SE	88	77	77	178		G75a
379	X	28	289	N19E	62 SE	19	62	62	109		G75a
380	X	29	297	N27E	61 SE	27	61	61	117		G75a
381	X	36	244	N26W	54 NE	334	54	54	64		G75a
382	X	15	273	N3E	75 SE	3	75	75	93		G75a
383	X	12	305	N35E	78 SE	35	78	78	125		G75a
384	X	16	265	N5W	74 NE	355	74	74	85		G75a
385	X	41	182	N88W	49 NE	272	49	49	2		G75a

FIELD OBSERVATIONS: Continued

No.	ID	Plng	Trnd	Strike	Dip	Azmth	Dip	Dip	DDir	Plt	Site
386	X	42	195	N75W	48 NE	285	48	48	15		G75a
387	X	50	262	N8W	40 NE	352	40	40	82		G75a
388	X	20	346	N76E	70 SE	76	70	70	166		G76
389	X	5	85	N5W	85 SW	175	85	85	265		G76
390	X	5	125	N35E	85 NW	215	85	85	305		G76
391	X	36	333	N63E	54 SE	63	54	54	153		G76
392	X	18	341	N71E	72 SE	71	72	72	161		G76
393	X	10	94	N4E	80 NW	184	80	80	274		G76
394	X	34	347	N77E	56 SE	77	56	56	167		G76
395	X	10	85	N5W	80 SW	175	80	80	265		G76
396	X	35	313	N43E	55 SE	43	55	55	133		G76
397	X	20	209	N61W	70 NE	299	70	70	29		G76
398	X	24	202	N68W	66 NE	292	66	66	22		G76
399	X	40	205	N65W	50 NE	295	50	50	25		G76
400	X	14	269	N1W	76 NE	359	76	76	89		G76
401	X	5	276	N6E	85 SE	6	85	85	96		G76
402	X	26	253	N17W	64 NE	343	64	64	73		G76
403	X	0	183	N87W	90 NE	273	90	90	3		G76
404	X	0	302	N32E	90 SE	32	90	90	122		G76
405	X	6	122	N32E	84 NW	212	84	84	302		G76
406	X	40	329	N59E	50 SE	59	50	50	149		G76
407	X	54	272	N2E	36 SE	2	36	36	92		G76
408	BDG	66	122	N32E	24 NW	212	24	24	302		G76
409	BDG	51	54	N36W	39 SW	144	39	39	234		G76
410	BDG	66	65	N25W	24 SW	155	24	24	245		G76
411	BDG	68	111	N21E	22 NW	201	22	22	291		G76
412	BDG	59	67	N23W	31 SW	157	31	31	247		G76
413	BDG	62	103	N13E	28 NW	193	28	28	283		G76
414	BDG	59	134	N44E	31 NW	224	31	31	314		G76
415	BDG	60	133	N43E	30 NW	223	30	30	313		G76
416	BDG	66	126	N36E	24 NW	216	24	24	306		G76
417	BDG	61	110	N20E	29 NW	200	29	29	290		G76
418	BDG	56	90	N0W	34 W	180	34	34	270		G76
419	BDG	61	104	N14E	29 NW	194	29	29	284		G76
420	X	8	280	N10E	82 SE	10	82	82	100		P77
421	X	52	196	N74W	38 NE	286	38	38	16		P77
422	X	17	324	N54E	73 SE	54	73	73	144		G77
423	X	35	169	N79E	55 NW	259	55	55	349		G77
424	X	25	285	N15E	65 SE	15	65	65	105		G77
425	X	34	300	N30E	56 SE	30	56	56	120		G77
426	X	40	188	N82W	50 NE	278	50	50	8		G77
427	X	15	265	N5W	75 NE	355	75	75	85		G77
428	X	31	171	N81E	59 NW	261	59	59	351		G77
429	X	48	198	N72W	42 NE	288	42	42	18		G77
430	X	4	264	N6W	86 NE	354	86	86	84		G77
431	X	48	201	N69W	42 NE	291	42	42	21		G77
432	X	8	293	N23E	82 SE	23	82	82	113		G77
433	X	35	195	N75W	55 NE	285	55	55	15		G77
434	X	29	272	N2E	61 SE	2	61	61	92		G77
435	X	31	289	N19E	59 SE	19	59	59	109		G77
436	X	5	80	N10W	85 SW	170	85	85	260		G77
437	X	15	255	N15W	75 NE	345	75	75	75		G77
438	X	42	269	N1W	48 NE	359	48	48	89		G77
439	X	31	255	N15W	59 NE	345	59	59	75		G77
440	X	37	322	N52E	53 SE	52	53	53	142		G77

FIELD OBSERVATIONS: Continued

No.	ID	Plng	Trnd	Strike	Dip	Azmth	Dip	Dip	DDir	Plt	Site
441	X	49	282	N12E	41 SE	12	41	41	102		G77
442	X	6	285	N15E	84 SE	15	84	84	105		G77
443	X	18	284	N14E	72 SE	14	72	72	104		G77
444	BDG	56	59	N31W	34 SW	149	34	34	239		G77
445	BDG	66	54	N36W	24 SW	144	24	24	234		G77
446	BDG	63	72	N18W	27 SW	162	27	27	252		G77
447	BDG	65	71	N19W	25 SW	161	25	25	251		G77
448	BDG	68	123	N33E	22 NW	213	22	22	303		G77
449	BDG	50	40	N50W	40 SW	130	40	40	220		G77
450	BDG	60	55	N35W	30 SW	145	30	30	235		G77
451	BDG	67	50	N40W	23 SW	140	23	23	230		G77
452	BDG	63	36	N54W	27 SW	126	27	27	216		G77
453	BDG	47	42	N48W	43 SW	132	43	43	222		G77
454	BDG	53	52	N38W	37 SW	142	37	37	232		G77
455	BDG	53	50	N40W	37 SW	140	37	37	230		G77
456	BDG	62	59	N31W	28 SW	149	28	28	239		G77
457	X	5	8	N82W	85 SW	98	85	85	188		P78
458	X	29	22	N68W	61 SW	112	61	61	202		P78
459	X	26	205	N65W	64 NE	295	64	64	25		P78
460	X	22	193	N77W	68 NE	283	68	68	13		P78
461	X	30	204	N66W	60 NE	294	60	60	24		P78
462	X	67	211	N59W	23 NE	301	23	23	31		P78
463	X	59	280	N10E	31 SE	10	31	31	100		P78
464	X	32	206	N64W	58 NE	296	58	58	26		P78
465	X	30	201	N69W	60 NE	291	60	60	21		P78
466	X	41	18	N72W	49 SW	108	49	49	198		P78
467	X	33	195	N75W	57 NE	285	57	57	15		P78
468	X	32	306	N36E	58 SE	36	58	58	126		P78
469	X	23	205	N65W	67 NE	295	67	67	25		P78
470	X	25	203	N67W	65 NE	293	65	65	23		P78
471	X	10	108	N18E	80 NW	198	80	80	288		P78
472	X	40	120	N30E	50 NW	210	50	50	300		P78
473	X	45	104	N14E	45 NW	194	45	45	284		P78
474	X	46	113	N23E	44 NW	203	44	44	293		P78
475	X	39	183	N87W	51 NE	273	51	51	3		G79
476	X	54	207	N63W	36 NE	297	36	36	27		G79
477	X	38	347	N77E	52 SE	77	52	52	167		G79
478	X	45	197	N73W	45 NE	287	45	45	17		G79
479	X	60	197	N73W	30 NE	287	30	30	17		G79
480	X	33	346	N76E	57 SE	76	57	57	166		G79
481	X	39	339	N69E	51 SE	69	51	51	159		G79
482	X	39	340	N70E	51 SE	70	51	51	160		G79
483	X	26	300	N30E	64 SE	30	64	64	120		G79
484	X	61	142	N52E	29 NW	232	29	29	322		G79
485	X	55	170	N80E	35 NW	260	35	35	350		G79
486	X	50	14	N76W	40 SW	104	40	40	194		G79
487	X	22	50	N40W	68 SW	140	68	68	230		G79
488	X	41	18	N72W	49 SW	108	49	49	198		G79
489	X	36	30	N60W	54 SW	120	54	54	210		G79
490	X	59	136	N46E	31 NW	226	31	31	316		G79
491	X	9	319	N49E	81 SE	49	81	81	139		G79
492	X	68	230	N40W	22 NE	320	22	22	50		G79
493	X	49	8	N82W	41 SW	98	41	41	188		G79
494	X	81	97	N7E	9 NW	187	9	9	277		G79
495	X	18	162	N72E	72 NW	252	72	72	342		P80

FIELD OBSERVATIONS: Continued

No.	ID	Plng	Trnd	Strike	Dip		Azmth	Dip	Dip	DDir	Plt	Site
496	X	24	172	N82E	66	NW	262	66	66	352		P80
497	X	46	148	N58E	44	NW	238	44	44	328		P80
498	X	0	150	N60E	90	NW	240	90	90	330		P80
499	X	17	163	N73E	73	NW	253	73	73	343		P80
500	X	40	60	N30W	50	SW	150	50	50	240		P80
501	X	10	326	N56E	80	SE	56	80	80	146		P80
502	X	11	323	N53E	79	SE	53	79	79	143		P80
503	X	15	167	N77E	75	NW	257	75	75	347		P80
504	X	15	319	N49E	75	SE	49	75	75	139		P80
505	X	12	151	N61E	78	NW	241	78	78	331		P80
506	X	49	289	N19E	41	SE	19	41	41	109		P80
507	X	15	152	N62E	75	NW	242	75	75	332		P80
508	X	46	225	N45W	44	NE	315	44	44	45		P80
509	X	35	323	N53E	55	SE	53	55	55	143		P80
510	X	36	6	N84W	54	SW	96	54	54	186		P80
511	X	15	153	N63E	75	NW	243	75	75	333		P80
512	X	42	280	N10E	48	SE	10	48	48	100		G80
513	X	6	331	N61E	84	SE	61	84	84	151		G80
514	X	20	151	N61E	70	NW	241	70	70	331		G80
515	X	38	287	N17E	52	SE	17	52	52	107		G80
516	X	2	162	N72E	88	NW	252	88	88	342		G80
517	X	10	327	N57E	80	SE	57	80	80	147		G80
518	X	20	158	N68E	70	NW	248	70	70	338		G80
519	X	55	220	N50W	35	NE	310	35	35	40		G80
520	X	31	150	N60E	59	NW	240	59	59	330		G80
521	X	16	157	N67E	74	NW	247	74	74	337		G80
522	X	58	238	N32W	32	NE	328	32	32	58		G80
523	X	30	258	N12W	60	NE	348	60	60	78		G80
524	X	38	242	N28W	52	NE	332	52	52	62		G80
525	BDG	70	208	N62W	20	NE	298	20	20	28		G80
526	BDG	70	225	N45W	20	NE	315	20	20	45		G80
527	BDG	65	235	N35W	25	NE	325	25	25	55		G80
528	BDG	25	218	N52W	65	NE	308	65	65	38		G80
529	BDG	53	219	N51W	37	NE	309	37	37	39		G80
530	BDG	76	1	N89W	14	SW	91	14	14	181		A81a
531	BDG	71	11	N79W	19	SW	101	19	19	191		A81a
532	BDG	77	13	N77W	13	SW	103	13	13	193		A81a
533	X	46	306	N36E	44	SE	36	44	44	126		A81a
534	X	47	294	N24E	43	SE	24	43	43	114		A81a
535	X	5	191	N79W	85	NE	281	85	85	11		A81a
536	X	5	90	N0W	85	W	180	85	85	270		A81a
537	X	5	90	N0W	85	W	180	85	85	270		A81a
538	X	10	91	N1E	80	NW	181	80	80	271		A81a
539	X	25	13	N77W	65	SW	103	65	65	193		A81a
540	X	14	132	N42E	76	NW	222	76	76	312		A81a
541	X	18	128	N38E	72	NW	218	72	72	308		A81a
542	X	0	5	N85W	90	SW	95	90	90	185		A81a
543	X	0	84	N6W	90	SW	174	90	90	264		A81a
544	X	32	284	N14E	58	SE	14	58	58	104		A81a
545	X	50	32	N58W	40	SW	122	40	40	212		A81b
546	X	6	305	N35E	84	SE	35	84	84	125		A81b
547	X	4	185	N85W	86	NE	275	86	86	5		A81b
548	X	6	186	N84W	84	NE	276	84	84	6		A81b
549	X	30	300	N30E	60	SE	30	60	60	120		A81b
550	X	31	312	N42E	59	SE	42	59	59	132		A81b

FIELD OBSERVATIONS: Continued

No.	ID	Plng	Trnd	Strike	Dip		Azmth	Dip	Dip	DDir	Plt	Site
551	X	56	46	N44W	34	SW	136	34	34	226		A81b
552	X	58	33	N57W	32	SW	123	32	32	213		A81b
553	BDG	55	81	N9W	35	SW	171	35	35	261		A82
554	BDG	66	80	N10W	24	SW	170	24	24	260		A82
555	BDG	56	42	N48W	34	SW	132	34	34	222		A82
556	BDG	55	58	N32W	35	SW	148	35	35	238		A82
557	X	5	38	N52W	85	SW	128	85	85	218		A82
558	X	26	207	N63W	64	NE	297	64	64	27		A82
559	X	48	214	N56W	42	NE	304	42	42	34		A82
560	X	2	235	N35W	88	NE	325	88	88	55		A82
561	X	1	299	N29E	89	SE	29	89	89	119		A82
562	X	2	119	N29E	88	NW	209	88	88	299		A82
563	X	4	300	N30E	86	SE	30	86	86	120		A82
564	X	5	240	N30W	85	NE	330	85	85	60		A82
565	X	4	67	N23W	86	SW	157	86	86	247		A82
566	X	1	338	N68E	89	SE	68	89	89	158		A82
567	X	64	325	N55E	26	SE	55	26	26	145		A82
568	X	28	185	N85W	62	NE	275	62	62	5		A82
569	X	50	220	N50W	40	NE	310	40	40	40		A82
570	X	38	262	N8W	52	NE	352	52	52	82		A82
571	X	11	223	N47W	79	NE	313	79	79	43		A82
572	X	28	235	N35W	62	NE	325	62	62	55		A82
573	X	25	133	N43E	65	NW	223	65	65	313		A82
574	X	41	129	N39E	49	NW	219	49	49	309		A82
575	X	14	230	N40W	76	NE	320	76	76	50		A82
576	BDG	47	156	N66E	43	NW	246	43	43	336		A82
577	BDG	51	22	N68W	39	SW	112	39	39	202		A82
578	BDG	49	33	N57W	41	SW	123	41	41	213		A82
579	X	74	311	N41E	16	SE	41	16	16	131		P83
580	X	62	330	N60E	28	SE	60	28	28	150		P83
581	X	70	320	N50E	20	SE	50	20	20	140		P83
582	X	63	328	N58E	27	SE	58	27	27	148		P83
583	X	67	325	N55E	23	SE	55	23	23	145		P83
584	X	18	120	N30E	72	NW	210	72	72	300		P83
585	X	19	116	N26E	71	NW	206	71	71	296		P83
586	X	43	135	N45E	47	NW	225	47	47	315		P83
587	X	42	0	N90E	48	S	90	48	48	180		P83
588	X	3	290	N20E	87	SE	20	87	87	110		P83
589	X	6	225	N45W	84	NE	315	84	84	45		P83
590	X	10	140	N50E	80	NW	230	80	80	320		P83
591	X	19	129	N39E	71	NW	219	71	71	309		P83
592	X	32	167	N77E	58	NW	257	58	58	347		P83
593	X	22	138	N48E	68	NW	228	68	68	318		P83
594	X	64	347	N77E	26	SE	77	26	26	167		P83
595	X	5	87	N3W	85	SW	177	85	85	267		P83
596	X	53	237	N33W	37	NE	327	37	37	57		P84
597	X	20	255	N15W	70	NE	345	70	70	75		P84
598	X	22	352	N82E	68	SE	82	68	68	172		P84
599	X	32	249	N21W	58	NE	339	58	58	69		P84
600	X	35	263	N7W	55	NE	353	55	55	83		P84
601	X	24	173	N83E	66	NW	263	66	66	353		P84
602	X	30	32	N58W	60	SW	122	60	60	212		P84
603	X	63	179	N89E	27	NW	269	27	27	359		P84
604	X	68	201	N69W	22	NE	291	22	22	21		P84
605	X	19	173	N83E	71	NW	263	71	71	353		P84

FIELD OBSERVATIONS: Continued

No.	ID	Plng	Trnd	Strike	Dip	Azmth	Dip	Dip	DDir	Plt	Site
606	X	17	349	N79E	73 SE	79	73	73	169		P84
607	X	6	91	N1E	84 NW	181	84	84	271		P84
608	X	15	197	N73W	75 NE	287	75	75	17		P84
609	X	10	285	N15E	80 SE	15	80	80	105		P84
610	X	13	330	N60E	77 SE	60	77	77	150		P84
611	X	45	284	N14E	45 SE	14	45	45	104		P84
612	X	10	4	N86W	80 SW	94	80	80	184		P84
613	X	65	39	N51W	25 SW	129	25	25	219		P84
614	X	42	236	N34W	48 NE	326	48	48	56		P84
615	X	58	88	N2W	32 SW	178	32	32	268		P84
616	X	49	27	N63W	41 SW	117	41	41	207		P84
617	X	25	231	N39W	65 NE	321	65	65	51		P84
618	X	5	160	N70E	85 NW	250	85	85	340		Q84
619	X	5	338	N68E	85 SE	68	85	85	158		Q84
620	X	6	154	N64E	84 NW	244	84	84	334		Q84
621	X	7	160	N70E	83 NW	250	83	83	340		Q84
622	X	34	61	N29W	56 SW	151	56	56	241		Q84
623	X	75	277	N7E	15 SE	7	15	15	97		Q84
624	X	28	41	N49W	62 SW	131	62	62	221		Q84
625	X	30	23	N67W	60 SW	113	60	60	203		Q84
626	X	10	181	N89W	80 NE	271	80	80	1		Q84
627	X	14	180	N90E	76 N	270	76	76	0		Q84
628	X	6	147	N57E	84 NW	237	84	84	327		Q84
629	X	14	211	N59W	76 NE	301	76	76	31		Q84
630	X	4	212	N58W	86 NE	302	86	86	32		Q84
631	BDG	37	90	N0W	53 W	180	53	53	270		G87
632	BDG	67	279	N9E	23 SE	9	23	23	99		G87
633	X	25	203	N67W	65 NE	293	65	65	23		G87
634	X	25	200	N70W	65 NE	290	65	65	20		G87
635	X	20	131	N41E	70 NW	221	70	70	311		G87
636	X	18	358	N88E	72 SE	88	72	72	178		G87
637	X	63	183	N87W	27 NE	273	27	27	3		P88
638	X	20	329	N59E	70 SE	59	70	70	149		P88
639	X	12	42	N48W	78 SW	132	78	78	222		P88
640	X	9	329	N59E	81 SE	59	81	81	149		P88
641	X	5	245	N25W	85 NE	335	85	85	65		P88
642	X	11	111	N21E	79 NW	201	79	79	291		P88
643	X	24	94	N4E	66 NW	184	66	66	274		P88
644	X	21	35	N55W	69 SW	125	69	69	215		P88
645	X	15	51	N39W	75 SW	141	75	75	231		P88
646	X	23	137	N47E	67 NW	227	67	67	317		P88
647	X	5	197	N73W	85 NE	287	85	85	17		P88
648	X	10	40	N50W	80 SW	130	80	80	220		P88
649	X	45	258	N12W	45 NE	348	45	45	78		P88
650	X	20	36	N54W	70 SW	126	70	70	216		P88
651	X	55	196	N74W	35 NE	286	35	35	16		P88
652	X	10	34	N56W	80 SW	124	80	80	214		P88
653	X	9	145	N55E	81 NW	235	81	81	325		P89
654	X	37	260	N10W	53 NE	350	53	53	80		P89
655	X	38	250	N20W	52 NE	340	52	52	70		P89
656	X	7	149	N59E	83 NW	239	83	83	329		P89
657	X	17	144	N54E	73 NW	234	73	73	324		P89
658	X	26	150	N60E	64 NW	240	64	64	330		P89
659	X	4	348	N78E	86 SE	78	86	86	168		P89
660	X	30	308	N38E	60 SE	38	60	60	128		P89

FIELD OBSERVATIONS: Continued

No.	ID	Plng	Trnd	Strike	Dip	Azmth	Dip	Dip	DDir	Plt	Site
661	X	15	153	N63E	75 NW	243	75	75	333		P89
662	X	15	335	N65E	75 SE	65	75	75	155		P89
663	X	12	60	N30W	78 SW	150	78	78	240		P89
664	X	12	58	N32W	78 SW	148	78	78	238		P89
665	X	10	20	N70W	80 SW	110	80	80	200		P89
666	X	24	24	N66W	66 SW	114	66	66	204		P89
667	X	39	25	N65W	51 SW	115	51	51	205		P89
668	X	35	225	N45W	55 NE	315	55	55	45		P89
669	X	72	180	N90E	18 N	270	18	18	0		P89
670	X	45	184	N86W	45 NE	274	45	45	4		P89
671	X	38	193	N77W	52 NE	283	52	52	13		P89
672	X	62	167	N77E	28 NW	257	28	28	347		P89
673	X	43	354	N84E	47 SE	84	47	47	174		P89
674	X	45	238	N32W	45 NE	328	45	45	58		P89
675	X	25	171	N81E	65 NW	261	65	65	351		P89
676	BDG	63	199	N71W	27 NE	289	27	27	19		G90gen
677	X	49	163	N73E	41 NW	253	41	41	343		G90
678	X	10	346	N76E	80 SE	76	80	80	166		G90
679	X	29	166	N76E	61 NW	256	61	61	346		G90
680	X	15	168	N78E	75 NW	258	75	75	348		G90
681	X	45	198	N72W	45 NE	288	45	45	18		G90
682	X	27	179	N89E	63 NW	269	63	63	359		G90
683	X	6	334	N64E	84 SE	64	84	84	154		G90
684	X	30	149	N59E	60 NW	239	60	60	329		G90
685	X	25	306	N36E	65 SE	36	65	65	126		G90
686	X	14	168	N78E	76 NW	258	76	76	348		G90
687	X	28	166	N76E	62 NW	256	62	62	346		G90
688	X	61	176	N86E	29 NW	266	29	29	356		G90
689	X	68	191	N79W	22 NE	281	22	22	11		G90
690	X	72	213	N57W	18 NE	303	18	18	33		G90
691	X	53	161	N71E	37 NW	251	37	37	341		G90
692	X	40	144	N54E	50 NW	234	50	50	324		G90
693	X	35	336	N66E	55 SE	66	55	55	156		G90
694	X	46	23	N67W	44 SW	113	44	44	203		G90
695	X	21	167	N77E	69 NW	257	69	69	347		G90
696	X	8	56	N34W	82 SW	146	82	82	236		G90
697	BDG	45	143	N53E	45 NW	233	45	45	323		A91a
698	BDG	40	133	N43E	50 NW	223	50	50	313		A91a
699	BDG	49	132	N42E	41 NW	222	41	41	312		A91a
700	BDG	38	142	N52E	52 NW	232	52	52	322		A91a
701	BDG	41	141	N51E	49 NW	231	49	49	321		A91a
702	BDG	40	127	N37E	50 NW	217	50	50	307		A91a
703	BDG	21	145	N55E	69 NW	235	69	69	325		A91a
704	BDG	35	41	N49W	55 SW	131	55	55	221		A91b
705	BDG	31	39	N51W	59 SW	129	59	59	219		A91b
706	BDG	40	18	N72W	50 SW	108	50	50	198		A91b
707	BDG	39	21	N69W	51 SW	111	51	51	201		A91b
708	X	19	165	N75E	71 NW	255	71	71	345	X	A91
709	X	30	184	N86W	60 NE	274	60	60	4		A91
710	X	30	189	N81W	60 NE	279	60	60	9		A91
711	X	41	254	N16W	49 NE	344	49	49	74		A91
712	X	60	243	N27W	30 NE	333	30	30	63		A91
713	X	9	323	N53E	81 SE	53	81	81	143		A91
714	X	4	296	N26E	86 SE	26	86	86	116		A91
715	X	10	133	N43E	80 NW	223	80	80	313		A91

FIELD OBSERVATIONS: Continued

No.	ID	Plng	Trnd	Strike	Dip	Azmth	Dip	Dip	DDir	Plt	Site
716	X	55	196	N74W	35 NE	286	35	35	16		A91
717	X	2	151	N61E	88 NW	241	88	88	331		A91
718	X	16	313	N43E	74 SE	43	74	74	133		A91
719	X	9	319	N49E	81 SE	49	81	81	139		A91
720	X	48	201	N69W	42 NE	291	42	42	21		A91
721	X	3	17	N73W	87 SW	107	87	87	197		A91
722	X	17	177	N87E	73 NW	267	73	73	357		A91
723	X	0	209	N61W	90 NE	299	90	90	29		A91
724	X	49	156	N66E	41 NW	246	41	41	336		A91
725	X	60	173	N83E	30 NW	263	30	30	353		A91
726	X	18	148	N58E	72 NW	238	72	72	328		A91
727	X	53	162	N72E	37 NW	252	37	37	342		A91
728	X	40	200	N70W	50 NE	290	50	50	20		A91
729	X	21	170	N80E	69 NW	260	69	69	350		P92
730	X	15	169	N79E	75 NW	259	75	75	349		P92
731	X	32	171	N81E	58 NW	261	58	58	351		P92
732	X	55	226	N44W	35 NE	316	35	35	46		P92
733	X	30	245	N25W	60 NE	335	60	60	65		P92
734	X	43	110	N20E	47 NW	200	47	47	290		P92
735	X	42	316	N46E	48 SE	46	48	48	136		P92
736	X	37	318	N48E	53 SE	48	53	53	138		P92
737	X	13	58	N32W	77 SW	148	77	77	238		P92
738	X	10	60	N30W	80 SW	150	80	80	240		P92
739	X	4	159	N69E	86 NW	249	86	86	339		P92
740	X	27	29	N61W	63 SW	119	63	63	209		P92
741	X	21	179	N89E	69 NW	269	69	69	359		P92
742	X	20	171	N81E	70 NW	261	70	70	351		P92
743	X	0	132	N42E	90 NW	222	90	90	312		P92
744	X	19	52	N38W	71 SW	142	71	71	232		P92
745	X	6	144	N54E	84 NW	234	84	84	324		P92
746	X	35	44	N46W	55 SW	134	55	55	224		P92
747	X	30	28	N62W	60 SW	118	60	60	208		P92
748	X	68	204	N66W	22 NE	294	22	22	24		P92
749	X	23	170	N80E	67 NW	260	67	67	350		P92
750	X	29	163	N73E	61 NW	253	61	61	343		P92
751	X	50	302	N32E	40 SE	32	40	40	122		P92
752	X	52	318	N48E	38 SE	48	38	38	138		P92
753	X	40	82	N8W	50 SW	172	50	50	262		P92
754	X	70	199	N71W	20 NE	289	20	20	19		P92
755	X	30	16	N74W	60 SW	106	60	60	196		P92
756	X	9	168	N78E	81 NW	258	81	81	348		A93
757	X	1	160	N70E	89 NW	250	89	89	340		A93
758	X	22	319	N49E	68 SE	49	68	68	139		A93
759	X	5	13	N77W	85 SW	103	85	85	193		A93
760	X	5	315	N45E	85 SE	45	85	85	135		A93
761	X	22	180	N90E	68 N	270	68	68	0		A93
762	X	5	319	N49E	85 SE	49	85	85	139		A93
763	X	2	317	N47E	88 SE	47	88	88	137		A93
764	X	8	200	N70W	82 NE	290	82	82	20		A93
765	X	6	195	N75W	84 NE	285	84	84	15		A93
766	X	34	6	N84W	56 SW	96	56	56	186		A93
767	X	17	274	N4E	73 SE	4	73	73	94		A93
768	X	19	311	N41E	71 SE	41	71	71	131		A93
769	X	26	324	N54E	64 SE	54	64	64	144		A93
770	X	6	260	N10W	84 NE	350	84	84	80		A93

FIELD OBSERVATIONS: Continued

No.	ID	Plng	Trnd	Strike	Dip		Azmth	Dip	Dip	DDir	Plt	Site
771	BDG	60	41	N49W	30	SW	131	30	30	221		A93
772	BDG	62	54	N36W	28	SW	144	28	28	234		A93
773	BDG	67	45	N45W	23	SW	135	23	23	225		A93
774	BDG	76	336	N66E	14	SE	66	14	14	156		A93
775	BDG	70	306	N36E	20	SE	36	20	20	126		A93
776	BDG	76	352	N62E	14	SE	82	14	14	172		A93
777	BDG	1	191	N79W	89	NE	281	89	89	11		A93
778	BDG	3	199	N71W	87	NE	289	87	87	19		A93
779	BDG	14	16	N74W	76	SW	106	76	76	196		A93
780	BDG	6	18	N72W	84	SW	108	84	84	198		A93
781	X	27	310	N40E	63	SE	40	63	63	130		A94
782	X	29	301	N31E	61	SE	31	61	61	121		A94
783	X	20	320	N50E	70	SE	50	70	70	140		A94
784	X	30	297	N27E	60	SE	27	60	60	117		A94
785	X	36	307	N37E	54	SE	37	54	54	127		A94
786	X	26	299	N29E	64	SE	29	64	64	119		A94
787	X	68	199	N71W	22	NE	289	22	22	19		A94
788	X	27	109	N19E	63	NW	199	63	63	289		A94
789	X	49	85	N5W	41	SW	175	41	41	265		A94
790	X	30	101	N11E	60	NW	191	60	60	281		A94
791	BDG	20	49	N41W	70	SW	139	70	70	229		A94
792	BDG	25	45	N45W	65	SW	135	65	65	225		A94
793	BDG	25	63	N27W	65	SW	153	65	65	243		A94
794	BDG	36	64	N26W	54	SW	154	54	54	244		A94
795	X	10	137	N47E	80	NW	227	80	80	317		G94
796	X	10	132	N42E	80	NW	222	80	80	312		G94
797	X	15	120	N30E	75	NW	210	75	75	300		G94
798	X	55	44	N46W	35	SW	134	35	35	224		G94
799	X	27	20	N70W	63	SW	110	63	63	200		G94
800	X	65	71	N19W	25	SW	161	25	25	251		G94
801	X	6	316	N46E	84	SE	46	84	84	136		G94
802	X	60	16	N74W	30	SW	106	30	30	196		G94
803	X	54	12	N78W	36	SW	102	36	36	192		G94
804	X	2	318	N48E	88	SE	48	88	88	138		G94
805	BDG	25	198	N72W	65	NE	288	65	65	18		G94
806	BDG	23	202	N68W	67	NE	292	67	67	22		G94
807	BDG	26	202	N68W	64	NE	292	64	64	22		G94
808	BDG	18	189	N81W	72	NE	279	72	72	9		G94
809	BDG	42	199	N71W	48	NE	289	48	48	19		G94
810	BDG	35	201	N69W	55	NE	291	55	55	21		G94
811	X	45	168	N78E	45	NW	258	45	45	348		P95
812	X	33	27	N63W	57	SW	117	57	57	207		P95
813	X	26	12	N78W	64	SW	102	64	64	192		P95
814	X	23	105	N15E	67	NW	195	67	67	285		P95
815	X	70	202	N68W	20	NE	292	20	20	22		P95
816	X	20	9	N81W	70	SW	99	70	70	189		P95
817	X	40	145	N55E	50	NW	235	50	50	325		P95
818	X	46	359	N89E	44	SE	89	44	44	179		P95
819	X	15	41	N49W	75	SW	131	75	75	221		P95
820	X	[illegible]	55	N35W	79	SW	145	79	79	235		P95
821	X	26	29	N61W	64	SW	119	64	64	209		P95
822	X	35	36	N54W	55	SW	126	55	55	216		P95
823	X	43	54	N36W	47	SW	144	47	47	234		P95
824	X	0	323	N53E	90	SE	53	90	90	143		P95
825	X	2	88	N2W	88	SW	178	88	88	268		P95

FIELD OBSERVATIONS: Continued

No.	ID	Plng	Trnd	Strike	Dip	Azmth	Dip	Dip	DDir	Plt	Site
826	X	29	48	N42W	61 SW	138	61	61	228		P95
827	X	44	168	N78E	46 NW	258	46	46	348		P95
828	X	48	175	N85E	42 NW	265	42	42	355		P95
829	X	20	38	N52W	70 SW	128	70	70	218		P96
830	X	25	67	N23W	65 SW	157	65	65	247		P96
831	X	1	303	N33E	89 SE	33	89	89	123		P96
832	X	18	43	N47W	72 SW	133	72	72	223		P96
833	X	64	56	N34W	26 SW	146	26	26	236		P96
834	X	54	52	N38W	36 SW	142	36	36	232		P96
835	X	31	52	N38W	59 SW	142	59	59	232		P96
836	X	4	140	N50E	86 NW	230	86	86	320		P96
837	X	63	58	N32W	27 SW	148	27	27	238		P96
838	X	63	44	N46W	27 SW	134	27	27	224		P96
839	X	0	298	N28E	90 SE	28	90	90	118		P96
840	X	2	116	N26E	88 NW	206	88	88	296		P96
841	X	19	35	N55W	71 SW	125	71	71	215		P96
842	X	25	24	N66W	65 SW	114	65	65	204		P96
843	X	25	41	N49W	65 SW	131	65	65	221		P96
844	X	45	100	N10E	45 NW	190	45	45	280		P96
845	X	23	100	N10E	67 NW	190	67	67	280		P96
846	X	11	109	N19E	79 NW	199	79	79	289		P96
847	X	14	92	N2E	76 NW	182	76	76	272		P96
848	X	30	39	N51W	60 SW	129	60	60	219		P96
849	X	16	329	N59E	74 SE	59	74	74	149		P96
850	X	7	257	N13W	83 NE	347	83	83	77		P96
851	X	20	7	N83W	70 SW	97	70	70	187		P96
852	X	25	31	N59W	65 SW	121	65	65	211		P96
853	X	24	356	N86E	66 SE	86	66	66	176		P96
854	X	33	52	N38W	57 SW	142	57	57	232		P96
855	X	25	329	N59E	65 SE	59	65	65	149		P96
856	X	24	326	N56E	66 SE	56	66	66	146		P96
857	X	10	114	N24E	80 NW	204	80	80	294		P97
858	X	2	113	N23E	88 NW	203	88	88	293		P97
859	X	34	265	N5W	56 NE	355	56	56	85		P97
860	X	15	148	N58E	75 NW	238	75	75	328		P97
861	X	20	291	N21E	70 SE	21	70	70	111		P97
862	X	30	47	N43W	60 SW	137	60	60	227		P97
863	X	15	147	N57E	75 NW	237	75	75	327		P97
864	X	18	149	N59E	72 NW	239	72	72	329		P97
865	X	22	331	N61E	68 SE	61	68	68	151		P97
866	X	32	244	N26W	58 NE	334	58	58	64		P97
867	X	25	250	N20W	65 NE	340	65	65	70		P97
868	X	10	106	N16E	80 NW	196	80	80	286		P97
869	X	52	100	N10E	38 NW	190	38	38	280		P97
870	X	34	193	N77W	56 NE	283	56	56	13		P97
871	X	10	330	N60E	80 SE	60	80	80	150		P97
872	X	18	222	N48W	72 NE	312	72	72	42		P97
873	X	42	152	N62E	48 NW	242	48	48	332		P97
874	X	33	328	N58E	57 SE	58	57	57	148		P97
875	X	25	164	N74E	65 NW	254	65	65	344		P97
876	X	25	103	N13E	65 NW	193	65	65	283		P97
877	X	30	169	N79E	60 NW	259	60	60	349		P97
878	X	15	160	N70E	75 NW	250	75	75	340		P97
879	X	5	194	N76W	85 NE	284	85	85	14		P97
880	X	15	173	N83E	75 NW	263	75	75	353		P97

FIELD OBSERVATIONS: Continued

No.	ID	Plng	Trnd	Strike	Dip	Azmth	Dip	Dip	DDir	Plt	Site
881	X	10	165	N75E	80 NW	255	80	80	345		P97
882	BDG	38	54	N36W	52 SW	144	52	52	234		Q97
883	BDG	26	66	N24W	64 SW	156	64	64	246		Q97
884	BDG	32	53	N37W	58 SW	143	58	58	233		Q97
885	BDG	25	55	N35W	65 SW	145	65	65	235		Q97
886	BDG	28	35	N55W	62 SW	125	62	62	215		Q97
887	BDG	26	44	N46W	64 SW	134	64	64	224		Q97
888	BDG	47	44	N46W	43 SW	134	43	43	224		Q97
889	BDG	49	31	N59W	41 SW	121	41	41	211		G97
890	X	57	217	N53W	33 NE	307	33	33	37		Q97
891	X	66	244	N26W	24 NE	334	24	24	64		Q97
892	X	46	280	N10E	44 SE	10	44	44	100		Q97
893	X	16	157	N67E	74 NW	247	74	74	337		Q97
894	X	32	188	N82W	58 NE	278	58	58	8		Q97
895	X	25	175	N85E	65 NW	265	65	65	355		Q97
896	X	8	355	N85E	82 SE	85	82	82	175		Q97
897	X	18	158	N68E	72 NW	248	72	72	338		Q97
898	X	10	163	N73E	80 NW	253	80	80	343		Q97
899	X	8	134	N44E	82 NW	224	82	82	314		Q97
900	X	0	328	N58E	90 SE	58	90	90	148		Q97
901	X	0	333	N63E	90 SE	63	90	90	153		Q97
902	X	4	155	N65E	86 NW	245	86	86	335		Q97
903	BDG	70	224	N46W	20 NE	314	20	20	44		G100
904	BDG	76	141	N51E	14 NW	231	14	14	321		G100
905	BDG	65	235	N35W	25 NE	325	25	25	55		G100
906	BDG	30	228	N42W	60 NE	318	60	60	48		G100
907	X	10	310	N40E	80 SE	40	80	80	130		G100
908	X	21	83	N7W	69 SW	173	69	69	263		G100
909	X	7	348	N78E	83 SE	78	83	83	168		G100
910	X	9	346	N76E	81 SE	76	81	81	166		G100
911	X	21	303	N33E	69 SE	33	69	69	123		G100
912	X	31	76	N14W	59 SW	166	59	59	256		G100
913	X	9	316	N46E	81 SE	46	81	81	136		G100
914	X	12	89	N1W	78 SW	179	78	78	269		G101
915	X	11	340	N70E	79 SE	70	79	79	160		G101
916	X	11	113	N23E	79 NW	203	79	79	293		G101
917	X	13	110	N20E	77 NW	200	77	77	290		G101
918	X	13	278	N8E	77 SE	8	77	77	98		G101
919	X	25	295	N25E	65 SE	25	65	65	115		G101
920	X	21	335	N65E	69 SE	65	69	69	155		G101
921	X	18	109	N19E	72 NW	199	72	72	289		G101
922	X	38	294	N24E	52 SE	24	52	52	114		G101
923	X	32	306	N36E	58 SE	36	58	58	126		G101
924	BDG	63	226	N44W	27 NE	316	27	27	46		G101
925	BDG	70	255	N15W	20 NE	345	20	20	75		G101
926	BDG	72	244	N26W	18 NE	334	18	18	64		G101
927	BDG	62	252	N18W	28 NE	342	28	28	72		G101
928	X	68	224	N46W	22 NE	314	22	22	44		G101a
929	X	75	235	N35W	15 NE	325	15	15	55		G101a
930	X	64	213	N57W	26 NE	303	26	26	33		G101a
931	X	76	224	N46W	14 NE	314	14	14	44		G101a
932	X	10	349	N79E	80 SE	79	80	80	169		G101a
933	X	13	156	N66E	77 NW	246	77	77	336		G101a
934	X	6	159	N69E	84 NW	249	84	84	339		G101a
935	X	18	158	N68E	72 NW	248	72	72	338		G101a

FIELD OBSERVATIONS: Continued

No.	ID	Plng	Trnd	Strike	Dip	Azmth	Dip	Dip	DDir	Plt	Site
936	X	18	233	N37W	72 NE	323	72	72	53		G101a
937	X	6	95	N5E	84 NW	185	84	84	275		G101a
938	X	15	265	N5W	75 NE	355	75	75	85		G101a
939	X	5	335	N65E	85 SE	65	85	85	155		G101a
940	X	5	231	N39W	85 NE	321	85	85	51		G101a
941	BDG	44	31	N59W	46 SW	121	46	46	211		G101a
942	BDG	58	16	N74W	32 SW	106	32	32	196		G101a
943	BDG	50	35	N55W	40 SW	125	40	40	215		G101a
944	BDG	50	45	N45W	40 SW	135	40	40	225		G101a
945	BDG	45	30	N60W	45 SW	120	45	45	210		G101a
946	X	13	299	N29E	77 SE	29	77	77	119		G105
947	X	70	292	N22E	20 SE	22	20	20	112		G105
948	X	65	222	N48W	25 NE	312	25	25	42		G105
949	X	20	293	N23E	70 SE	23	70	70	113		G105
950	X	22	86	N4W	68 SW	176	68	68	266		G105
951	X	16	294	N24E	74 SE	24	74	74	114		G105
952	X	18	154	N64E	72 NW	244	72	72	334		G105
953	X	15	288	N18E	75 SE	18	75	75	108		G105
954	X	8	297	N27E	82 SE	27	82	82	117		G105
955	X	29	156	N66E	61 NW	246	61	61	336		G105
956	X	24	89	N1W	66 SW	179	66	66	269		G105
957	X	14	310	N40E	76 SE	40	76	76	130		G105
958	X	11	299	N29E	79 SE	29	79	79	119		G105
959	X	19	178	N88E	71 NW	268	71	71	358		G105
960	X	30	161	N71E	60 NW	251	60	60	341		G105
961	BDG	0	209	N61W	90 NE	299	90	90	29		G105
962	BDG	0	205	N65W	90 NE	295	90	90	25		G105
963	BDG	0	205	N65W	90 NE	295	90	90	25		G105
964	BDG	9	205	N65W	81 NE	295	81	81	25		G105
965	BDG	10	203	N67W	80 NE	293	80	80	23		G105
966	BDG	15	203	N67W	75 NE	293	75	75	23		G105
967	BDG	80	95	N5E	10 NW	185	10	10	275		G105a
968	BDG	36	182	N88W	54 NE	272	54	54	2		G105a
969	BDG	61	143	N53E	29 NW	233	29	29	323		G105a
970	BDG	1	182	N88W	89 NE	272	89	89	2		G105a
971	BDG	8	195	N75W	82 NE	285	82	82	15		G105a
972	BDG	34	181	N89W	56 NE	271	56	56	1		G105a
973	BDG	40	178	N88E	50 NW	268	50	50	358		G105a
974	X	44	107	N17E	46 NW	197	46	46	287		A107
975	X	39	110	N20E	51 NW	200	51	51	290		A107
976	X	28	122	N32E	62 NW	212	62	62	302		A107
977	X	28	125	N35E	62 NW	215	62	62	305		A107
978	X	21	127	N37E	69 NW	217	69	69	307		A107
979	X	31	14	N76W	59 SW	104	59	59	194		A107
980	X	35	3	N87W	55 SW	93	55	55	183		A107
981	X	40	10	N80W	50 SW	100	50	50	190		A107
982	X	15	19	N71W	75 SW	109	75	75	199		A107

No comment attached to this file.
From file WASATCHII on WASTCH
Created at 16:44:22 on 31 Aug 1988
Last Modified at 12:47:18 on 6 Sep 1988
Printed on: 15 Jul 1990 at: 20:14:53

WASATCH3

No.	ID	Plng	Trnd	Strike	Dip	Azmth	Dip	Dip	DDir	Plt	Site
1	X	68	196	N74W	22 NE	286	22	22	16		G108
2	X	35	238	N32W	55 NE	328	55	55	58		G108
3	X	15	148	N58E	75 NW	238	75	75	328		G108
4	X	52	147	N57E	38 NW	237	38	38	327		G108
5	X	40	151	N61E	50 NW	241	50	50	331		G108
6	X	2	357	N87E	88 SE	87	88	88	177		G108
7	X	14	204	N66W	76 NE	294	76	76	24		G108
8	X	21	206	N64W	69 NE	296	69	69	26		G108
9	X	18	200	N70W	72 NE	290	72	72	20		G108
10	X	25	201	N69W	65 NE	291	65	65	21		G108
11	X	18	208	N62W	72 NE	298	72	72	28		G108
12	X	25	208	N62W	65 NE	298	65	65	28		G108
13	X	40	177	N87E	50 NW	267	50	50	357		G108
14	X	54	250	N20W	36 NE	340	36	36	70		G108
15	X	38	245	N25W	52 NE	335	52	52	65		G108
16	X	5	175	N85E	85 NW	265	85	85	355		G108
17	X	18	210	N60W	72 NE	300	72	72	30		G108
18	X	21	220	N50W	69 NE	310	69	69	40		G108
19	X	8	137	N47E	82 NW	227	82	82	317		G108
20	X	68	196	N74W	22 NE	286	22	22	16		G108
21	X	35	238	N32W	55 NE	328	55	55	58		G108
22	BDG	47	21	N69W	43 SW	111	43	43	201		G108
23	BDG	40	19	N71W	50 SW	109	50	50	199		G108
24	BDG	47	22	N68W	43 SW	112	43	43	202		G108
25	BDG	30	33	N57W	60 SW	123	60	60	213		G108
26	BDG	52	33	N57W	38 SW	123	38	38	213		G108
27	X	30	75	N15W	60 SW	165	60	60	255		A109
28	X	60	237	N33W	30 NE	327	30	30	57		A109
29	X	12	160	N70E	78 NW	250	78	78	340		A109
30	X	36	111	N21E	54 NW	201	54	54	291		A109
31	X	54	115	N25E	36 NW	205	36	36	295		A109
32	X	59	219	N51W	31 NE	309	31	31	39		A109
33	X	35	75	N15W	55 SW	165	55	55	255		A109
34	X	59	236	N34W	31 NE	326	31	31	56		A109
35	X	34	101	N11E	56 NW	191	56	56	281		A109
36	X	51	226	N44W	39 NE	316	39	39	46		A109
37	X	34	26	N64W	56 SW	116	56	56	206		A109
38	X	4	281	N11E	86 SE	11	86	86	101		A109
39	X	48	108	N18E	42 NW	198	42	42	288		A109
40	X	38	99	N9E	52 NW	189	52	52	279		A109
41	X	49	103	N13E	41 NW	193	41	41	283		A109
42	X	12	220	N50W	78 NE	310	78	78	40		A109
43	X	40	59	N31W	50 SW	149	50	50	239		A109
44	X	25	78	N12W	65 SW	168	65	65	258		A109
45	X	33	336	N66E	57 SE	66	57	57	156		G111
46	X	69	192	N78W	21 NE	282	21	21	12		G111
47	X	72	182	N88W	18 NE	272	18	18	2		G111
48	X	55	294	N24E	35 SE	24	35	35	114		G111
49	X	56	295	N25E	34 SE	25	34	34	115		G111
50	X	7	98	N8E	83 NW	188	83	83	278		G111
51	X	18	98	N8E	72 NW	188	72	72	278		G111
52	X	6	275	N5E	84 SE	5	84	84	95		G111
53	X	37	297	N27E	53 SE	27	53	53	117		G111
54	X	2	100	N10E	88 NW	190	88	88	280		G111
55	X	7	102	N12E	83 NW	192	83	83	282		G111

WASATCH3: Continued

No.	ID	Plng	Trnd	Strike	Dip		Azmth	Dip	Dip	DDir	Plt	Site
56	X	19	290	N20E	71	SE	20	71	71	110		G111
57	X	19	169	N79E	71	NW	259	71	71	349		G111
58	X	69	304	N34E	21	SE	34	21	21	124		G111
59	X	55	284	N14E	35	SE	14	35	35	104		G111
60	X	55	288	N18E	35	SE	18	35	35	108		G111
61	X	39	288	N18E	51	SE	18	51	51	108		G111
62	X	57	294	N24E	33	SE	24	33	33	114		G111
63	X	15	97	N7E	75	NW	187	75	75	277		G111
64	X	12	166	N76E	78	NW	256	78	78	346		G111
65	X	43	209	N61W	47	NE	299	47	47	29		G111
66	X	35	229	N41W	55	NE	319	55	55	49		G111
67	X	35	212	N58W	55	NE	302	55	55	32		G111
68	X	11	173	N83E	79	NW	263	79	79	353		G111
69	X	15	170	N80E	75	NW	260	75	75	350		G111
70	X	4	9	N81W	86	SW	99	86	86	189		G111
71	BDG	17	199	N71W	73	NE	289	73	73	19		G111
72	BDG	9	197	N73W	81	NE	287	81	81	17		G111
73	BDG	11	28	N62W	79	SW	118	79	79	208		G111
74	BDG	16	17	N73W	74	SW	107	74	74	197		G111
75	BDG	23	25	N65W	67	SW	115	67	67	205		G111
76	BDG	6	202	N68W	84	NE	292	84	84	22		G111
77	BDG	58	44	N46W	32	SW	134	32	32	224		G111
78	BDG	45	39	N51W	45	SW	129	45	45	219		G111
79	BDG	71	85	N5W	19	SW	175	19	19	265		G111
80	BDG	49	40	N50W	41	SW	130	41	41	220		G111
81	X	34	309	N39E	56	SE	39	56	56	129		G112
82	X	51	176	N86E	39	NW	266	39	39	356		G112
83	X	47	179	N89E	43	NW	269	43	43	359		G112
84	X	8	108	N18E	82	NW	198	82	82	288		G112
85	X	10	95	N5E	80	NW	185	80	80	275		G112
86	X	35	75	N15W	55	SW	165	55	55	255		G112
87	X	8	108	N18E	62	NW	198	82	82	288		G112
88	X	30	303	N33E	60	SE	33	60	60	123		G112
89	X	14	93	N3E	76	NW	183	76	76	273		G112
90	X	52	215	N55W	38	NE	305	38	38	35		G112
91	X	28	301	N31E	62	SE	31	62	62	121		G112
92	X	30	300	N30E	60	SE	30	60	60	120		G112
93	X	26	308	N38E	64	SE	38	64	64	128		G112
94	X	34	304	N34E	56	SE	34	56	56	124		G112
95	X	4	95	N5E	86	NW	185	86	86	275		G112
96	X	8	86	N4W	82	SW	176	82	82	266		G112
97	X	4	78	N12W	86	SW	168	86	86	258		G112
98	X	6	95	N5E	84	NW	185	84	84	275		G112
99	X	54	200	N70W	36	NE	290	36	36	20		G112
100	X	48	194	N76W	42	NE	284	42	42	14		G112
101	BDG	64	53	N37W	26	SW	143	26	26	233		112
102	BDG	49	48	N42W	41	SW	138	41	41	228		112
103	BDG	22	30	N60W	68	SW	120	68	68	210		112
104	BDG	32	39	N51W	58	SW	129	58	58	219		112
105	BDG	56	56	N34W	34	SW	146	34	34	236		112
106	BDG	53	66	N24W	37	SW	156	37	37	246		112
107	X	2	333	N63E	88	SE	63	88	88	153		AG113
108	X	32	139	N49E	58	NW	229	58	58	319		AG113
109	X	0	291	N21E	90	SE	21	90	90	111		AG113
110	X	34	310	N40E	56	SE	40	56	56	130		AG113

WASATCH3: Continued

No.	ID	Plng	Trnd	Strike	Dip	Azmth	Dip	Dip	DDir	Plt	Site
111	X	5	325	N55E	85 SE	55	85	85	145		AG113
112	X	35	303	N33E	55 SE	33	55	55	123		AG113
113	X	0	324	N54E	90 SE	54	90	90	144		AG113
114	X	0	325	N55E	90 SE	55	90	90	145		AG113
115	X	40	306	N36E	50 SE	36	50	50	126		AG113
116	X	40	310	N40E	50 SE	40	50	50	130		AG113
117	X	2	154	N64E	88 NW	244	88	88	334		AG113
118	X	34	17	N73W	56 SW	107	56	56	197		AG113
119	X	35	294	N24E	55 SE	24	55	55	114		AG113
120	X	9	347	N77E	81 SE	77	81	81	167		AG113
121	X	32	300	N30E	58 SE	30	58	58	120		AG113
122	X	20	153	N63E	70 NW	243	70	70	333		AG113
123	X	1	150	N60E	89 NW	240	89	89	330		AG113
124	X	7	129	N39E	83 NW	219	83	83	309		AG113
125	X	17	301	N31E	73 SE	31	73	73	121		AG113
126	X	9	351	N81E	81 SE	81	81	81	171		AG113
127	X	30	320	N50E	60 SE	50	60	60	140		AG113
128	X	23	316	N46E	67 SE	46	67	67	136		AG113
129	X	6	173	N83E	84 NW	263	84	84	353		AG113
130	BDG	14	41	N49W	76 SW	131	76	76	221		AG113
131	BDG	15	44	N46W	75 SW	134	75	75	224		AG113
132	BDG	8	43	N47W	82 SW	133	82	82	223		AG113
133	BDG	5	47	N43W	85 SW	137	85	85	227		AG113
134	BDG	16	35	N55W	74 SW	125	74	74	215		AG113
135	BDG	7	33	N57W	83 SW	123	83	83	213		AG113
136	BDG	6	202	N68W	84 NE	292	84	84	22		AG113
137	BDG	10	27	N63W	80 SW	117	80	80	207		AG113
138	BDG	21	28	N62W	69 SW	118	69	69	208		AG113
139	X	40	210	N60W	50 NE	300	50	50	30		SCH44
140	X	45	211	N59W	45 NE	301	45	45	31		SCH44
141	X	44	200	N70W	46 NE	290	46	46	20		SCH44
142	X	5	184	N86W	85 NE	274	85	85	4		SCH44
143	X	31	167	N77E	59 NW	257	59	59	347		SCH44
144	X	41	157	N67E	49 NW	247	49	49	337		SCH44
145	X	43	203	N67W	47 NE	293	47	47	23		SCH44
146	X	10	201	N69W	80 NE	291	80	80	21		SCH44
147	X	2	5	N85W	88 SW	95	88	88	185		SCH44
148	X	48	353	N83E	42 SE	83	42	42	173		SCH44
149	X	39	204	N66W	51 NE	294	51	51	24		SCH44
150	X	42	0	N90E	48 S	90	48	48	180		SCH44
151	X	45	82	N8W	45 SW	172	45	45	262		G45
152	X	41	72	N18W	49 SW	162	49	49	252		G45
153	X	39	68	N22W	51 SW	158	51	51	248		G45
154	X	18	350	N80E	72 SE	80	72	72	170		G45
155	X	61	322	N52E	29 SE	52	29	29	142		G45
156	X	17	38	N52W	73 SW	128	73	73	218		PG46
157	X	20	144	N54E	70 NW	234	70	70	324		PG46
158	X	30	355	N85E	60 SE	85	60	60	175		PG46
159	X	20	308	N38E	70 SE	38	70	70	128		G47
160	X	17	306	N36E	73 SE	36	73	73	126		G47
161	X	40	296	N26E	50 SE	26	50	50	116		G47
162	X	24	319	N49E	66 SE	49	66	66	139		G47
163	X	18	336	N66E	72 SE	66	72	72	156		G47
164	X	2	327	N57E	88 SE	57	88	88	147		P48
165	X	11	275	N5E	79 SE	5	79	79	95		P48

WASATCH3: Continued

No.	ID	Plng	Trnd	Strike	Dip	Azmth	Dip	Dip	DDir	Plt	Site
166	X	15	42	N48W	75 SW	132	75	75	222		P48
167	X	15	228	N42W	75 NE	318	75	75	48		P48
168	X	4	57	N33W	86 SW	147	86	86	237		P48
169	X	21	43	N47W	69 SW	133	69	69	223		P48
170	X	6	335	N65E	84 SE	65	84	84	155		P48
171	X	20	188	N82W	70 NE	278	70	70	8		P48
172	X	41	201	N69W	49 NE	291	49	49	21		P48
173	X	40	288	N18E	50 SE	18	50	50	108		G49
174	X	39	282	N12E	51 SE	12	51	51	102		G49
175	X	24	338	N68E	66 SE	68	66	66	158		G49
176	X	20	348	N78E	70 SE	78	70	70	168		G49
177	X	31	254	N16W	59 NE	344	59	59	74		G49
178	X	40	112	N22E	50 NW	202	50	50	292		G49
179	X	25	314	N44E	65 SE	44	65	65	134		G49
180	X	25	325	N55E	65 SE	55	65	65	145		G49
181	X	20	334	N64E	70 SE	64	70	70	154		G49
182	X	24	326	N56E	66 SE	56	66	66	146		G49
183	X	20	92	N2E	70 NW	182	70	70	272		G49
184	X	26	78	N12W	64 SW	168	64	64	258		G49
185	X	5	117	N27E	85 NW	207	85	85	297		G50
186	X	14	114	N24E	76 NW	204	76	76	294		G50
187	X	48	310	N40E	42 SE	40	42	42	130		G50
188	X	42	83	N7W	48 SW	173	48	48	263		G50
189	X	51	301	N31E	39 SE	31	39	39	121		G50
190	X	20	336	N66E	70 SE	66	70	70	156		G50
191	X	24	329	N59E	66 SE	59	66	66	149		G50
192	X	40	326	N56E	50 SE	56	50	50	146		G50
193	X	24	337	N67E	66 SE	67	66	66	157		G50
194	X	41	289	N19E	49 SE	19	49	49	109		G50
195	X	4	169	N79E	86 NW	259	86	86	349		G50
196	X	46	40	N50W	44 SW	130	44	44	220		G50
197	X	40	42	N48W	50 SW	132	50	50	222		G50
198	X	40	291	N21E	50 SE	21	50	50	111		G50
199	X	13	323	N53E	77 SE	53	77	77	143		G51
200	X	40	280	N10E	50 SE	10	50	50	100		G51
201	X	30	222	N48W	60 NE	312	60	60	42		G51
202	X	25	322	N52E	65 SE	52	65	65	142		G51
203	X	28	281	N11E	62 SE	11	62	62	101		G51
204	X	8	65	N25W	82 SW	155	82	82	245		G51
205	X	24	318	N48E	66 SE	48	66	66	138		G51
206	X	18	324	N54E	72 SE	54	72	72	144		G51
207	X	32	281	N11E	58 SE	11	58	58	101		G51
208	X	14	335	N65E	76 SE	65	76	76	155		G51
209	X	15	318	N48E	75 SE	48	75	75	138		G51
210	X	5	262	N8W	85 NE	352	85	85	82		G51
211	X	34	54	N36W	56 SW	144	56	56	234		G51
212	X	35	53	N37W	55 SW	143	55	55	233		G51
213	X	31	288	N18E	59 SE	18	59	59	108		G51
214	X	10	119	N29E	80 NW	209	80	80	299		G51
215	X	11	43	N47W	79 SW	133	79	79	223		G51
216	X	20	302	N32E	70 SE	32	70	70	122		A52
217	X	23	300	N30E	67 SE	30	67	67	120		A52
218	X	30	300	N30E	60 SE	30	60	60	120		A52
219	X	16	85	N5W	74 SW	175	74	74	265		A52
220	X	19	80	N10W	71 SW	170	71	71	260		A52

WASATCH3: Continued

No.	ID	Plng	Trnd	Strike	Dip	Azmth	Dip	Dip	DDir	Plt	Site
221	X	22	77	N13W	68 SW	167	68	68	257		A52
222	X	75	72	N18W	15 SW	162	15	15	252		A52
223	X	80	146	N56E	10 NW	236	10	10	326		A52
224	X	41	324	N54E	49 SE	54	49	49	144		A52
225	X	84	25	N65W	6 SW	115	6	6	205		A52
226	X	17	299	N29E	73 SE	29	73	73	119		A52
227	X	70	8	N82W	20 SW	98	20	20	188		A52
228	X	25	301	N31E	65 SE	31	65	65	121		A52
229	X	76	40	N50W	14 SW	130	14	14	220		A52
230	X	20	189	N81W	70 NE	279	70	70	9		G52
231	X	20	50	N40W	70 SW	140	70	70	230		G52
232	X	5	335	N65E	85 SE	65	85	85	155		G52
233	X	26	184	N86W	64 NE	274	64	64	4		G52
234	X	25	76	N14W	65 SW	166	65	65	256		G52
235	X	35	66	N24W	55 SW	156	55	55	246		G52
236	X	30	289	N19E	60 SE	19	60	60	109		G52
237	X	31	172	N82E	59 NW	262	59	59	352		G52
238	X	17	34	N56W	73 SW	124	73	73	214		G52
239	X	1	152	N62E	89 NW	242	89	89	332		G52
240	X	18	66	N24W	72 SW	156	72	72	246		G52
241	X	3	164	N74E	87 NW	254	87	87	344		G52
242	X	7	154	N64E	83 NW	244	83	83	334		G36
243	X	5	128	N38E	85 NW	218	85	85	308		G36
244	X	48	344	N74E	42 SE	74	42	42	164		G36
245	X	11	155	N65E	79 NW	245	79	79	335		G36
246	X	41	325	N55E	49 SE	55	49	49	145		G36
247	X	4	301	N31E	86 SE	31	86	86	121		G36
248	X	1	185	N85W	89 NE	275	89	89	5		G36
249	X	60	96	N6E	30 NW	186	30	30	276		G36
250	X	49	50	N40W	41 SW	140	41	41	230		G36
251	X	35	215	N55W	55 NE	305	55	55	35		G36
252	X	48	324	N54E	42 SE	54	42	42	144		A36
253	X	31	321	N51E	59 SE	51	59	59	141		A36
254	X	0	175	N85E	90 NW	265	90	90	355		A36
255	X	15	62	N28W	75 SW	152	75	75	242		A36
256	X	35	332	N62E	55 SE	62	55	55	152		A36
257	X	17	326	N56E	73 SE	56	73	73	146		A36
258	X	15	118	N28E	75 NW	208	75	75	298		A36
259	X	15	125	N35E	75 NW	215	75	75	305		A36
260	X	14	16	N74W	76 SW	106	76	76	196		A36
261	X	60	108	N18E	30 NW	198	30	30	288		A36
262	BDG	1	33	N57W	89 SW	123	89	89	213		A36
263	BDG	4	37	N53W	86 SW	127	86	86	217		A36
264	X	32	274	N4E	58 SE	4	58	58	94		A34
265	X	19	237	N33W	71 NE	327	71	71	57		A34
266	X	16	234	N36W	74 NE	324	74	74	54		A34
267	X	21	3	N87W	69 SW	93	69	69	183		A34
268	X	28	246	N24W	62 NE	336	62	62	66		A34
269	X	26	268	N2W	64 NE	358	64	64	88		A34
270	X	26	228	N42W	64 NE	318	64	64	48		A34
271	X	60	5	N85W	30 SW	95	30	30	185		A34
272	X	47	21	N69W	43 SW	111	43	43	201		A34
273	X	37	355	N85E	53 SE	85	53	53	175		A34
274	X	30	268	N2W	60 NE	358	60	60	88		A34
275	X	29	290	N20E	61 SE	20	61	61	110		A34

WASATCH3: Continued

No.	ID	Plng	Trnd	Strike	Dip		Azmth	Dip	Dip	DDir	Plt	Site
276	X	28	222	N48W	62	NE	312	62	62	42		A34
277	X	38	15	N75W	52	SW	105	52	52	195		A34
278	X	53	110	N20E	37	NW	200	37	37	290		Q35
279	X	29	253	N17W	61	NE	343	61	61	73		Q35
280	X	27	11	N79W	63	SW	101	63	63	191		Q35
281	X	56	129	N39E	34	NW	219	34	34	309		Q35
282	X	0	137	N47E	90	NW	227	90	90	317		Q35
283	X	1	181	N89W	89	NE	271	89	89	1		Q35
284	X	27	249	N21W	63	NE	339	63	63	69		Q35
285	X	8	332	N62E	82	SE	62	82	82	152		Q35
286	X	62	129	N39E	28	NW	219	28	28	309		Q35
287	X	4	183	N87W	86	NE	273	86	86	3		Q35
288	X	2	180	N90E	88	N	270	88	88	0		Q35
289	X	10	15	N75W	80	SW	105	80	80	195		Q35
290	X	46	99	N9E	44	NW	189	44	44	279		Q35
291	X	38	240	N30W	52	NE	330	52	52	60		Q35
292	BDG	17	63	N27W	73	SW	153	73	73	243		Q35
293	BDG	34	13	N77W	56	SW	103	56	56	193		Q35
294	X	20	330	N60E	70	SE	60	70	70	150		G35
295	X	20	330	N60E	70	SE	60	70	70	150		G35
296	X	14	326	N56E	76	SE	56	76	76	146		G35
297	X	31	296	N26E	59	SE	26	59	59	116		G35
298	X	36	294	N24E	54	SE	24	54	54	114		G35
299	X	31	310	N40E	59	SE	40	59	59	130		G35
300	X	3	165	N75E	87	NW	255	87	87	345		G35
301	X	13	86	N4W	77	SW	176	77	77	266		G35
302	X	10	164	N74E	80	NW	254	80	80	344		G35
303	X	15	355	N85E	75	SE	85	75	75	175		G35
304	X	72	120	N30E	18	NW	210	18	18	300		P35
305	X	14	160	N70E	76	NW	250	76	76	340		P35
306	X	5	152	N62E	85	NW	242	85	85	332		P35
307	X	43	165	N75E	47	NW	255	47	47	345		P35
308	X	2	35	N55W	88	SW	125	88	88	215		P35
309	X	0	330	N60E	90	SE	60	90	90	150		P35
310	X	7	225	N45W	83	NE	315	83	83	45		P35
311	X	5	150	N60E	85	NW	240	85	85	330		P35
312	X	18	151	N61E	72	NW	241	72	72	331		P35
313	X	14	335	N65E	76	SE	65	76	76	155		P35
314	BDG	43	41	N49W	47	SW	131	47	47	221		GP35
315	BDG	1	201	N69W	89	NE	291	89	89	21		GP35
316	BDG	70	84	N6W	20	SW	174	20	20	264		GP35
317	BDG	71	89	N1W	19	SW	179	19	19	269		GP35
318	BDG	71	118	N28E	19	NW	208	19	19	298		GP35
319	BDG	43	29	N61W	47	SW	119	47	47	209		GP35
320	BDG	53	39	N51W	37	SW	129	37	37	219		GP35
321	BDG	39	182	N88W	51	NE	272	51	51	2		QP35
322	BDG	49	171	N81E	41	NW	261	41	41	351		QP35
323	BDG	50	170	N80E	40	NW	260	40	40	350		QP35
324	X	1	103	N13E	89	NW	193	89	89	283		QP35
325	X	15	271	N1E	75	SE	1	75	75	91		QP35
326	X	0	288	N18E	90	SE	18	90	90	108		QP35
327	X	9	279	N9E	81	SE	9	81	81	99		QP35
328	X	10	200	N70W	80	NE	290	80	80	20		QP35
329	X	0	103	N13E	90	NW	193	90	90	283		QP35
330	X	14	88	N2W	76	SW	178	76	76	268		QP35

WASATCH3: Continued

No.	ID	Plng	Trnd	Strike	Dip	Azmth	Dip	Dip	DDir	Plt	Site
331	X	10	290	N20E	80 SE	20	80	80	110		QP35
332	BDG	60	200	N70W	30 NE	290	30	30	20		A25
333	X	48	30	N60W	42 SW	120	42	42	210		A25
334	X	10	321	N51E	80 SE	51	80	80	141		A25
335	X	5	340	N70E	85 SE	70	85	85	160		A25
336	X	52	20	N70W	38 SW	110	38	38	200		A25
337	X	55	23	N67W	35 SW	113	35	35	203		A25
338	X	50	25	N65W	40 SW	115	40	40	205		A25
339	X	42	209	N61W	48 NE	299	48	48	29		A25
340	X	63	201	N69W	27 NE	291	27	27	21		A25
341	X	15	322	N52E	75 SE	52	75	75	142		A25
342	X	14	121	N31E	76 NW	211	76	76	301		A25
343	X	18	121	N31E	72 NW	211	72	72	301		A25
344	X	56	54	N36W	34 SW	144	34	34	234		A26
345	X	63	53	N37W	27 SW	143	27	27	233		A26
346	X	56	56	N34W	34 SW	146	34	34	236		A26
347	X	61	51	N39W	29 SW	141	29	29	231		A26
348	X	9	185	N85W	81 NE	275	81	81	5		A26
349	X	4	131	N41E	86 NW	221	86	86	311		A26
350	X	8	275	N5E	82 SE	5	82	82	95		A26
351	X	0	278	N8E	90 SE	8	90	90	98		A26
352	X	5	5	N85W	85 SW	95	85	85	185		A26
353	X	16	206	N64W	74 NE	296	74	74	26		P27
354	X	22	219	N51W	68 NE	309	68	68	39		P27
355	X	7	203	N67W	83 NE	293	83	83	23		P27
356	X	14	210	N60W	76 NE	300	76	76	30		P27
357	X	74	118	N28E	16 NW	208	16	16	298		P27
358	X	80	53	N37W	10 SW	143	10	10	233		P27
359	X	84	4	N86W	6 SW	94	6	6	184		P27
360	X	1	96	N6E	89 NW	186	89	89	276		P27
361	X	11	262	N8W	79 NE	352	79	79	82		P27
362	X	35	63	N27W	55 SW	153	55	55	243		Q27a
363	X	31	57	N33W	59 SW	147	59	59	237		Q27a
364	X	48	265	N5W	42 NE	355	42	42	85		Q27a
365	X	56	246	N24W	34 NE	336	34	34	66		Q27a
366	X	44	268	N2W	46 NE	358	46	46	88		Q27a
367	X	19	17	N73W	71 SW	107	71	71	197		Q27a
368	X	16	23	N67W	74 SW	113	74	74	203		Q27a
369	X	32	157	N67E	58 NW	247	58	58	337		Q27a
370	X	5	172	N82E	85 NW	262	85	85	352		Q27a
371	X	20	180	N90E	70 N	270	70	70	0		P28
372	X	0	185	N85W	90 NE	275	90	90	5		P28
373	X	5	180	N90E	85 N	270	85	85	0		P28
374	X	5	287	N17E	85 SE	17	85	85	107		P28
375	X	6	288	N18E	84 SE	18	84	84	108		P28
376	X	10	284	N14E	80 SE	14	80	80	104		P28
377	X	18	352	N82E	72 SE	82	72	72	172		P28
378	X	31	351	N81E	59 SE	81	59	59	171		P28
379	X	12	330	N60E	78 SE	60	78	78	150		P28
380	X	5	22	N68W	85 SW	112	85	85	202		P28
381	X	4	269	N1W	86 NE	359	86	86	89		P28a
382	X	5	255	N15W	85 NE	345	85	85	75		P28a
383	X	4	182	N88W	86 NE	272	86	86	2		P28a
384	X	11	3	N87W	79 SW	93	79	79	183		P28a
385	X	8	355	N85E	82 SE	85	82	82	175		P28a

WASATCH3: Continued

No.	ID	Plng	Trnd	Strike	Dip		Azmth	Dip	Dip	DDir	Plt	Site
386	X	6	353	N83E	84	SE	83	84	84	173		P28a
387	X	7	355	N85E	83	SE	85	83	83	175		P28a
388	X	3	304	N34E	87	SE	34	87	87	124		P28a
389	X	39	200	N70W	51	NE	290	51	51	20		P28a
390	X	48	55	N35W	42	SW	145	42	42	235		A29
391	X	44	57	N33W	46	SW	147	46	46	237		A29
392	X	62	54	N36W	28	SW	144	28	28	234		A29
393	X	64	45	N45W	26	SW	135	26	26	225		A29
394	X	1	4	N86W	89	SW	94	89	89	184		A29
395	X	8	21	N69W	82	SW	111	82	82	201		A29
396	X	11	305	N35E	79	SE	35	79	79	125		A29
397	X	7	308	N38E	83	SE	38	83	83	128		A29
398	X	35	346	N76E	55	SE	76	55	55	166		A29
399	X	50	6	N84W	40	SW	96	40	40	186		A29
400	X	16	202	N68W	74	NE	292	74	74	22		Q30
401	X	8	203	N67W	82	NE	293	82	82	23		Q30
402	X	73	114	N24E	17	NW	204	17	17	294		Q30
403	X	72	109	N19E	18	NW	199	18	18	289		Q30
404	X	37	201	N69W	53	NE	291	53	53	21		Q30
405	X	44	211	N59W	46	NE	301	46	46	31		Q30
406	X	50	223	N47W	40	NE	313	40	40	43		A30
407	X	34	213	N57W	56	NE	303	56	56	33		A30
408	X	46	218	N52W	44	NE	308	44	44	38		A30
409	X	5	345	N75E	85	SE	75	85	85	165		A30
410	X	5	8	N82W	85	SW	98	85	85	188		A30
411	X	12	1	N89W	78	SW	91	78	78	181		A30
412	X	15	325	N55E	75	SE	55	75	75	145		A30
413	X	30	64	N26W	60	SW	154	60	60	244		A30
414	X	33	109	N19E	57	NW	199	57	57	289		A30
415	X	44	354	N84E	46	SE	84	46	46	174		A30
416	X	1	213	N57W	89	NE	303	89	89	33		A30
417	X	4	342	N72E	86	SE	72	86	86	162		Q30
418	X	19	346	N76E	71	SE	76	71	71	166		Q30
419	X	13	337	N67E	77	SE	67	77	77	157		Q30
420	X	0	315	N45E	90	SE	45	90	90	135		Q30
421	X	24	214	N56W	66	NE	304	66	66	34		Q30
422	X	27	215	N55W	63	NE	305	63	63	35		Q30
423	X	50	47	N43W	40	SW	137	40	40	227		Q30
424	X	66	119	N29E	24	NW	209	24	24	299		Q30
425	X	28	325	N55E	62	SE	55	62	62	145		A25
426	X	50	30	N60W	40	SW	120	40	40	210		A25
427	X	58	24	N66W	32	SW	114	32	32	204		A25
428	X	62	30	N60W	28	SW	120	28	28	210		A25
429	X	30	110	N20E	60	NW	200	60	60	290		A25
430	X	30	320	N50E	60	SE	50	60	60	140		A25
431	X	0	305	N35E	90	SE	35	90	90	125		A25
432	X	14	40	N50W	76	SW	130	76	76	220		A25
433	X	15	122	N32E	75	NW	212	75	75	302		A25
434	X	28	110	N20E	62	NW	200	62	62	290		A25
435	X	12	125	N35E	78	NW	215	78	78	305		A25
436	X	10	275	N5E	80	SE	5	80	80	95		A26
437	X	60	50	N40W	30	SW	140	30	30	230		A26
438	X	30	176	N86E	60	NW	266	60	60	356		A26
439	X	36	212	N58W	54	NE	302	54	54	32		A26
440	X	15	280	N10E	75	SE	10	75	75	100		A26

WASATCH3: Continued

No.	ID	Plng	Trnd	Strike	Dip	Azmth	Dip	Dip	DDir	Plt	Site
441	X	40	230	N40W	50 NE	320	50	50	50		A26
442	X	10	320	N50E	80 SE	50	80	80	140		A26
443	X	26	220	N50W	64 NE	310	64	64	40		P27
444	X	26	70	N20W	64 SW	160	64	64	250		P27
445	X	70	150	N60E	20 NW	240	20	20	330		P27
446	X	10	210	N60W	80 NE	300	80	80	30		P27
447	X	2	230	N40W	88 NE	320	88	88	50		P27
448	X	10	214	N56W	80 NE	304	80	80	34		P27
449	X	25	250	N20W	65 NE	340	65	65	70		Q27a
450	X	26	182	N88W	64 NE	272	64	64	2		Q27a
451	X	10	188	N82W	80 NE	278	80	80	8		Q27a
452	X	0	352	N82E	90 SE	82	90	90	172		Q27a
453	X	14	70	N20W	76 SW	160	76	76	250		Q27a
454	X	30	270	N0E	60 E	0	60	60	90		P28
455	X	2	294	N24E	88 SE	24	88	88	114		P28
456	X	0	290	N20E	90 SE	20	90	90	110		P28
457	X	2	292	N22E	88 SE	22	88	88	112		P28
458	X	0	30	N60W	90 SW	120	90	90	210		P28
459	X	0	10	N80W	90 SW	100	90	90	190		P28
460	X	10	280	N10E	80 SE	10	80	80	100		P28
461	X	1	0	N90E	89 S	90	89	89	180		P28a
462	X	2	325	N55E	88 SE	55	88	88	145		P28a
463	X	0	356	N86E	90 SE	86	90	90	176		P28a
464	X	0	350	N80E	90 SE	80	90	90	170		P28a
465	X	50	230	N40W	40 NE	320	40	40	50		P28a
466	X	16	0	N90E	74 S	90	74	74	180		P28a
467	X	20	80	N10W	70 SW	170	70	70	260		P28a
468	X	0	305	N35E	90 SE	35	90	90	125		A29
469	X	1	304	N34E	89 SE	34	89	89	124		A29
470	X	38	200	N70W	52 NE	290	52	52	20		A29
471	X	50	195	N75W	40 NE	285	40	40	15		A29
472	X	10	115	N25E	80 NW	205	80	80	295		A29
473	X	30	200	N70W	60 NE	290	60	60	20		A29
474	X	0	5	N85W	90 SW	95	90	90	185		A29
475	BDG	38	200	N70W	52 NE	290	52	52	20		Q30
476	BDG	30	210	N60W	60 NE	300	60	60	30		Q30
477	BDG	34	204	N66W	56 NE	294	56	56	24		Q30
478	BDG	34	200	N70W	56 NE	290	56	56	20		Q30
479	X	60	70	N20W	30 SW	160	30	30	250		Q30
480	X	62	56	N34W	28 SW	146	28	28	236		Q30
481	X	58	60	N30W	32 SW	150	32	32	240		Q30
482	X	32	0	N90E	58 S	90	58	58	180		A30
483	X	32	15	N75W	58 SW	105	58	58	195		A30
484	X	40	208	N62W	50 NE	298	50	50	28		A30
485	X	12	332	N62E	78 SE	62	78	78	152		A30
486	X	60	190	N80W	30 NE	280	30	30	10		A30
487	X	28	170	N80E	62 NW	260	62	62	350		A30
488	X	10	112	N22E	80 NW	202	80	80	292		A30
489	X	55	190	N80W	35 NE	280	35	35	10		A30
490	X	18	337	N67E	72 SE	67	72	72	157		Q30
491	X	30	210	N60W	60 NE	300	60	60	30		Q30
492	X	0	322	N52E	90 SE	52	90	90	142		Q30

No comment attached to this file.
From file WASATCH3 on WASTCH
Created at 16:53:40 on 7 Sep 1988

WHOLEOUTCROP

No.	ID	Plng	Trnd	Strike	Dip	Azmth	Dip	Dip	DDir	Plt	Site
1	X	24	314	N44E	66 SE	44	66	66	134		G47*
2	X	3	160	N70E	87 NW	250	87	87	340		G59
3	X	30	254	N16W	60 NE	344	60	60	74		A34
4	X	37	192	N78W	53 NE	282	53	53	12		SCH44
5	X	18	213	N57W	72 NE	303	72	72	33		27
6	X	26	64	N26W	64 SW	154	64	64	244		27
7	X	71	222	N48W	19 NE	312	19	19	42		G101s
8	X	15	40	N50W	75 SW	130	75	75	220		P88
9	X	29	202	N68W	61 NE	292	61	61	22		P78
10	X	35	284	N14E	55 SE	14	55	55	104		G51
11	X	25	330	N60E	65 SE	60	65	65	150		G49
12	X	37	317	N47E	53 SE	47	53	53	137		G50
13	X	41	358	N88E	49 SE	88	49	49	178		G79
14	X	16	308	N38E	74 SE	38	74	74	128		G94
15	X	27	42	N48W	63 SW	132	63	63	222		P92
16	X	20	164	N74E	70 NW	254	70	70	344		P92
17	X	7	154	N64E	83 NW	244	83	83	334		80
18	X	60	201	N69W	30 NE	291	30	30	21		72
19	X	20	332	N62E	70 SE	62	70	70	152		66
20	X	7	78	N12W	83 SW	168	83	83	258		G64
21	X	60	68	N22W	30 SW	158	30	30	248		A56
22	X	41	75	N15W	49 SW	165	49	49	255		G45
23	X	66	78	N12W	24 SW	168	24	24	258		30
24	X	38	209	N61W	52 NE	299	52	52	29		30
25	X	2	306	N36E	88 SE	36	88	88	126		A29
26	X	5	288	N18E	85 SE	18	85	85	108		28
27	X	9	278	N8E	81 SE	8	81	81	98		A26
28	X	55	29	N61W	35 SW	119	35	35	209		A25
29	X	23	118	N28E	67 NW	208	67	67	298		A25
30	X	57	228	N42W	33 NE	318	33	33	48		A109
31	X	40	90	N0W	50 W	180	50	50	270		A109
32	X	51	176	N86E	39 NW	266	39	39	356		55
33	X	42	307	N37E	48 SE	37	48	48	127		55
34	X	14	145	N55E	76 NW	235	76	76	325		70
35	X	36	166	N76E	54 NW	256	54	54	346		G90
36	X	20	207	N63W	70 NE	297	70	70	27		G108
37	X	3	158	N68E	87 NW	248	87	87	338		35
38	X	60	116	N26E	30 NW	206	30	30	296		35
39	X	3	308	N38E	87 SE	38	87	87	128		AG113
40	X	47	181	N89W	43 NE	271	43	43	1		A91
41	X	40	300	N30E	50 SE	30	50	50	120		A81
42	X	4	87	N3W	86 SW	177	86	86	267		G76
43	X	26	280	N10E	64 SE	10	64	64	100		G77
44	X	40	183	N87W	50 NE	273	50	50	3		G77
45	X	10	319	N49E	80 SE	49	80	80	139		A93
46	X	14	155	N65E	76 NW	245	76	76	335		97
47	X	30	31	N59W	60 SW	121	60	60	211		P95
48	X	43	162	N72E	47 NW	252	47	47	342		P95
49	X	19	320	N50E	71 SE	50	71	71	140		G51
50	X	38	357	N87E	52 SE	87	52	52	177		72
51	X	54	197	N73W	36 NE	287	36	36	17		P73
52	X	9	0	N90E	81 S	90	81	81	180		28
53	X	60	56	N34W	30 SW	146	30	30	236		A26
54	X	3	159	N69E	87 NW	249	87	87	339		71
55	X	80	53	N37W	10 SW	143	10	10	233		A52

WHOLEOUTCROP: Continued

No.	ID	Plng	Trnd	Strike	Dip	Azmth	Dip	Dip	DDir	Plt	Site
56	X	20	81	N9W	70 SW	171	70	70	261		A52
57	X	25	300	N30E	65 SE	30	65	65	120		A52
58	X	31	338	N68E	59 SE	68	59	59	158		AG113
59	X	32	185	N85W	58 NE	275	58	58	5		G22
60	X	42	172	N82E	48 NW	262	48	48	352		70
61	X	60	23	N67W	30 SW	113	30	30	203		A75
62	X	17	208	N62W	73 NE	298	73	73	28		G69
63	X	30	305	N35E	60 SE	35	60	60	125		G112
64	X	10	93	N3E	80 NW	183	80	80	273		G112
65	X	51	190	N80W	39 NE	280	39	39	10		G112
66	X	4	97	N7E	86 NW	187	86	86	277		G111
67	X	52	290	N20E	38 SE	20	38	38	110		G111
68	X	37	326	N56E	53 SE	56	53	53	146		36

No comment attached to this file.
From file WHOLOUTCRP on DISC6
Created at 13:00:37 on 1 Feb 1990
Last Modified at 13:22:28 on 23 Apr 1990
Printed on: 15 Jul 1990 at: 20:25:28

MEAN POLES TO BEDDING

No.	ID	Plng	Trnd	Strike	Dip		Azmth	Dip	Dip	DDir	Plt	Site
1	X	6	37	N53W	84	SW	127	84	84	217		AG113
2	X	50	48	N42W	40	SW	138	40	40	228		112
3	X	57	50	N40W	33	SW	140	33	33	230		A82
4	X	50	28	N62W	40	SW	118	40	40	208		G66
5	X	55	118	N28E	35	NW	208	35	35	298		G58
6	X	48	173	N83E	42	NW	263	42	42	353		35
7	X	70	100	N10E	20	NW	190	20	20	280		35
8	X	46	35	N55W	44	SW	125	44	44	215		35
9	X	36	180	N90E	54	N	270	54	54	0		G105s
10	X	7	202	N68W	83	NE	292	83	83	22		G105s
11	X	2	34	N56W	88	SW	124	88	88	214		A36*
12	X	57	221	N49W	33	NE	311	33	33	41		G80*
13	X	74	22	N68W	16	SW	112	16	16	202		A93*
14	X	29	200	N70W	61	NE	290	61	61	20		G94
15	X	61	56	N34W	29	SW	146	29	29	236		G77*
16	X	40	139	N49E	50	NW	229	50	50	319		A91a
17	X	30	37	N53W	60	SW	127	60	60	217		A91b
18	X	53	64	N26W	37	SW	154	37	37	244		70*
19	X	61	156	N66E	29	NW	246	29	29	336		G72*
20	X	9	20	N70W	81	SW	110	81	81	200		G69
21	X	64	101	N11E	26	NW	191	26	26	281		G76*
22	X	60	200	N70W	30	NE	290	30	30	20		A25
23	X	64	221	N49W	26	NE	311	26	26	41		G100*
24	X	37	151	N61E	53	NW	241	53	53	331		A75*
25	X	76	121	N31E	14	NW	211	14	14	301		G75a*
26	X	43	26	N64W	47	SW	116	47	47	206		G108*
27	X	3	21	N69W	87	SW	111	87	87	201		G111
28	X	52	42	N48W	38	SW	132	38	38	222		G111
29	X	34	48	N42W	56	SW	138	56	56	228		97*
30	X	34	204	N66W	56	NE	294	56	56	24		Q30*
31	X	49	32	N58W	41	SW	122	41	41	212		G101a
32	X	67	244	N26W	23	NE	334	23	23	64		G101
33	X	15	190	N80W	75	NE	280	75	75	10		S55
34	X	70	125	N35E	20	NW	215	20	20	305		A68
35	X	69	267	N3W	21	NE	357	21	21	87		A68
36	X	74	118	N28E	16	NW	208	16	16	298		G59*
37	X	20	19	N71W	70	SW	109	70	70	199		G71

No comment attached to this file.
From file MEANPLBDG on DISC6
Created at 20:58:03 on 12 Feb 1990
Last Modified at 21:35:32 on 4 Jun 1990
Printed on: 15 Jul 1990 at: 20:27:17

APPENDIX 5

ORIGINAL CONDUCTIVITY DATA MEASURED BY WADI

STEED CANYON

X (m)	Y (m)	ECD	Quad.	ECD-avg.	Quad.-avg.
20	120	-2.5	-0.5	-1.42001	0.168
30	120	1	0	2.07999	0.668
40	120	6	-3	7.07999	-2.332
50	120	-6	-3	-4.92001	-2.332
60	120	-11	1	-9.92001	1.668
70	120	1	0.5	2.07999	1.168
80	120	-3.5	-1	-2.42001	-0.332
90	120	-4.5	-2	-3.42001	-1.332
100	120	1	0	2.07999	0.668
110	120	0.0001	-1.5	1.08009	-0.832
120	120	-1	-0.5	0.07999	0.168
130	120	0.5	0.5	1.57999	1.168
140	120	0.5	1	1.57999	1.668
150	120	1	2.5	2.07999	3.168
160	120	1.5	2	2.57999	2.668
170	120	-0.5	0	0.57999	0.668
180	120	3.5	-1	4.57999	-0.332
190	120	-0.5	-1	0.57999	-0.332
200	120	-4	1	-2.92001	1.668
210	120	9.5	9	10.58	9.668
220	120	2.5	4	3.57999	4.668
230	120	-9.5	-3.5	-8.42001	-2.832
240	120	-6	-0.5	-4.92001	0.168
250	120	-5	-4	-3.92001	-3.332
260	120	-3.5	-1.5	-2.42001	-0.832
270	120	-1	0.5	0.07999	1.168
280	120	-2.5	-1.5	-1.42001	-0.832
290	120	-1	-1.5	0.07999	-0.832
300	120	-1.5	-1.5	-0.42001	-0.832
310	120	-0.5	0	0.57999	0.668
320	120	-1	-0.5	0.07999	0.168
20	90	-3	-3	-1.92001	-2.332
30	90	1	-1	2.07999	-0.332

X (m)	Y (m)	ECD	Quad.	ECD-avg.	Quad.-avg.
40	90	3.5	3.5	4.57999	4.168
50	90	5	7.5	6.07999	8.168
60	90	-1.5	-1.5	-0.42001	-0.832
70	90	-14	-13.5	-12.92	-12.832
80	90	-2	-2.5	-0.92001	-1.832
90	90	4	0	5.07999	0.668
100	90	2.5	1	3.57999	1.668
110	90	0	0	1.07999	0.668
120	90	-4.5	-2.5	-3.42001	-1.832
128	92	-2	0	-0.92001	0.668
134	90	2.5	3	3.57999	3.668
142	90	5.5	2	6.57999	2.668
150	90	-1.5	-2	-0.42001	-1.332
160	90	-4.5	-1	-3.42001	-0.332
170	90	0.5	3.5	1.57999	4.168
180	90	0.5	3.5	1.57999	4.168
190	90	-8.5	-6	-7.42001	-5.332
200	90	-5.5	-4.5	-4.42001	-3.832
210	90	8	7	9.07999	7.668
220	90	3	2.5	4.07999	3.168
230	90	-5.5	-5.5	-4.42001	-4.832
240	90	-7	-7	-5.92001	-6.332
250	90	-8	-8	-6.92001	-7.332
260	90	-4	-3.5	-2.92001	-2.832
270	90	-3.5	-2	-2.42001	-1.332
280	90	-1.5	0	-0.42001	0.668
290	90	0.5	-0.5	1.57999	0.168
300	90	0.5	-1	1.57999	-0.332
310	90	3.5	2.5	4.57999	3.168
320	90	5	3	6.07999	3.668
20	60	-7	-10	-5.92001	-9.332
30	60	-6.5	-7.5	-5.42001	-6.832
40	60	0	-1	1.07999	-0.332
50	60	-0.5	1	0.57999	1.668
60	60	-1	0	0.07999	0.668
70	60	0	-2.5	1.07999	-1.832
80	60	-0.5	-2.5	0.57999	-1.832
90	60	-3	-4	-1.92001	-3.332
100	60	-1.5	-1	-0.42001	-0.332
110	60	0	1	1.07999	1.668
120	60	0	0	1.07999	0.668
130	60	-1	0	0.07999	0.668
140	60	1	1	2.07999	1.668

X (m)	Y (m)	ECD	Quad.	ECD-avg.	Quad.-avg.
150	60	3.5	2	4.57999	2.668
160	60	0	3	1.07999	3.668
170	60	-3	0.5	-1.92001	1.168
180	60	-2	-0.5	-0.92001	0.168
190	60	-4	-1.5	-2.92001	-0.832
200	60	-6	-2	-4.92001	-1.332
210	60	-5	-3	-3.92001	-2.332
220	60	-1.5	-1	-0.42001	-0.332
230	60	-3.5	-3	-2.42001	-2.332
240	60	-3.5	-2	-2.42001	-1.332
250	60	-1.5	0.5	-0.42001	1.168
260	60	-1.5	-1	-0.42001	-0.332
270	60	-0.5	-1	0.57999	-0.332
280	60	-1.5	-1	-0.42001	-0.332
290	60	-1	0	0.07999	0.668
300	60	0	-0.5	1.07999	0.168
310	60	0.5	1	1.57999	1.668
320	60	0	1	1.07999	1.668
20	30	6	6.5	7.07999	7.168
30	30	15	15	16.08	15.668
40	30	5	5	6.07999	5.668
50	30	-10.5	-10	-9.42001	-9.332
60	30	-5.5	-6.5	-4.42001	-5.832
70	30	-3.5	-5.5	-2.42001	-4.832
80	30	-1	-0.5	0.07999	0.168
90	30	2	2	3.07999	2.668
100	30	3	3	4.07999	3.668
110	30	-3.5	-1.5	-2.42001	-0.832
120	30	-0.5	2.5	0.57999	3.168
130	30	1.5	4.5	2.57999	5.168
140	30	0	0	1.07999	0.668
150	30	-3	-2.5	-1.92001	-1.832
160	30	6.5	9.5	7.57999	10.168
170	30	-6.5	-6.5	-5.42001	-5.832
180	30	-11	-12.5	-9.92001	-11.832
190	30	-6.5	-10	-5.42001	-9.332
200	30	-5.5	-9	-4.42001	-8.332
210	30	-4.5	-2.5	-3.42001	-1.832
220	30	-4	-1	-2.92001	-0.332
230	30	0	-1.5	1.07999	-0.832
240	30	-2	-1.5	-0.92001	-0.832
250	30	2	0.5	3.07999	1.168
260	30	2	-1	3.07999	-0.332

X(m)	Y (m)	ECD	Quad.	ECD-avg.	Quad.-avg.
270	30	-3.5	-4	-2.42001	-3.332
280	30	-0.5	-1	0.57999	-0.332
290	30	3.5	3	4.57999	3.668
300	30	6	6	7.07999	6.668
310	30	4	3	5.07999	3.668
320	30	-1.5	-1	-0.42001	-0.332

UPPER FORD CANYON SWALE

X(in.)	Y(in.)	ECD	Quad.	ECD-avg.	Quad.-avg.
0.9	8.94	6.5	-1.5	5.78209	-1.17911
1.38	8.82	6.5	-1	5.78209	-0.67911
1.87	8.7	8	2	7.28209	2.32089
2.35	8.58	4	1	3.28209	1.32089
2.84	8.46	-7	-2	-7.71791	-1.67911
3.34	8.35	-2	-1	-2.71791	-0.67911
3.8	8.22	-3	-2	-3.71791	-1.67911
1.13	7.84	3.5	-0.5	2.78209	-0.17911
1.64	7.73	5	-0.5	4.28209	-0.17911
2.1	7.62	1.5	0	0.782088	0.32089
2.61	7.49	0.00001	0.5	-0.71790	0.82089
3.07	7.38	-0.6	0	-1.31791	0.32089
3.59	7.26	0.5	-1	-0.21791	-0.67911
4.04	7.14	-4.5	-0.5	-5.21791	-0.17911
1.36	6.77	1	1	0.282088	1.32089
1.88	6.64	1.5	-0.5	0.782088	-0.17911
2.33	6.53	7	-2.5	6.28209	-2.17911
2.82	6.41	3.5	-1	2.78209	-0.67911
3.3	6.3	-4.5	-1	-5.21791	-0.67911
3.78	6.17	-1	-1	-1.71791	-0.67911
4.27	6.05	0.00001	-0.5	-0.71790	-0.17911
1.7	6.18	11.5	-1	10.7821	-0.67911
2.24	6.04	4	-1	3.28209	-0.67911
2.79	5.9	-9.5	-1	-10.2179	-0.67911
3.32	5.77	-2	-1.5	-2.71791	-1.17911
3.84	5.64	1.5	-2	0.782088	-1.67911
4.4	5.5	3.5	-1.5	2.78209	-1.17911
1.6	5.67	-3	-0.5	-3.71791	-0.17911
2.1	5.55	-4	-0.5	-4.71791	-0.17911
2.58	5.43	0.00001	0	-0.71790	0.32089
3.07	5.31	8	-1	7.28209	-0.67911
3.55	5.19	8	-1	7.28209	-0.67911
4.3	5.08	-6	1.5	-6.71791	1.82089
4.5	4.95	-7.5	1.5	-8.21791	1.82089

X(in.)	Y(in.)	ECD	Quad.	ECD-avg.	Quad.-avg.
1.95	5.07	9.5	-1	8.78209	-0.67911
2.5	4.93	-2	-0.5	-2.71791	-0.17911
3.02	4.81	-15	0.5	-15.7179	0.82089
3.57	4.67	-4.5	0	-5.21791	0.32089
4.1	4.53	-4	0	-4.71791	0.32089
4.61	4.4	-2.5	-0.5	-3.21791	-0.17911
1.84	4.58	-5	0	-5.71791	0.32089
2.32	4.46	4.5	-1	3.78209	-0.67911
2.81	4.35	-3	-0.5	-3.71791	-0.17911
3.29	4.22	-13.5	0.5	-14.2179	0.82089
3.78	4.11	4.5	-1	3.78209	-0.67911
4.28	3.99	-3	0	-3.71791	0.32089
4.73	3.87	-5.5	0	-6.21791	0.32089
2.32	3.44	0.5	-1	-0.21791	-0.67911
2.86	3.31	0.00001	0.5	-0.71790	0.82089
3.4	3.17	1	2	0.282088	2.32089
3.91	3.04	3	0	2.28209	0.32089
4.45	2.91	0.00001	-0.5	-0.71790	-0.17911
4.98	2.78	-0.5	0.5	-1.21791	0.82089
2.52	2.36	1	-1	0.282088	-0.67911
3.06	2.22	2.2	-1	1.48209	-0.67911
3.58	2.09	4.5	-1	3.78209	0.67911
4.13	1.95	0.00001	0	-0.71790	0.32089
4.65	1.83	-4.5	1	-5.21791	1.32089
5.19	1.69	-1.5	0.5	-2.21791	0.82089
2.04	1.45	6.5	-4.5	5.78209	-4.17911
2.54	1.33	12.5	-2	11.7821	-1.67911
3	1.2	14	1.5	13.2821	1.82089
3.5	1.1	8.5	-0.5	7.78209	-0.17911
3.98	0.97	-2.5	1	-3.21791	1.32089
4.48	0.84	1.5	1	0.782088	1.32089
4.95	0.73	8.5	1	7.78209	1.32089
5.44	0.6	2.5	0	1.78209	0.32089
6	8.1	-17.5	-29	-17.2785	-29.3038
6.48	8.2	-22.5	-28	-22.2785	-28.3038
1.15	8.31	0	0.5	0.22151	0.196202
2.3	8.42	4	0	4.22151	-0.30379
2.8	8.52	3.5	-1	3.72151	-1.3038
3.35	8.63	-1	-1.5	-0.77849	-1.8038
3.9	8.72	3	-1.5	3.22151	-1.8038
4.45	8.81	3	-1.5	3.22151	-1.8038
4.98	8.91	2	-3	2.22151	-3.3038

X(in.)	Y(in.)	ECD	Quad.	ECD-avg.	Quad.-avg.
5.55	9.09	5	-3.5	5.22151	-3.8038
6.05	9.13	-3	1.5	-2.77849	1.1962
6.6	9.24	-7.5	4	-7.27849	3.6962

LOWER FORD CANYON SWALE

X(in.)	Y(in.)	ECD	Quad.	ECD-avg.	Quad.-avg.
1.46	0.1	2.5	-19.5	2.72151	-19.8038
1.95	0.21	4.5	-18	4.72151	-18.3038
2.45	0.3	4.5	1	4.72151	0.696202
2.94	0.4	4.5	3	4.72151	2.6962
1.3	1.1	5.5	-1	5.72151	-1.3038
1.8	1.2	13.5	-4	13.7215	-4.3038
2.3	1.3	6	-3	6.22151	-3.3038
2.79	1.4	-14.5	-7.5	-14.2785	-7.8038
3.28	1.49	-19.5	-20	-19.2785	-20.3038
3.78	1.59	-24.5	41	-24.2785	40.6962
4.26	1.68	-29.5	46	-29.2785	45.6962
1.9	2.15	3.5	0	3.72151	-0.30379
2.05	2.26	4.5	0.5	4.72151	0.196202
2.6	2.38	3.5	1.5	3.72151	1.1962
3.3	2.5	5	2	5.22151	1.6962
3.96	2.62	0.5	2.5	0.72151	2.1962
4.6	2.75	-2.5	2.5	-2.27849	2.1962
0.7	3.03	-7	0.5	-6.77849	0.196202
1.26	3.12	-10	3.5	-9.77849	3.1962
1.88	3.24	-5	3	-4.77849	2.6962
2.48	3.36	1	-1	1.22151	-1.3038
3.05	3.47	4	-2	4.22151	-2.3038
3.63	3.58	2.5	1	2.72151	0.696202
4.21	3.69	6	2.5	6.22151	2.1962
4.82	3.8	2.5	2.5	2.72151	2.1962
5.4	3.91	-6	1.5	-5.77849	1.1962
1	4.1	-4	1.5	-3.77849	1.1962
1.59	4.2	1	2.5	1.22151	2.1962
2.18	4.3	5	3.5	5.22151	3.1962
2.25	4.42	4	2	4.22151	1.6962
3.35	4.55	6.5	-0.5	6.72151	-0.80379
3.85	4.66	-1.5	2	-1.27849	1.6962
4.54	4.77	2.5	1	2.72151	0.696202
5.11	4.88	12.5	-1.5	12.7215	-1.8038

X(in.)	Y(in.)	ECD	Quad.	ECD-avg.	Quad.-avg.
5.71	5	3	3.5	3.22151	3.1962
6.25	5.1	-3	4.5	-2.77849	4.1962
1.3	5.19	1.5	-3	1.72151	-3.3038
1.8	5.28	12	-1	12.2215	-1.3038
2.4	5.39	11	1.5	11.2215	1.1962
2.92	5.48	-5.5	-1	-5.27849	-1.3038
3.46	5.6	-4	-0.5	-3.77849	-0.80379
4	5.69	4.5	0.5	4.72151	0.196202
4.55	5.8	4.5	2	4.72151	1.6962
5.15	5.9	0.5	2	0.72151	1.6962
5.71	6	7.5	1.5	7.72151	1.1962
6.35	6.11	11.5	0	11.7215	-0.30379
0.64	6.08	-6	5.5	-5.77849	5.1962
1.11	6.18	-2	4	-1.77849	3.6962
1.6	6.26	3.5	-1	3.72151	-1.3038
2	6.32	2.5	0	2.72151	-0.30379
2.5	6.41	6	1	6.22151	0.696202
3	6.51	1	-0.5	1.22151	-0.80379
3.48	6.6	-1.5	-3.5	-1.27849	-3.8038
3.95	6.7	-1.5	0	-1.27849	-0.30379
4.45	6.8	-3	5.5	-2.77849	5.1962
4.95	6.9	-0.5	6	-0.27849	5.6962
5.47	6.99	-1	-1.5	-0.77849	-1.8038
5.94	7.08	0	0.5	0.22151	0.196202
6.4	7.16	0	0	0.22151	-0.30379
1.6	7.28	-1	-1	-0.77849	-1.3038
2.22	7.4	1.5	-1	1.72151	-1.3038
2.75	7.49	3	-1	3.22151	-1.3038
3.3	7.6	3.5	-1.5	3.72151	-1.8038
3.8	7.7	1	-1.5	1.22151	-1.8038
4.4	7.8	-5	-0.5	-4.77849	-0.80379
4.92	7.9	-4.5	-1	-4.27849	-1.3038
5.45	8	-12.5	-7.5	-12.2785	-7.8038
6	8.1	-17.5	-29	-17.2785	-29.3038
6.48	8.2	-22.5	-28	-22.2785	-28.3038
1.15	8.31	0	0.5	0.22151	0.196202
2.3	8.42	4	0	4.22151	-0.30379
2.8	8.52	3.5	-1	3.72151	-1.3038
3.35	8.63	-1	-1.5	-0.77849	-1.8038
3.9	8.72	3	-1.5	3.22151	-1.8038
4.45	8.81	3	-1.5	3.22151	-1.8038
4.98	8.91	2	-3	2.22151	-3.3038

X(in.)	Y(in.)	ECD	Quad.	ECD-avg.	Quad.-avg.
5.55	9.09	5	-3.5	5.22151	-3.8038
6.05	9.13	-3	1.5	-2.77849	1.1962
6.6	9.24	-7.5	4	-7.27849	3.6962

VITA

Souren Nariman Ala was born on April 4, 1960, in the County of Surrey, England. He is the second of three children of Ann Pelham Sealy and Fereydoun Abolghassem Ala. After graduating from Edinburgh Academy, Scotland, he enrolled in Princeton University in September 1977. He received a Bachelor of Arts degree in Geology from Princeton University in June 1981. From October 1981 to May 1986 he worked as a well site geologist in petroleum and natural gas exploration. In September 1986, he enrolled in the Geology program at Texas A&M University. He was married to Natalyn Louise Kraemer on March 16, 1990. He received a Master of Science degree in Geology from Texas A&M University in December 1990. His permanent address is:

c/o Ala
Hall Farm
Weatheroak Hill
Alvechurch
Birmingham
England B48 7EG

VITA

Souren Nariman Ala was born on April 4, 1960, in the County of Surrey, England. He is the second of three children of Ann Pelham Sealy and Fereydoun Abolghassem Ala. After graduating from Edinburgh Academy, Scotland, he enrolled in Princeton University in September 1977. He received a Bachelor of Arts degree in Geology from Princeton University in June 1981. From October 1981 to May 1986 he worked as a well site geologist in petroleum and natural gas exploration. In September 1986, he enrolled in the Geology program at Texas A&M University. He was married to Natalyn Louise Kraemer on March 16, 1990. He received a Master of Science degree in Geology from Texas A&M University in December 1990. His permanent address is:

c/o Ala
Hall Farm
Weatheroak Hill
Alvechurch
Birmingham
England B48 7EG